

**Role of PROTEIN PHOSPHATASE 7-LIKE  
and the EUKARYOTIC TRANSLATION  
ELONGATION FACTOR COMPLEX 1B in  
plant development and stress responses in  
*Arabidopsis thaliana***

Dissertation with the aim of achieving a doctoral degree at the faculty of Mathematics,

Informatics and Natural Sciences

Department of Biology

University of Hamburg

Submitted by Julia Christin Lohmann

Hamburg, 2024



1. Referee: Dr. Magdalena Weingartner

2. Referee: Prof. Dr. Julia Kehr

Disputation date: 10.10.2024

# Table of Content

Abbreviations .....	
1 Introduction .....	1
1.1 Plant development and genome stability .....	1
1.1.1 Embryo development .....	1
1.1.2 Root apical meristem and regulation of stem cell maintenance .....	3
1.1.3 Genome stability and cell death .....	4
1.1.4 MAINTENANCE OF MERISTEMS (MAIN) protein family .....	5
1.1.5 PROTEIN PHOSPHATASE 7-LIKE .....	7
1.2 Protein biosynthesis .....	8
1.2.1 Canonical translation initiation, elongation and termination .....	9
1.2.2 Translation elongation factor complex eEF1B .....	10
1.3 Abiotic stress responses .....	11
1.3.1 ROS act as signaling molecules and as inducers of oxidative stress response .....	12
1.3.2 Response to elevated temperatures .....	13
1.3.3 Stress-induced biomolecular condensate formation .....	15
1.4 Aim of the thesis .....	18
2 Material and Methods .....	19
2.1 Organisms and Media .....	19
2.1.1 Media additives .....	20
2.2 Biomolecular Methods .....	21
2.2.1 Polymerase chain reaction (PCR) for fragment amplification .....	21
2.2.2 Electrophoretic separation of nucleic acids .....	21
2.2.3 Isolation of DNA fragments from agarose gels .....	22
2.2.4 Gateway cloning - BP reaction .....	22
2.2.5 Transformation of <i>Escherichia coli</i> .....	22
2.2.6 Colony-PCR .....	22
2.2.7 Isolation of plasmid DNA from <i>E. coli</i> and sequencing .....	23
2.2.8 Site-directed mutagenesis .....	23
2.2.9 Gateway cloning - LR reaction .....	24
2.2.10 Transformation of competent <i>Agrobacterium tumefaciens</i> .....	25
2.3 Plant work .....	25
2.3.1 <i>Arabidopsis thaliana</i> growth conditions .....	25
2.3.2 Plant phenotyping methods .....	27
2.3.3 Heat sensitivity assays .....	29

2.3.4 Assays testing for oxidative stress sensitivity.....	30
2.3.5 Genotyping.....	31
2.3.6 Gene expression analysis .....	32
2.3.7 Transient expression in Arabidopsis protoplasts .....	33
2.3.8 Agrobacterium-mediated transient expression in <i>Nicotiana benthamiana</i> leaves...	34
2.3.9 Stable transformation of <i>Arabidopsis thaliana</i> by floral painting .....	34
2.3.10 Suppressor-Screen.....	35
2.4 Protein Analysis.....	36
2.4.1 Protein extraction from plants.....	36
2.4.2 Protein extraction from protoplasts.....	37
2.4.3 Protein concentration measurement .....	37
2.4.4 Sodium dodecyl-sulfate polyacrylamide gel electrophoresis for protein separation	37
2.4.5 Western Blot .....	37
2.4.6 Total protein staining on nitrocellulose membranes .....	39
2.4.7 Stripping of nitrocellulose membranes .....	39
2.4.8 SUnSET .....	40
2.4.9 Polysome Profiling.....	41
2.4.10 Co-Immunoprecipitation for MS analysis .....	42
2.4.11 Co-Immunoprecipitation for western blot analysis.....	42
2.4.12 Yeast-Two-Hybrid .....	43
2.5 Microscopy .....	44
2.5.1 Confocal laser scanning microscopy.....	44
2.5.2 Quantification of cytoplasmic condensates from confocal images.....	45
2.6 Bioinformatics .....	45
2.7 Primers.....	46
3 Results: Functional analysis of inactive protein phosphatase PP7L.....	51
3.1 Interaction studies of MAIL1 and PP7L.....	51
3.1.1 MAIL1 interacts with PP7L in Y2H.....	51
3.1.2 Inactive site of PP7L phosphatase domain is not essential for interaction with MAIL1 in Y2H .....	52
3.1.3 N-terminus of PP7L is necessary for interaction with MAIL1 in Y2H.....	54
3.2 Subcellular localization studies of PP7L .....	56
3.2.1 N-terminus of PP7L, including the NLS, determines nuclear localization of PP7L	56
3.2.2 Inactive motif in phosphatase domain of PP7L does not influence its localization	60
3.3 Suppressor screen .....	60

3.4	Finding new protein interaction partners of PP7L using proteomics .....	67
3.4.1	Proteomic identification of new PP7L interaction partners .....	67
3.4.2	NIT1 and PP7L display no interaction in Y2H or Co-IP/Western .....	68
3.4.3	eEF1B subunits and PP7L do not interact in Y2H or Co-IP/Western .....	70
4	Results: Characterization of translation elongation complex eEF1B .....	73
4.1	Compositional analysis of the eEF1B complex.....	73
4.2	Analysis of the eEF1B $\beta$ subunit.....	76
4.2.1	Expression level of the two eEF1B $\beta$ genes .....	76
4.2.2	Two splicing variants of the eEF1B $\beta$ 1 gene.....	77
4.2.3	Characterization of T-DNA insertion lines of eEF1B $\beta$ 1 and eEF1B $\beta$ 2 .....	79
4.2.4	Generation of eEF1B $\beta$ double mutants.....	83
4.3	Analysis of the eEF1B $\gamma$ subunit .....	85
4.3.1	Expression of the two eEF1B $\gamma$ genes in WT .....	85
4.3.2	N-terminus of eEF1B $\gamma$ is necessary for interaction with eEF1B $\beta$ .....	86
4.3.2	Characterization of T-DNA insertional lines of eEF1B $\gamma$ 1 and eEF1B $\gamma$ 2 .....	88
4.3.4	Phenotypical analysis of <i>eef1b<math>\gamma</math>1/2</i> double mutants .....	90
4.3.5	Complementation studies in <i>eef1b<math>\gamma</math>1/2</i> .....	96
4.3.6	The role of eEF1B $\gamma$ in translation regulation .....	99
4.3.7	eEF1B $\gamma$ does not influence heat stress response .....	106
4.3.8	eEF1B $\gamma$ has an influence on the oxidative stress level in plants .....	112
4.4	Subcellular localization of the three plant eEF1B subunits.....	116
4.4.1	eEF1B subunits accumulate in cytoplasmic condensates after heat stress.....	116
4.4.2	eEF1B-containing condensates are partially overlapping with stress granules after heat stress .....	119
4.4.3	Short digression: Quantification of condensates – possibilities and disadvantages .....	125
4.4.4	eEF1B $\beta$ shows a different condensation behavior than the other eEF1B subunits	128
4.5	Interaction networks of eEF1B $\beta$ and eEF1B $\gamma$ .....	132
5	Discussion .....	142
5.1	PP7L as part of MAIN-MAIL1-PP7L interaction complex .....	142
5.2	eEF1B $\beta$ is central to the plant eEF1B complex.....	146
5.3	The canonical function of Arabidopsis eEF1B in translation elongation and its influence on general translation efficiency.....	149
5.4	Translation factor complex eEF1B impacts plant development.....	151
5.4.1	Loss of eEF1B $\beta$ might be lethal.....	152

5.4.2	Reduction of eEF1B $\gamma$ levels delays plant development and disturbs cell division .....	153
5.5	eEF1B $\gamma$ does play a role for specific stress responses.....	155
5.5.1	eEF1B $\gamma$ modulates ROS homeostasis in Arabidopsis .....	156
5.5.2	eEF1B $\gamma$ is not directly involved in heat stress response.....	157
5.6	eEF1B subunits accumulate in heat-induced stress granules .....	159
6	Summary .....	166
6.1	Zusammenfassung .....	167
7	References .....	169
8	Appendix .....	189
9	List of publications .....	191
	Acknowledgements .....	193
	Affidavit .....	194

## Abbreviations

<i>A. thaliana</i>	<i>Arabidopsis thaliana</i>
AD	Activation domain
AT	3-Aminotriazol
ATM	ATAXIA TELANGIECTASIA MUTATED
ATP	Adenosintriphosphat
ATR	ATM AND RAD3-RELATED
BD	DNA-binding domain
BT	Basal thermotolerance
CAF1	CHROMATIN ASSEMBLY FACTOR 1
cDNA	Complementary DNA
CDS	Coding sequence
CHX	Cycloheximide
CMT2	CHROMO-METHYLASE 2
Co-IP	Co-immunoprecipitation
DAB	3,3'-Diaminobenzidine
dag	days after germination
DNA	Desoxyribonucleic acid
DDR	DNA damage response
DRM1	DOMAINS REARRANGED METHYLATTRANSFERASE 1
eEF1B	Eukaryotic ELONGATION FACTOR 1B
<i>E. coli</i>	<i>Escherichia coli</i>
EMS	Ethylmethanesulfonate
ERF115	ETHYLENE RESPONSE FACTOR 115
FAS	FASCIATA
FDR	False Discovery Rate
gDNA	Genomic DNA
GDP	Guanosindiphosphat
GEF	Guanine exchange factor domain

GFP	Green fluorescent protein
GST	Glutathione S-transferase
GTP	Guanosintriphosphat
G3BP1	Ras GTPase-activating protein-binding protein 1
h	hour
HIRA	HISTONE REGULATOR A
HIS	Histidine
HSG	Heat stress granule
HSP	HEAT SHOCK PROTEIN
HYG	Hygromycin B
H <sub>2</sub> O <sub>2</sub>	Hydrogen peroxide
IDR	Intrinsically disordered region
IP-MS	Immunoaffinity purification with following mass spectrometry
kb	kilobases
kDa	kilodalton
LAT	Long-term acquired thermotolerance
LLPS	Liquid-liquid phase separation
MAIN	MAINTENANCE OF MERISTEMS
MAIL1	MAINTENANCE OF MERISTEMS-LIKE 1
MES	2-( <i>N</i> -morpholino)ethanesulfonic acid
5mC	5-methylcytosine
min	minute
MORC	MICRORCHIDIA
MS	Murashige and Skoog
MV	Methylviologen (N-,N'-dimethyl-4,-4'-bipyridinium dichloride)
<i>N. benthamiana</i>	<i>Nicotiana benthamiana</i>
NIT1	NITRILASE 1
NLS	Nuclear localization signal
PAB	POLY-A-BINDING PROTEIN

PB	Processing body
PCR	Polymerase chain reaction
PI	Propidium iodide
pI	Isoelectric point
PLTs	PLETHORA transcription factors
PMD	Plant mobile domain
PPD	Serine-/Threonine-phosphatase domain
PPP	Phosphoprotein phosphatase
PP7	PROTEIN PHOSPHATASE 7
PP7L	PROTEIN PHOSPHATASE 7-LIKE
PRLD	Prion-like domain
QC	Quiescent center
qPCR	Quantitative Real-Time PCR
RBGD2	RNA-binding glycine rich D2
RBP	RNA-BINDING-PROTEIN
RFP	Red fluorescent protein
RNA	Ribonucleic acid
ROS	Reactive oxygen species
RP	Ribosomal proteins
RT	Room temperature
RT-PCR	Reverse transcriptase PCR
s	Second
<i>S. cerevisiae</i>	<i>Saccharomyces cerevisiae</i>
SAT	Short-term acquired thermotolerance
SCN	Stem cell niche
SCR	SCARECROW
SDS	Sodium dodecyl sulfate
SG	Stress granule
SHR	SHORT-ROOT

sHSP	Small HEAT SHOCK PROTEIN
SnRK1	SNF1-RELATED PROTEIN KINASE 1
SOG1	SUPPRESSOR OF GAMMA RESPONSE 1
TIA1	T-cell-restricted intracellular antigen-1
TOR	TARGET OF RAPAMYCIN
TSN	TUDOR-STAPHYLOCOCCUS-NUCLEASE
UBP1b	OLIGOURIDYLATE BINDING PROTEIN 1b
UTR	Untranslated region
V	Volt
YFP	Yellow fluorescent protein
Y2H	Yeast two-hybrid

# 1 Introduction

Plants are sessile organisms, consequently they have to develop and survive at the place of their germination, no matter which environmental challenges are occurring. During embryonal and postembryonal development, plants are able to renew their cells. The replenishment of cells is conceived by a specific cell tissue, called meristem. A tight regulation of cell replenishment and maintenance of genome integrity are essential for correct growth and development.

An essential process for plant growth is protein biosynthesis, which produces enzymes that are required to run the metabolism and catabolism. One important step during protein biosynthesis is the translation of the mRNA sequence into proteins. Translation is known as regulatory step, which is downregulated if plants are exposed to extreme conditions. Especially in times of climate change an adaption of plants to stress conditions like heat, drought or salt stress is required to ensure plant survival. Understanding the mechanisms of plant stress responses in greater detail will help in the long term to ensure sufficient crop yields for human food production.

In the following, the development of plants including important factors for meristem maintenance will be introduced. Additionally, an overview of plant abiotic stress responses, especially focusing on oxidative stress, heat stress and the formation of stress-induced biomolecular condensates in regard of translational regulation will be given.

## 1.1 Plant development and genome stability

### 1.1.1 Embryo development

All cells of the mature plant originate from the zygote, which is formed upon fertilization of the egg cell with the sperm. Through highly coordinated cell division and differentiation processes of the zygote cell lineages, tissue types and body axis are already established during embryogenesis (Capron et al. 2009; Armenta-Medina et al. 2021). Cell division and cell patterning is strongly influenced by domain-specific gene expression and cell-cell communication. The different stages of embryonal development are clearly distinguishable in *Arabidopsis* and are defined by expression of certain marker genes. These steps of embryogenesis are visualized in Fig. 1.

First, the zygote elongates and an asymmetric cell division leads to formation of the apical and basal cell. The elongation and first division of the zygote is regulated by homeobox transcription factor family *WUSCHEL-RELATED HOMEODOMAIN* (*WOX*) (Haecker et al. 2004)

and the YODA-MPK pathway (Ueda et al. 2017). Both, *WOX2* and *WOX8*, are expressed together in the zygote. Activation of *WRKY2* through the YODA-MPK pathway leads to increased *WOX8* expression and cell division. Afterwards, *WOX2* is only expressed in the apical cell, while *WOX8* is expressed solely in the basal cell.

The apical cell will lead to formation of the embryo and later on to all above-ground tissues. Auxin-mediated coordination of cell division of the apical cell leads to radial patterning of the apical domain. Auxin efflux facilitator *PINFORMED1* (*PIN1*) is expressed in the apical proembryo and establishes the apical-basal embryo axis. The basal cell will form the suspensor including hypophysis and the root cap (Capron et al. 2009). The suspensor is an extra-embryonal structure that connects the embryo to the tissue of the mother cell. The uppermost suspensor cell is the hypophysis, which later forms the quiescent center (QC) and the central root cap initials in root apical meristem. This is largely determined by the expression of the transcription factor *WOX5* in the hypophysis and later in the QC cells during embryogenesis and post-germination growth (Forzani et al. 2014).

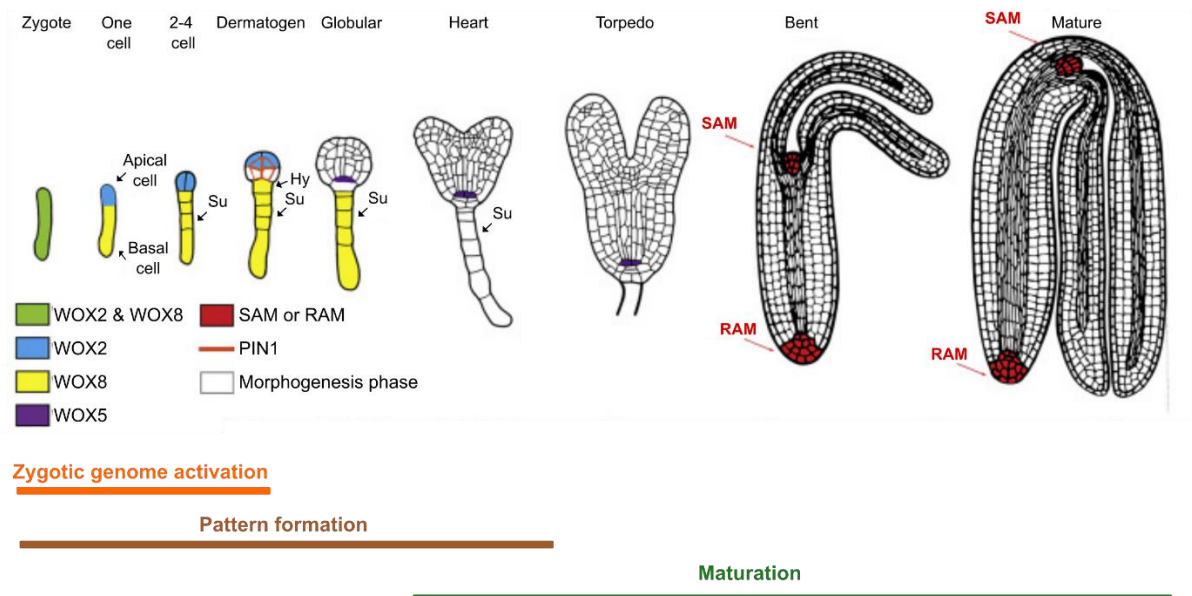


**Figure 1: Embryo development in Arabidopsis.** (A) Scheme of different developmental stages of embryo development from zygote to mature embryo with different colors showing the cell identity markers of the different stages. Hy: hypophysis, Su: suspensor, SAM: Shoot apical meristem, RAM: Root apical meristem. The figure has been adapted from (Armenta-Medina et al. 2021).

In the ‘globular stage’, when the embryo contains 32 cells, the shoot apical meristem (SAM) and the root apical meristem (RAM) are being initiated (Jurgens et al. 1994). Upon localized

growth at the opposing apical regions, the embryo becomes triangular and reaches early ‘heart stage’, when it contains around 200 cells. At heart stage, the major organs, cotyledons, hypocotyl and primary root are recognizable and pattern formation is completed. Further growth elongates the hypocotyl and the cotyledons and brings the embryo to ‘torpedo stage’. Cotyledons start to fold over, when the embryo is in ‘bent stage’. The mature embryo contains full SAM and RAM and maturation ends with the fully desiccated seed (Armenta-Medina et al. 2021).

### 1.1.2 Root apical meristem and regulation of stem cell maintenance

The root apical meristem (RAM) is located at the root tip and gives rise to all cells of the primary root (Fig. 2). In the center of the meristematic zone are four mitotically inactive cells, which are called ‘quiescent center’ (QC). The QC is surrounded by five sets of mitotically active stem cells (also known as initials), which divide asymmetrically and give rise to a self-replenishing daughter cell and a daughter cell that divides and after several rounds of cell division and differentiation builds distinct root cell types (van den Berg et al. 1995; Scheres 2007). The QC together with the stem cells form the stem cell niche (SCN) (van den Berg et al. 1995; Jiang and Feldman 2005). Distal of the QC are the columella initials, which later on will form the columella cells (Fig. 2B).

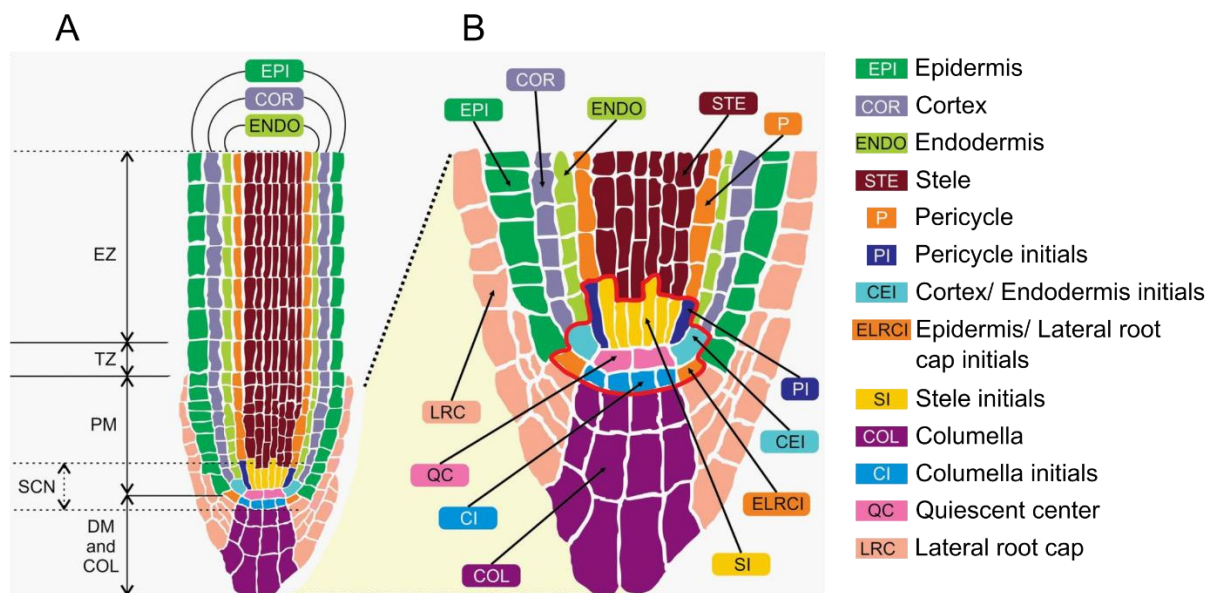


**Figure 2: Arabidopsis root architecture and root apical meristem.** (A) Graphical overview of a longitudinal section of an Arabidopsis root. The root is structured in three zones, the meristematic zone (MZ), the transition zone (TZ) and the elongation zone (EZ). In the center of the meristematic zone is the stem cell niche (SCN). Above the SCN is the proximal meristem (PM) and below the SCN is the distal meristem (DM) and the columella (COL).

(B) Longitudinal section of the meristematic zone. The stem cell niche is circled in red. The figure has been adapted from (Lee, Lee, and Kim 2012).

Proximal of the QC are the stele initials and pericycle initials, which will develop the vasculature tissues. Lateral of the QC are the cortex/endodermis initials, which divide asymmetrically to build a cortex and an endodermis daughter cell. Similarly, lateral to QC and dividing asymmetrically are the epidermis/lateral root cap initials (Dolan et al. 1993). At the root transition zone, cells exit the cell cycle and start to differentiate into the above-named tissue types (Dello Ioio et al. 2007). The differentiated cells do not divide anymore, but grow by cell elongation and are forming the so called elongation zone (Perilli, Di Mambro, and Sabatini 2012).

Similar to the formation of the RAM during embryogenesis, the maintenance of the stem cell niche in post-embryonic growth requires a tight and coordinated regulation to secure correct radial patterning and development of root tissues. A large network of different molecular factors, predominantly transcription factors and several phytohormones, act together as regulatory hub for stem cell maintenance (reviewed in (Di Mambro and Dello Ioio 2020; Strotmann and Stahl 2021; Lee, Lee, and Kim 2012)). Transcription factor *WOX5* is not only an important regulator for RAM formation during embryogenesis, but is also essential for stem cell maintenance. Mutants of *WOX5* lose QC cell identity and QC cells become mitotically active (Sarkar et al. 2007). *WOX5* controls the division rate in the QC by repressing the expression of cell cycle regulators including *CYCLIND3;3* and *CYCLIND1;1*. *WOX5* maintains the columella stem cells by controlling transcription factors including *CYCLING DOF FACTOR4* (Forzani et al. 2014; Pi et al. 2015). Additionally, the PLETHORA (PLTs) transcription factors are induced through *WOX5* activity. Through a highly balanced PLT protein gradient, which is coordinated with the auxin gradient within the root meristematic zone, stem cell proliferation and differentiation are regulated (Aida et al. 2004; Galinha et al. 2007; Mähönen et al. 2014). Another important pathway for correct positioning of QC and the regulation of QC maintenance is dependent on the two GRAS transcription factors, *SHORT-ROOT (SHR)* and *SCARECROW (SCR)* (Sabatini et al. 2003). *SHR* activates *SCR* forming an *SHR/SCR* protein complex, whose concentration and localization regulates the division of cortex/ endodermis initials and QC cells (Clark et al. 2020).

### 1.1.3 Genome stability and cell death

Since all below-ground cells originate from the root stem cell niche, it is essential to ensure genomic stability within the stem cells. Cells are permanently exposed to DNA damaging

agents, e.g. UV light or reactive oxygen species (ROS) resulting from metabolic processes or abiotic stresses. To counteract the DNA damage, plants have evolved a highly sophisticated network of DNA repair mechanisms, called DNA damage response (DDR); (reviewed in (Nisa et al. 2019)). This process is dependent on the two checkpoint kinases, ATAXIA TELANGIECTASIA MUTATED (ATM) and ATM AND RAD3-RELATED (ATR); (Fulcher and Sablowski 2009; Furukawa et al. 2010). ATM phosphorylates the transcription factor SUPPRESSOR OF GAMMA RESPONSE 1 (SOG1), which is an important regulator of cell cycle progression, DNA repair activation and induction of stem cell death (Yoshiyama et al. 2013). If possible, the DDR induces repair of DNA single or double strand breaks and thereby ensures continued cell cycle activity. Upon more severe DNA damage either endoreduplication (Adachi et al. 2011) or, most severely, programmed cell death (PCD) is induced to avoid proliferation of cells with damaged DNA (Furukawa et al. 2010). Consequently, stem cells and their early descendants are selectively entering cell death under DNA damaging conditions. To replenish the damaged stem cells in the meristem, cell division of QC cells is initiated by the transcription factor ETHYLENE RESPONSE FACTOR 115 (ERF115), which is transcriptionally upregulated in cells in direct contact to dead cells (Heyman et al. 2013; Heyman et al. 2016).

#### 1.1.4 MAINTENANCE OF MERISTEMS (MAIN) protein family

Meristem function strongly relies on genome integrity, as several DDR mutants are also affected in meristem organization (Nisa et al. 2019). The gene *MAINTENANCE OF MERISTEMS (MAIN)* is an important factor for the post-embryonic development and maintenance of the RAM in Arabidopsis. *Loss-of-MAIN* leads to a strong short-root phenotype associated with accumulation of dead cells within the meristem, increased DNA damage and the up-regulation of DNA damage-induced transcripts (Wenig et al. 2013). MAIN belongs to a protein family of in total four proteins (MAIN, MAINTENANCE OF MERISTEMS-LIKE 1 (MAIL1), MAIL2 and MAIL3). All four MAIN family proteins contain an aminotransferase-like, ‘plant mobile domain’ (PMD) and a ‘nuclear localization signal’ (Fig. 3B). Indeed, MAIN family proteins were found to be expressed exclusively in the nucleus (Wenig et al. 2013; Uhlken et al. 2014). The phylogenetic tree in Fig. 3A shows all proteins belonging to the MAIN protein family from thirty different eudicots indicating that the MAIN protein family is conserved (Nicolau et al. 2020). The highest similarity to MAIN has MAINTENANCE OF MERISTEMS-LIKE 1 (MAIL1), which shares 68% protein sequence identity in Arabidopsis. MAIL2 is also relatively similar, whereas MAIL3 belongs to another subclade in the

phylogenetic tree (Fig. 3A). MAIL3 contains, in addition to the PMD domain, a ‘serine/threonine protein phosphatase’ (PPD)-domain at the C-terminus (Fig. 3B).

In depth analysis of T-DNA insertion lines of MAIN family proteins revealed that *main* and *mail1* mutants show highly similar short root phenotypes, whereas *mail3* mutants resemble the WT plant phenotype. RNAi-lines of *MAIL2* did show a minor developmental defect in leaf formation, but no defects in primary root development (PhD thesis, Christine Ühlken, 2014). *mail1* mutants display accumulation of damaged DNA and cell death in the root meristem starting at 2-3 dag, similar to *main*. Both mutants are able to survive and to reproduce due to formation of adventitious roots compensating for defects in the primary root and anchor root formation (Uhlken et al. 2014; Uhlken, Hoth, and Weingartner 2014). Double mutant analysis of *main mail1* showed that both proteins act redundantly in the same signaling pathway as the double mutant phenotype mirrors the single mutant phenotype (Uhlken et al. 2014).

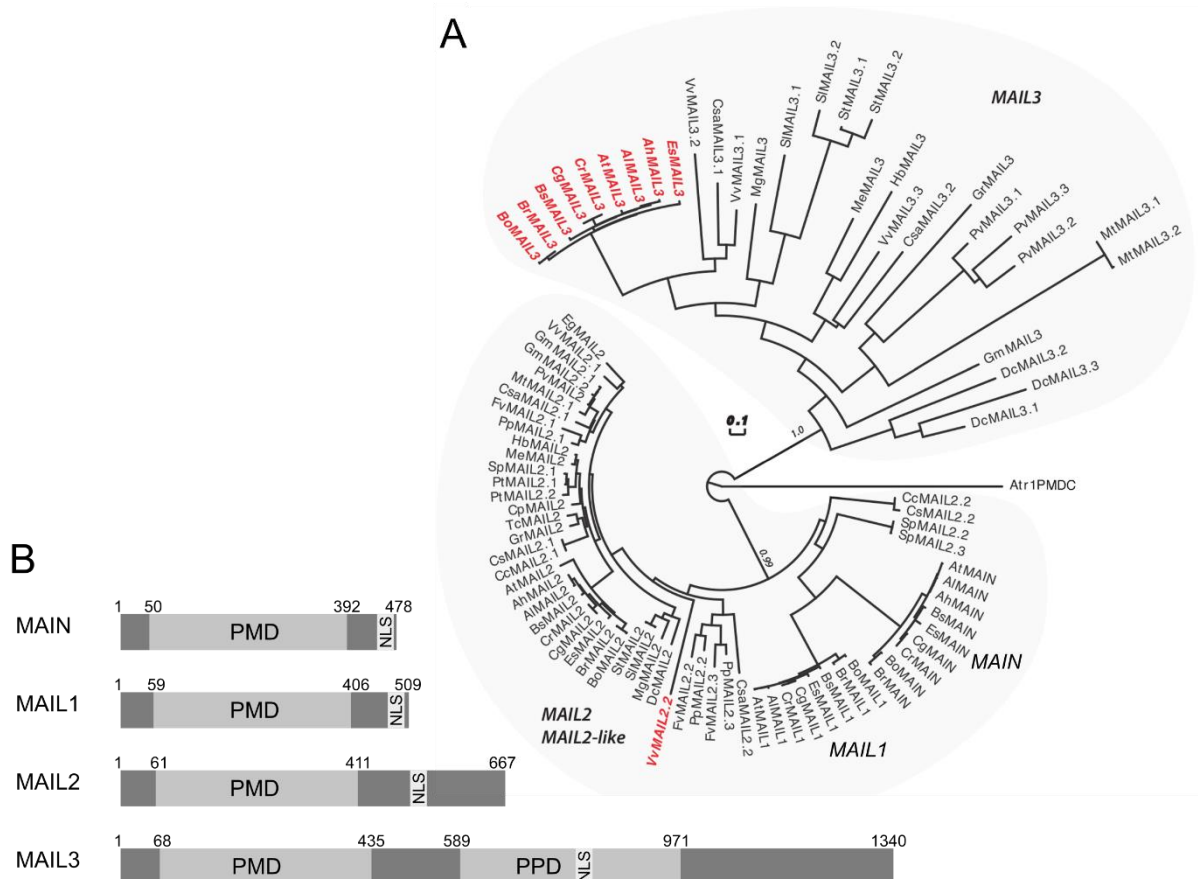


**Figure 3: Conservation of PMD domains and structures of Arabidopsis MAIN family proteins. (A)** Phylogenetic tree showing the PMD motif containing proteins from 30 representative Eudicot species. The major clades MAIL2/MAIL2-like (including MAIN and MAIL1) and MAIL3 are indicated. Genes containing both, a PMD and a PPD motif, are marked in red. The image was taken from (Nicolau et al. 2020). **(B)** Protein structures

of Arabidopsis MAIN, MAIL1, MAIL2 and MAIL3. PMD: Plant mobile domain, PPD: Protein phosphatase domain, NLS: Nuclear localization signal.

In addition to the function in primary root development and genome integrity in the RAM, MAIN and MAIL1 were identified in independent studies as important factors for silencing of transposable elements (Ikeda et al. 2017; Nicolau et al. 2020). Both *main* and *mail1* mutants show release of transposon silencing, mainly of loci that are located in the pericentromeric heterochromatin associated with partial decondensation of the pericentromeric heterochromatin (Ikeda et al. 2017). The mechanism leading to release of TE silencing as consequence of loss of MAIN or MAIL1 is still unsure. MAIL1 was described to act independently of the most common pathways for TE silencing, DNA methylation and siRNA-mediated silencing pathway (Ikeda et al. 2017). For MAIN, it was suggested to act in a complex ‘multiple layer’ regulation network together with factors involved in DNA methylation and other epigenetic regulatory pathways (Nicolau et al. 2020). Overall, it is also unknown, whether the observed release of TEs in *main* and *mail1* is connected to the defects in primary root growth and genome integrity.

#### 1.1.5 PROTEIN PHOSPHATASE 7-LIKE

Our group and another independent group from France searched for protein interaction partners of MAIN and MAIL1 and we both identified PROTEIN PHOSPHATASE 7-LIKE (PP7L) as being part of a MAIN-MAIL1-PP7L complex (de Luxan-Hernandez et al. 2020; Nicolau et al. 2020). PP7L belongs to the plant-specific serine/threonine protein phosphatase family of PROTEIN PHOSPHATASE 7 (PP7) together with MAIL3 (Farkas et al. 2007; Uhrig, Labandera, and Moorhead 2013). PP7 is involved in phytochrome signaling (Genoud et al. 2008) and has been associated with the regulation of HEAT SHOCK PROTEIN (HSP) expression under heat stress (LIU et al. 2007). In comparison to PP7, PP7L also contains a PP7-like protein phosphatase domain, but which contains several mutations within the catalytic center and is therefore designated as being inactive (Goldberg et al. 1995). Additionally, PP7L contains an N-terminal domain, which includes the NLS (Fig. 4).

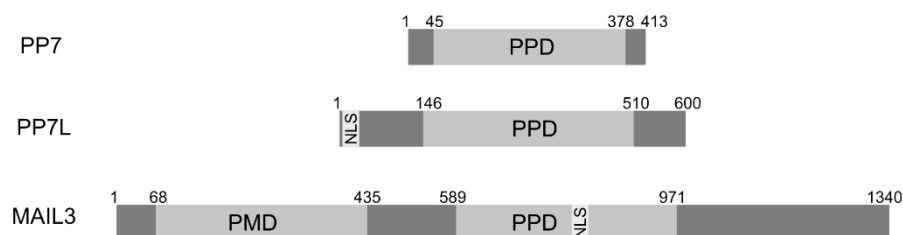


**Figure 4: Structures of Arabidopsis PROTEIN PHOSPHATASE 7 (PP7) protein family members.** PMD: Plant mobile domain, PPD: Protein phosphatase domain, NLS: nuclear localization signal.

Analysis of *pp7l* mutants mirrored the phenotype of *mail1*. *pp7l* mutants showed normal embryogenesis, but showed impaired primary root growth and accumulated dead cells in the RAM at 3 dag. This was associated with an increased expression of several DNA repair genes. Interestingly, the induction of DNA damage response in *pp7l* mutants was not dependent on the main DDR regulator SOG1 (de Luxan-Hernandez et al. 2020). A similar set of TEs was released from silencing in *pp7l* as had been shown for *main* and *mail1* mutants (de Luxan-Hernandez et al. 2020; Nicolau et al. 2020). Analysis of *main pp7l* and *mail1 pp7l* double mutants underlined that PP7L acts in the same signaling pathway as MAIN and MAIL1 (de Luxan-Hernandez et al. 2020). Nonetheless, it still remains unknown in which pathway the MAIN-MAIL1-PP7L complex is involved.

Another study found a function for PP7L in chloroplast biogenesis (Xu et al. 2019). It was shown that *pp7l* mutants are defective in chloroplast ribosomal RNA (rRNA) biogenesis and therefore also in messenger RNA (mRNA) translation. Additionally, seed germination of *pp7l* was impaired under salt and high light, whereas overexpression of PP7L increased tolerance to these stresses. This implied a possible role of PP7L in abiotic stress responses (Xu et al. 2019).

## 1.2 Protein biosynthesis

Plant growth and development strongly rely on proper and coordinated gene expression. Proteins are involved in a multitude of cellular processes. Thus, maintenance of protein homeostasis is essential for plant survival. Translation describes the process of translating the genetic information from mRNA into a polypeptide chain and production of the final protein. The process of translation is a highly conserved mechanism, including the three steps, initiation, elongation and termination, with a consequent recycling step. The most important factors involved in translation are mRNAs, tRNAs, ribosomes and translation factors. Based on the high conservation of translation mechanisms between different species, conserved translation factors have been identified in plants and Arabidopsis. Despite the high conservation, there are several plant-specific translation factors (Browning and Bailey-Serres 2015; Moore, Gossmann, and Dietz 2016; Wu, Jen, and Hsu 2023).

The process of translation is highly energy-dependent and cost-intensive, so it has to be tightly regulated. Especially in response to adverse environmental conditions, translation needs to be adapted quickly to conserve energy and prevent damage (Advani and Ivanov 2019). Therefore, it is not surprising that many translation factors have been shown to play a role in abiotic stress responses in plants (Castellano and Merchante 2021).

### 1.2.1 Canonical translation initiation, elongation and termination

Canonical initiation of translation is dependent on the 5' m<sup>7</sup>Gppp cap structure of the messenger RNA (mRNA) and occurs during favorable conditions. The 5' cap is bound by the eukaryotic INITIATION FACTOR COMPLEX 4F, which is formed by the subunits, eIF4E, eIF4G and eIF4A. The 3' poly-(A)-tail of the mRNA is bound by POLY-A-BINDING PROTEINS (PABs). Simultaneously, the GTP-bound eIF2 binds to an initiator tRNA (Met-tRNA<sub>i</sub><sup>Met</sup>) and further assembles with 40S ribosomal subunits, eIF1, eIF3 and eIF4A to form the 43S pre-initiation complex (43S PIC). 43S PIC binds eIF4F, consequently bringing mRNA and initiator tRNA together. Consequently, scanning of the mRNA for a start codon can begin at the 5'UTR. Start codon recognition leads to recruitment of 60S ribosomal subunits. Once several eIFs are released, the fully assembled ribosome, called 80S ribosome, can begin translation elongation.

Translation elongation is dependent on the delivery of aminoacyl-tRNAs to the ribosome. The start codon paired with the initiator tRNA is placed in the P-site of the ribosome. The following codon is placed in the A-site of the ribosome and the appropriate anticodon containing aminoacyl-tRNA has to be delivered. This is mediated by the eukaryotic TRANSLATION ELONGATION FACTOR 1A (eEF1A). eEF1A binds aminoacyl-tRNAs and releases them to the A-site upon codon:anticodon pairing. A peptide-bond between initiator tRNA and the aminoacyl-tRNA is formed. The transfer of the aminoacyl-tRNA from eEF1A to the A-site is energy-dependent and requires the hydrolysis of GTP to GDP, which is bound to eEF1A. For eEF1A to be able to deliver a new aminoacyl-tRNA, it has to be recharged with GTP. This GDP/GTP exchange is promoted by the eukaryotic TRANSLATION ELONGATION FACTOR COMPLEX 1B (eEF1B). Subsequently, the mRNA is translocated by one codon, which shifts the peptidyl-tRNA to P-site and the deacylated tRNA to the E-site of the ribosome. The translocation is mediated by eEF2 and also requires GTP hydrolysis. Afterwards, the A-site of the ribosome is again free for the next aminoacyl-tRNA and a new round of elongation cycling. An overview of the translation elongation cycle is demonstrated in Fig. 5.

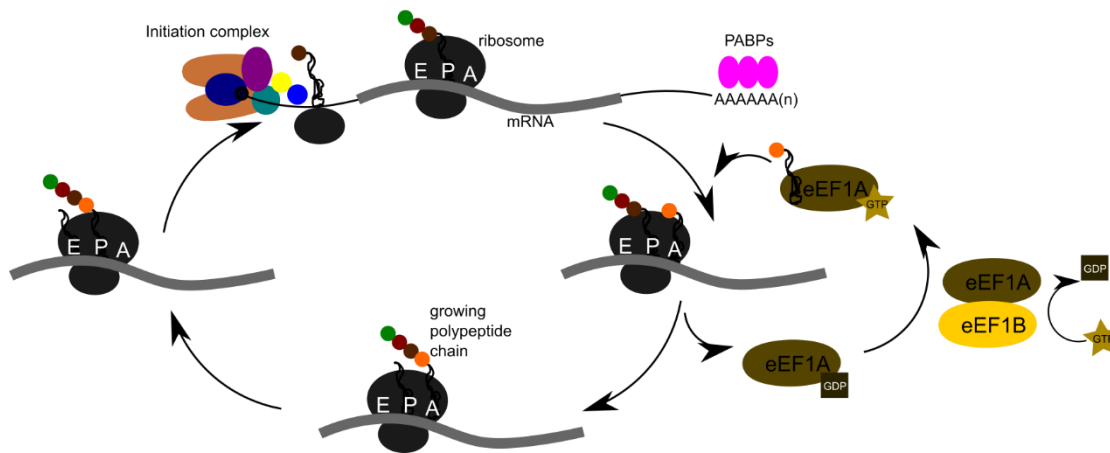


**Figure 5: Overview of translation elongation.** Once the initiation-tRNA is bound to the AUG of the mRNA, translation elongation starts. GTP-bound eEF1A delivers aminoacyl-tRNAs to the ribosome. Upon correct codon:anticodon pairing a peptide bond is formed and the mRNA is translocated by three nucleotides, which shifts the peptidyl-tRNA to the P-site, the deacylated tRNA to the E-site and frees the A-site for the next aminoacyl tRNA. The figure has been adapted from (Browning and Bailey-Serres 2015).

The elongation cycle is stopped, when a stop codon is encountered in the A-site. The eukaryotic RELEASE FACTORS 1 and 3 (eRF1 and eRF3) mediate translation termination in a GTP-dependent manner and lead to the release of the peptide from the ribosome. To completely finish the translation cycle and to be able to start a new round of translation, the ribosomal subunits are recycled by the ATP-binding cassette subfamily E member 1 (ABCE1) (Pisarev et al. 2010).

### 1.2.2 Translation elongation factor complex eEF1B

The translation elongation factor complex is highly conserved among yeast, metazoa and plants, although the number and composition of the subunits within the eEF1B complex are diverse between different species. In the following, the nomenclature suggested by Le Sourd et al. will be used to describe the eEF1B complex subunits. In plants, the eEF1B complex is composed of three subunits: alpha ( $\alpha$ ), beta ( $\beta$ ) and gamma ( $\gamma$ ); (Le Sourd et al. 2006). Two genes are encoding for each subunit in Arabidopsis, which produce highly similar proteins (Browning and Bailey-Serres 2015). Yeast eEF1B is composed of only two subunits, alpha and gamma (Miyazaki et al. 1988), while metazoa contain alpha, gamma and delta subunits. The beta subunit is plant-specific (Le Sourd et al. 2006). The canonical functions of the subunits are described based on the high sequence homology of plant eEF1B subunits to their corresponding homologs in yeast and metazoa. Table 1 shows the accessions numbers and the assigned functions of the subunits in Arabidopsis.

**Table 1: Subunits of the Arabidopsis eEF1B complex:** Functions, protein isoforms and gene identifiers.

eEF1B subunit	Function	Protein isoform	Gene identifier
alpha	GDP/GTP exchange	eEF1B $\alpha$ 1	AT5G12110
		eEF1B $\alpha$ 2	AT5G19510
beta	GDP/GTP exchange	eEF1B $\beta$ 1	AT1G30230
		eEF1B $\beta$ 2	AT2G18110
gamma	Structural component and possible GST activity	eEF1B $\gamma$ 1	AT1G09640
		eEF1B $\gamma$ 2	AT1G57720

The plant eEF1B $\alpha$  and eEF1B $\beta$  subunit possess guanine exchange factor activity, which is necessary for recharging eEF1A. The eEF1B $\gamma$  subunit is supposedly a structural subunit, which keeps the complex together. Besides these canonical functions, additional non-canonical functions have been described for the eEF1B complex of different organisms, including cell cycle regulation, virus replication, DNA repair, alternate splicing and stress responses (Sasikumar, Perez, and Kinzy 2012; Negrutskii 2020). In Arabidopsis, eEF1B $\beta$  is playing a role in plant development and cell wall biosynthesis (Hossain et al. 2012). Several studies indicate that eEF1B $\gamma$  is involved in oxidative stress. Loss of eEF1B $\gamma$  in yeast results in altered oxidative stress response (Olarewaju et al. 2004; Esposito and Kinzy 2010). eEF1B $\gamma$  mutants of *Aspergillus fumigatus* are more sensitive towards oxidative stress (O'Keeffe et al. 2013). eEF1B $\gamma$  from *Phanerochaete chrysosporium* has been shown to be an active Glutathione-S-transferase (GST) and to interact with other GSTs (Bchini et al. 2020).

### 1.3 Abiotic stress responses

Throughout their life cycle, plants are exposed to different kinds of abiotic stress including heat, drought, cold, nutrient deficiencies, excess salt or toxic metal stress. Under stress conditions, growth, development, yield and metabolism of plants are severely affected. In regard of climate change, plants are confronted with more extreme weather conditions. Recently, it was shown that the occurrence of combined heat and drought during growing season of the most important crop plants (wheat, maize, soybean, rice), which leads to severe yield reduction, significantly increased from 1980 to 2009 (Heino et al. 2023). Another study indicated that the 'primary climatic driver' influencing crop yields in the future is temperature increase (Ortiz-Bobea et al. 2019). Therefore, it is of utmost importance to understand the plant stress signaling pathways

and response mechanisms to be able to ensure plant survival and sufficient crop yields in the future.

Plants stress responses can be non-adaptive or adaptive (Zhang et al. 2022). Non-adaptive responses mirror the damage resulting from stress and include changes in membrane fluidity, protein structure or disorder of enzyme kinetics. Adaptive responses are responsible for increased stress tolerance and are therefore most interesting for engineering of more stress robust plants. Adaptive responses include repair of stress-induced damage, rebalancing of cellular homeostasis and adaption of growth and development (Zhang et al. 2022). This implies that plants have to constantly balance their growth rate and their stress responses resulting in a growth-stress response-trade-off (Zhang, Zhao, and Zhu 2020).

Plant stress responses can be divided into general stress response mechanisms, which are induced in response to any kind of stress, and stress-specific response mechanisms, which are dependent on the type of stress. Stress responses are induced via various cellular processes including: stress sensing, signal transduction, transcription, transcript processing, translation and post-translational modifications (Zhang et al. 2022). In the following, the specific responses to oxidative and heat stress will be introduced with special emphasis on the regulation of translation. Another potential factor for regulating stress responses is the subcellular localization of mRNA and proteins in cytoplasmic biomolecular condensates, which will also be introduced.

### 1.3.1 ROS act as signaling molecules and as inducers of oxidative stress response

ROS are built as side-products during photosynthesis and aerobic processes. The most often generated ROS are singlet oxygen, hydrogen peroxide, superoxide anion and hydroxyl radical (Mittler 2002). In low concentrations, ROS are dynamic and important signaling messengers regulating plant growth, development and abiotic stress responses. Coordinated oxygen and ROS signaling is required for correct function and patterning of the stem cell niche (Considine and Foyer 2021). Various stresses, including heat, cold, drought or heavy metal stress, can induce high concentrations of ROS (reviewed in (Huang et al. 2019)). High concentrations of ROS can cause cellular damage through oxidation of proteins, lipids and other metabolites. But high ROS levels can also induce programmed cell death, which can be required for survival during stress conditions. Different pathways are scavenging ROS and help to maintain ROS homeostasis. Many of these pathways include the scavenging enzymes, superoxide dismutase, ascorbate peroxidase or catalase (Mittler 2002). Furthermore, antioxidants like ascorbate and glutathione are important for removal of ROS (Noctor and Foyer 1998). Loss of glutathione

synthase enzymes can be embryo-lethal or induce strong developmental defects (Vernoux et al. 2000; Cairns et al. 2006). Glutathione is a low-molecular weight thiol and can exist in two free forms, reduced or oxidized form. Reduced glutathione is required for detoxification of ROS and needs to be transferred to ROS. This is mediated by glutathione-S-transferases (GSTs). Plants have 14 classes of GSTs, which have canonical catalytic activity, but are also involved in mediating biotic and abiotic stress resistance and plant development (reviewed in (Nianiou-Obeidat et al. 2017)).

### 1.3.2 Response to elevated temperatures

Plants are highly responsive to changes of temperature, even differences of 1°C can be sensed (Jung et al. 2016). High temperatures lead to several physiological changes in plants that are recognized by different sensors (reviewed in (Zhang et al. 2022)). During high temperatures membrane fluidity is altered (Sangwan et al. 2002) and free cytosolic Ca<sup>2+</sup> concentration is increased. This might be due to alterations of membrane-bound cyclic nucleotide-gated ion channels, which regulate Ca<sup>2+</sup> signaling and confer heat tolerance in rice (Cui et al. 2020). Temperature stress also leads to decreased protein stability, which is recognized for example by the temperature-dependent switch phyB. At elevated temperatures, phyB switches to inactive state and releases the transcription factor PIF4. Increased PIF4 activity leads to thermomorphogenesis, including elongation of growth of petioles, hypocotyl and primary root as well as increased expression of heat-responsive genes (Franklin et al. 2011; Jung et al. 2016). Thermomorphogenesis occurs mainly in response to moderately elevated temperatures. During extremely high temperatures, the heat stress response is mediated through the Heat Shock Transcription Factor (HSF)-Heat Shock Protein pathway (Zhou et al. 2022). In Arabidopsis, HSFA1 has been described as main regulator of heat stress response at the transcriptional level. Mutants lacking multiple *HsfA1* genes display altered morphology and retarded growth under control conditions and reduced expression of several heat responsive genes and increased heat sensitivity during heat stress (Liu, Liao, and Charng 2011).

At the translational level, two main regulatory mechanisms are initiated upon heat stress. One of the two main mechanisms is the global repression of general protein biosynthesis. In Arabidopsis seedlings, only 50% of bulk mRNAs are associated with polysomes after heat stress (Yanguéz et al. 2013). This is mainly regulated through inhibition of translation initiation. In mammalian cells, the phosphorylation of translation initiation factor eIF2 $\alpha$  through a specific protein kinase is the main regulatory switch leading to downregulation of translation initiation (Lu, Han, and Chen 2001). In plants, eIF2 $\alpha$  is not phosphorylated in response to heat stress

(Gallie et al. 1997; Zhigailov et al. 2020). Instead, other mechanisms including those involved in control of the formation of the eIF4F complex, often depending on the activity of the central signaling hub TARGET OF RAPAMYCIN (TOR) and its antagonist SNF1-related protein kinase 1 (SnRK1), were suggested to lead to inhibition of translation initiation in response to various stresses in plants (Bruns et al. 2019; Nukarinen et al. 2016; Scarpin, Leiboff, and Brunkard 2020; Son and Park 2023; Castellano and Merchante 2021).

The second of the two main mechanisms at the translational level is the induction of stress-specific gene expression. HSFs and other heat-specific transcription factors induce the expression of HEAT SHOCK PROTEINS (HSPs) in response to heat stress. HSPs act as molecular chaperones, which support correct protein folding and prevent aggregation of nascent polypeptide chains. Heat stress leads to an increased number of misfolded proteins, whose refolding is supported by HSPs or which are targeted by HSP and other co-chaperones for degradation (Zhang and Qian 2011). Thereby, HSPs help to maintain protein homeostasis. There are five families of HSP proteins, which are clustered according to their molecular weight: HSP60, HSP70, HSP90, HSP100 and small HSPs (Bascos and Landry 2019; Ul Haq et al. 2019). Arabidopsis mutants lacking several *HSP70* genes show severe developmental defects under control conditions and are hypersensitive to heat stress (Leng et al. 2017). Targets of HSC70/HSP70 are degraded in co-translational decay through the exoribonuclease XRN4 (Merret et al. 2013; Merret et al. 2015). HSC70/HSP70 also mediates the downregulation of general translation rates at the translation elongation step. The heat-induced increase of misfolded proteins leads to reduced availability of HSC70/HSP70, which provokes ribosome pausing during translation elongation (Merret et al. 2015). This shows that translation elongation plays a role for global translational repression during heat stress.

HSP101 is an important protein disaggregase in Arabidopsis, which confers heat stress resistance. *hsp101* mutants do show minor developmental defects under control conditions, but are strongly heat sensitive (Hong and Vierling 2001; Tiwari et al. 2021). Therefore, *hsp101* mutants are often used as control line for heat stress experiments (McLoughlin et al. 2016; Zhang, Liu, et al. 2017). HSP101 has been shown to act together with HSP70 and small HSPs (sHSPs) to solubilize proteins that aggregate in response to heat. The group of proteins, which are re-solubilized by HSP101 included translation initiation factor eIF4A, translation elongation factors eEF1B $\alpha$ , eEF1B $\beta$  and eEF1B $\gamma$  as well as an RNA helicase (McLoughlin et al. 2016). It was suggested that the re-solubilization of these factors might be important for recovery of translation rates after stress relief. Indeed, *hsp101* mutants show a defect in polysome recovery

after heat stress-recovery. Additionally, *hsp101* is defective in the disassembly of heat-induced cytoplasmic biomolecular condensates, called stress granules (Merret et al. 2017).

### 1.3.3 Stress-induced biomolecular condensate formation

Biomolecular condensates are microscopically observable, membrane-less sites containing increased numbers of specific mRNAs and proteins. High numbers of low-affinity interactions between multivalent molecules lead to liquid-liquid phase separation (LLPS), which is essential for biomolecular condensate formation (Banani et al. 2017). Multivalent molecules known to enhance LLPS are on the one hand RNAs with specific properties, e.g. secondary structures or chemical modifications (Tauber, Tauber, and Parker 2020; Campos-Melo et al. 2021). On the other hand are RNA-binding proteins (RBPs), especially proteins containing intrinsically disordered regions (IDRs), prion-like domains (PLDs) or low complexity domains (LCDs), enhancing biomolecular condensate formation (Wiedner and Giudice 2021). Proteins, that are driving the process of biomolecular condensate formation and that are found at the core of biomolecular condensates, are called ‘scaffolds’. Proteins, that are only associating with the shell of biomolecular condensates, are called ‘clients’.

Upon stress conditions different types of biomolecular condensates are formed within cells. Two types of cytosolic biomolecular condensates have predominantly been described in mammalian, yeast and plant cells: stress granules (SGs) and processing bodies (PBs). Upon stress conditions, translation is downregulated and polysomes are released from mRNAs. Free untranslated mRNAs are a prerequisite for SG and PB formation. PBs are present within the cytosol prior to stress conditions, but their quantity and size increase upon stress. Untranslated, deadenylated mRNA and mRNA decay factors like decapping enzymes and exoribonucleases have been identified as components of PBs (Teixeira et al. 2005; Zheng et al. 2008). Therefore, it was initially assumed that PBs are active sites of mRNA decay and mRNAs are targeted to PBs for their degradation. But different studies challenged this hypothesis. Currently, it is not finally cleared up in which way PBs are regulating mRNA translation, both, selective stabilization or decay of mRNA, are possible. Such a dual function of PBs has been proposed (Aizer et al. 2014). Interestingly, PBs and SGs can share or exchange their components (Kedersha et al. 2005).

SGs form quickly after stress initiation. Key components of SGs are untranslated poly(A)-mRNAs, specific translation initiation factors and 40S ribosomal subunits (Kedersha et al. 1999). Important examples of SG scaffold proteins from mammalian cells are Ras GTPase-activating protein-binding protein 1 (G3BP1), T-cell-restricted intracellular antigen-1 (TIA1)

and TIA1-related (TIAR) (Yang et al. 2020; Rayman and Kandel 2017; Kedersha et al. 2000). Upon stress relief, SGs are disassembled with the help of different chaperones, like HSP101 (Merret et al. 2017). Thus, it was suggested that SGs play a role in storage and protection of mRNAs and proteins during stress conditions. A simplified overview of the formation of SGs and PBs in response elevated temperatures is shown in Fig. 6.

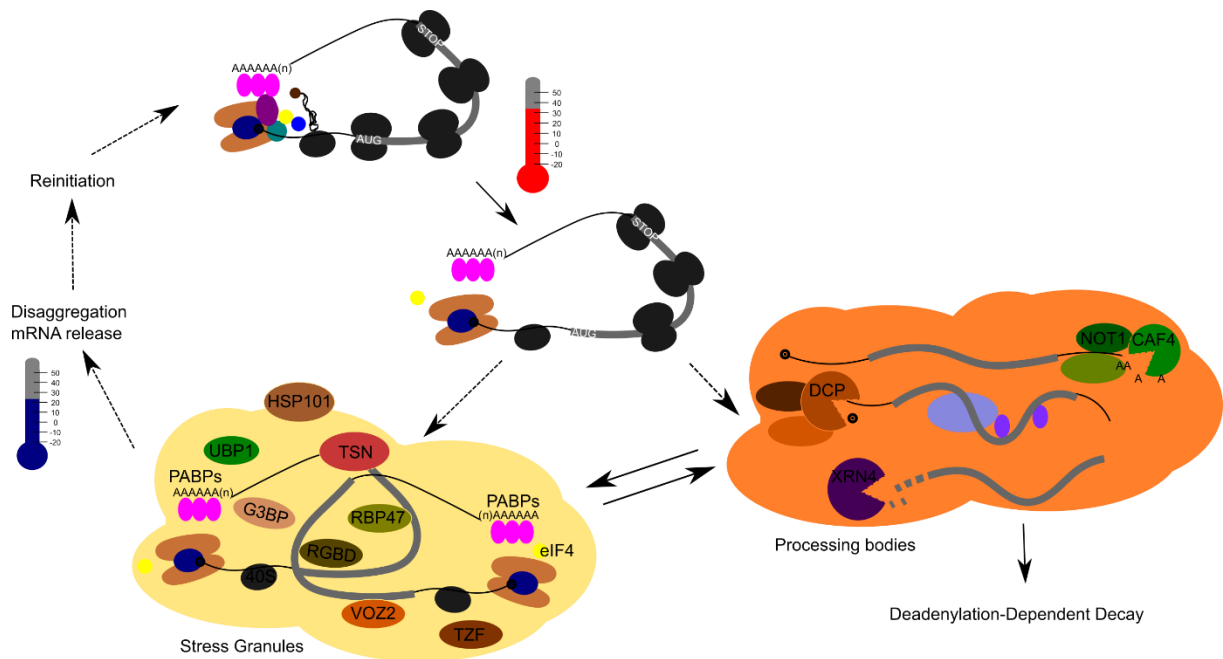


**Figure 6: Stress Granules and Processing Bodies assemble upon polysomal mRNA run-off in response to heat stress.** In response to heat stress, polysomes disassemble from the translated mRNA. Untranslated mRNAs and proteins are reversibly stored in stress granules and processing bodies. Upon stress relief, proteins and mRNAs are released from stress granules and can re-enter the translation. The figure has been adapted from (Chantarachot and Bailey-Serres 2018).

The details of assembly, disassembly, composition and function of mammalian SGs and PBs in response to different stresses have been thoroughly reviewed in mammalian cells (Hofmann et al. 2021; Glauninger et al. 2022; Millar et al. 2023). Mis-regulated biomolecular condensation was shown to lead to severe diseases in humans (Baradaran-Heravi, Van Broeckhoven, and van der Zee 2020; Niu et al. 2023; Silva et al. 2023). The analysis of biomolecular condensates is an active research area in plants. Newest insights on SG and PB characteristics in plants have been reviewed recently (Maruri-Lopez et al. 2021; Kearly et al. 2022; Londoño Vélez et al. 2022; Solis-Miranda et al. 2023; Yan et al. 2022). While many aspects of SGs and PBs are shared between mammalian, yeast and plant cells, there are also differences. One of which is that in plants, an additional class of biomolecular condensate has been proposed in response to

heat stress. While SGs assemble quickly in response to heat stress and lack HSPs, plant heat-stress granules (HSGs) assemble only under long-term heat stress, contain HSPs and are not dependent on untranslated RNAs (Weber, Nover, and Fauth 2008). The distinct separation of SGs and HSGs has later on been questioned, because at least some HSP-containing condensates contain mRNA (McLoughlin et al. 2016).

#### 1.3.3.1 Scaffold proteins in heat-induced stress granules

Stress granules in plants are formed in response to diverse stress conditions, but high temperature is one of the most commonly used conditions for induction of stress granule assembly in plants. Thereby, important scaffold proteins of heat-induced stress granules have been identified. OLIGOURIDYLATE BINDING PROTEIN 1b (UBP1b), a homolog of mammalian SG-scaffold protein TIA1, is a SG-nucleating protein, whose overexpression promotes thermotolerance (Sorenson and Bailey-Serres 2014; Nguyen et al. 2016). It was suggested that mRNAs associated with UBP1b-SGs are protected from degradation during heat stress (Nguyen et al. 2016). Direct evidence for this hypothesis is missing so far.

RBP47, plant homolog of mammalian TIAR, is also essential for SG formation upon heat stress (Weber, Nover, and Fauth 2008; Bhasin and Hülskamp 2017). RBP47 was used as bait to identify the first heat-induced SG proteome in plants (Kosmacz et al. 2019) and revealed an overlap of 28% with human SG proteome (Jain et al. 2016). It was shown that similar to mammalian SGs, many RBPs are localizing to plant SGs (Kosmacz et al. 2019).

RNA-binding glycine rich D2 and 4 (RBGD2 and RBGD4) are RBPs that confer thermotolerance and localize to heat-induced SGs. A low complexity domain that is capable of LLPS *in vitro* and *in vivo* after heat stress is present in both proteins and is required for heat stress resistance (Zhu et al. 2022).

Tudor Staphylococcal Nuclease (TSN) is another scaffold protein in heat-induced SGs, which contains an intrinsically disordered region (Gutierrez-Beltran et al. 2015; Gutierrez-Beltran et al. 2021). The analysis of the TSN interactome showed that 70% of TSN interactors form a preassembled interaction network already at control conditions, whereas 30% of the TSN interactome are recruited to SGs *de novo* upon heat induction. So, TSN might act as docking platform for SG-associated proteins and could thereby support early steps of SG formation (Gutierrez-Beltran et al. 2021).

### 1.3.3.2 Translation elongation factors in heat-induced biomolecular condensates

While the presence of translation initiation factors has long been established, the occurrence of translation elongation factors in biomolecular condensates has been discovered more recently. In yeast, the translation elongation factor subunit eEF1B $\gamma$  has been found in heat-shock induced SGs (Grousl et al. 2013). Several lines of evidence indicated that subunits of the translation elongation factor complex eEF1B are also present in heat-induced SGs in Arabidopsis. First, all eEF1B subunits do colocalize with HSP101 in heat-induced cytoplasmic condensates (McLoughlin et al. 2016). Second, in the proteomic analysis of the RBP47 interactors in SGs, all three eEF1B subunits have been identified (Kosmacz et al. 2019). Third, the SG scaffold protein TSN does interact with eEF1B $\gamma$  in a heat-dependent manner (Gutierrez-Beltran et al. 2021). This led to the hypothesis that the subcellular localization of the eEF1B subunits might play a role in response to heat stress. Thus, the analysis of the changes in the subcellular localization of eEF1B complex components upon heat stress has been one focus of this thesis.

## 1.4 Aim of the thesis

PP7L is an inactive phosphatase that belongs to a protein complex involved in maintenance of root meristem and genome integrity. In order to understand the function of PP7L within the interplay of the three-protein MAIN-MAIL1-PP7L complex, protein-protein interaction and subcellular localization studies have been performed as part of this thesis. The signaling pathway, in which PP7L and its complex partners work, is still unknown. To this end, two experimental approaches were followed. First, a suppressor screen was initiated with *pp7l* mutants and second, new potential protein interactors were identified.

The eEF1B complex has a canonical function in translation elongation and several non-canonical functions, which had not been studied in plants. Analysis of T-DNA insertion lines was performed to identify the function of eEF1B $\gamma$  in protein biosynthesis, growth and development and heat stress response. Since biomolecular condensates play a role in abiotic stress response and several studies indicated the localization of eEF1B subunits in biomolecular condensates upon heat stress, the subcellular localization of the three eEF1B subunits was analyzed using GFP fusion proteins. The studies should especially elucidate how the recruitment of eEF1B subunits to biomolecular condensates upon heat stress might influence the control of translation.

## 2 Material and Methods

### 2.1 Organisms and Media

Organism	Strain	Genotype	Reference
OneShot® Top10	<i>Escherichia coli</i>	F- <i>mcrA</i> Δ( <i>mrr-hsdRMS-mcrBC</i> ) Φ80 <i>LacZ</i> Δ <i>M15</i> Δ <i>LacX74</i> <i>recA1</i> <i>araD139</i> Δ( <i>araleu</i> )7697 <i>galU</i> <i>galK</i> <i>rpsL</i> (StrR) <i>endA1</i> <i>nupG</i>	Thermo Fisher Scientific
DH5α	<i>Escherichia coli</i>	F- <i>endA1</i> <i>glnV44</i> <i>thi-1</i> <i>recA1</i> <i>relA1</i> <i>gyrA96</i> <i>deoR</i> <i>nupG</i> <i>purB20</i> φ80 <i>dlacZ</i> Δ <i>M15</i> Δ( <i>lacZYA-argF</i> )U169, <i>hsdR17</i> (rK -mK +), λ-	(Hanahan 1983)
GV3101	<i>Agrobacterium tumefaciens</i>	C58 (Rif <sup>R</sup> ), pMP90 (Gent <sup>R</sup> )	(Koncz and Schell 1986)
C58C1	<i>Agrobacterium tumefaciens</i>	C58 (Rif <sup>R</sup> )	(Van Larebeke et al. 1974)
AH109	<i>Saccharomyces cerevisiae</i>	<i>MATa</i> , <i>trp1-901</i> , <i>leu2-3, 112</i> , <i>ura3-52</i> , <i>his3-200</i> , <i>gal4Δ</i> , <i>gal80Δ</i> , <i>LYS2::GAL1<sub>UAS</sub>-</i> <i>GAL1<sub>TATA</sub>-HIS3</i> , <i>GAL2<sub>UAS</sub>-GAL2<sub>TATA</sub>-</i> <i>ADE2</i> , <i>URA3::MEL1<sub>UAS</sub>-MEL1<sub>TATA</sub>-lacZ</i>	(James, Halladay, and Craig 1996)

#### LB medium (Luria and Bertani-Medium)

Trypton	0,5 % (w/v)
Yeast extract	1 % (w/v)
NaCl	0,5 % (w/v)

LB medium was autoclaved before use. For solid medium 1,5 % (w/v) agar was added.

#### YPDA (Yeast Peptone Dextrose Adenine-Medium)

Yeast extract	1 % (w/v)
Peptone	2 % (w/v)
Glucose	2 % (w/v)
Adenine hemisulfate	0,003 % (w/v)

YPDA medium was autoclaved before use. Glucose and adenine hemisulfate were dissolved in ddH<sub>2</sub>O, sterile-filtrated and added after autoclaving. pH has been adjusted to 5.8 using HCl. For solid medium 2 % (w/v) agar was added.

SD-Medium (Synthetic Defined Growth-Medium)

Glucose	2 % (w/v)
Yeast Nitrogen base without amino acids	6,7 g/L
Adenine hemisulfate	20 mg/L
Arginine	20 mg/L
Histidine (not in -Leu-Trp-His)	20 mg/L
Isoleucine	20 mg/L
Myo-Inositol	20 mg/L
Leucine (not in -Leu-Trp or -Leu-Trp-His)	40 mg/L
Lysine	20 mg/L
Methionine	20 mg/L
Phenylalanine	30 mg/L
Serine	20 mg/L
Threonine	20 mg/L
Tryptophan (not in -Leu-Trp or -Leu-Trp-His)	30 mg/L
Tyrosine	20 mg/L
Uracil	12 mg/L
Valine	90 mg/L

SD-Medium was sterile-filtrated before use. If SD-Medium was used for selection of positive yeast transformants, the appropriate amino acids were left out of the medium. To increase stringency of yeast selection 3-aminotriazol was added to the medium.

2.1.1 Media additives

<b>Additive</b>	<b>Solvent</b>	<b>Stock solution</b>	<b>Final concentration</b>
Ampicillin	ddH <sub>2</sub> O	100 mg/ml	100 µg/ml
Kanamycin	ddH <sub>2</sub> O	50 mg/ml	50 µg/ml
Spectinomycin	ddH <sub>2</sub> O	100 mg/ml	100 µg/ml
3-aminotriazol	ddH <sub>2</sub> O	1 M	0,5 mM to 1 mM

## 2.2 Biomolecular Methods

### 2.2.1 Polymerase chain reaction (PCR) for fragment amplification

Amplification of genomic or coding sequences for cloning was performed by PCR using Phusion™ High Fidelity DNA-Polymerase (Thermo Fisher, Schwerte, Germany). All primers used in this study are listed in 2.7. The PCR reaction mix was set up as following:

<b>Reagent</b>	<b>Volume</b>
Phusion™ High Fidelity Buffer	10 µl
10 mM dNTPs	1 µl
10 µM Forward primer	2,5 µl
10 µM Reverse Primer	2,5 µl
DMSO	1,5 µl
DNA template	2 µl
Phusion™ High Fidelity DNA-Polymerase	0,5 µl
ddH <sub>2</sub> O	ad 50 µl

The following PCR program was used for amplification (Cycling between denaturation and elongation step 29x):

<b>Step</b>	<b>Temperature</b>	<b>Time</b>
Initial denaturation	98°C	3 min
Denaturation	98°C	10 s
Annealing	x°C (dependent on primer melting T)	30 s
Elongation	72°C	x min (30s per 1 kb)
Final Elongation	72°C	8 min
Hold	10°C	∞

### 2.2.2 Electrophoretic separation of nucleic acids

Agarose gel electrophoresis was used to separate DNA fragments. Therefore, an agarose gel was prepared with 0,8 % (w/v) agarose (Genaxxon bioscience GmbH) in 1x TAE buffer (40 mM Tris-acetate, 1 mM EDTA) and 0,05 µg/mL ethidiumbromide. As marker, 4 µl of GeneRuler 1 kb Plus DNA Ladder (Thermo Fisher Scientific, Schwerte, Germany) were loaded onto the gel. Phusion PCR products were mixed with 5x loading dye before loading. Gel

electrophoresis was run at 120 V for 30 – 50 min. DNA was detected under UV light with PEQLAB E-BOX VX2 imaging system (VWR International GmbH, Darmstadt, Germany).

### 2.2.3 Isolation of DNA fragments from agarose gels

Pieces of agarose gel containing DNA fragments of interest were cut from the gel. DNA was isolated and cleaned using the NucleoSpin® Gel and PCR Clean-up Kit (MACHEREY-NAGEL GmbH & Co. KG, Düren, Germany) according to manufacturer's information. For elution of DNA from the column, 20 µl of ddH<sub>2</sub>O was used.

### 2.2.4 Gateway cloning - BP reaction

Isolated amplicons of genes of interest were transferred into entry vectors using Gateway® BP Clonase™ II Enzyme Mix. The reaction was performed for 1-12 h at room temperature and the reaction mix was set up as following:

<b>Reagent</b>	<b>Volume</b>
PCR product (ca. 15-150 ng)	2 µl
Entry vector (pDONR221 or pDONR223; 150 ng/µl)	1 µl
BP Clonase™ II Enzyme Mix	0,5 µl
TE buffer (10 mM Tris-HCl, 1 mM EDTA, pH 8.0)	2,5 µl

### 2.2.5 Transformation of *Escherichia coli*

Chemically competent *E. coli* cells were thawed on ice for 20 min. For transformation of BP or LR reaction, 5 µl of reaction mix was added to 25 µl of competent cells, mixed gently by flicking and incubated for 10 min on ice. For retransformation of plasmid DNA into *E. coli*, 1 µl DNA was added to 25 µl of competent cells. The cells were heat-shocked for 45 s at 42°C and afterwards cooled on ice for 2 min. Recovery of heat-shocked cells was performed by addition of 250 µl LB medium and incubation for 1 h at 37°C and 450 rpm. Then, cells were plated on LB plates containing the respective antibiotics and grown overnight at 37°C.

### 2.2.6 Colony-PCR

Single colonies were tested for correct insertion of plasmids by Colony-PCR. Therefore, bacteria were picked with a tooth pick and dispersed in 25 µl of ddH<sub>2</sub>O. From this bacteria solution 2 µl were used as DNA template in PCR reaction mix. The primers were chosen to make sure that the correct plasmid was inserted in the correct orientation. Therefore, one primer

was binding in the vector sequence, while the other primer was binding in the gene of interest. The reaction was set up as following:

<b>Reagent</b>	<b>Volume</b>
10x DreamTaq DNA Polymerase Buffer	2 $\mu$ l
10 mM dNTPs	0,4 $\mu$ l
10 $\mu$ M Forward primer	0,4 $\mu$ l
10 $\mu$ M Reverse Primer	0,4 $\mu$ l
Bacteria solution as DNA template	2 $\mu$ l
DreamTaq DNA-Polymerase	0,1 $\mu$ l
ddH <sub>2</sub> O	ad 20 $\mu$ l

The following PCR program was used for amplification (Cycling between denaturation and elongation step 35x):

<b>Step</b>	<b>Temperature</b>	<b>Time</b>
Initial denaturation	95°C	8 min
Denaturation	95°C	30 s
Annealing	x°C (dependent on primer melting T)	30 s
Elongation	72°C	x min (1 min per kb)
Final Elongation	72°C	8 min
Hold	10°C	$\infty$

PCR products were analyzed for correct size via agarose gel electrophoresis.

### 2.2.7 Isolation of plasmid DNA from *E. coli* and sequencing

Positive colonies were grown overnight in 5 ml LB medium with the respective antibiotics. Plasmid DNA was isolated from bacteria with NucleoSpin Plasmid EasyPure Mini Kit (MACHEREY-NAGEL GmbH & Co. KG, Düren, Germany). 40  $\mu$ l of ddH<sub>2</sub>O were used for elution. Plasmid-DNA concentration and DNA quality was controlled at NanoDrop2000 Spectrophotometer (Thermo Fisher Scientific, Schwerte, Germany). Plasmids were sent for sequencing with Eurofins Genomics GmbH (Ebersberg, Germany) or GeneWiz Germany GmbH (Leipzig, Germany). Primers are listed in 2.7.

### 2.2.8 Site-directed mutagenesis

For generation of PP7L (active) and eEF1B $\beta$ 1.2 constructs, site-directed mutagenesis was performed. The entry clones containing the cDNA of PP7L or cDNA of eEF1B $\beta$ 1.1 were used

as templates for PCR amplification. Overlapping complementing primers containing the desired nucleotide exchange were used in a PCR reaction. Primers are listed in 2.7. PCR was set up as described in 2.2.1.

The following PCR program was used for amplification (Cycling between denaturation and elongation step 18x):

<b>Step</b>	<b>Temperature</b>	<b>Time</b>
Initial denaturation	95°C	2 min
Denaturation	95°C	30 s
Annealing	60°C (for eEF1B $\beta$ 1)	10 s
Elongation	68°C	6 min (for eEF1B $\beta$ 1)
Final Elongation	68°C	6 min
Hold	10°C	$\infty$

PCR fragments were isolated as described in 2.2.3. The cleaned PCR products were incubated for 1 h with 1  $\mu$ l of DpnI at 37°C. DpnI is a restriction enzyme that specifically cuts methylated DNA, therefore only the plasmid DNA that was used as template is being cut by DpnI. Consequently, only the newly synthesized mutated DNA will be successfully transformed into *E. coli* afterwards.

### 2.2.9 Gateway cloning - LR reaction

To generate expression constructs, genes of interest were shuttled from entry vectors into destination vectors with help of Gateway<sup>®</sup> LR Clonase<sup>™</sup> II. All destination vectors used for this study are listed below.

<b>Vector</b>	<b>Promotor</b>	<b>Tag</b>	<b>Resistance</b>	<b>Reference</b>
pEarleyGate 104	<i>CaMV 35S</i>	N-terminal YFP	Kanamycin	(Earley et al. 2006)
pEarleyGate 203	<i>CaMV 35S</i>	N-terminal MYC	Kanamycin	(Earley et al. 2006)
pGBT9	<i>pADH</i>	N-terminal BD	Ampicillin	Clontech
pGAD424	<i>pADH</i>	N-terminal AD	Ampicillin	Clontech
pGADCF	<i>pADH</i>	C-terminal AD	Ampicillin	Clontech
pGADCg	<i>pADH</i>	C-terminal AD	Ampicillin	(Stellberger et al. 2010)

pAB117	<i>CaMV 35S</i>	C-terminal GFP	Spectinomycin	(Bleckmann et al. 2010)
pAB118	<i>CaMV 35S</i>	C-terminal mCherry	Spectinomycin	(Bleckmann et al. 2010)
pMDC107	<i>Native promotor</i>	C-terminal GFP	Kanamycin	(Curtis and Grossniklaus 2003)

The Gateway® LR Clonase™ II reaction was performed for 1-12 h at room temperature and the reaction mix was set up as following:

Reagent	Volume
Entry clone (150 ng/μl)	1 μl
Destination (150 ng/μl)	1 μl
LR Clonase™ II Enzyme Mix	0,5 μl
TE buffer (10 mM Tris-HCl, 1 mM EDTA, pH 8.0)	2,5 μl

After LR reaction, the reaction mix was transformed into *E. coli*, tested by Colony-PCR and send for sequencing (see above).

### 2.2.10 Transformation of competent *Agrobacterium tumefaciens*

Electro-competent *A. tumefaciens* cells were thawed on ice for 20 min. For transformation of plasmid DNA, 100 ng DNA was gently mixed with 80 μl of competent cells. The cells were transferred into an ice-cold electroporation cuvette and electroporation was performed for 5 ms at 1440 V. Then, 400 μl of LB medium was added and cells were transferred into an 1,5 ml tube. Recovery of electroporated cells was performed by incubation for 2 h at 28°C and 450 rpm. Afterwards, cells were plated on LB plates containing the respective antibiotics and grown for two days at 28°C.

## 2.3 Plant work

### 2.3.1 *Arabidopsis thaliana* growth conditions

All experiments in this study were performed with *Arabidopsis thaliana* from the ecotype *Columbia-0*. This applies also for each T-DNA insertional line analyzed and each transgenic line produced in this study. All T-DNA insertional lines were obtained from the Nottingham Arabidopsis Stock Centre (NASC; (Alonso et al. 2003)).

<b>Line</b>	<b>Gene identifier</b>	<b>NASC identifier</b>	<b>Publications</b>
<i>pp7l-1</i>	AT5G10900	SALK_018295	(Xu et al. 2019)
<i>pp7l-3</i>	AT5G10900	SALK_022053	(Xu et al. 2019)
<i>eef1bβ1-1</i>	AT1G30230	SALK_046102C	(Hossain et al. 2012)
<i>eef1bβ1-2</i>	AT1G30230	SALK_102754	-
<i>eef1bβ1-3</i>	AT1G30230	SALK_026418	-
<i>eef1bβ2-1</i>	AT2G18110	SALK_107994	-
<i>eef1bβ2-2</i>	AT2G18110	SAIL_241G10	-
<i>eef1bγ1-1</i>	AT1G09640	SAIL_450_F07	-
<i>eef1bγ1-2</i>	AT1G09640	GABI_920E04	-
<i>eef1bγ2-1</i>	AT1G57720	GABI_041E07	-
<i>eef1bγ2-2</i>	AT1G57720	GABI_473B05	-
<i>hsp101</i> ( <i>hot1-3</i> )	AT1G74310		(Hong and Vierling 2001; McLoughlin et al. 2019)
<i>eif5b (hot3-2)</i>	AT1G76810		(Zhang, Liu, et al. 2017)
<i>phb3-3</i>	AT5G40770	SALK_020707	(Van Aken et al. 2007)

Plants were either grown on soil or on Murashige and Skoog (MS) growth medium. For soil grown plants, seeds were stratified in H<sub>2</sub>O for two days at 4°C in the dark, before sowing on a wet soil mixture (60% soil, 30% sand and 10% expanded clay). For MS grown plants, seeds were first sterilized using fumigation with chlorine gas (mix of 50 ml NaOCl (Chemsolute<sup>®</sup>, Th. Geyer GmbH & Co. KG, Renningen, Germany) with 2.3 ml of 32% HCl) for 3 h. Seeds were sown on MS (Duchefa Biochemie, Harleem, Netherlands) plates or transferred in liquid MS cultures containing 1 % sucrose. Plates or flasks were kept at 4°C in the dark for two days for stratification, before the plates were placed in climate chambers (CLF Plant climatics) for growth. Flasks were placed on a shaker (70 rpm) within a climate chamber. Standard growth conditions were 16 h of light at 22°C and 8 h of darkness at 18°C.

### 2.3.1.2 Generation of double mutants by crossing

To generate double mutants, homozygous single mutant plants were grown on soil. Closed flower buds were opened carefully and emasculated. Stigmas were then pollinated with the

pollen of mature flowers from the corresponding other single mutant. Below are all crosses produced during this study listed.

<b>Line</b>	<b>Genes</b>
<i>eef1bβ1-3 eef1bβ2-1</i>	AT1G30230 and AT2G18110
<i>eef1bβ1-1 eef1bβ2-1</i>	AT1G30230 and AT2G18110
<i>eef1bγ1-1 eef1bγ2-1</i>	AT1G09640 and AT1G57720
<i>eef1bγ1-1 eef1bγ2-2</i>	AT1G09640 and AT1G57720
<i>eef1bγ1-2 eef1bγ2-1</i>	AT1G09640 and AT1G57720
<i>eef1bγ1-2 eef1bγ2-2 (named as eef1bγ1/2)</i>	AT1G09640 and AT1G57720

### 2.3.2 Plant phenotyping methods

#### 2.3.2.1 Primary root length measurement and lateral root counting

For primary root length and lateral root measurements, seedlings were germinated and grown on vertically placed MS plates. For documentation the plates were scanned with an Epson Perfection V700 Photo Scanner. Primary root length was measured using the freehand tool in ImageJ software (<https://imagej.nih.gov/ij/>) and lateral roots were counted individually for each seedling. For measurement of primary root length under translation inhibition, seeds were germinated and grown on MS plates supplemented with cycloheximide (CHX, 0.05 μM or 0.1 μM) or with hygromycin B (HYG; 10 mg/ml or 20 mg/ml).

#### 2.3.2.2 Propidium iodide staining of root tips to analyze the root apical meristem

Seedlings were grown on vertically placed MS plates for 7 d. Root tips were dissected using a binocular microscope and emerged in 10 μg/ml propidium iodide (PI) solution for at least 1 min. Fluorescence was observed at a confocal laser scanning microscope (Leica TCS SP8 Confocal Platform, Leica Microsystems) using an excitation wavelength of 561 nm and an emission wavelength of 610-650 nm. Numbers of dividing cells were defined by counting the number of cortical cells in the meristematic zone.

#### 2.3.2.3 FM4-64 staining in leaves

Seedlings were grown for 7 d on horizontally placed MS plates. First true leaves were dissected from the seedlings and stained for 30 min in FM4-64 solution. Leaves were washed twice before observation of the adaxial epidermal leaf cells at the confocal laser scanning microscope (Leica TCS SP8 Confocal Platform, Leica Microsystems) using an excitation wavelength of 514 nm and an emission wavelength of 586-666 nm. Cells were counted in four categories: pavement

cells, guard cell couples, meristemoid/mother cell couples or meristemoids (Larkin, Brown, and Schiefelbein 2003) using ImageJ Plugin Cell Counter.

#### 2.3.2.4 True leaf formation

Numbers of true leaves were counted on seedlings, which had germinated and grown on horizontally placed MS plates at the indicated timepoints.

#### 2.3.2.5 Size of biggest rosette leaf

The size of the biggest rosette leaf was determined on 28 d-old plants, which were germinated and grown on soil. The biggest leaf was determined by measuring the length from the leaf petiole to the tip of the leaf blade. The biggest rosette leaf was in each analyzed plant among the leaves number 9-12.

#### 2.3.2.6 Number of rosette leaves at flowering time point

Plants were germinated and grown on soil. From day 21 after germination, plants were observed every second day for the formation of bolts. Number of rosette leaves were counted for each plant, which started bolting and exhibited visible flower buds.

#### 2.3.2.7 Seed counting in siliques

For counting the number of seeds and empty spots in siliques, plants were germinated and grown on soil. Siliques from the main shoot were carefully opened using a razor blade and observed with an Olympus MVX10 Macroscope. A camera (Olympus DP73) was attached to the macroscope and used for documentation.

#### 2.3.2.8 Clearing of seeds for analysis of embryo development

For analysis of embryo development, plants were germinated and grown on soil. Different siliques were collected from plants and carefully opened using a razor blade. Seeds were transferred directly into Hoyer's solution (50 g chloral hydrate, 3.75 g gum arabic, 2.5 ml glycine, 15 ml ddH<sub>2</sub>O), which was placed on a microscope slide. Seeds were covered with a cover slip and incubated in Hoyer's solution overnight. The de-stained seeds were analyzed and documented using an Olympus MVX10 Macroscope with a coupled camera system (Olympus DP73).

#### 2.3.2.9 Seed germination rate

To test the seed germination rate, seeds were sown on MS plates. MS plates were kept for 3 days at 4°C in the dark for stratification of the seeds. Plates were vertically placed in the growth chamber and germination was observed every 12 h after the transfer to light. Seeds were defined as germinated, when the radical emerged through the seed coat.

### 2.3.3 Heat sensitivity assays

#### 2.3.3.1 Basal thermotolerance

Basal thermotolerance was assessed by analyzing the seed germination. Seeds were imbibed in 2 ml H<sub>2</sub>O and stratified for 3 d at 4°C in the dark. Imbibed seeds were either directly sown on MS plates for control conditions or incubated for 3,5 h at 45° in MaxQ 6000 thermo shaker (Thermo Fisher Scientific) and then sown on MS plates. MS plates were immediately moved into growth chambers into the light. Germination was observed every 24 h after transfer to light. Seeds were counted as germinated when the radicle emerged from seed coat.

#### 2.3.3.2 Short-term acquired thermotolerance

Acquired thermotolerance assays have been partially adapted from (Kim et al. 2017). The heat treatments were performed using a thermo incubator MaxQ 6000 thermo shaker (Thermo Fisher Scientific). The hypocotyl elongation was assayed on seedlings that were grown for 2,5 d on vertical MS plates in the dark, mildly pre-heat treated for 90 min at 38°C, recovered for 120 min at 22°C, severely heat stressed for 180 min at 45°C and again recovered for 2,5 d. Before the pre-heat treatment the position of the hypocotyl tip was marked on the plate. After recovery for 2,5 d the growth of the hypocotyl tip from the marked position to current position was measured. Seedlings were kept in the dark as much as possible to avoid phototropism. The root growth was assessed from seedlings that were grown for 4 d at 22°C and then heat-treated in the following way: 90 min at 38°C, 2 h at 22°C, 2 h at 45°C. The root length was measured 5 days after the heat treatment. Hypocotyl length and root length was measured using ImageJ software.

Seedling survival was measured after seedlings were grown for 7 days on horizontal MS plates, then treated for 90 min at 38°C, 120 min at 22°C, 150 min at 45°C and after 5 d at 22°C. Seedling survival was defined by plants developing green leaves.

#### 2.3.3.3 Long-term acquired thermotolerance

Protocol for long-term acquired thermotolerance (LAT) assay has been adapted from (Fernández-Bautista et al. 2018). The LAT of seedlings was approached by growing seedlings for 6d on MS plates, pre-heat-stress for 90 min at 38°C, recover for 2 d at 22°C before heat stress for 100 min at 45°C. The number of green leaves per plant was counted 7 days after the second heat stress.

#### 2.3.3.4 Ambient temperature resistance

To analyze ambient temperature response, seeds were sown on MS plates, stratified for three days and then transferred into the light in growth chambers in vertical position. Seeds were incubated at 22°C for 24 h to germinate and then either kept at 22°C for control conditions or moved to 27°C for ambient temperature increase. At 7 dag, MS plates were scanned and the hypocotyl length or root length was measured from scans using ImageJ software.

#### 2.3.3.5 Heat stress conditions to induce cytoplasmic condensates in root cells

Seeds were germinated and grown for 4 days on vertical placed MS plates. Seedlings were carefully transferred to a curved microscope slide and fixed with a small piece of MS medium on top. Microscope slides were placed directly on a heating plate at 42°C for 20 min. After heat incubation, root epidermal cells were immediately analyzed using a confocal laser scanning microscope. After imaging the seedlings were kept on the microscope slide with the MS agar piece at 22°C for 12 h. The same root cells were imaged after recovery time.

### 2.3.4 Assays testing for oxidative stress sensitivity

#### 2.3.4.1 Sensitivity assay on methylviologen

Sensitivity of seedlings towards oxidative stress was tested on MS plates supplemented with methylviologen (MV). For fresh weight measurements, seeds were germinated and grown for 21 d on horizontally placed MS plates containing 25 nM or 50 nM MV. For root length measurements, seeds were germinated and grown for the indicated times on vertical MS plates containing 100 nM MV. Primary root length was measured using ImageJ.

#### 2.3.4.2 DAB staining

DAB staining is a method used for in situ staining of hydrogen peroxide (H<sub>2</sub>O<sub>2</sub>). 3,3'-diaminobenzidine (DAB) is oxidized in presence of H<sub>2</sub>O<sub>2</sub> and forms brown precipitates, which is visible in de-stained plant tissue. For DAB staining, seedlings were grown for 8 d on vertical MS plates. DAB staining was performed according to (Daudi and O'Brien 2012). In brief, DAB solution was freshly prepared by solving 50 mg DAB in 45 ml ddH<sub>2</sub>O. pH was adjusted to 3 using 0.2 M HCl, then 25 µl Tween20 and 2.5 ml 200 mM Na<sub>2</sub>HPO<sub>4</sub> were added. Seedlings were placed in 1 ml of DAB solution; 5 min of vacuum infiltration was applied before incubation for 12-14 h at room temperature and 100 rpm in the dark. DAB solution was discarded and seedlings were boiled in 1 ml bleaching solution (ethanol:acetic acid:glycerol = 3:1:1) for 15 min. If necessary, de-staining was repeated with fresh bleaching solution. Photographs were taken directly after de-staining using a Canon EOS 600D Camera.

### 2.3.5 Genotyping

#### 2.3.5.1 Isolation of genomic DNA

Frozen plant material was grinded with a small pestle in a 1,5 ml tube. Powdered plant material was resuspended in 400 µl lysis buffer (200 mM Tris-HCl, 250 mM NaCl, 25 mM EDTA, 0,5% SDS (w/v), pH 7,5). After centrifugation for 5 min at 22°C and 14000 rpm, supernatant was transferred to a new tube. Supernatant was added to 300 µl ice-cold isopropanol, mixed well and incubated for at least 10 min at -20°C for DNA precipitation. DNA was pelleted by centrifugation for 5 min at 22°C and 14000 rpm. Supernatant was discarded and pellet was washed with 500 µl of 70 % ethanol (v/v). Pellet was dried by short incubation at 50°C and then resuspended in 50 µl of ddH<sub>2</sub>O.

#### 2.3.5.2 Genotyping PCR

The genotype of T-DNA insertion lines was tested by PCR. Two PCR reactions were set up. One PCR reaction tested for a wild type allele. Primers were designed to amplify a region of the genomic sequence of the gene of interest, in which the T-DNA insertion was expected. A second PCR reaction with a gene-specific primer and a primer binding in the T-DNA. Thereby, it is possible to determine, whether an analyzed gDNA sample contains only WT alleles, only the T-DNA alleles or both. All primers used for genotyping are listed in 2.7. The PCR reactions were set up as following:

<b>Reagent</b>	<b>Volume</b>
10x DreamTaq DNA Polymerase Buffer	2 µl
10 mM dNTPs	0,4 µl
10 µM Forward primer	0,4 µl
10 µM Reverse Primer	0,4 µl
gDNA	2 µl
DreamTaq DNA-Polymerase	0,1 µl
ddH <sub>2</sub> O	ad 20 µl

The PCR was performed using the following conditions:

<b>Step</b>	<b>Temperature</b>	<b>Time</b>
Initial denaturation	95°C	3 min
Denaturation	95°C	30 s
Annealing	x°C (dependent on primer melting T)	30 s

Elongation	72°C	x min (1 min per kb)
Final Elongation	72°C	8 min
Hold	10°C	∞

The PCR products were analyzed using agarose gel electrophoresis (see 2.2.2).

### 2.3.6 Gene expression analysis

#### 2.3.6.1 RNA isolation

Plant material was snap-frozen in liquid nitrogen and homogenized using the Tissue Lyser II (Qiagen, Hilden, Germany) for 30s at 25 Hz. RNA was isolated using the innuPrep Plant RNA Kit (Analytik Jena GmbH, Jena, Germany) following the manufacturer's specifications.

#### 2.3.6.2 cDNA synthesis

To perform semiquantitative Reverse Transcriptase-PCR (RT-PCR) or quantitative RealTime-PCR (qPCR), RNA was first transcribed to cDNA using the QuantiTect® Reverse Transcription kit (Qiagen, Hilden, Germany) following the manufacturer's specifications.

#### 2.3.6.3 RT-PCR and qPCR

For RT-PCR, cDNA was used as template in PCR reaction, which was set-up exactly as in 2.3.5.2. Primers used for RT-PCR are listed in 2.7. For qPCR, a PCR reaction was set up using QuantiFast SYBR Green PCR Master Mix (Qiagen, Hilden, Germany). The PCR reaction mix included the following:

Reagent	Volume
QuantiFast SYBR Green PCR Master Mix	5 µl
10 µM Forward primer	0,5 µl
10 µM Reverse Primer	0,5 µl
cDNA	4 µl

The PCR was run in a Rotor-Gene Q (Qiagen, Hilden, Germany) using the following programme:

Step	Temperature	Time
Initial denaturation	95°C	5 min
Denaturation	95°C	10 s
Combined annealing and elongation	60°C	30 s
Melting curve	65-95°C	x

Gene expression was normalized against two of the following housekeeping genes: Ubiquitin10 (AT4G05320), FASS (AT5G18580) or SAND (AT2G28390). For data analysis, the qBASE Plus software was used (Hellemans et al. 2007). All primers used in this study for qPCR are listed in 2.7.

#### 2.3.6.4 BioAnalyzer analysis

To analyze the characteristics of total RNA with an Agilent 2100 BioAnalyzer System (Agilent Technologies), the concentration of isolated RNA (2.3.6.1) was adjusted to 250 ng/μl and 1.1 μl RNA sample was loaded onto an RNA NanoChip according to the manufacturer's direction.

#### 2.3.7 Transient expression in Arabidopsis protoplasts

Transient transformation of Arabidopsis mesophyll protoplasts is a fast and powerful method to analyze gene expression pattern in living cells (Yoo, Cho, and Sheen 2007). For protoplast isolation, leaves from 4-6 weeks-old plants grown in short day-conditions (8 h light, 16 h darkness) were cut in small stripes and incubated in 20 ml digestion buffer (0,25 % macerozyme (w/v), 1 % cellulase (w/v), 500 mM sorbitol, 1 mM CaCl<sub>2</sub>, 10 mM MES, pH 5.6) for 2 h at 25°C and 50 rpm. Protoplasts were filtered through nylon mesh and centrifuged for 3 min at 100 g. Supernatant was discarded and protoplasts were washed with 20 ml MaMg buffer (450 mM sorbitol, 15 mM MgCl<sub>2</sub>, 5 mM MES, pH 5.6). Afterwards, protoplasts were taken up in appropriate amount of MaMg buffer depending on the number of transformations needed per experiment. For confocal laser scanning microscopy 150 μl of protoplasts in MaMg buffer were transformed per construct, for detection on western blot 300 μl of protoplasts and for co-immunoprecipitation experiments followed by western blot 1,5 ml of protoplasts were transformed.

Protoplasts were transformed by addition of 10 μg plasmid DNA per 150 μl of protoplasts and 1,1x volume of PEG-Ca buffer (40% PEG4000 (w/v), 0,2 M mannitol, 100 mM CaCl<sub>2</sub>), gentle mixing and incubation for 20-30 min at 22°C. 4,4x volumes of W5 buffer (154 mM NaCl, 125 mM CaCl<sub>2</sub>, 5 mM KCl, 5 mM glucose, 2 mM MES, pH 5.7) were added to wash out PEG. Protoplasts were centrifuged for 3 min at 100 g and supernatant was discarded. Protoplasts were washed twice again with 4,4x volumes of W5 buffer and finally stored for overnight incubation at 22°C in 3 ml W5 buffer in a small petri dish. If constructs with an estradiol inducible promotor should be expressed, 10 μM estradiol was added to protoplasts before overnight incubation.

To analyze heat-induced cytoplasmic condensates in protoplasts, the small petri dish with the transformed protoplasts (including the 3 ml W5 buffer) was transferred into a heat incubator at the indicated temperature for 60 min. Afterwards, protoplasts were carefully pipetted onto a microscope slide and immediately analyzed at the confocal laser scanning microscope. To reduce the possibility of condensate disassembly due to temperature reduction, protoplasts were only observed and imaged within the next 15 min after removal from the heat incubator.

### 2.3.8 Agrobacterium-mediated transient expression in *Nicotiana benthamiana* leaves

For transient expression of proteins of interest in *Nicotiana benthamiana*, 6 ml liquid cultures of *Agrobacterium tumefaciens* (strain: GV3101 or C58C1) transformed with the desired construct were grown in LB medium with appropriate antibiotics overnight at 28°C and 160 rpm. In addition, a liquid overnight culture of *Agrobacterium tumefaciens* carrying the gene-silencing suppressor p19 (Voinnet et al. 2003) was prepared. Grown overnight cultures were centrifuged for 10 min at 5000 rpm and 4°C. Supernatant was discarded and pellets were resuspended in 7,5 ml freshly prepared infiltration solution (10 mM MgCl<sub>2</sub>, 10 mM sodium phosphate buffer (pH 7.0), 200 µM acetosyringone). Agrobacteria was incubated for 2 h at 28°C and 60 rpm to regenerate. Afterwards, each Agrobacterium harboring a construct of interest was mixed 1:1 with Agrobacterium carrying p19 gene. The mixture was carefully infiltrated into tobacco leaves with a syringe (Wroblewski, Tomczak, and Michelmore 2005).

Two days after infiltration, expression of proteins of interest expressed under a constitutive promotor was checked at Olympus MVX10 Fluorescence Macroscope. Positive transformants were further analyzed using a confocal laser-scanning microscope Leica SP8. For expression of proteins with an estradiol inducible promotor, tobacco leaves were sprayed with estradiol (20 µM estradiol in 0,1 % Tween20) two days after infiltration. Protein expression was analyzed two days after spraying.

### 2.3.9 Stable transformation of *Arabidopsis thaliana* by floral painting

Creation of stably transformed *Arabidopsis* lines was performed via floral painting with *Agrobacterium tumefaciens* (strain: GV3101 or C58C1) carrying the desired construct. Therefore, the first bolts of flowers were cut from plants that should be transformed. Then, a pre-culture of agrobacteria in 5 ml LB medium with appropriate antibiotics were grown overnight at 28°C and 160 rpm. 2,5 ml of grown pre-culture was used to inoculate a fresh 50 ml culture, which was again grown overnight at 28°C and 160 rpm. Cells were pelleted by centrifugation for 10 min at 22°C and 4700 rpm. Pellets were resuspended in 50 ml sucrose-silwet-solution (5 % sucrose (w/v), 0,05 % silwet-77 (v/v)). The suspension was applied on floral

buds with a soft paint brush. Painted plants were covered with cling film for 24–48 h to increase humidity, which favors bacterial survival. Seeds of painted plants were selected depending on the introduced construct. Plants transformed with pEG104 vector were grown on soil and selected by three rounds of spraying BASTA (Bayer AG, Leverkusen, Germany). Plants transformed with pMDC107 or pABind vectors were selected on hygromycin B-containing MS plates (Carl Roth®, Karlsruhe, Germany). All transgenic lines generated during this study are listed below.

<b>Transgenic line</b>	<b>Plasmid</b>	<b>Resistance</b>	<b>Description</b>
		<b>in plants</b>	
<i>eef1bγ1/2::p35S-YFP-eEF1Bγ1</i>	pEG104	BASTA	Complementation line
<i>eef1bγ1/2::p35S-YFP-eEF1Bγ1ΔN</i>	pEG104	BASTA	Complementation line
<i>eef1bγ1/2::p35S-YFP-eEF1Bγ1ΔC</i>	pEG104	BASTA	Complementation line
<i>eef1bγ1/2::p35S-YFP-eEF1Bγ2ΔN</i>	pEG104	BASTA	Complementation line
<i>eef1bγ1/2::p35S-YFP-eEF1Bγ2ΔC</i>	pEG104	BASTA	Complementation line
<i>eef1bβ1-3::p35S-YFP-eEF1Bβ1</i>	pEG104	BASTA	Transgenic line
<i>WT::p35S-YFP-eEF1Bγ1</i>	pEG104	BASTA	Overexpression line

### 2.3.10 Suppressor-Screen

Ethylmethanesulfonate (EMS) is a powerful mutagen used to introduce mutations in DNA (Sega 1984). For mutagenesis, 1 g of *pp7l-1* seeds were incubated in 50 ml of 0,3 % (v/v) aqueous solution of EMS for 13 h. Seeds were washed four times with 60 ml ddH<sub>2</sub>O. Again, seeds were washed intensively by pouring 250 ml water on them and afterwards decanting it (10–15 times). EMS-mutagenized seeds were then transferred in 0,1 % (w/v) aqueous phytoagar solution and single seeds were sown in soil-filled 96-pot trays. In total, 5000 seeds were sown. M1 generation was grown and self-fertilized. Seeds of each M1 plants were individually harvested. M2 plants were screened for mutants suppressing the short-root phenotype of *pp7l* mutants. Therefore, 30 seeds from each M2 line were sown on MS plates and root length was monitored in comparison to WT and *pp7l-1* mutant. M2 plants with longer roots than those of *pp7l-1* mutant were transferred to soil, genotyped for *pp7l* mutation, self-fertilized and seeds (M3) were individually harvested. Roots of M3 plants were again analyzed for long root phenotype to check, if the phenotype seen in M2 was heritable. Homozygous *pp7l-1* mutations in M3 plants were again checked by genotyping. Additionally, root meristems of M3 plants

were stained with propidium iodide (PI) and monitored by confocal laser-scanning microscopy to test if suppressors still accumulated dead cells in the meristematic zone. Interesting M3 suppressor candidates were backcrossed twice to original not-EMS-mutagenized parent *pp7l*. Phenotype of F1 generation was analyzed to find out whether the suppressing mutation is recessive or dominant.

## 2.4 Protein Analysis

### 2.4.1 Protein extraction from plants

For protein extraction from plant tissue, the plant tissue was collected and snap-frozen in liquid nitrogen. Frozen plant tissue was grinded with mortar and pestle. The plant tissue was transferred into a cooled and weighed 2 ml tube. The frozen plant tissue in the tube was weighed and per 0.1 g of plant tissue, 200 µl of ice-cold lysis buffer was added. Co-IP lysis buffer was used for extraction of cytosolic proteins. RIPA buffer was used for nuclear or membrane proteins. Directly before use protease inhibitor cocktail was added 1:1000 to the corresponding lysis buffer (cOmplete, EDTA free from Roche Diagnostics GmbH, Mannheim, Germany). Plant tissue was carefully resuspended in the lysis buffer by vortexing (air bubble formation was tried to be avoided). Samples were incubated on ice for 30 min. During incubation time, the samples were at least three times vortexed. Samples were centrifuged for 20 min at 10000 rpm and 4°C. The supernatant was transferred into a new tube and kept on ice until use or stored at -20°C.

#### Co-IP lysis buffer

Tris-HCl (pH 7-8)	10 mM
NaCl	150 mM
EDTA	0,5 mM
Triton X-100	0.1 %

#### RIPA lysis buffer

Tris-HCl (pH 7-8)	50 mM
NaCl	150 mM
Sodium deoxycholate	0.5 %
Triton X-100	1 %
SDS	0.1 %

#### 2.4.2 Protein extraction from protoplasts

For detection of proteins from protoplasts by western blot, protoplasts were transformed with the protocol described in 2.3.7 with the following adaptations. Instead of 150  $\mu$ l protoplast suspension, 300  $\mu$ l of protoplasts were transformed with 20  $\mu$ g plasmid DNA and 330  $\mu$ l of PEG solution. After overnight incubation of the protoplasts for protein expression. The protoplasts were transferred into 1.5 ml tubes and centrifuged for 5s at 14000 rpm. The supernatant was immediately removed and discarded. The pellet was resuspended in 20  $\mu$ l of 2x SDS loading dye by careful pipetting to avoid air bubble formation. The samples were boiled for 5 min at 95°C and were then loaded directly on a SDS gel or frozen at -20°C for storage.

#### 2.4.3 Protein concentration measurement

Protein concentrations in protein extracts were measured with the Pierce™ 660 nm Protein Assay (ThermoScientific, Rockford, IL, USA). The assay was performed according to the manufacturers protocol with some adaptations. In brief, 50  $\mu$ l of protein extract were mixed with 750  $\mu$ l of Protein Assay Reagent. The tubes were incubated for 5 min at room temperature and in the dark. The absorbance of the samples was measured at 660 nm using the NanoDrop2000 Spectrophotometer (Thermo Fisher Scientific, Schwerte, Germany). The protein concentrations of the unknown samples were determined using a standard curve of samples with a known BSA concentration.

#### 2.4.4 Sodium dodecyl-sulfate polyacrylamide gel electrophoresis for protein separation

The sodium dodecyl-sulfate polyacrylamide gel electrophoresis (SDS-PAGE) was performed with discontinuous gels with a pH shift between separating and stacking gel (Laemmli 1970). Separating gels were prepared with 10 or 12% of polyacrylamide according to the molecular weight of proteins of interest. Stacking gels were prepared with 5% polyacrylamide.

Protein samples were mixed with 1x loading dye (25 % Tris (w/v), 20 % glycerol (w/v), 4 % SDS (w/v), 2 % dithiothreitol (DTT; w/v), 0,05 % bromophenol blue (w/v)) and denatured at 95°C for 5 min before loading on the gel. Gel electrophoresis was performed in 1x Laemmli running buffer (3 g/L Tris, 14,4 g/L glycine, 1 g/L SDS) and at 120V. As standard, 4  $\mu$ l of PageRuler™ Prestained Protein Ladder (Thermo Scientific, Schwerte, Germany) was used.

#### 2.4.5 Western Blot

Proteins separated by SDS-PAGE can be transferred from the gel to membranes with protein-binding capacity (Towbin, Staehelin, and Gordon 1979). This can be useful for several downstream applications including immunodetection of specific proteins. In this study, proteins

were transferred with the SemiDry blotting system “Fastblot B43” (Biometra GmbH, Göttingen, Germany) using 1x Blotting buffer (24 mM Tris, 192 mM glycine, 0,04 % SDS (w/v), 20 % ethanol (v/v)) onto nitrocellulose membrane (Roti®-NC 0,2 µm, Carl Roth GmbH&Co.KG, Karlsruhe, Germany) or PVDF membrane (PVDF 0,45 µm transfer membrane, SERVA Electrophoresis GmbH, Heidelberg, Germany). Transfer was performed at 1 mA per 1 cm<sup>2</sup> of membrane for 60 min.

To reduce unspecific binding of antibodies to the membrane, the free protein binding capacities have to be blocked. The membrane was blocked with a 5 % (w/v) milk powder solution in TBST buffer (10 mM Tris-HCl, 150 mM NaCl, 0,5 % Tween 20 (v/v), pH 7.5) for at least 60 min. Next, the membrane was incubated with the primary antibody, which was diluted to the required concentration in a 5 % milk powder solution in TBST buffer for at least 60 min. Unbound primary antibody was washed off by four washing steps, each with TBST buffer for 10 min. If necessary, the secondary antibody was applied to the membrane diluted in a 5 % milk powder solution in TBST buffer and incubated for at least 45 min. Again, unbound antibodies were washed off by four washing steps with TBST buffer for 5 min each. All antibodies used in this study are listed below. To detect the desired bands on the membrane the membrane was incubated with Pierce™ ECL Western Blotting Substrate or SuperSignal™ West Atto Ultimate Sensitivity Chemiluminescent Substrate (Thermo Scientific, Germany). Signal detection was performed using the ChemiDoc™ Imaging System (Bio-Rad Laboratories GmbH, Feldkirchen, Germany).

Quantification of western blot band intensities was analyzed using ImageJ software and normalized to ACTIN as shown in (Stael et al. 2022).

#### Primary antibodies

<b>Antibody</b>	<b>Order number</b>	<b>Company</b>	<b>Dilution</b>
Anti-MYC-HRP	R951-25	Thermo Fisher Scientific	1:1000
Anti-GFP	G1544	Sigma-Aldrich	1:2500
Anti-RFP	5F8	ChromoTek	1:5000
Anti-eEF1B $\alpha$	AS10678	Agrisera	1:2000
Anti-eEF1B $\beta$	AS10677	Agrisera	1:3000
Anti-eEF1B $\gamma$	AS10676	Agrisera	1:3000
Anti-ACTIN	A0480	Sigma-Aldrich	1:1000

Anti-HSP70	AS08371	Agrisera	1:2000
Anti-HSP90	AS08346	Agrisera	1:3000

### Secondary antibodies

<b>Antibody</b>	<b>Order number</b>	<b>Company</b>	<b>Dilution</b>
Anti-rabbit-HRP	4750.1	Carl Roth	1:5000
Anti-mouse-HRP	A4416	Sigma-Aldrich	1:5000
Anti-rat-HRP	ab97057	Abcam	1:10000

## 2.4.6 Total protein staining on nitrocellulose membranes

### 2.4.6.1 Ponceau staining

For control of correct protein transfer after semi-dry blotting, total protein staining was performed using Ponceau S solution. Ponceau staining can also be used for total protein normalization on western blot membranes (Sander et al. 2019). The membrane was removed from the transfer sandwich and washed once in ddH<sub>2</sub>O. Then Ponceau S solution (0,1 % Ponceau S (w/v), 5 % acetic acid (glacial, v/v)) was added and the membrane was gently rotated at room temperature until the big subunit of Rubisco (ca. 55 kDa) was nicely detected. Membrane was washed 3x with ddH<sub>2</sub>O until background staining was removed. The stained membrane was photographed before Ponceau staining was completely removed by washing in 1x TBST. Afterwards, the membrane could be further used for immunodetection.

### 2.4.6.2 Amido black staining

For several experiments, amido black staining was used for checking loading equality on the membranes (Gultekin and Heermann 1988). First, the membrane was washed once in ddH<sub>2</sub>O after immunodetection. Then, it was gently rotated in amido black stain (0,1 % amido black (w/v), 25 % isopropanol (v/v), 10 % acetic acid (v/v)) until the big subunit of Rubisco protein (ca. 55 kDa) was clearly visible. The membrane was washed repeatedly with ddH<sub>2</sub>O until background staining was reduced. The stained membrane was immediately photographed.

## 2.4.7 Stripping of nitrocellulose membranes

To detect several proteins with different tags on the same membrane, the membrane was stripped. Thereby, antibodies bound to the membrane could be removed, while proteins transferred onto the membrane were kept. The membrane was incubated in stripping buffer (0,2 M glycine, 0,1 % SDS (w/v), pH 2.0) for 30 min, washed three times with ddH<sub>2</sub>O and one time

with TBST buffer for 5 min each. In the end, the membrane was newly blocked and subsequently incubated with new antibody.

#### 2.4.8 SUnSET

SURface SENSing of Translation (SUnSET) is a method to measure the protein synthesis in eukaryotic cells. The method has been adapted for Arabidopsis tissues in 2016 (Van Hoewyk 2016). For this method, puromycin is added to the plants. Puromycin is an analogue of the tyrosyl-tRNA, therefore it is being transported to the growing polypeptide chain during active translation and can be incorporated in the nascent polypeptide. Upon the incorporation of puromycin, the translation is terminated. Consequently, during active translation many polypeptide chains of different length will be labeled with puromycin. The amount of protein synthesis can be measured by quantifying the amount of puromycin-labeled proteins using a puromycin-antibody for western blot. The principle of the SUnSET method is shown in Fig. 7.

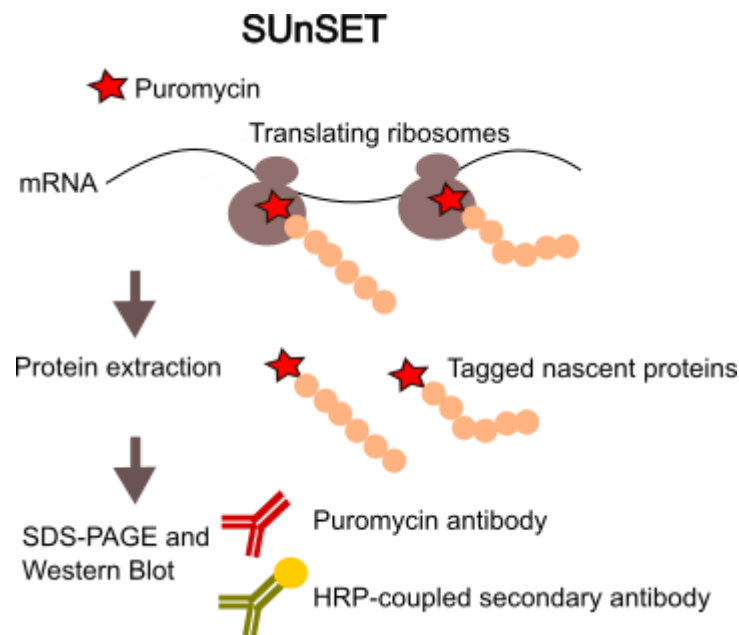


**Figure 7: Principle of SUnSET method.** Nascent polypeptides are labeled with the tyrosyl-tRNA analogue puromycin, which terminates translation upon incorporation. The level of puromycin-labeled proteins resembles the amount of protein synthesis. Puromycin-labeled proteins are detected by western blot with a puromycin-specific antibody. The figure has been adapted from (Iwasaki and Ingolia 2017).

For SUnSET method, seeds were germinated and grown for 7 d in 100 ml liquid MS medium at 100 rpm in an Erlenmeyer flask. If not stated otherwise, for control samples (active translation), 100  $\mu$ M of puromycin were added directly into the MS medium and seedlings were incubated at 150 rpm for 2 h. Afterwards, seedlings were washed 3x with ddH<sub>2</sub>O, shortly dried between two filter papers and then snap-frozen in liquid nitrogen.

For inhibition of translation by translation elongation inhibitor cycloheximide (CHX), the appropriate amount of CHX was added to the seedlings in the Erlenmeyer flask and seedlings were incubated for 4 h. Afterwards, puromycin was added to the seedlings and handling was performed as described before.

For heat treatment, the seedlings were transferred inside the Erlenmeyer flask to a water bath and incubated at the indicated temperature and time. The puromycin labeling was performed afterwards as described above.

Protein extraction was performed with Co-IP lysis buffer as described in 2.4.1 and protein concentration was measured as described in 2.4.3. 20 µg protein was loaded per sample on a 10% SDS gel and western blot was performed as described previously (2.4.4 to 2.4.7). The membrane was first probed with anti-PUROMYCIN/ anti-MOUSE for detection of puromycin-labeled proteins. Afterwards, the membrane was stripped and incubated with anti-ACTIN/anti-MOUSE as loading control or Ponceau S staining was used for loading control.

#### 2.4.9 Polysome Profiling

Polysome analysis examines the association of mRNAs with ribosomes and is a measure for translation efficiency. WT and *eef1bγ1/2* plants were grown for 24 d on soil, leaves were harvested and snap-frozen in liquid nitrogen and sent on dry ice to our collaboration partners, Yang Gao and Reimo Zoschke (at MPI Potsdam). Polysomes were analyzed by them according to a previously published protocol with several adaptations (Barkan 1998). 400 mg frozen plant material per sample was grinded to prepare 4 ml of lysate with polysome extraction buffer (0.2 M Tris-HCl (pH 9), 0.2 M KCl, 35 mM MgCl<sub>2</sub>, 25 mM EGTA, 0.2 M sucrose, 1% Triton X-100, 2% polyoxy-ethylene-10-tridecyl ether, 0.5mg/ml heparin, 100 mM 2-mercaptoethanol, 100 µg/ml chloramphenicol, 25 µg/ml cycloheximide). The lysate was loaded onto a 1 ml sucrose cushion (30% (w/v) sucrose, 100 mM KCl, 40 mM Tris-acetate (pH 8.0), 15 mM MgCl<sub>2</sub>, 5 mM 2-mercaptoethanol, 100 µg/ml chloramphenicol, 100 µg/ml cycloheximide). Large ribonucleotides, monosomes and polysomes were pelleted by centrifugation for 90 min at 303800 g and 4°C. The mRNAs contained in the pellet were size-separated according to their ribosome loading by ultracentrifugation for 4 h at 4 °C and 169000 g in sucrose density gradients as described in (Barkan 1998). A continuous UV absorbance profile at 254 nm was assembled for the sucrose gradient by using a density gradient fractionation system (Teledyne ISCO). Briefly, the bottom of the ultracentrifuge tube containing the sucrose gradient was pierced to allow the subsequent introduction of a dense chase buffer [65% (w/v) sucrose], which raised the gradient through the UV detector and into the collection tubes by a peristaltic pump.

#### 2.4.10 Co-Immunoprecipitation for MS analysis

For the PP7L-GFP pulldown (Table 2), transgenic seedlings expressing PP7L-GFP or GFP were grown for 6 days on MS medium and 3 g of plant material was harvested. The protein extraction, co-immunoprecipitation and MS analysis was performed by Geert Persiau and Dominique Eeckhout at VIB-UGent Center for Plant Systems Biology. A Q-Exactive Orbitrap was used for MS analysis and MAXQUANT and PERSEUS software were used for quantitative analysis. Protocols were used as described previously (Wendrich et al. 2017).

For the YFP-eEF1B $\beta$  and YFP-eEF1B $\gamma$  pull down (Chapter 4.5), transgenic seedlings were grown in 100 ml liquid MS medium for 7 days in an Erlenmeyer flask. Seedlings used for control were dried quickly between filter paper and frozen in liquid nitrogen. Heat treatment was performed by incubating the seedlings in the Erlenmeyer flask for 30 min at 42°C in a water bath. Afterwards, seedlings were also dried between filter paper and snap-frozen in liquid nitrogen. For each sample, three replicates with each 3 g of plant material was sent to VIB-UGent Center for Plant Systems Biology. The protein extraction using standard extraction buffer (25 mM Tris/HCl pH 7.6, 15 mM MgCl<sub>2</sub>, 150 mM NaCl, 15 mM pNO<sub>2</sub>-phenyl-PO<sub>4</sub>, 60 mM  $\beta$ -glycerophosphate, 0.1% NP-40, 0.1 mM Na<sub>3</sub>VO<sub>4</sub>, 1 mM NaF, 1 mM PMSF, 1  $\mu$ M E64, cOmplete™ ULTRA Tablet, Mini, EDTA-free (1 mini tablet/10 mL), 5% ethyleenglycol, Benzonase® Nuclease, Purity > 99% (MilliporeSigma, Novagen, 70664-3, 10 ku), 1/1000), co-immunoprecipitation and MS analysis was again performed by Geert Persiau and Dominique Eeckhout. A Q-Exactive Orbitrap was used for MS analysis and MAXQUANT and PERSEUS software were used for quantitative analysis. Protocols were used as described previously (Wendrich et al. 2017).

#### 2.4.11 Co-Immunoprecipitation for western blot analysis

Co-immunoprecipitation with following western blot analysis was performed from protein extracts obtained from transiently transformed protoplasts. The protoplasts were transformed as described in 2.3.7 with the following adaptations. For each combination of proteins of interest, 1.5 ml protoplast suspension was transformed with 50  $\mu$ g plasmid DNA of each construct. It was mixed with 1.65 ml PEG-Ca-buffer. Each washing step was performed with 5 ml W5 buffer. For overnight incubation, protoplasts were incubated in 3 ml W5 buffer.

Transformed protoplasts were transferred into two 1.5 ml tubes. Cut pipette tips were used for pipetting of the protoplasts. The protoplasts were pelleted by centrifugation for 10 s at 14.000 rpm. The supernatant was immediately discarded. Each pellet was resuspended in 500  $\mu$ l Co-IP lysis buffer (see 2.4.1) and the extract of the same constructs were reunited in one tube. The

samples were vortexed thoroughly, kept on ice for 15 min and vortexed several times during this incubation. Samples were centrifuged for 10 min at 14.000rpm and 4°C. The supernatant was transferred into a new tube. 50 µl of the supernatant was kept as “input” sample. The remaining supernatant was diluted 1:1 with Co-IP wash buffer. The diluted supernatant was added to 15 µl GFP-Trap® Magnetic Agarose (ChromoTek GmbH, Planegg-Martinsried, Germany), which were previously washed and equilibrated according to ChromoTek user manual. Beads and supernatant were incubated on a rotating wheel for 1-2 h at 4°C. Supernatant was discarded and beads were washed three times with 500 µl Co-IP wash buffer. For elution, 50 µl 2x SDS loading dye was added to the beads and beads were boiled for 10 min at 95°C. Supernatant was transferred to a fresh tube and used as “IP” sample.

#### Co-IP wash buffer

Tris-HCl (pH 7-8)	10 mM
NaCl	150 mM
EDTA	0,5 mM

#### 2.4.12 Yeast-Two-Hybrid

##### Preparation of competent cells of *Saccharomyces cerevisiae*

The yeast-two-hybrid assay performed in this study is based on the protocol from Takara Clontech (Clontech, [www.takarabio.com](http://www.takarabio.com)) and yeast transformation is based on previous publication (Gietz et al. 1997). First, a colony of yeast strain AH109 was inoculated in 3 ml YPDA medium for each transformation and grown overnight at 30°C and 200 rpm. The OD<sub>600</sub> of this pre-culture was measured and an appropriate amount of pre-culture was added to fresh YPDA medium to an OD<sub>600</sub> of 0.3. The culture was grown for 3 h at 30°C and 200 rpm. Afterwards the cells were centrifuged for 8 min at 22°C and 1000 g. The pellet was resuspended in 2 ml of 1xTE buffer (10 mM Tris-HCl, 1 mM EDTA, pH 7.5) per transformation. Centrifugation for 8 min at 22°C and 1000 g was repeated. The pellet was resuspended in 0.1 ml of TE/LiAc buffer (10 mM Tris-HCl, 1 mM EDTA, 100 mM Lithium acetate, pH 7.5) per transformation. The competent cells were prepared fresh each time directly before transformation.

##### Heat-Shock transformation of *Saccharomyces cerevisiae*

For each transformation, 100 µl of competent cells were vigorously mixed with 10 µl of carrier DNA (10 mg/mL), 0.1 µg of each plasmid DNA and 600 µl of PEG/LiAc solution (40% PEG 4000, 10 mM Tris-HCl, 1 mM EDTA, 100 mM Lithium acetate, pH 7.5). Carrier DNA had

been boiled for 15 min at 99°C and cooled on ice before use. The transformation mix was incubated for 30 min at 30°C and 400 rpm. Then 70 µl DMSO were added to the transformation mix, vortexed and heat shocked for 15 min at 42°C. After 2 min incubation on ice, the transformation mix was centrifuged for 5 s at 22°C and 14000 rpm. The pellet was resuspended in 100 µl of 1x TE buffer and plated on respective selection SD-medium (-Leu-Trp). The plates were incubated for 2-4 d at 28°C until colonies were visible. Colonies were tested by PCR for successful transformation before use for spotting in yeast two-hybrid assay.

### Spotting for yeast two-hybrid assay

Three positive colonies per combination were inoculated in 3 ml of SD medium (-Leu-Trp) and grown overnight at 30°C and 180 rpm. The OD<sub>600</sub> was measured and the appropriate amount of culture was centrifuged for 2 min at 22°C and 5000 rpm to get an OD<sub>600</sub> of 4 after resuspension of the pellet in 500 µl of 0,9% NaCl. A serial dilution of 10<sup>-1</sup>, 10<sup>-2</sup> and 10<sup>-3</sup> was prepared for each sample. 5 µl of sample, undiluted and dilution series, was dropped on selective SD medium. SD-Leu-Trp was used for growth control. SD-Leu-Trp-His was used to test for protein-protein interaction. Stringency of test for protein-protein interaction was enhanced by adding 3-aminotriazol to the SD-Leu-Trp-His medium. Yeast were grown for several days at 28°C. Growth monitored every day and pictures were taken when desired.

## 2.5 Microscopy

### 2.5.1 Confocal laser scanning microscopy

Leica TCS SP8 Confocal Platform (Leica Microsystems) was used for confocal laser scanning microscopy. The excitation wavelength and the wavelength, at which emission was detected for different fluorescent proteins or dyes are listed below.

<b>Fluorescent protein or dye</b>	<b>Excitation wavelength (nm)</b>	<b>Emission range (nm)</b>
GFP	488	498-514
YFP	514	522-540
mCherry/RFP	561	590-630
Propidium iodide	561	610-650
FM4-64	514	586-666
Autofluorescence of chlorophyll	-	712-724

Confocal images are either shown as single image or as 2D maximum intensity projection from z-stacks generated using Las X software (Leica Microsystems).

### 2.5.2 Quantification of cytoplasmic condensates from confocal images

Number of cytoplasmic condensates were quantified from confocal images of protoplasts using the ‘Analyze Particles’ function of ImageJ version 1.53n (<https://imagej.nih.gov/ij/index.html>). Before use of ‘Analyze Particles’ function, the colors of the image were split. The channel containing the color of interest was chosen and the threshold defined using ‘Intermodes’. To reduce background signal, images were ‘despeckled’ once. Using the ‘Analyze particles’ function only condensates with a size between 0.05 and 5  $\mu\text{m}$  were counted. Calculation of the Pearson and Spearman’s rank correlation coefficients to quantify the co-localization of proteins was performed using the ImageJ Plugin Coloc2. Coefficient values can vary from -1 (negative correlation) to +1 (positive correlation). The percentage of condensates showing both GFP and mCherry fluorescence compared to the total number of condensates inside a protoplast is shown as frequency of co-localization. GFP-fluorescent condensates, mCherry-fluorescent condensates, and condensates showing both fluorophores were counted using the ImageJ Plugin Cell Counter.

## 2.6 Bioinformatics

Sequence alignments were performed by inserting DNA or protein sequences from TAIR ([www.arabidopsis.org](http://www.arabidopsis.org)) into Clustal Omega (<https://www.ebi.ac.uk/Tools/msa/clustalo/>). RNA-Seq data used to analyze the gene expression levels were derived from Arabidopsis eFP Browser 2.0 and visualized using ePlant (Waese et al. 2017).

Proteomics data were searched for enriched biological processes or molecular functions using Gene Ontology (GO) enrichment analysis performed as described previously (Bonnot, Gillard, and Nagel 2019) using a combination of Panther ([www.pantherdb.org/](http://www.pantherdb.org/)), Revigo (Supek et al. 2011) and R version 4.2.2 ([www.r-project.org/](http://www.r-project.org/)). Analysis of subcellular localization was performed using SUBA4 (Hooper et al. 2017). Network of HS-dependent interactors of eEF1B $\gamma$  was assembled using STRING:protein query from public databases in Cytoscape version 3.8.2 ([www.cytoscape.org](http://www.cytoscape.org)). Proteins were clustered using MCODE version 2.0.2 (Bader and Hogue 2003). Proteins that were not found in clusters were excluded from Fig. 67. Annotation of functions to each cluster was assigned using STRING enrichment.

Identification of RNA binding proteins in proteomics datasets was performed using RNApred (Kumar, Gromiha, and Raghava 2011). Fasta identifiers and amino acid sequences retrieved from TAIR Sequence Bulk Download were used as input for the prediction approach “amino acid composition” and SVM score was set to 0.5.

Identification of prion-like domain containing proteins from proteomics data was performed using PLAAC (Lancaster et al. 2014). Settings for analysis were as following: Lcore=60, background frequencies were used from *Arabidopsis thaliana* with  $\alpha=1$ . Only proteins with a positive LLR score were chosen as prion-like domain containing protein.

Identification of proteins with ATPase activity were identified using Panther Protein Class ([www.pantherdb.org/](http://www.pantherdb.org/)).

## 2.7 Primers

Name	Sequence	Purpose
pp7l-1_fw	ATGCCGTCAACTTCAACAATC	Genotyping of SALK_018295
pp7l-1_rev	CATTCTTGAAGCTAAGTGCGG	Genotyping of SALK_018295
pp7l-3_fw	CCAATGTAGCTTTCGTCTTCG	Genotyping of SALK_022053
pp7l-3_rev	TTACAAGGGACTTCTTTGGGG	Genotyping of SALK_022053
eef1b $\beta$ 1-1_fw	CAGCCACAGAACCGAAATAAC	Genotyping of SALK_046102C
eef1b $\beta$ 1-1_rev	GTTGACCTTTTTCGGAGAGGAG	Genotyping of SALK_046102C
eef1b $\beta$ 1-2_fw	AACTGAGGAGATAATTGGGCC	Genotyping of SALK_102754
eef1b $\beta$ 1-2_rev	AGCCTCCTCAGTGATAGGAGC	Genotyping of SALK_102754
eef1b $\beta$ 1-3_fw	CTGATGCTGGATTGAAGAAGC	Genotyping of SALK_026418
eef1b $\beta$ 1-3_rev	GCAGGCCATAACAGAG	Genotyping of SALK_026418
eef1b $\beta$ 2-1_fw	GCCTTTACACCTGTAGTTTAC	Genotyping of SALK_107994
eef1b $\beta$ 2-1_rev	AAGTCATCTCCATTCCCATCC	Genotyping of SALK_107994
eef1b $\beta$ 2-2_fw	TCATAATGCAGGAGGATGGAG	Genotyping of SAIL_241G10
eef1b $\beta$ 2-2_rev	TTCAAACGTTTTGTTGGAACC	Genotyping of SAIL_241G10
eef1b $\gamma$ 1-1_fw	TCTTTCCCCTTGGATCTTCTC	Genotyping of SAIL_450_F07
eef1b $\gamma$ 1-1_rev	TAAACCCAAACGACAACAAGC	Genotyping of SAIL_450_F07
eef1b $\gamma$ 1-2_fw	CTTGTCGGACACTCTATTACCC	Genotyping of GABI_920E04
eef1b $\gamma$ 1-2_rev	GTTCTTTTATTAGAGTTGTGTG GCGT	Genotyping of GABI_920E04
eef1b $\gamma$ 2-1_fw	CTATTAAGCTCAATGCCTTGAA TG	Genotyping of GABI_041E07
eef1b $\gamma$ 2-1_rev	TCTGAATCATCAAGTTAGAGAC GTG	Genotyping of GABI_041E07
eef1b $\gamma$ 2-2_fw	CTCTCTAAACAATTCACAGCTG CTC	Genotyping of GABI_473B05

eef1by2-2_rev	CTTGAGTGATTTTAAGCCTCTC GG	Genotyping of GABI_473B05
GABIKAT_LB_o8474	ATAATAACGCTGCGGACATCT	Genotyping of GABIKAT lines
Lbb1.3	ATTTTGCCGATTTTCGGAAC	Genotyping of SALK lines
LB3sail	GCATCTGAATTTTCATAACCAAT CTCGATACAC	Genotyping of SAIL lines
hsp101_fw	CATGCCTCCTCGCTCTCTCGCA ATTCAC	Genotyping of <i>hsp101</i>
hsp101_rev	TTTGGCCAAGTCTCGTCAC	Genotyping of <i>hsp101</i>
hsp101_TDNA	CAGTCATAGCCGAATAGCCTCT CCACCC	Genotyping of <i>hsp101</i>
PP7L_fw	GGGGACAAGTTTGTACAAAAA AGCAGGCTTAATGCCGCCTCCA GAAATTTTCG	Cloning of PP7L with stop
PP7L_rev	GGGGACCACTTTGTACAAGAA AGCTGGGTCTTATACCCTTGTT TGAATCTC	Cloning of PP7L with stop
PP7L $\Delta$ N $\Delta$ C_fw	GGGGACAAGTTTGTACAAAAA AGCAGGCTTAGGTGACATTGTT TTGGAGCCAA	Cloning of PP7L $\Delta$ N $\Delta$ C with stop
PP7L $\Delta$ N $\Delta$ C_rev	GGGGACCACTTTGTACAAGAA AGCTGGGTCTTATACCCTTGTT ATGATTTGAT	Cloning of PP7L $\Delta$ N $\Delta$ C with stop
PP7L $\Delta$ N $\Delta$ C_rev w/o stop	GGGGACCACTTTGTACAAGAA AGCTGGGTCTTATACCCTTGTT ATTTGAT	Cloning of PP7L $\Delta$ N $\Delta$ C or PP7L $\Delta$ C without stop
PP7L $\Delta$ NLS_fw	GGGGACAAGTTTGTACAAAAA AGCAGGCTCCATGAACTATAA GCAACTGCGTACT	Cloning of PP7L $\Delta$ NLS with stop
PP7L_rev	GGGGACCACTTTGTACAAGAA AGCTGGGTCTTATACCCTTGTT TGAATCTC	Cloning of PP7L $\Delta$ NLS with stop
PP7L_fw	GGGGACAAGTTTGTACAAAAA AGCAGGCTTAATGCCGCCTCCA GAAATTTTCG	Cloning of PP7L Nterm with stop
PP7L Nterm_rev	GGGGACCACTTTGTACAAGAA AGCTGGGTCTTATGGTTCGTAT TTTCTACTACC	Cloning of PP7L Nterm with stop
PP7L $\Delta$ N_fw	GGGGACAAGTTTGTACAAAAA AGCAGGCTTCATGGGTGACATT GTTTTGGAGCCAA	Cloning of PP7L $\Delta$ N (reverse primer also for PP7L $\Delta$ NLS or PP7L without stop)
PP7L_rev w/o stop	CAAGAAAGCTGGGTTTACCCTT GTTTGAATCTCCTG	

eEF1B $\alpha$ 2_fw	GGGGACAAGTTTGTACAAAAA AGCAGGCTTAATGGCCGTTACC TTTTCAGA	Cloning of eEF1B $\alpha$ 2 with stop
eEF1B $\alpha$ 2_rev+stop	GGGGACCACTTTGTACAAGAA AGCTGGGTATAGCTAAATCTTG TTGAAAGCGA	Cloning of eEF1B $\alpha$ 2 with stop
eEF1B $\alpha$ 2_fw	GGGGACAAGTTTGTACAAAAA AGCAGGCTTAATGGCCGTTACC TTTTCAGA	Cloning of eEF1B $\alpha$ 2 without stop
eEF1B $\alpha$ 2_rev-stop	GGGGACCACTTTGTACAAGAA AGCTGGGTCAATCTTGTTGAAA GCGACAATGTC	Cloning of eEF1B $\alpha$ 2 without stop
eEF1B $\beta$ 1_fw	CACCATGGCAGCATTCCTAAC CT	Cloning of eEF1B $\beta$ 1 with stop
eEF1B $\beta$ 1_rev+stop	CTACAAAACTTGGGAAACT	Cloning of eEF1B $\beta$ 1 with stop
eEF1B $\beta$ 1.2_fw	GTTGCCTTCAACAAGATATGTA AGATGGAGAAAGCTTCAAG	Site-directed mutagenesis for cloning of eEF1B $\beta$ 1.2
eEF1B $\beta$ 1.2_rev	CTTGAAGCTTTCTCCATCTTAC ATATCTTGTTGAAGGCAAC	Site-directed mutagenesis for cloning of eEF1B $\beta$ 1.2
eEF1B $\beta$ 1_fw_pDONR 221	GGGGACAAGTTTGTACAAAAA AGCAGGCTTAATGGCAGCATTC CCTAACCTTA	Cloning of eEF1B $\beta$ 1 without stop
eEF1B $\beta$ 1_rev- stop_DONR221	GGGGACCACTTTGTACAAGAA AGCTGGGTATATCTTGTTGAAG GCAACAATGTC	Cloning of eEF1B $\beta$ 1 without stop
eEF1B $\gamma$ 1_fw	GGGGACAAGTTTGTACAAAAA AGCAGGCTTAATGGCTTTGGTC TTGCACAC	Cloning of eEF1B $\gamma$ 1 with stop
eEF1B $\gamma$ 1_rev+stop	GGGGACCACTTTGTACAAGAA AGCTGGGTATAGTCACTTGAAG CACTTGGCGT	Cloning of eEF1B $\gamma$ 1 with stop
eEF1B $\gamma$ 1_fw	GGGGACAAGTTTGTACAAAAA AGCAGGCTTAATGGCTTTGGTC TTGCACAC	Cloning of eEF1B $\gamma$ 1 without stop
eEF1B $\gamma$ 1_rev-stop	GGGGACCACTTTGTACAAGAA AGCTGGGTACTTGAAGCACTTG GCGTCCAAGAG	Cloning of eEF1B $\gamma$ 1 without stop
eEF1B $\gamma$ 1_fw	GGGGACAAGTTTGTACAAAAA AGCAGGCTTAATGGCTTTGGTC TTGCACAC	Cloning of eEF1B $\gamma$ 1 $\Delta$ C with stop
eEF1B $\gamma$ 1 $\Delta$ C_rev	GGGGACCACTTTGTACAAGAA AGCTGGGTCTCACTTAGGTGCC TCTGCTACTGG	Cloning of eEF1B $\gamma$ 1 $\Delta$ C with stop

eEF1B $\gamma$ 1 $\Delta$ N_fw	GGGGACAAGTTTGTACAAAAA AGCAGGCTCCCTTGCTGAAGAG GAAGAGGCA	Cloning of eEF1B $\gamma$ 1 $\Delta$ N with stop
eEF1B $\gamma$ 1_rev-stop	GGGGACCACTTTGTACAAGAA AGCTGGGTACTTGAAGCACTTG GCGTCCAAGAG	Cloning of eEF1B $\gamma$ 1 $\Delta$ N with stop
eEF1B $\gamma$ 2_fw	CACCATGGCGTTGGTCATGCAC ACATACA	Cloning of eEF1B $\gamma$ 2 with stop
eEF1B $\gamma$ 2_rev+stop	TCACTTAAAGCATTGCGT	Cloning of eEF1B $\gamma$ 2 with stop
eEF1B $\gamma$ 2 $\Delta$ C_fw	GGGGACAAGTTTGTACAAAAA AGCAGGCTCCATGGCGTTGGTC ATGCACACATAC	Cloning of eEF1B $\gamma$ 2 without stop
eEF1B $\gamma$ 2_rev-stop	GGGGACCACTTTGTACAAGAA AGCTGGGTACTTAAAGCATTG GCGTCCAAAAG	Cloning of eEF1B $\gamma$ 2 without stop
eEF1B $\gamma$ 2 $\Delta$ C_fw	GGGGACAAGTTTGTACAAAAA AGCAGGCTCCATGGCGTTGGTC ATGCACACATAC	Cloning of eEF1B $\gamma$ 2 $\Delta$ C with stop
eEF1B $\gamma$ 2 $\Delta$ C_rev	GGGGACCACTTTGTACAAGAA AGCTGGGTCTTAAAGGCTGTGGA GCTTCTTAGTAGG	Cloning of eEF1B $\gamma$ 2 $\Delta$ C with stop
eEF1B $\gamma$ 2 $\Delta$ N_fw	GGGGACAAGTTTGTACAAAAA AGCAGGCTCCGCTAAGCCCAA GGAGGAGCCC	Cloning of eEF1B $\gamma$ 2 $\Delta$ N with stop
eEF1B $\gamma$ 2 $\Delta$ N_rev	GGGGACCACTTTGTACAAGAA AGCTGGGTCTCACTTAAAGCAT TTGGCGTC	Cloning of eEF1B $\gamma$ 2 $\Delta$ N with stop
eef1b $\beta$ 1_RTfw	CACCATGGCAGCATTCCTAAC CT	RT-PCR of <i>eef1b<math>\beta</math>1-2</i> and <i>eef1b<math>\beta</math>1-3</i>
eef1b $\beta$ 1_RTrev	CTACAAAACCTGGGAAACT	RT-PCR of <i>eef1b<math>\beta</math>1-2</i> and <i>eef1b<math>\beta</math>1-3</i>
eef1b $\beta$ 2_RTfw	CATCACCTATCACAGAAG	RT-PCR of <i>eef1b<math>\beta</math>2-1</i>
eef1b $\beta$ 2_RTrev	GAGTTGGTAAAAGCCC	RT-PCR of <i>eef1b<math>\beta</math>2-1</i>
eEF1B $\beta$ 1-qPCR-4 fw	CAGCTCCTATCACTGAGG	qRT-PCR of WT
eEF1B $\beta$ 1-qPCR-4 rev	GACTTCACAGCTTCTCAAG	qRT-PCR of WT
eEF1B $\beta$ 2-qPCR-3 fw	CATCACCTATCACAGAAG	qRT-PCR of WT
eEF1B $\beta$ 2-qPCR-3 rev	GATCTTACAGCTTCTCTA	qRT-PCR of WT
eef1by1_fw	CTTCCAAGAAAGCTGCCAG	RT-PCR of <i>eef1by1-1</i> and <i>eef1by1-2</i>
eef1by1_3'UTRrev	GCCAGTCTACCCTGGCAATAG	RT-PCR of <i>eef1by1-1</i> and <i>eef1by1-2</i>
eef1by2_fw	GGCGTCACTAACAAGTCACC	RT-PCR of <i>eef1by2-1</i> and <i>eef1by2-2</i>
eef1by2_3'UTRrev	CCAAACTCGTGTGTGTGAC	RT-PCR of <i>eef1by2-1</i> and <i>eef1by2-2</i>

Ubiquitin10_fw	CAGTTGGAGGATGGCAGAAC	Reference gene for RT-PCR
Ubiquitin10_rev	GACGCAAGACCAAGTGGAGT	Reference gene for RT-PCR
eef1bγ1_fw	CTTCCAAGAAAGCTGCCAG	qRT-PCR of <i>eef1bγ1-1</i> and <i>eef1bγ1-2</i> and WT
eef1bγ1_rev	TGGTGCCTCTTCCTCTTCAG	qRT-PCR of <i>eef1bγ1-1</i> and <i>eef1bγ1-2</i> and WT
eef1bγ2_fw	GGCGTCACTAACAAGTCACC	qRT-PCR of <i>eef1bγ2-1</i> and <i>eef1bγ2-2</i> and WT
eef1bγ2_rev	GCTCACATATCGGGCAATGG	qRT-PCR of <i>eef1bγ2-1</i> and <i>eef1bγ2-2</i> and WT
FASS_fw	GGTGAAACCGTCTGACCCAT	Reference gene for qRT-PCR
FASS_rev	TCTCACGGTTGTCATGAGCC	Reference gene for qRT-PCR
SAND_fw	AACTCTATGCAGCATTGATCC AC	Reference gene for qRT-PCR
SAND_rev	TGATTGCATATCTTTATCGCCA TC	Reference gene for qRT-PCR

### 3 Results: Functional analysis of inactive protein phosphatase PP7L

PP7L is part of the MAIN-MAIL1 protein complex, which plays an important role in plant development, genome stability and silencing of transposable elements (de Luxan-Hernandez et al. 2020; Nicolau et al. 2020; Xu et al. 2019). The interaction of full length PP7L with MAIL1 and MAIN was proven in Y2H assays, bimolecular fluorescence complementation and co-immunoprecipitation experiments (de Luxan-Hernandez et al. 2020; Nicolau et al. 2020). Here, interaction and localization studies of mutated and truncated versions of PP7L were performed to analyze which domains are essential for PP7Ls function and localization.

The phenotype of *pp7l* mutants has been described in several publications. *pp7l* mutants show delayed chloroplast development in young tissue, which is due to impaired translation in chloroplasts (Xu et al. 2019). Also, primary root growth of *pp7l* mutants is impaired with increased cell death in the RAM (de Luxan-Hernandez et al. 2020). Interestingly, transposable elements are released from silencing in *pp7l* (de Luxan-Hernandez et al. 2020; Nicolau et al. 2020). Although, the phenotype is clearly described, the signaling pathway, which is influenced by PP7L, MAIN and MAIL1 has still not been determined. To tackle this challenge, two different approaches were followed in this study. On the one hand, a suppressor screen was started to find mutations suppressing the *pp7l* phenotype. On the other hand, co-immunoprecipitation coupled with mass spectrometric analysis was used to identify possible interaction partners of PP7L.

#### 3.1 Interaction studies of MAIL1 and PP7L

##### 3.1.1 MAIL1 interacts with PP7L in Y2H

Physical interaction between proteins can be analyzed by Y2H assays. As previously published MAIL1 and PP7L have been found to interact (de Luxan-Hernandez et al. 2020; Nicolau et al. 2020). A previous Y2H study showed a positive interaction of MAIL1 with PP7L, when each protein was N-terminally tagged. This result was reproduced in this study using a GAL4-based Y2H assay (Fig. 8A), where proteins of interest were N-terminally fused to DNA-binding domain (BD) or activation domain (AD). It has to be noticed that the BD-MAIL1 construct shows a slight auto-activation of yeast growth, as weak yeast growth can be seen for the interaction of BD-MAIL1 with the negative control AD-Citrine. To find out if the position of the tag influences the interaction, PP7L was C-terminally tagged with the AD-domain (PP7L (-C)) and tested for interaction with BD-MAIL1. This combination also showed a positive interaction (Fig. 8A).

MAIL1 contains a large plant mobile domain (PMD) domain flanked by two undefined protein regions (Figure 8B). To analyze which part of MAIL1 is interacting with PP7L, a truncated version of MAIL1 was tested for interaction with PP7L. MAIL1 $\Delta$ N (258-509aa) is lacking the N-terminus (1-257aa) and is schematically shown in Figure 8B. Y2H assay showed that MAIL1 $\Delta$ N is not sufficient for interaction with PP7L, no yeast growth was observed (Fig 8C).

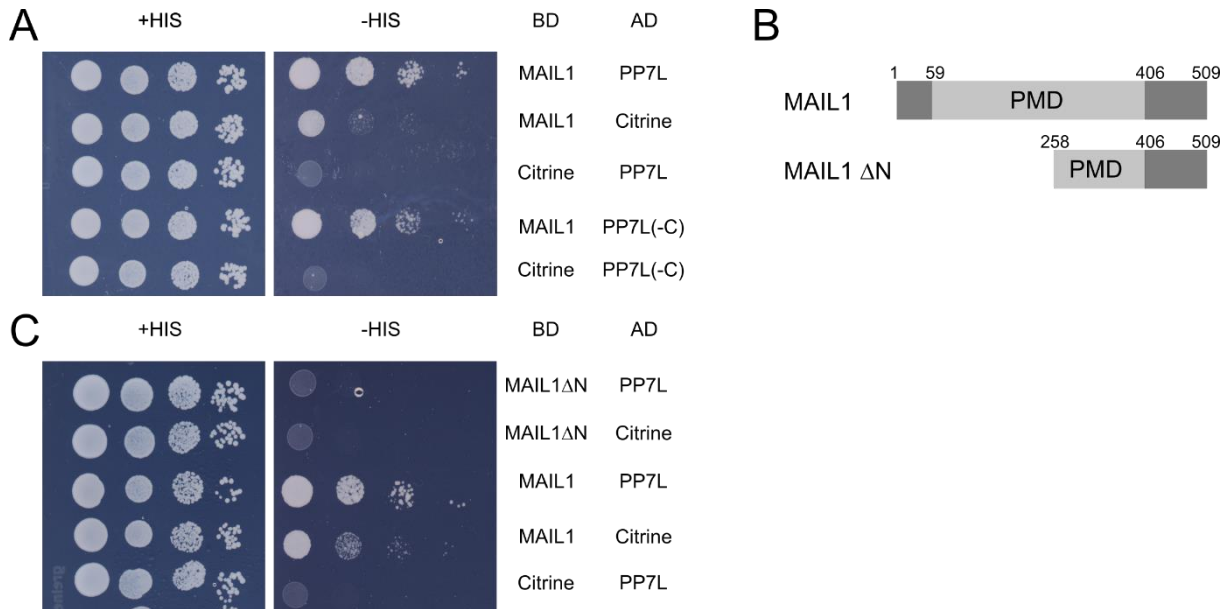


**Figure 8: MAIL1 interacts with PP7L in Y2H.** (A) Y2H assay showing physical interaction between full length MAIL1 and PP7L, independent of position of the tag. A serial dilution of yeast colonies was spotted on medium lacking tryptophan and leucine (+HIS) for growth control and on selective medium additionally lacking histidine (-HIS) to analyze the protein-protein interaction. Citrine was used as negative control. BD: DNA-binding domain (pGBT9 vector, N-terminal tag). AD: Activation domain (pGAD424 vector, N-terminal tag or pGADCg vector, C-terminal tag). (-C) indicates C-terminally tagged protein, all other proteins are N-terminally tagged. The data are representative for three independent colonies. (B) Structure of MAIL1 and the truncated version MAIL1 $\Delta$ N used for Y2H assay shown in (C). PMD: Plant Mobile Domain. (C) Y2H assay showing no interaction of MAIL1 $\Delta$ N with PP7L. The data are representative for three independent colonies. The constructs used for Y2H assay had been previously cloned in our lab by Teresa Wulf and Giuliana Heßler.

### 3.1.2 Inactive site of PP7L phosphatase domain is not essential for interaction with MAIL1 in Y2H

PP7L is described as ‘inactive homolog of serine/threonine protein phosphatase 7 (PP7)’ according to Uniprot database (<https://www.uniprot.org/uniprotkb/Q9LEV0/entry>; (Xu et al. 2019)). The active phosphatase PP7 contains a phosphatase domain with several conserved motifs important for metal ion binding, phosphate binding and catalytic activity (Goldberg et al. 1995; Uhrig, Labandera, and Moorhead 2013). Among these motifs is a stretch of the following amino acids: -LRGNHE-, which is positioned at 142-147aa in PP7 (Fig. 9). PP7L



At position 287-292aa of PP7L the not conserved motif -LRG**SSE**- is located. The change in amino acid sequence from asparagine (**N**) and histidine (**H**) to two serines (**S**) possibly decreases phosphatase activity of PP7L. To test whether the inactive site of PP7L is important for its interaction with MAIL1, site-directed mutagenesis was performed to generate a putatively active version of PP7L. The -LRG**SSE**- motif in PP7L was changed to the PP7 originated motif -LRG**NHE**- (Fig. 10A), the construct was hereafter named ‘PP7L (active)’. Interaction of PP7L (active) with MAIL1 was compared to the interaction between PP7L and MAIL1, but no difference was detected (Fig. 10B). PP7L with a putatively active catalytic domain is still able to bind MAIL1.

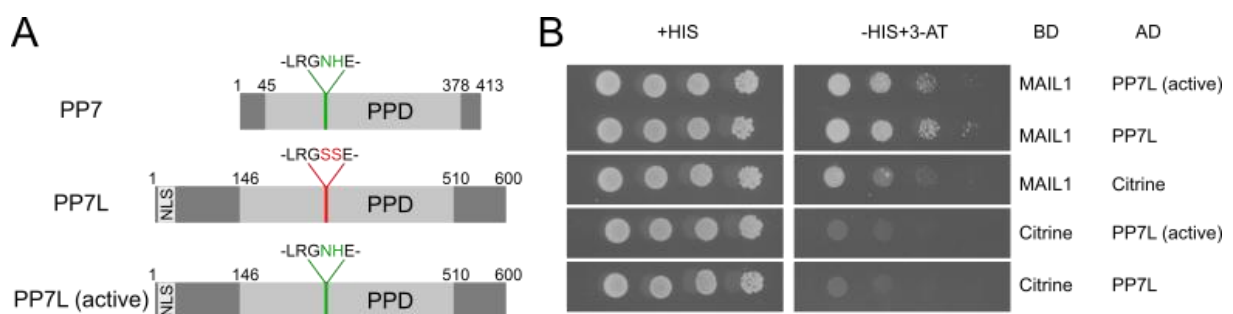


**Figure 10: Inactive catalytic site of phosphatase domain in PP7L is not required for MAIL1 interaction. (A)** Structure of PP7, PP7L and the mutated version of PP7L active used for Y2H assay shown in (B). Colored amino acids show that the catalytic site of PP7L active is similar to PP7, while PP7L catalytic site is described as inactive. PPD: Serine-/Threonine-Phosphatase Domain. **(B)** Y2H assay showing strong interaction between full length MAIL1 and full length PP7L as well as with PP7L active. A serial dilution of yeast colonies was spotted on medium lacking tryptophan and leucine (+HIS) for growth control, and on selective medium lacking histidine containing 3-aminotriazol (-HIS+3-AT) to analyze the protein-protein interaction. Citrine was used as negative control. BD: DNA-binding domain (pGBT9 vector, N-terminal tag). AD: Activation domain (pGAD424 vector, N-terminal tag). The data are representative for three independent colonies.

### 3.1.3 N-terminus of PP7L is necessary for interaction with MAIL1 in Y2H

The full length PP7L protein contains 600 amino acids and the inactive serine/threonine phosphatase domain (PPD) is located in the center of the protein from amino acid 146 to 510. The protein domains N-terminal and C-terminal of the PPD show no homology to any known protein domain. A bipartite nuclear localization signal (NLS) has been predicted by the cNLS mapper at the N-terminus of PP7L from amino acid 6 to 34 (Kosugi et al., 2009; [http://nls-mapper.iab.keio.ac.jp/cgi-bin/NLS\\_Mapper\\_form.cgi](http://nls-mapper.iab.keio.ac.jp/cgi-bin/NLS_Mapper_form.cgi) as shown in (Xu et al. 2019)). To find out, which part of PP7L is important for the interaction with MAIL1, different truncated versions of PP7L were created and cloned into vectors for Y2H assay. The constructs PP7L $\Delta$ N and PP7L $\Delta$ C have been cloned by Giuliana Heßler. The constructs PP7L $\Delta$ N $\Delta$ C, which only

contains the PPD domain (146-510aa), PP7L N-term, which contains only the part located N-terminal of the PPD (1-145aa) and PP7L $\Delta$ NLS, which lacks the NLS (35-600aa), were generated in this study (Fig. 11A). The interaction of these truncated PP7L versions with MAIL1 was tested in Y2H. To determine fine differences in yeast growth, selection medium lacking histidine but containing 3-aminotriazol (-HIS+3-AT) was used (Fig. 11B). As expected, the strongest interaction with MAIL1 was found for full length PP7L. No interaction was found for PP7L $\Delta$ N, PP7L $\Delta$ N $\Delta$ C and PP7L N-term with MAIL1. A positive, but weak interaction was found for PP7L $\Delta$ C and PP7L $\Delta$ NLS. The results indicate that the N-terminal part of PP7L is important for the interaction with MAIL1, but only the N-terminus without the PPD is not sufficient. Additionally, the NLS of PP7L is not absolutely necessary for the interaction with MAIL1, since PP7L $\Delta$ NLS is still able to weakly interact.

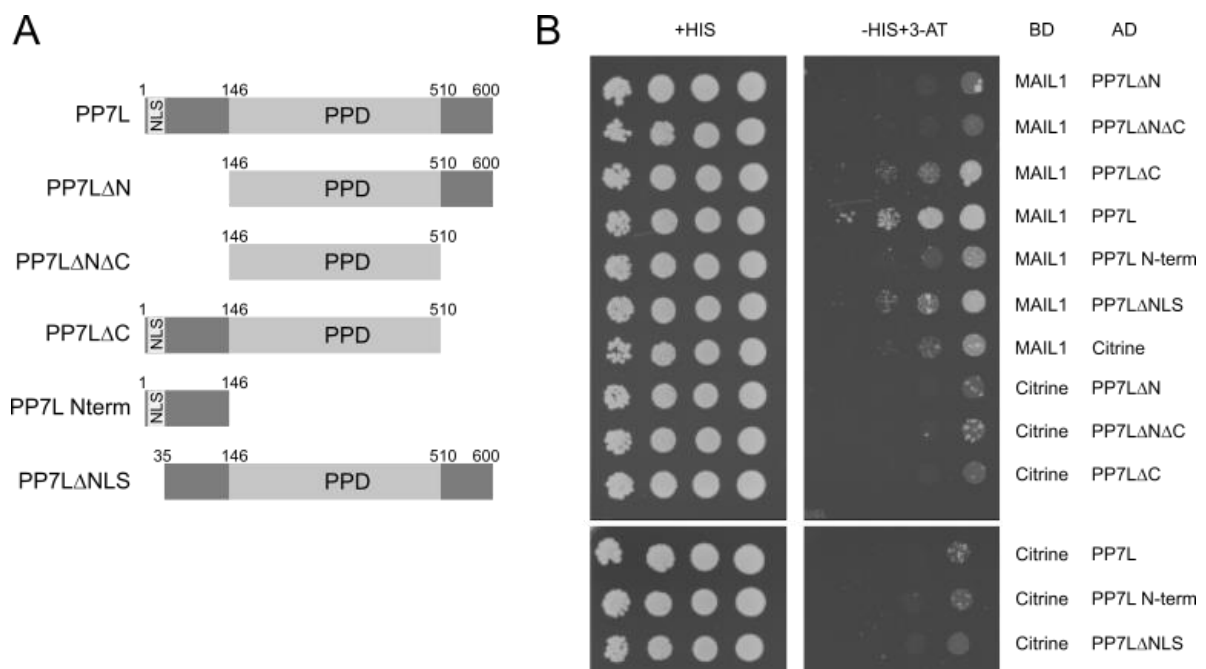


**Figure 11: N-terminus of PP7L is necessary for interaction with MAIL1 in Y2H.** (A) Structure of PP7L and the truncated versions of PP7L used for Y2H assay shown in (B). PPD: Serine-/Threonine-Phosphatase Domain. (B) Y2H assay showing strong interaction between full length MAIL1 and full length PP7L, weak interaction between full length MAIL1 and PP7L $\Delta$ C and PP7L $\Delta$ NLS, but no interaction for PP7L $\Delta$ N, PP7L $\Delta$ N $\Delta$ C or PP7L N-term. A serial dilution of yeast colonies was spotted on medium lacking tryptophan and leucine (+HIS) for growth control and on selective medium lacking histidine containing 3-aminotriazol (-HIS+3-AT) to analyze the protein-protein interaction. Citrine was used as negative control. BD: DNA-binding domain (pGBT9 vector, N-terminal tag). AD: Activation domain (pGAD424 vector, N-terminal tag). Data are representative for three independent colonies.

## 3.2 Subcellular localization studies of PP7L

3.2.1 N-terminus of PP7L, including the NLS, determines nuclear localization of PP7L  
The full length PP7L has been described to localize mainly in the nucleus, but is partially also found in cytoplasm (de Luxan-Hernandez et al. 2020). This was in accordance with the prediction score of 5.1 from the cNLS mapper, which also indicated a dual localization in the nucleus and the cytoplasm. The truncated versions PP7L $\Delta$ NLS and PP7L $\Delta$ N are both lacking the NLS and were therefore expected to localize only in the cytoplasm, if the nuclear transport of PP7L was solely dependent on the NLS. To test the subcellular localization of PP7L $\Delta$ NLS, PP7L $\Delta$ N and PP7L $\Delta$ C, the proteins were C-terminally fused to the Green Fluorescent Protein (GFP) and expressed under an estradiol-inducible 35S-promotor in epidermal cells of *Nicotiana benthamiana* (Fig. 12A and 12B). As expected, PP7L-GFP and PP7L $\Delta$ C-GFP localized to the nucleus and the cytoplasm, while PP7L $\Delta$ NLS-GFP and PP7L $\Delta$ N-GFP did not localize to the nucleus (Fig. 12A).

Since PP7L interacts with the nuclear localized protein MAIL1, we questioned whether MAIL1 might be able to promote the transport of PP7L to the nucleus. To this end, we co-expressed PP7L-GFP and its truncated versions with MAIL1-mCherry and observed whether the presence of MAIL1 enhances the nuclear localization of PP7L. PP7L-GFP perfectly co-localizes with MAIL1-mCherry in the nucleus, but is still present in the cytoplasm (Fig. 12C). The localization of PP7L $\Delta$ N and PP7L $\Delta$ C were not influenced by the co-expression of MAIL1-mCherry. PP7L $\Delta$ N was still excluded from the nucleus. A slight difference was observed for PP7L $\Delta$ NLS, when co-expressed with MAIL1. Some cells showed the same localization as before, but in others PP7L $\Delta$ NLS was present in the nucleus when MAIL1 was present. Taken together, these results indicate that the N-terminus (including the NLS) of PP7L is important for its nuclear localization. The observed results in *N. benthamiana* are qualitative observations. To verify the results a quantitative evaluation of localization was performed in transiently transformed *Arabidopsis* protoplasts.

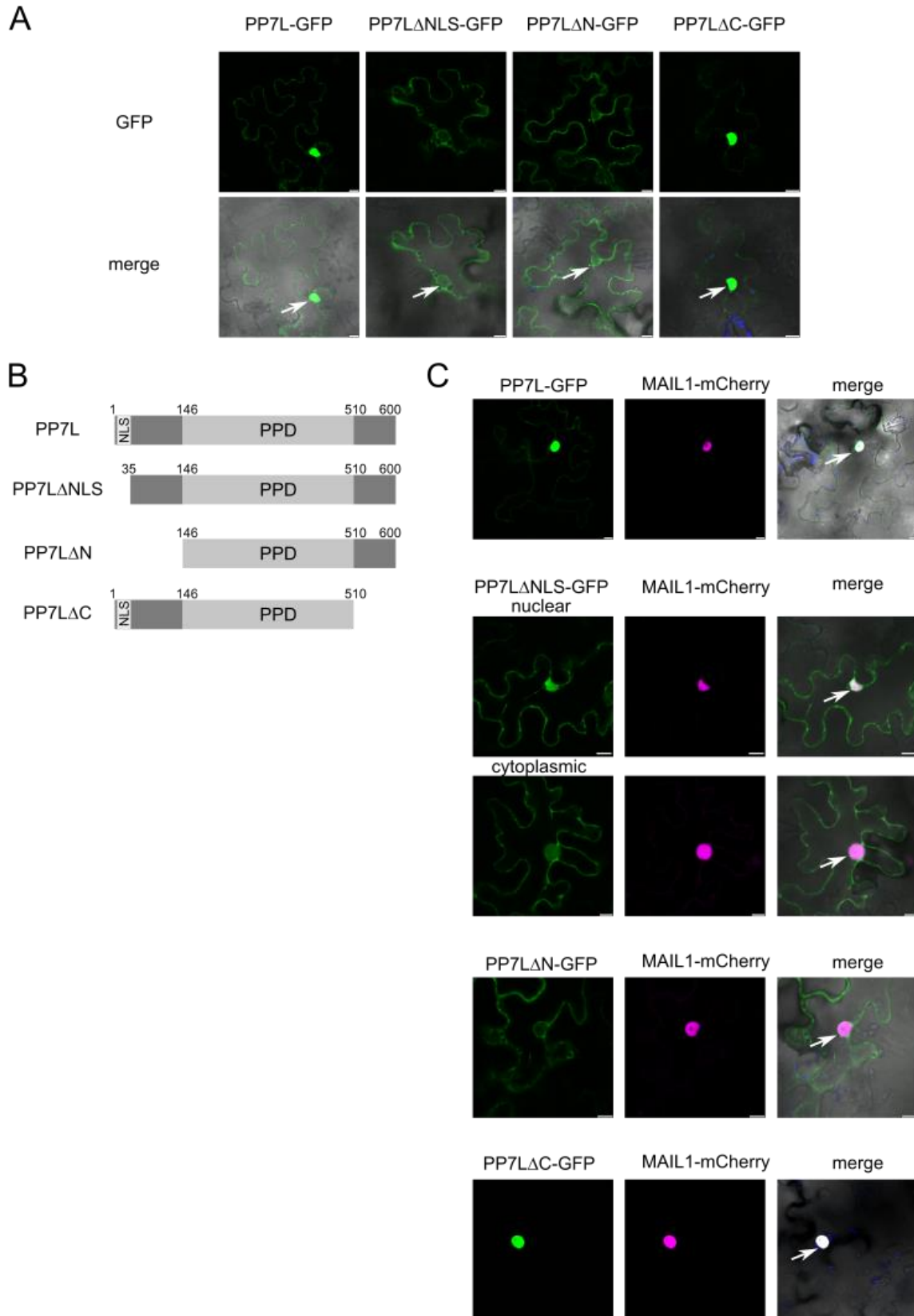


**Figure 12: N-terminal domain of PP7L is important for its nuclear localization.** (A) Representative confocal images of epidermal leaf cells of *Nicotiana benthamiana* expressing indicated PP7L-GFP versions. Full length PP7L mainly localizes to the nucleus, but some cells show dual localization in the nucleus and cytoplasm.

PP7L $\Delta$ NLS and PP7L $\Delta$ N do not localize in the nucleus, but only in the cytoplasm, whereas PP7L $\Delta$ C localizes mainly in the nucleus. Merged picture shows GFP signal in green, autofluorescence of chloroplasts in blue and bright field. Scale bar is 10  $\mu$ m. Arrows show expected position of the nucleus. **(B)** Structure of PP7L, PP7L $\Delta$ NLS, PP7L $\Delta$ N and PP7L $\Delta$ C used for localization studies shown in (A) and (C). PPD: Serine-/Threonine-Phosphatase Domain. NLS: Nuclear Localization Signal. **(C)** Representative confocal images of epidermal leaf cells of *Nicotiana benthamiana* co-expressing indicated PP7L-GFP versions with MAIL1-mCherry. Localization of PP7L constructs did not change in comparison to single expression, only PP7L $\Delta$ NLS showed in some cells still nuclear localization. Merged picture shows GFP signal in green, autofluorescence of chloroplasts in blue and bright field. Scale bar is 10  $\mu$ m. Arrows show expected position of the nucleus. Cloning of PP7L $\Delta$ N and PP7L $\Delta$ C into pABind vectors and localization studies in *Nicotiana benthamiana* were performed by Florian Pomrehn (as part of his lab rotation under my supervision).

To this end, the plasmid DNA of PP7L-GFP and the truncated versions were first transiently expressed in WT protoplasts. PP7L mainly localized to the nucleus, but in some protoplasts a dual localization in the nucleus and in the cytoplasm could be observed (Fig. 13A and 13B). To quantify the percentage of protoplasts showing solely nuclear localization or dual localization, we counted 50 protoplasts in each of the two independent experiments and found that about 75% of WT protoplasts expressing PP7L-GFP showed a nuclear localization, 5% showed only cytoplasmic localization and 20% showed a dual localization in the nucleus and the cytoplasm (Fig. 13B). Similar to the observations in *N. benthamiana*, PP7L $\Delta$ NLS and PP7L $\Delta$ N were mostly excluded from the nucleus (Fig. 13A). About 70 - 80 % of WT protoplasts showed solely nuclear localization, while the remaining protoplasts expressing PP7L $\Delta$ NLS or PP7L $\Delta$ N showed a dual localization in nucleus and cytoplasm (Fig. 13B). PP7L $\Delta$ C was observed mainly in the nucleus with few protoplasts showing a dual localization, similar to full length PP7L.

To analyze the role of MAIL1 and MAIN in the transport of PP7L to the nucleus in more detail, the different PP7L versions were next transiently expressed in protoplasts of the *mainmail1* double mutant. If the nuclear localization of PP7L in the nucleus would rely on MAIN or MAIL1 to drag PP7L with them into the nucleus, no nuclear localization of PP7L should be observed in *mainmail1* protoplasts. But localization studies in *mainmail1* protoplasts revealed no differences compared to the observed localizations of the PP7L versions in WT protoplasts (Fig. 13A and B). Together with the results from *N. benthamiana*, where the vice versa approach with overexpression of MAIL1 yielded the same results, this indicates that the N-terminus of PP7L, including its NLS, is determining the presence of PP7L in the nucleus, but

the interaction with MAIL1, which is also conferred by the N-terminus is not playing a role in the nuclear localization.

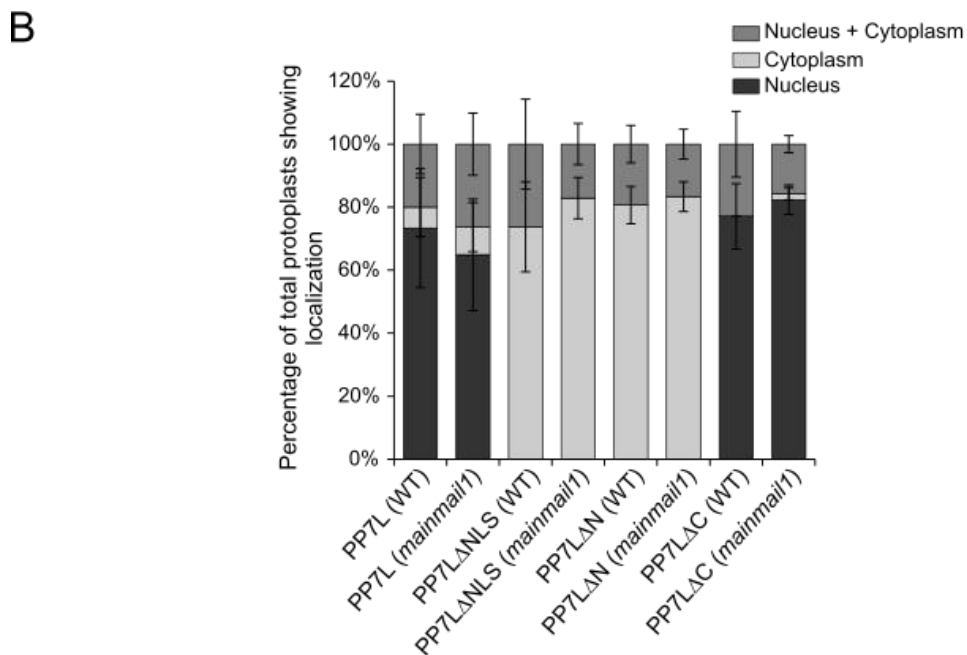
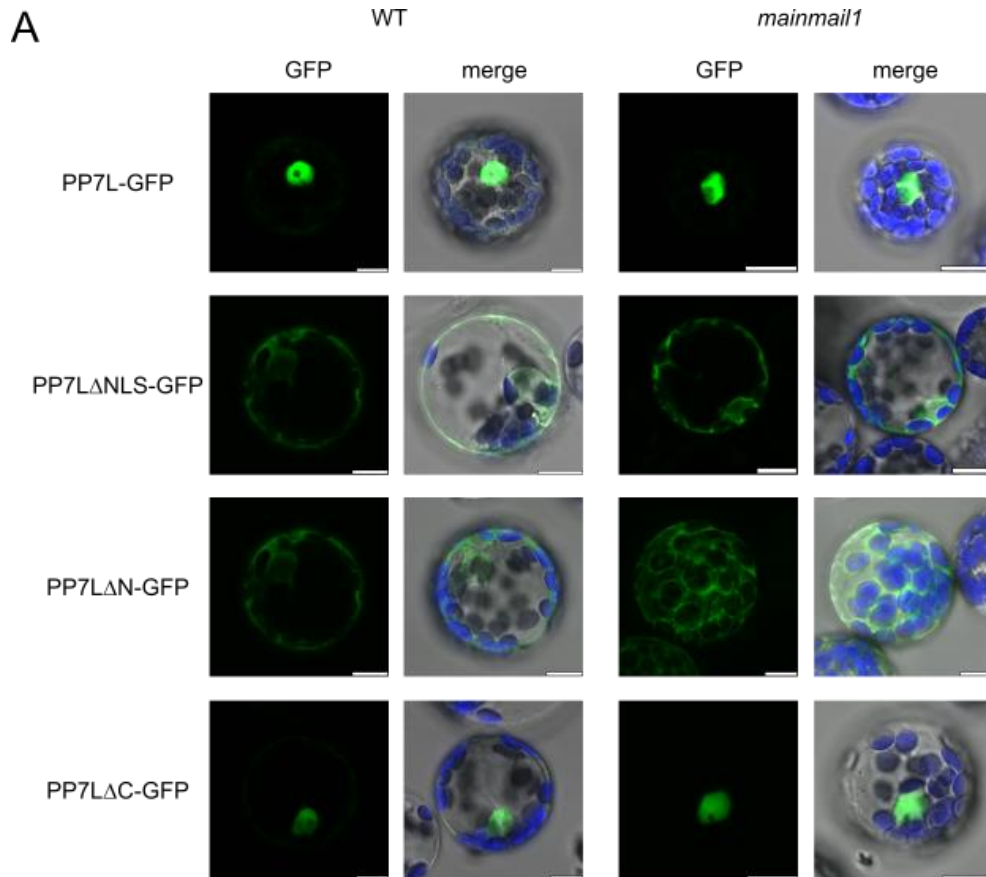


**Figure 13: N-terminal domain of PP7L is essential for its nuclear localization.** (A) Representative confocal images of WT or *mainmail1* protoplasts transiently transformed with indicated C-terminally GFP-tagged versions of PP7L under an estradiol-inducible 35S-promotor. Merged picture shows combination of GFP signal in green, chloroplast autofluorescence in blue and bright field. Scale bar is 10  $\mu$ m. (B) Quantification of localization of

protoplasts showing a GFP-signal only in the nucleus, only in the cytoplasm or in both, nucleus and cytoplasm. Data represent means from two independent experiments (n=50).

### 3.2.2 Inactive motif in phosphatase domain of PP7L does not influence its localization

In 3.1.2, a mutated ‘active’ version of PP7L was generated, which did still interact with MAIL1 in Y2H. To find out whether the mutated PP7L (active) is still localizing in the same cellular compartments as the native PP7L, the subcellular localization was analyzed in *N. benthamiana*. Therefore, PP7L (active) was expressed under an estradiol-inducible 35S promotor and C-terminally tagged with GFP. The subcellular localization of PP7L (active) was similar to PP7L. It localized in the nucleus and the cytoplasm (Fig. 14). Hence, the mutation in the PPD domain of PP7L does not change the subcellular localization of PP7L.

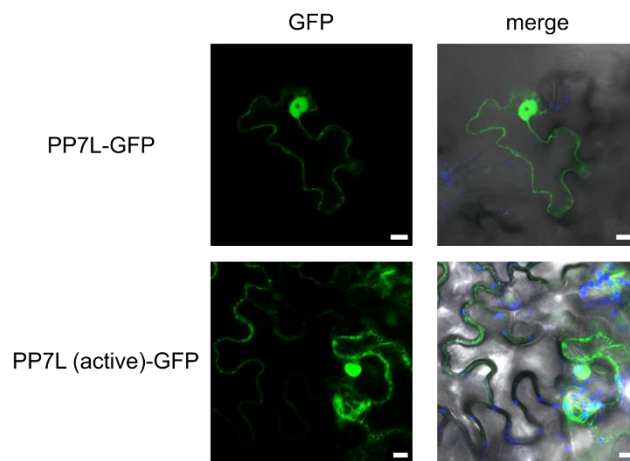


**Figure 14: PP7L (active) localizes to the nucleus and the cytoplasm, similar to PP7L.** Representative confocal images of epidermal leaf cells of *Nicotiana benthamiana* expressing PP7L-GFP or PP7L (active)-GFP. Both proteins localize to the nucleus and the cytoplasm. Merged picture shows GFP signal in green, autofluorescence of chloroplasts in blue and bright field. Scale bar is 10  $\mu$ m.

### 3.3 Suppressor screen

PP7L is important for genome stability and works in complex with MAIN and MAIL1. Nonetheless, the signaling pathway, in which PP7L is involved is so far unknown. One method to elucidate the signaling network of a protein is a suppressor screen. *pp7l* mutant shows a clear and easy-to-observe short root phenotype, which makes it an ideal candidate for a suppressor screen. The screen aimed at finding second-site mutants of *pp7l*, which show a restored root growth and therefore might harbor mutations in genes that act in parallel or downstream of PP7L. The workflow for the suppressor screen is outlined in Fig. 15.

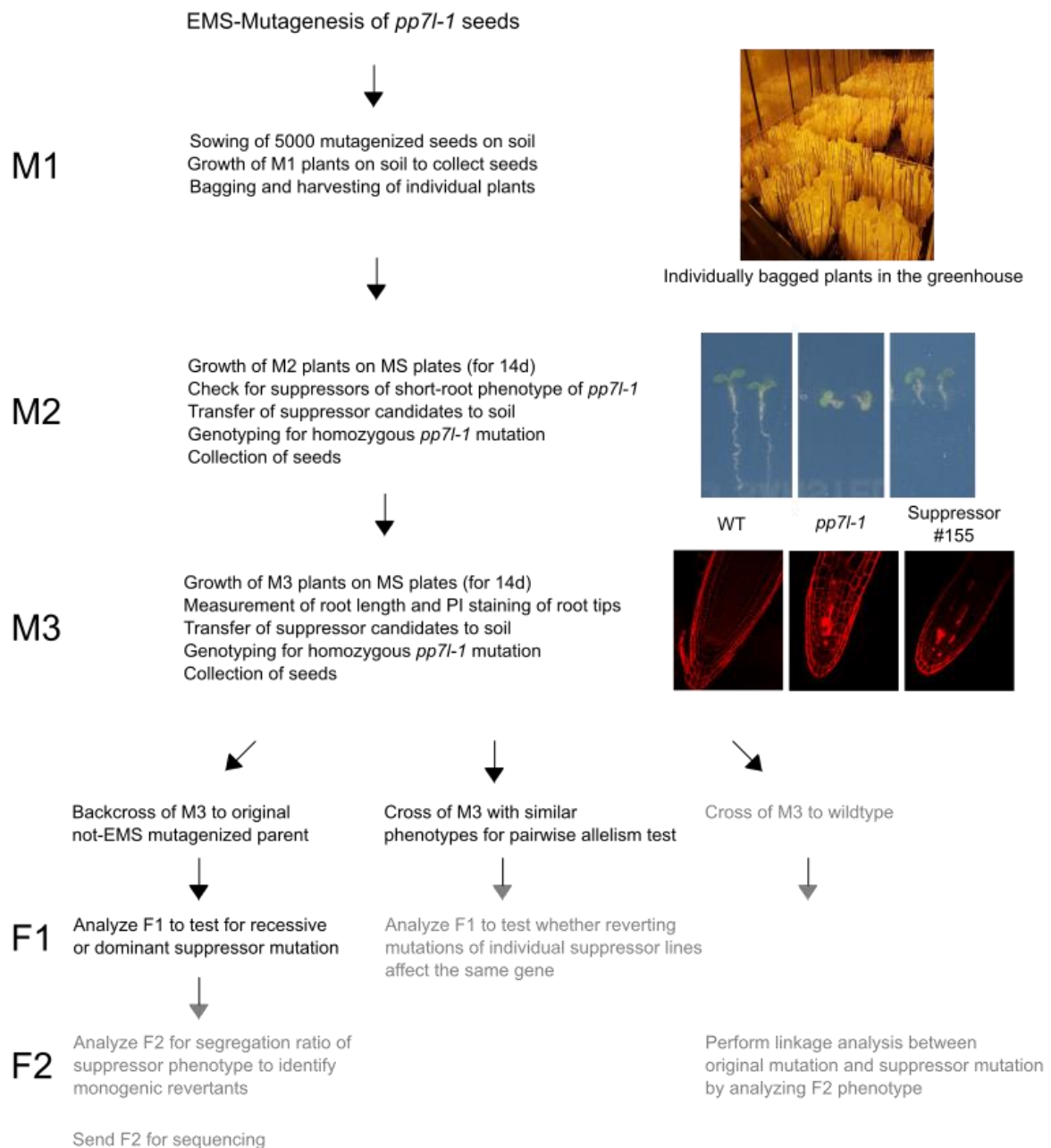


**Figure 15:** Workflow showing the screening for suppressors of *pp7l-1*. Steps that were performed during this study are written in black, pending steps are written in grey.

Seeds of *pp7l-1* were mutagenized with EMS and 5000 seeds were sown on soil. M1 plants were grown and self-fertilized to collect seeds. An indicator for successful mutagenesis of Arabidopsis seeds is the occurrence of mutants with defects in chlorophyll biosynthesis. Several M1 plants with partially or complete albino leaves were observed (Fig. 16C), suggesting an efficacious mutagenesis. During observation of the development of M1 plants, it was noticed that several plants showed wild-type like growth. This was unexpected, because in the M1 generation the EMS-introduced mutations are still heterozygous and would in most cases not

be able to suppress the *pp7l* phenotype. An image of several four weeks-old M1 plants is shown in Figure 16A. Numerous seeds did not germinate, which could be explained with a mutagenesis affecting genes involved in germination. Most plants (e.g. #1, #2, #3) are still small, which is comparable to the slow *pp7l-1* mutant development. In contrast, plant #4 has already developed flowers and siliques. To ensure that these fast developing, large M1 plants were indeed homozygous for the *pp7l-1* T-DNA insertion, plants were genotyped. The genotyping results of the plants #1 - #4 (shown in Fig. XA) are displayed in Fig. 16B. Small M1 plants (#1, #2, #3) were homozygous for the *pp7l-1* T-DNA insertion, but the large M1 plant (#4) was heterozygous. Therefore, all plants, which grew faster or similar to wild type, were genotyped. In total, 220 plants were heterozygous and were subsequently excluded from further experiments. From the originally 5000 sown seeds, 2970 plants developed siliques and were bagged and harvested as individual suppressor lines. To analyze the M2 generation for a restored root phenotype, 30 seeds from each line were sown and grown on vertically placed MS plates. Plates were scanned weekly and individual suppressor lines showing increased root-length compared to *pp7l-1* mutants were identified, transferred to soil, genotyped and grown to collect seeds. So far, 1280 M2 lines have been analyzed. We found 128 lines, which showed at least partially restored root growth. Genotyping revealed that 25 lines of these were heterozygous for *pp7l-1* mutation and were therefore discarded.

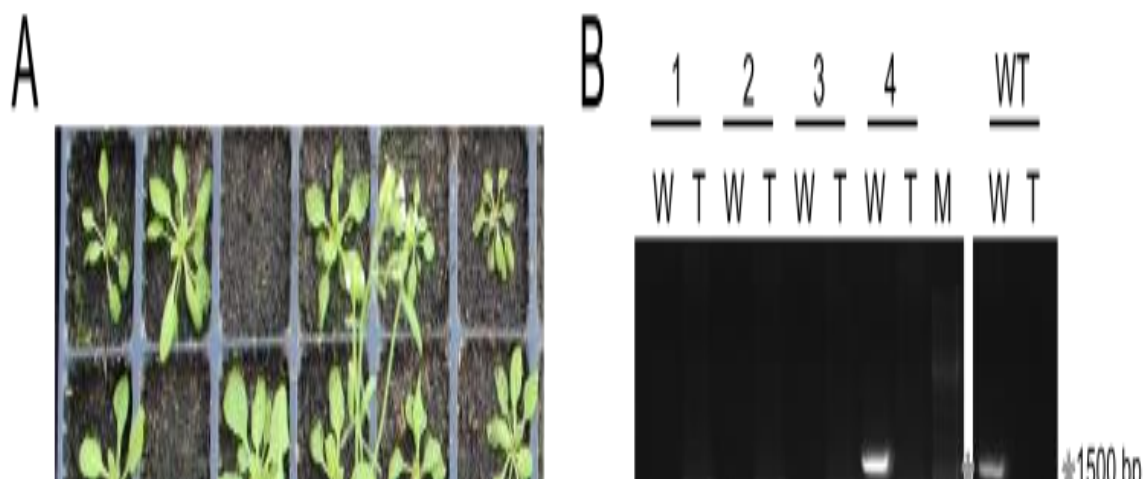


**Figure 16: Phenotypes and Genotypes of M0 generation of *pp7l-1* suppressors.** (A) Example tray with four weeks-old EMS-mutagenized *pp7l-1* seeds sown on soil demonstrating the variety of phenotypes observed in M0 generation. Single plants like #4 show wild type-like growth and development. Numbers show plants chosen for genotyping in (B); (1-4). (B) Genotyping for *pp7l-1* T-DNA insertion in potential *pp7l-1* suppressor lines. gDNA of plants shown and numbered in (A) was isolated and used for genotyping PCR using primers amplifying the wild type allele of *PP7L* with expected size of 1112 bp (W) or the T-DNA insertion with expected size of 770 bp (T).

As wild type control, gDNA from Columbia-0 was tested (WT). GeneRuler 1 kb Plus DNA Ladder was used as marker (M). (C) Four weeks-old potential suppressor of *pp7l-1* showing chlorophyll deficient leaf sections.

Seeds from the remaining 103 lines were harvested and M3 generation was again checked for root growth restoration. Repetition of root growth restoration would indicate that the observed suppression phenotype was heritable. Therefore, 30 seeds from each line were sown on MS plates and root length was measured. Many of the 103 chosen M2 lines did not germinate in the next generation or did not develop longer roots compared to *pp7l-1* mutants, indicating a non-heritable trait in the M2 generation. But seven lines appeared to be interesting suppressor candidates and were further characterized. Each line showed a significant increase in root length compared to *pp7l-1* mutants (Fig. 17A and 17B). Line 438-2 and line 469-1 showed the highest increase in root length compared to *pp7l-1*. However, root length of all seven lines was still very short compared to WT root length indicating that the *pp7l-1* short root-phenotype was not completely rescued by the suppressor mutations.

Another phenotypic trait of *pp7l-1* roots is the accumulation of dead cells in the meristematic zone (de Luxan-Hernandez et al. 2020). In root tips, the accumulation of dead cells can be visualized by propidium iodide (PI) staining. PI intercalates with the bases of DNA and can therefore be used as stain for DNA. Additionally, PI can be used as viability marker. It is membrane-impermeant, so that it can only enter dead cells with damaged membranes and stain intracellular DNA (Jones and Senft 1985). Root tips of suppressor candidate seedlings were analyzed with PI staining and confocal laser-scanning microscopy of root tips at 3 dag (Fig. 17C). Wild type seedlings show no dead cells in the meristematic zone, whereas *pp7l-1* mutants show many dead cells. Similarly, lines 143-5, 155-2, 254-2, 263-3 and 484-3 showed many dead cells. For line 438-2 fewer dead cells were observed, but dead cells were still present in every analyzed root tip of 438-2. Only, in seedlings of line 469-1 no dead cells were observed in the meristematic zone, making it the most interesting suppressor candidate for further analysis.

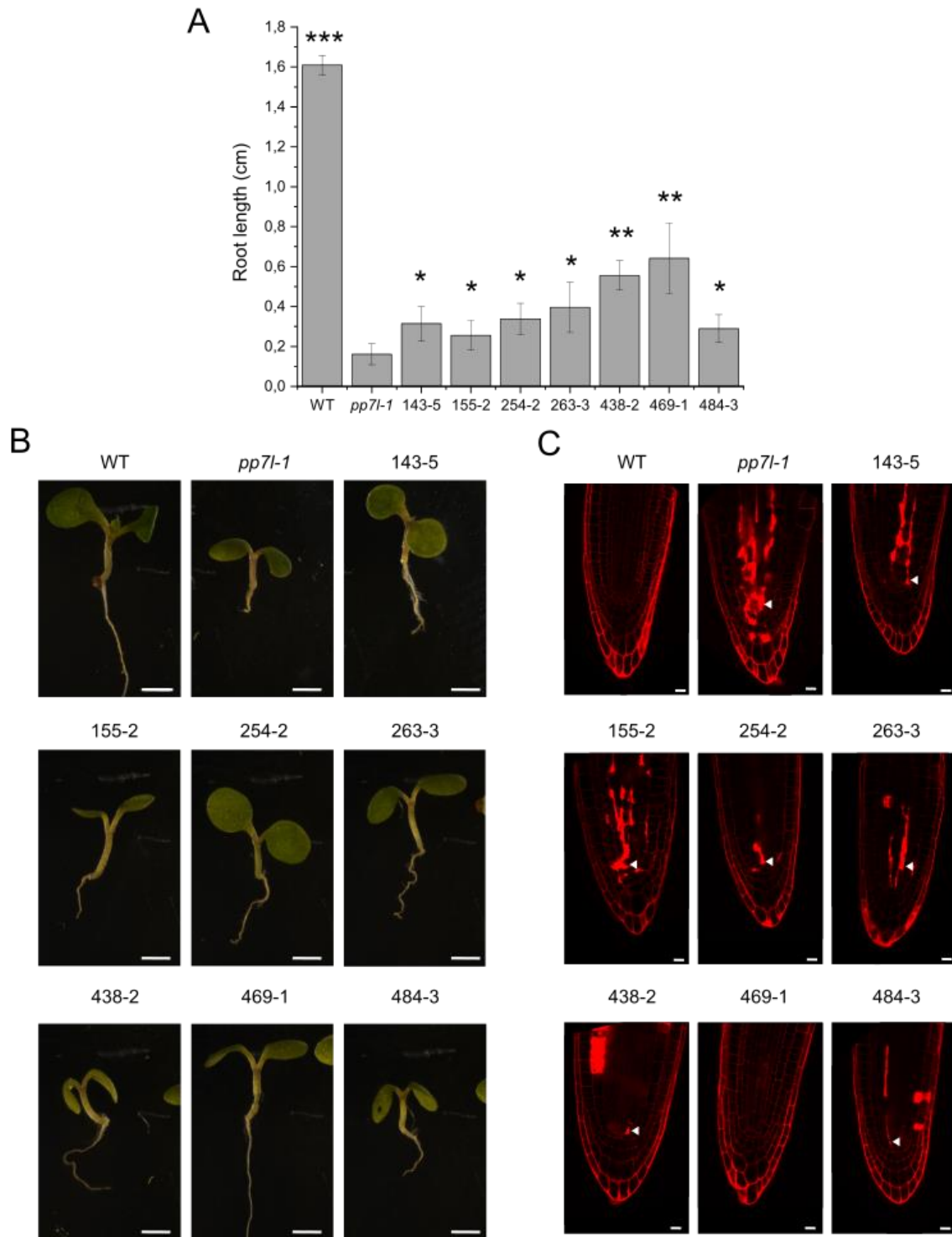


**Figure 17: Root phenotypes of suppressor candidates.** (A) Wild type, *pp7l-1* mutant and suppressor candidates were grown on vertical MS plates and root length was measured at 6 dag. Graphs represent mean  $\pm$  SE from the following number of roots (WT: n=10, *pp7l-1*: n=29, 143-5: n=13, 155-2: n=17, 254-2: n=23, 263-3: n=17, 438-2: n= 11, 469-1: n=29, 484-3: n=8). Asterisks show significant difference to *pp7l-1* (\* P<0,05; \*\* P<0,01). (B) Representative images of the indicated lines at 6 dag. Scale bar is 10 mm. (C) Confocal images of propidium iodide-stained root tips of the indicated lines at 3 dag. Arrowheads point to PI stained dead cells in the meristematic zone. Scale bar is 10  $\mu$ m.

Seedlings of interest were transferred to soil at 9 dag. Representative photographs of plants grown on soil for three weeks are shown in Figure 18. Wild-type plants did already develop shoots and first flowers, while *pp7l-1* mutants were still significantly smaller and had not started with shoot development. Phenotypes of lines 143-5 and 155-2 were comparable to *pp7l-1*. Also lines 254-2, 263-3 and 438-2 appeared to have a similar development. Plants of line 484-3 did not survive after transfer to soil. One possible explanation might be a defect in photosynthesis, so that plants cannot produce sugar. The defect was not noticeable on MS plates, which contained sucrose, but would become obvious on soil without the additional sugar source. In accordance with the previously observed most extensive restoration of root growth in line 469-1, also the development of leaves and the first bolts was more advanced in line 469-1 compared to *pp7l-1* mutants and the other suppressor candidates.

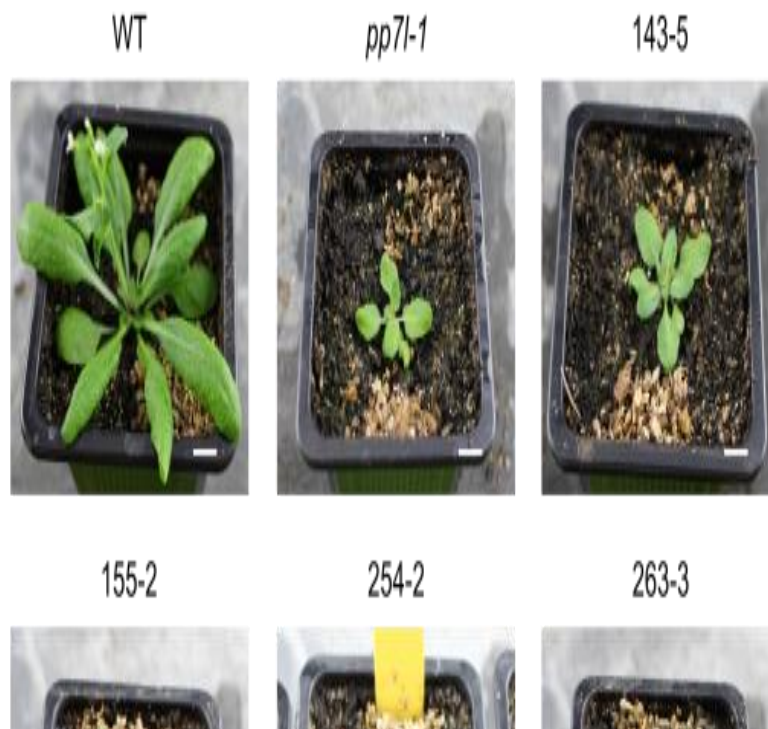


**Figure 18: Above-ground phenotypes of suppressor candidates.** Seeds of indicated lines were germinated on MS plates and seedlings were transferred to soil at 9 dag. Photographs of representative plants were taken after 21 days of growth on soil. Scale bar is 1 cm.

Mutagenesis with EMS can lead to many different point mutations throughout the genome of an individual plant. To simplify the identification of the mutation being responsible for the observed suppression of *pp7l-1* phenotype, it is important to cross-out “unwanted” point mutations. This can be achieved by backcrossing of the suppressor candidates with the original not-EMS mutagenized parent. Therefore, the M3 plants shown in Fig. 18 were crossed with

*pp7l-1* mutants. After successful backcrossing, it was expected that the suppressor mutation would be heterozygous again. Subsequently, the seedlings of the F1 generation would show a short-root phenotype like *pp7l-1*, if the suppressor mutation was recessive. Backcrosses of line 143-5, 254-2, 438-2 and 469-1 produced seeds, which were sown on MS plates and photographs of 10 days-old seedlings are shown in Fig. 19. All seedlings showed short roots like *pp7l-1* implying a recessive suppressor mutation.

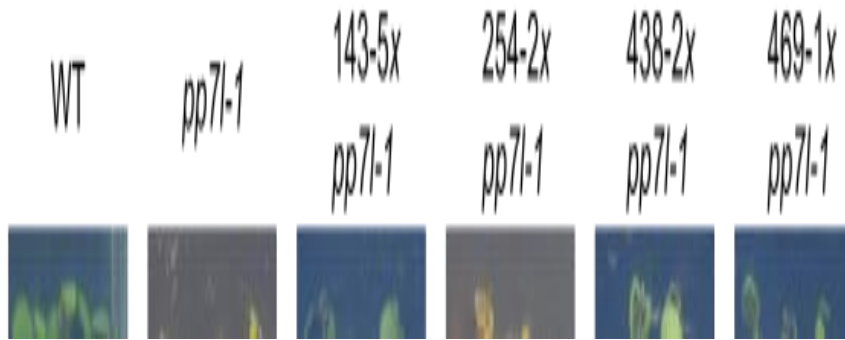


**Figure 19: F1 generation of backcrosses of suppressor candidates to *pp7l-1*.** Representative photographs of 10 days-old seedlings grown on vertical MS plates of the indicated lines. Scale bar is 0,5 cm.

Due to time reasons further experiments could not be performed during this study, so that the the affected gene of suppressor mutations remain unknown. To identify the position of the suppressor mutation, it would be necessary to analyze the F2 generation of the backcrosses to *pp7l-1*. The segregation ratio of the suppressor phenotype would indicate which mutants are monogenic revertants. Identified monogenic revertants could be send for whole-genome sequencing and bioinformatics would be performed to find the suppressor mutation.

In addition to this work process, two more work strands should be followed. First, it would be advantageous to perform a pairwise allelism test by crossing the M3 generation with mutants of similar phenotypes. In consequence, the different suppressor mutant lines should be crossed with each other. The F1 generation should be analyzed to find out, which reverting mutations are affecting the same gene. Second, the M3 generation should be crossed to wild type. This is necessary to perform a linkage analysis between the original mutation (*pp7l-1*) and the suppressor mutation in F2 generation.

### 3.4 Finding new protein interaction partners of PP7L using proteomics

#### 3.4.1 Proteomic identification of new PP7L interaction partners

PP7L was found to work in a complex with MAIN and MAIL1. The complex has a strong influence on plant development, maintenance of genome stability and silencing of transposable elements (Nicolau et al. 2020; de Luxan-Hernandez et al. 2020). In an independent study, PP7L was found as player involved in chloroplast biogenesis (Xu et al. 2019). Loss of PP7L led to reduced translation and ribosomal rRNA maturation in chloroplasts (Xu et al. 2019). To find out how PP7L can be involved in these different processes and which interaction partners are involved in the signaling pathway, a co-immunoprecipitation experiment coupled with MS analysis was performed. PP7L-GFP expressed from its native promotor in six days-old *pp7l* seedlings was used as bait. Seedlings expressing free GFP expressed from 35S promotor served as negative control. The MS analysis was performed by Dominique Eckhorst and Geert Peersiau at the protein complex purification platform at Vlaams Instituut voor Biotechnologie (VIB, Center for Plant Systems Biology, Belgium). The results of MS analysis showing the nine proteins with the highest significance are shown in Table 2.

**Table 2: Potential protein interactors of PP7L identified by Co-IP/MS.** Results of MS analysis showing the nine most significant potential interactors of PP7L-GFP, which was used as bait.

Leading Protein ID	Protein name	Peptide count	Sequence coverage (%)	P-value (-log)
AT5G10900	<b>PP7L:</b> Calcineurin-like metallo-phosphoesterase superfamily protein	15	34,7	4,225
AT3G44310	<b>NIT1:</b> ATNIT1, nitrilase 1	15	38,4	3,406
AT1G17930	<b>MAIN:</b> Aminotransferase-like, plant mobile domain family protein	18	47,5	4,598
AT2G25010	<b>MAIL1:</b> Aminotransferase-like, plant mobile domain family protein	14	36	6,659
AT5G19510	<b>eEF1B<math>\alpha</math>2:</b> Translation elongation factor EF1B/ribosomal protein S6 family protein	7	42	4,093
AT1G30230	<b>eEF1B<math>\beta</math>1:</b> Glutathione-S-transferase, C-terminal-like, Translation elongation factor EF1B/ribosomal protein S6 family protein	7	38,5	3,603

AT3G09440	<b>HSP70:</b> Heat shock protein70 protein family	23	46,5	2,638
AT1G57720	<b>eEF1B<math>\gamma</math>2:</b> Translation elongation factor EF1B, gamma chain	12	40,9	3,551
AT1G09640	<b>eEF1B<math>\gamma</math>1:</b> Translation elongation factor EF1B, gamma chain	11	36,2	3,647

As expected, MAIN and MAIL1 were found among the most significant potential interactors that specifically co-purified with PP7L. This indicates the Co-IP/MS analysis did indeed reveal already verified interaction partners of PP7L (de Luxan-Hernandez et al. 2020; Nicolau et al. 2020). None of the additional potential interactors had been found in Co-IP/MS analysis, which was previously performed in our lab and used MAIL1-GFP as bait, indicating that these are PP7L-specific interactors. The second most abundant potential interactor of PP7L found in the Co-IP/MS analysis was NITRILASE 1 (NIT1; AT3G44310). It yielded a peptide count of 15 and 38,4% sequence coverage. Additionally, four proteins belonging to the same protein complex were found among the top nine potential interactors. eEF1B $\alpha$ 2 (AT5G19510), eEF1B $\beta$ 1 (AT1G30230), eEF1B $\gamma$ 2 (AT1G57720) and eEF1B $\gamma$ 1 (AT1G09640) belong to the EUKARYOTIC TRANSLATION ELONGATION FACTOR COMPLEX 1B (eEF1B). Also, the HEAT SHOCK PROTEIN 70 (HSP70) was found with a high peptide count of 23 and 46,5% sequence coverage.

#### 3.4.2 NIT1 and PP7L display no interaction in Y2H or Co-IP/Western

NITRILASE 1 (NIT1; AT3G44310) is part of the nitrilase protein superfamily, which is known for catalyzing the hydrolysis of nitriles to carboxylic acids and ammonia (Pace and Brenner 2001). Plant nitrilases have been attributed to be involved in several processes including: cyanide detoxification and catabolism of cyanogenic glycosides (Piotrowski 2008), a minor role in auxin biosynthesis by conversion of indole-3-acetonitrile to indole-3-acetic acid (Zhao 2010) or repair of damaged glutathione (Niehaus et al. 2019). Interestingly, loss of NIT1/2/3 led to severe developmental defects in Arabidopsis roots and leaves. It was shown that NIT1 is important for cell cycle exit during differentiation, correct cytokinesis and maintaining genome integrity (Dorskocilova et al. 2013). These studies indicate some similarities in phenotype and function between *PP7L* and *NIT1*, leading us to the assumption that NIT1 is a strong candidate for interaction with PP7L. Therefore, we aimed at confirming the interaction between NIT1 and PP7L by two independent methods. First, we used the GAL4-based yeast-two-hybrid system.

The cDNA of NIT1 and PP7L was cloned into the Y2H vectors, pGBT9 and pGAD424, which allow expression with an N-terminally attached activation domain or DNA-binding domain of the GAL4 transcription factor. As negative control, we tested NIT1 together with the unrelated synthetic Citrine protein. The transformed yeast was spotted on selective medium lacking leucine and tryptophan for growth control and on medium lacking leucine, tryptophan and histidine to test for protein-protein interaction. The spotting results are shown in Fig. 20A. No physical interaction was observed for PP7L with NIT1. Negative controls with Citrine show no interaction, while the positive control PP7L with MAIL1 showed a positive interaction, implying that the Y2H assay was technically working correctly. We have observed a strong self-interaction of NIT1 with itself. This is in line with previous findings, which demonstrated that NIT1 is present in high molecular weight mass polymers (Dokocilova et al. 2013).

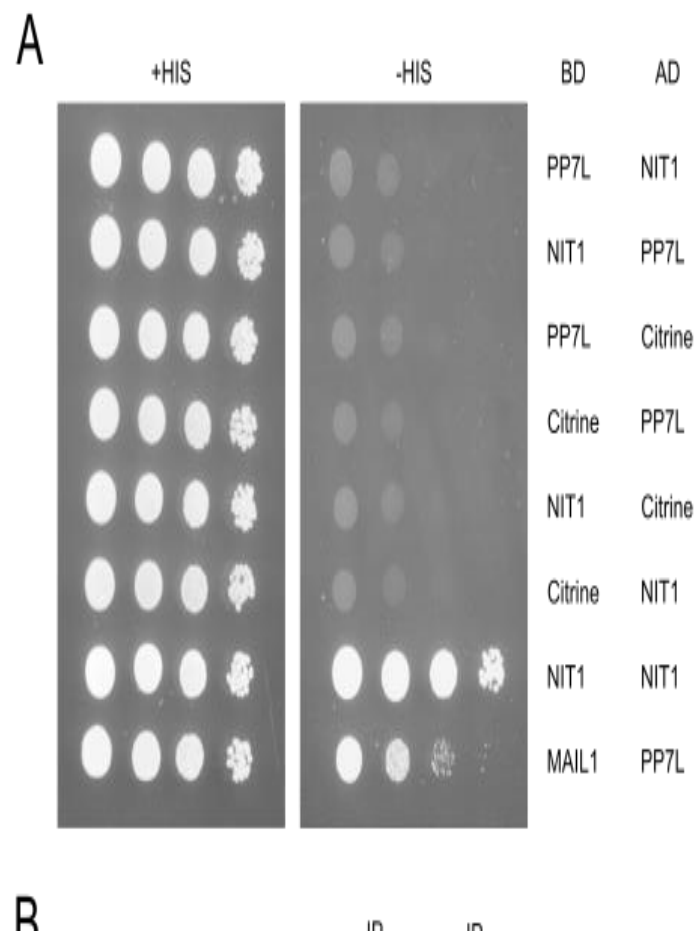


**Figure 20: PP7L and NIT1 do not interact in Y2H or Co-IP/Western blot.** (A) Y2H assay showing no interaction between PP7L and NIT1, but strong NIT1 self-interaction. A serial dilution of yeast colonies was spotted on medium lacking tryptophan and leucine (+HIS) for growth control and on selective medium additionally lacking histidine (-HIS), to analyze the protein-protein interaction. Citrine was used as negative control. PP7L interaction with MAIL1 was used as positive control. BD: DNA-binding domain (pGBT9 vector, N-terminal tag).

AD: Activation domain (pGAD424 vector, N-terminal tag). The data are representative for three independent colonies. **(B)** Co-immunoprecipitation of NIT1 with GFP-tagged PP7L. Proteins were extracted from 7 days-old *pp7l* seedlings expressing PP7L-GFP under its native promoter (Input) or from seedlings expressing gamma-tubulin-GFP, which was used as positive control for GFP antibody (PC). GFP-tagged PP7L or gamma-tubulin were enriched from protein extract using GFP-trap beads and for the PP7L-GFP sample two amounts of IP fraction were loaded (4  $\mu$ l and 30  $\mu$ l). Upper image: White arrowhead mark gamma-tubulin-GFP and black arrowheads mark PP7L-GFP with the expected size of 94 kDa. Asterisks mark unspecific high molecular weight protein detected by GFP antibody. Lower image: Co-immunoprecipitates were probed with anti-NIT1/2/3. Black arrowheads mark NIT1 at the expected size of 40 kDa.

Y2H assay shows physical interaction between proteins, which was not detected for NIT1 and PP7L. This could mean that NIT1 does not directly interact with PP7L, but is still present in the same complex or is connected to PP7L by another protein. To confirm the results from Co-IP/MS analysis, we performed another independent co-immunoprecipitation experiment followed by western blot analysis. Again, PP7L-GFP was extracted from 7 d-old transgenic seedlings precipitated with GFP-trap beads. Immunoprecipitants were analyzed by western blot with GFP-specific antibody to confirm precipitation of PP7L-GFP and a NIT1-specific antibody, which was obtained from our collaboration partner Dr. Pavla Binarova. The results are shown in Fig. 20B. As positive control (PC), immunoprecipitants of GFP-tagged gamma-tubulin were used, which was previously identified as interactor of NIT1 (Doskocilova et al. 2013). As expected, gamma-tubulin-GFP was detected at approximately 80 kDa (white asterisk). In addition, an unspecific high molecular weight protein was detected by the GFP antibody in both, the positive control and the input sample (black asterisks). PP7L-GFP was detected at its expected size of 94 kDa in the input sample and strongly enriched in the IP samples (black arrowheads). NIT1 was detected in the positive control and the input sample at approx. 40 kDa (black arrowheads). No NIT1 could be observed in the IP samples, meaning that NIT1 did not co-immunoprecipitate with PP7L in our experiment. The results from Co-IP/MS analysis could not be reproduced, therefore NIT1 was not further analyzed regarding a functional connection to PP7L.

### 3.4.3 eEF1B subunits and PP7L do not interact in Y2H or Co-IP/Western

The translation elongation factor complex eEF1B is known for its canonical function of GDP/GTP exchange of the eEF1A complex, which transports aminoacyl-tRNAs to the ribosome during translation elongation (Le Sourd et al. 2006). Several additional non-canonical functions have been attributed to eEF1B subunits in various organisms (Sasikumar, Perez, and Kinzy 2012; Negrutskii 2020). In Arabidopsis, the complex consists of three subunits: alpha ( $\alpha$ ), beta ( $\beta$ ) and gamma ( $\gamma$ ). Each subunit is encoded by two genes, whose protein products

show a high sequence similarity (Browning and Bailey-Serres 2015). In the Co-IP/MS experiment of PP7L, we found one alpha-isoform eEF1B $\alpha$ 2, one beta-isoform eEF1B $\beta$ 1 and both gamma isoforms eEF1B $\gamma$ 1 and eEF1B $\gamma$ 2. Each of these isoforms were cloned into the respective Y2H vectors, co-transformed with PP7L in yeast and spotted on selective medium to test for interaction. PP7L-MAIL1 interaction served as positive control and interaction with Citrine served as negative control. However, none of the tested eEF1B subunits showed a positive interaction with PP7L (Figure 21).

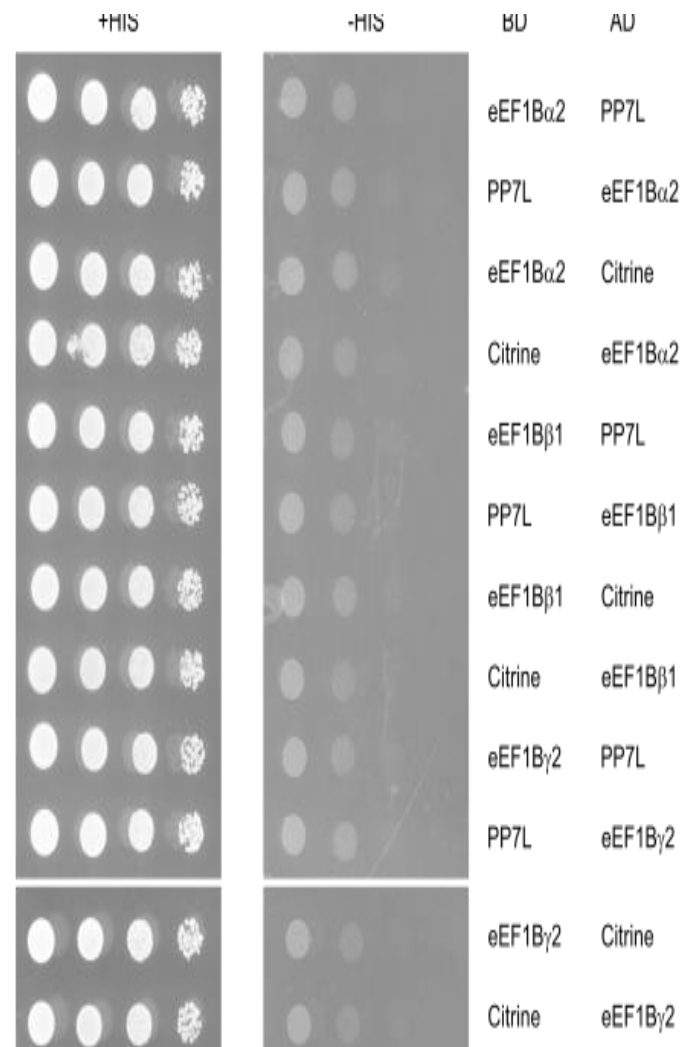


**Figure 21: PP7L and eEF1Bs do not interact in Y2H assay.** Y2H assay testing the interaction between PP7L and the subunits of the eEF1B complex. A serial dilution of yeast colonies was spotted on medium lacking tryptophan and leucine (+HIS) for growth control and on selective medium additionally lacking histidine (-HIS), to analyze the protein-protein interaction. Citrine was used as negative control. PP7L interaction with MAIL1 was used as positive control. BD: DNA-binding domain (pGBT9 vector, N-terminal tag). AD: Activation domain (pGAD424 vector, N-terminal tag). The data are representative for three independent colonies.

To exclude negative effects of the tag orientation of PP7L on the interaction with eEF1B subunits, we additionally tested the interaction of C-terminally tagged PP7L with eEF1B subunits. But again, did not find a positive interaction (Fig. 22).

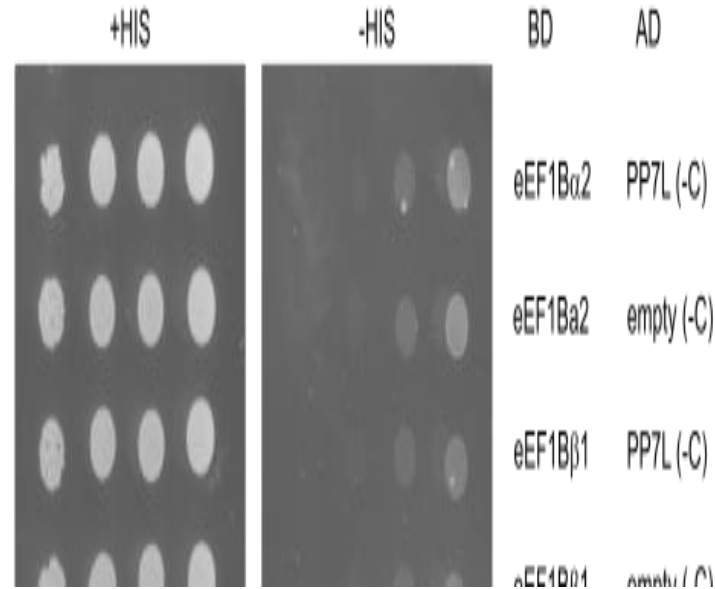


**Figure 22: C-terminally tagged PP7L and eEF1Bs do not interact in Y2H assay.** Y2H assay showing no interaction between PP7L and the indicated subunits of the eEF1B complex. A serial dilution of yeast colonies was spotted on medium lacking tryptophan and leucine (+HIS) for growth control and on selective medium additionally lacking histidine (-HIS), to analyze the protein-protein interaction. Citrine was used as negative control. PP7L interaction with MAIL1 was used as positive control. BD: DNA-binding domain (pGBT9 vector, N-terminal tag). AD: Activation domain (pGADCF vector, C-terminal tag). The data are representative for two independent colonies.

Altogether, the interaction of PP7L with potential interaction partners identified in Co-IP/MS could not be confirmed. Neither interaction with NIT1 nor interaction with eEF1B subunits could be verified. Nonetheless, they might still be part of the same complex and/or be connected to PP7L by another protein. Nitrilases have been extensively studied and mutants have been characterized (Piotrowski 2008; Duskocilova et al. 2013). Therefore, NIT1 has not been further analyzed in my studies. eEF1B subunits have not been fully characterized in plants so far. Studies from other organisms showed that eEF1Bs have, in addition to their canonical function in protein translation, also important roles in different developmental processes and stress responses. To find out whether plant eEF1B has similar canonical and non-canonical functions, deeper analysis of eEF1B subunits in *Arabidopsis* was performed during my PhD.

## 4 Results: Characterization of translation elongation complex eEF1B

Functional protein biosynthesis and homeostasis is essential for plant survival. Translation is an important step during protein synthesis, which is a highly regulated process ensuring protein homeostasis. At unfavorable conditions, general translation is downregulated to protect newly synthesized proteins e.g. against misfolding. Regulation of translation at the initiation step has been extensively studied in different organisms and has been regarded as rate-limiting step (Shah et al. 2013). The importance of regulation at translation elongation and termination has been neglected for a long time, but has lately become of interest. In yeast and in human cells, different mechanisms regulating protein biosynthesis rates by adaption of translation elongation have been described (Torrent et al. 2018; Negrutskii et al. 2018). The translation elongation factor complex eEF1B is known for its canonical function as GDP/GTP exchange factor in translation elongation. In different mammalian cells, several non-canonical functions have additionally been attributed to the different eEF1B subunits (Le Sourd et al. 2006; Sasikumar, Perez, and Kinzy 2012; Negrutskii 2020), but whether eEF1B is part of translational downregulation in response to stress is not yet elucidated. The knowledge of plant eEF1B is largely based upon sequence homology to mammalian eEF1B. Only one study has analyzed the function of the eEF1B $\beta$  subunit in Arabidopsis (Hossain et al. 2012). Here, the Arabidopsis eEF1B subunits have been studied regarding their role in plant development, stress response and translational regulation.

### 4.1 Compositional analysis of the eEF1B complex

The structure of the eEF1B complex is differing between organisms. In yeast, the complex is composed of two subunits eEF1B $\alpha$  and eEF1B $\gamma$  (Jeppesen et al. 2003). In human cells, the eEF1B complex was shown to form a heterotrimeric complex of eEF1Ba, eEF1B $\beta$  (alternatively named as eEF1B $\delta$  in literature) and eEF1B $\gamma$  (Bondarchuk et al. 2022). All described structures of eEF1B complexes have in common that the eEF1B $\gamma$  is described as the structural component connecting the other subunits (Sasikumar, Perez, and Kinzy 2012). The structure of the eEF1B complex in plants has not been studied so far. From literature, it is known that in plants, three subunits, eEF1B $\alpha$ , eEF1B $\beta$  and eEF1B $\gamma$  are part of the complex (Le Sourd et al. 2006). Here, we used two different methods to analyze the intra-complex interactions. First, we used yeast-two hybrid assays to detect physical protein-protein interactions. Second, we analyzed these interactions *in planta* with co-immunoprecipitation assays.

Each eEF1B subunit is encoded by two genes in Arabidopsis (see Table 1). Expression studies published in the eFP browser showed that the eEF1B $\alpha$ 2 and the eEF1B $\beta$ 1 gene were higher expressed than the corresponding second gene (Klepikova et al. 2016). Therefore, the higher expressed eEF1B $\alpha$ 2 and the eEF1B $\beta$ 1 were chosen for interaction assays, while for eEF1B $\gamma$  subunit both genes (eEF1B $\gamma$ 1 and eEF1B $\gamma$ 2) were tested. Upon interaction between the tested proteins, transformed yeast is able to grow on selection medium (-HIS). The same clones as used for interaction test with PP7L (Fig. 21) were utilized. Interestingly, positive interactions were found for eEF1B $\beta$ 1 with eEF1B $\alpha$ 2, with eEF1B $\gamma$ 1 and with eEF1B $\gamma$ 2. No interaction was detected between eEF1B $\alpha$ 2 with eEF1B $\gamma$ 1 or with eEF1B $\gamma$ 2 (Fig. 23A). Also, eEF1B $\gamma$ 1 and eEF1B $\gamma$ 2 did not interact with each other. Negative controls testing for interaction of eEF1B subunits with the unrelated Citrine protein remained without yeast growth. Interaction between MAIL1 and PP7L served as positive control (Fig. 23A).

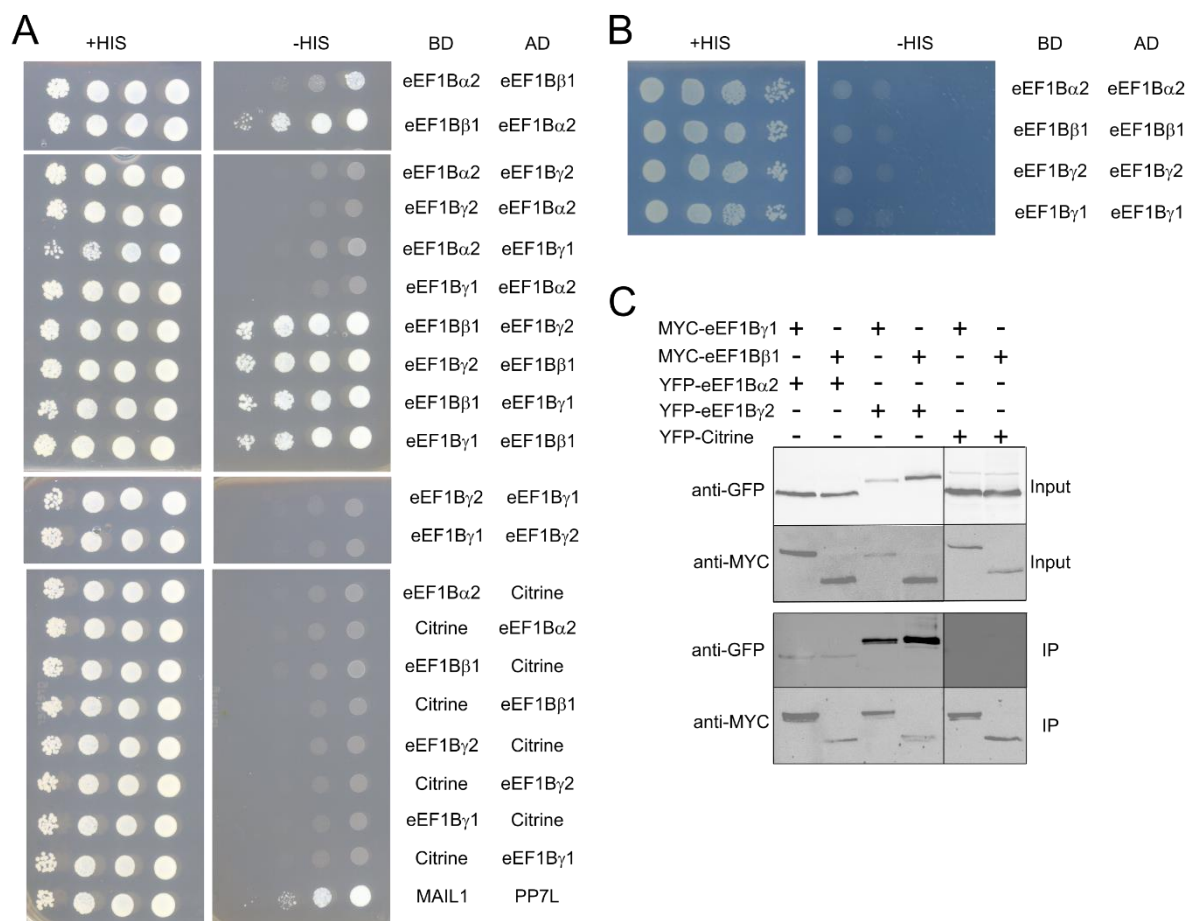


**Figure 23: Interaction studies of eEF1B complex.** (A) GAL4-based yeast-two-hybrid assay (Y2H) testing for direct interaction of eEF1B $\alpha$ 2, eEF1B $\beta$ 1, eEF1B $\gamma$ 1 and eEF1B $\gamma$ 2 with each other on growth control medium (+HIS) and selection medium (-HIS). As negative control, the interaction of eEF1B subunits with Citrine was tested. As positive control, the interaction between MAIL1 and PP7L was used. BD: DNA-binding domain, AD:

Activation domain. Data are representative for three independent replicates. **(B)** GAL4-based yeast-two-hybrid assay (Y2H) testing the interaction of eEF1B $\alpha$ 2, eEF1B $\beta$ 1, eEF1B $\gamma$ 1 and eEF1B $\gamma$ 2 with themselves on growth control medium (+HIS) and selection medium (-HIS). BD: DNA-binding domain, AD: Activation domain. Data are representative for three independent replicates. **(C)** Co-immunoprecipitation assay to test for *in planta*-interaction between different eEF1B subunits. MYC-tagged eEF1B $\gamma$ 1 and eEF1B $\beta$ 1 were co-expressed with YFP-eEF1B $\gamma$ 2 or eEF1B $\alpha$ 2 in Arabidopsis protoplasts (Input). MYC tagged proteins were coupled to MYC trap beads and co-immunoprecipitating YFP-tagged protein interaction partners were detected with western blot analysis (IP). Data are representative for three independent replicates.

In other organisms, the eEF1B complex is found as dimer or trimer showing that the eEF1B subunits not only interact with each other, but also with themselves (Sasikumar, Perez, and Kinzy 2012; Mansilla et al. 2002; Bondarchuk et al. 2022). For example, human eEF1B $\beta$  self-associates and is thereby responsible for the trimerization of the human eEF1B complex (Bondarchuk et al. 2022). To analyze a possible oligomerization of the Arabidopsis eEF1B complex, eEF1B $\alpha$ 2, eEF1B $\beta$ 1, eEF1B $\gamma$ 1 and eEF1B $\gamma$ 2 were tested in Y2H assays for self-interaction. None of the proteins self-interacted (Fig. 23B).

The Y2H assays showed that the eEF1B subunits physically interacted with each other. Next, the interaction should be analyzed in plant cells using co-immunoprecipitation. To this end, eEF1B $\gamma$ 1 and eEF1B $\beta$ 1 were cloned into the plant expression vector pEG203, which allowed expression under a 35S-promotor with an N-terminally coupled MYC-tag. eEF1B $\gamma$ 2, eEF1B $\alpha$ 2 and Citrine were cloned into the plant expression vector pEG104, which enabled expression under a 35S-promotor with an N-terminal YFP-tag. MYC-tagged and YFP-tagged proteins were transiently co-expressed in Arabidopsis protoplasts. A fraction of protoplasts co-expressing the corresponding two proteins was used as 'Input' sample. For immunoprecipitation, protein extracts from protoplasts were mixed with MYC-trap beads. Immunoprecipitated MYC-tagged proteins and co-immunoprecipitated YFP-tagged proteins were detected by western blot. Overall, an interaction between each of the tested eEF1B subunits was found (Fig. 23C). No interaction was found between YFP-Citrine and MYC-eEF1B $\gamma$ 1 or MYC-eEF1B $\beta$ 1. Together these results show that, as expected from other organisms, all three subunits are part of the same protein complex. Interestingly, the Y2H results indicate an important structural role of the eEF1B $\beta$  subunit in the eEF1B complex.

## 4.2 Analysis of the eEF1B $\beta$ subunit

### 4.2.1 Expression level of the two eEF1B $\beta$ genes

The eEF1B $\beta$  subunit is described to be plant-specific. It contains a C-terminal guanine exchange factor domain, which is responsible for its canonical function in GDP/GTP exchange on eEF1A (Le Sourd et al. 2006). The eEF1B $\beta$  subunit is encoded by two genes, *eEF1B $\beta$ 1* (AT1G30230) and *eEF1B $\beta$ 2* (AT2G18110). According to RNA-Seq data from the eFP browser both genes are expressed in all plant tissues, but *eEF1B $\beta$ 1* is generally higher expressed than *eEF1B $\beta$ 2* in most tissues (Klepikova et al. 2016).

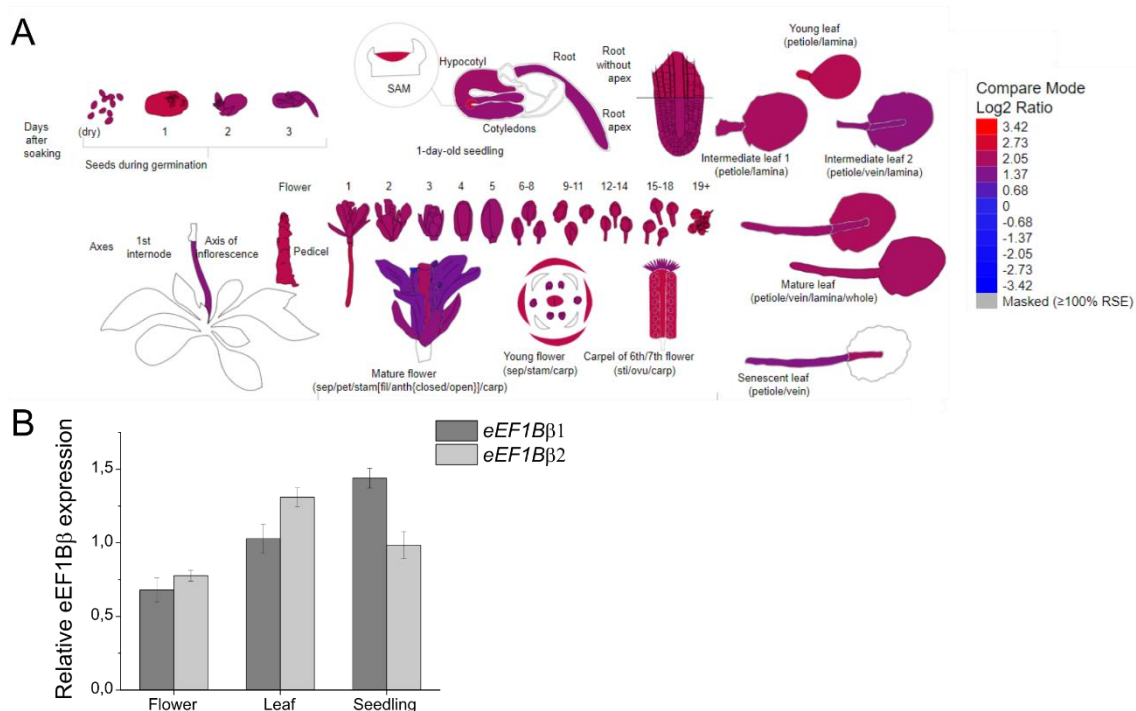


**Figure 24: Comparison of transcript levels of eEF1B $\beta$ 1 and eEF1B $\beta$ 2 in different tissues of WT plants. (A)** Image showing the comparison of eEF1B $\beta$ 1 to eEF1B $\beta$ 2 expression levels in different WT plant tissues. The red color demonstrates that eEF1B $\beta$ 1 is expressed log2 ratio of 3.42 higher expressed than eEF1B $\beta$ 2, while blue color would demonstrate a lower expression of eEF1B $\beta$ 1 compared to eEF1B $\beta$ 2. This image was generated with the Klepikova eFP (RNA-Seq data) at [bar.utoronto.ca/eplant](http://bar.utoronto.ca/eplant) by (Waese et al. 2017). **(B)** Relative transcript levels of eEF1B $\beta$ 1 and eEF1B $\beta$ 2 found in RNA extracted from WT flowers, leaves or seedlings using qRT-PCR. Data represent means from three independent replicates  $\pm$ SE. No significant differences were found between eEF1B $\beta$ 1 and eEF1B $\beta$ 2 expression in any tested tissue using Student's *t*-test ( $P \leq 0.05$ ).

A comparison showing the log<sub>2</sub> fold change between the expression level of eEF1B $\beta$ 1 and eEF1B $\beta$ 2 in different tissues according to the Klepikova RNA-Seq data is presented in Fig 24A. The RNA-Seq data suggests a log<sub>2</sub> fold higher expression of eEF1B $\beta$ 1 in seedlings and leaves

of 1 to 2, whereas the difference is less pronounced in mature flowers. To validate the higher expression of eEF1B $\beta$ 1 with an independent method, RT-qPCR was performed on RNA extracted from mature flowers, mature leaves (both from 4 weeks-old plants) and from 7 days-old seedlings. Since both eEF1B $\beta$  genes have a sequence similarity of 92% (see Fig. 73 - Sequence alignment of cDNAs in Appendix), primers used for RT-qPCR were first tested for specificity on plasmid DNA. Only primers specifically binding to one of the two genes were used. RT-qPCR revealed no significant differences between eEF1B $\beta$ 1 and eEF1B $\beta$ 2 expression in any of the tested tissues (Fig. 24B).

#### 4.2.2 Two splicing variants of the eEF1B $\beta$ 1 gene

The eEF1B $\beta$  subunit contains several conserved protein domains. A glutathione *S*-transferase-like domain is located at the N-terminus and the guanine exchange factor (GEF) domain is located at the C-terminus (Fig. 25A). In the linker region between both domains are two intrinsically disordered regions (IDRs). These domains are present in both protein isoforms, eEF1B $\beta$ 1 and eEF1B $\beta$ 2. For *eEF1B $\beta$ 1*, two splicing variants, *eEF1B $\beta$ 1.1* and *eEF1B $\beta$ 1.2*, are annotated in TAIR with *eEF1B $\beta$ 1.2* being suggested as representative gene model ([www.arabidopsis.org](http://www.arabidopsis.org)). The differential splicing leads to two different protein splicing variants. eEF1B $\beta$ 1.1 is lacking the last 29 amino acids at the C-terminus (behind the GEF domain), because the differential splicing leads to a premature STOP codon in *eEF1B $\beta$ 1.1* (Fig. 25A). This led us to analyze, whether there is a difference in the functionality of both proteins resulting from differential splicing. During the PCR amplification of *eEF1B $\beta$ 1* sequence from cDNA for cloning using primers designed for *eEF1B $\beta$ 1.2*, only the *eEF1B $\beta$ 1.1* splicing variant harboring the premature STOP codon could be obtained. Clones containing this *eEF1B $\beta$ 1.1* sequence have been used in Y2H assays (Fig. 23A) showing a positive interaction with eEF1B $\alpha$  and eEF1B $\gamma$  subunits. Site-directed mutagenesis was used to generate *eEF1B $\beta$ 1.2* sequence. Afterwards, it was cloned in the yeast expression vectors pGBT9 and pGAD424 and its interaction with the other subunits of the eEF1B complex was analyzed (Fig. 25B). In contrast to eEF1B $\beta$ 1.1, the eEF1B $\beta$ 1.2 splicing variant protein did not interact with eEF1B $\alpha$ 2, eEF1B $\gamma$ 1 or eEF1B $\gamma$ 2.

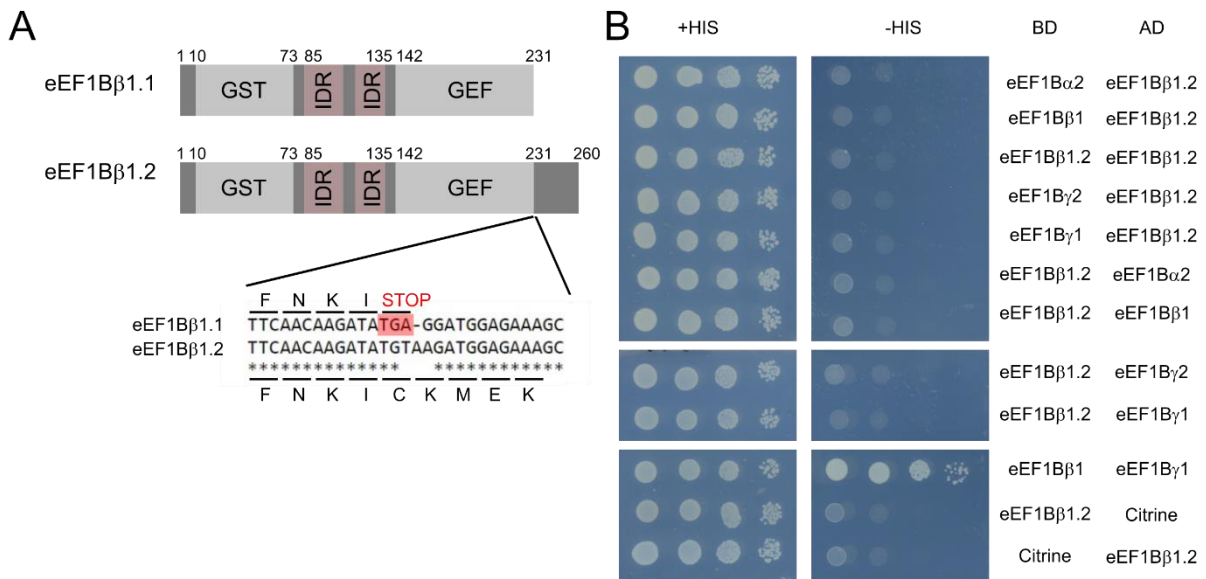


**Figure 25: Differences in protein structure and protein interactions of the two splicing variants of eEF1Bβ1.**

(A) Protein structures with the annotated domains of eEF1Bβ1.1 and eEF1Bβ1.2 (GST: glutathione S-transferase-like domain; IDR: intrinsically disordered region; GEF: guanine exchange factor domain). Until the end of the GEF domain, protein sequences of the two splicing variants are 100% identical. Due to the differential splicing, a premature STOP codon originated at the end of the GEF domain in eEF1Bβ1.1. Alignment of the cDNAs of the two splicing variants at the affected site together with the resulting translated sequences are shown. Alignment was performed with Clustal Omega (<https://www.ebi.ac.uk/Tools/msa/clustalo/>). (B) Y2H assay testing the interaction of eEF1Bβ1.2 with the other subunits of the eEF1B complex shows that eEF1Bβ1.2 does not interact with the other eEF1B subunits. Dilution series of transformed yeast was spotted on growth control medium (+HIS) and selection medium (-HIS). As negative control, the interaction of eEF1Bβ1.2 with Citrine was tested. As positive control, the interaction between eEF1Bβ1 and eEF1Bγ1 was used. BD: DNA-binding domain, AD: Activation domain. Data are representative for three independent replicates.

To find out, whether the different protein splicing variants are influencing subcellular protein localization, both proteins were transiently expressed in Arabidopsis protoplasts as N-terminally tagged YFP-fusion proteins. YFP-eEF1Bβ1.1 showed a uniform cytosolic localization. Contrarily, YFP-eEF1Bβ1.2 localized in large aggregates in the cytosol (Fig. 26). Collectively, the data indicate that eEF1Bβ1.2 might not be expressed normally inside the cell and high expression of eEF1Bβ1.2 leads to incorrect protein folding. Instead eEF1Bβ1.1 appears to be the functional protein, which is why eEF1Bβ1.1 was used in all subsequent experiments.

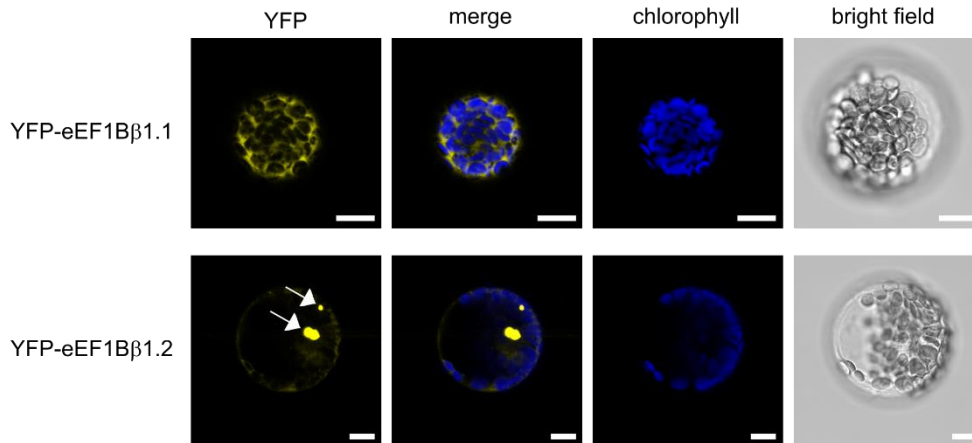


**Figure 26: Subcellular localization of the two splicing variants of eEF1B $\beta$ 1.** Representative confocal images of protoplasts transiently expressing N-terminally tagged YFP-eEF1B $\beta$ 1.1 or YFP-eEF1B $\beta$ 1.2 under a 35S promoter. Arrows indicate large protein aggregates. Scale bar is 10  $\mu$ m.

#### 4.2.3 Characterization of T-DNA insertion lines of eEF1B $\beta$ 1 and eEF1B $\beta$ 2

So far, only one functional characterization of eEF1B $\beta$  was published in plants describing functions of Arabidopsis eEF1B $\beta$  in plant development and cell wall formation. A loss-of-function mutant of *eEF1B $\beta$ 1* (named hereafter *eef1b $\beta$ 1-1*) showed a severe dwarf phenotype with reduced vascular apparatus, lignin and cellulose levels (Hossain et al. 2012). To analyze the role of eEF1B $\beta$  in plant development and translational regulation in detail, two additional T-DNA insertion lines for *eEF1B $\beta$ 1* and also two T-DNA insertion lines for *eEF1B $\beta$ 2* were obtained. Plants were identified as homozygous by genotyping. PCR products of genotyping for the T-DNA insertion were analyzed by sequencing to identify the exact T-DNA insertion site. In line *eef1b $\beta$ 1-2*, the T-DNA was inserted in the first intron and in line *eef1b $\beta$ 1-3* it was positioned in the fourth intron (Fig. 27A). The insertion site in line *eef1b $\beta$ 2-1* was placed in the fourth exon, while the T-DNA was inserted in extragenic region behind the 3'UTR of *eEF1B $\beta$ 2* in line *eef1b $\beta$ 2-2* (Fig. 27A). Line *eef1b $\beta$ 2-2* was excluded from further experiments, because the T-DNA position is far away from the gene of interest.

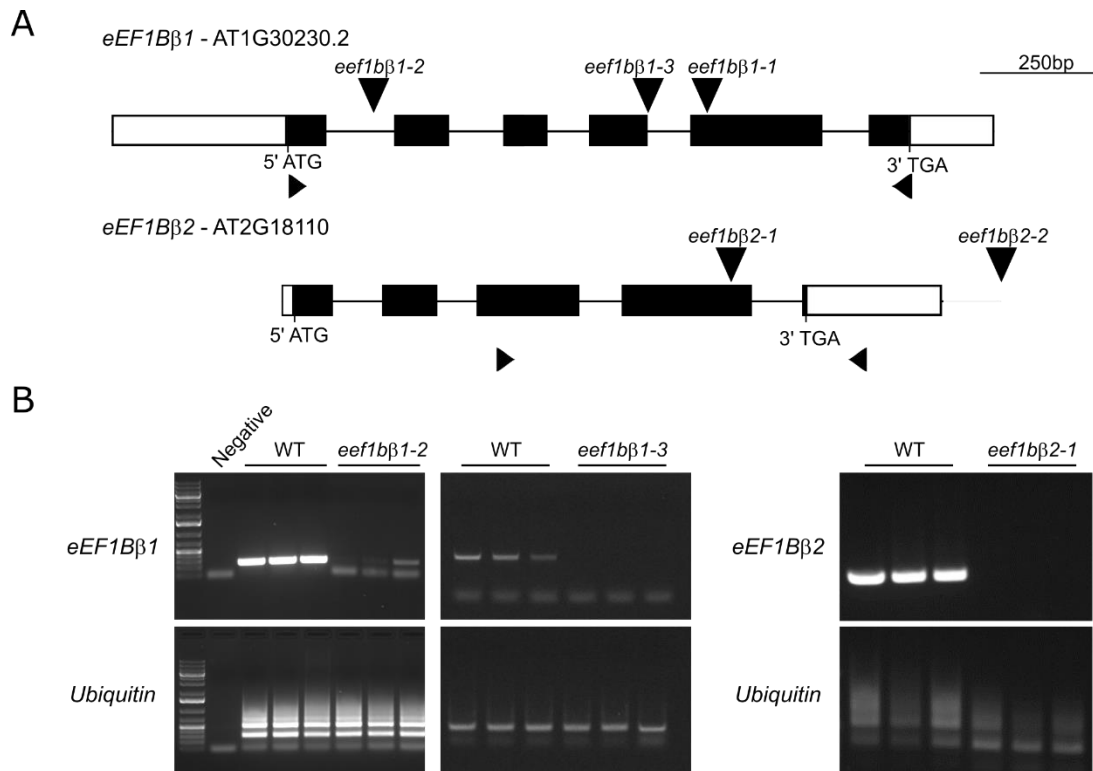


**Figure 27: Analysis of T-DNA insertion lines of *eEF1Bβ1* and *eEF1Bβ2*.** (A) Gene structure of *eEF1Bβ1* and *eEF1Bβ2* with exons (black boxes), introns (black lines), 5'- and 3'-UTRs (white boxes), T-DNA insertion sites (black, vertical arrowheads), and primers used for RT-PCR shown in (B) (small, black arrowheads). Grey line in gene structure of *eEF1Bβ2* represents extragenic region after the 3'-UTR. (B) RT-PCR products separated on an agarose gel. RT-PCR was performed on RNA isolated from three independent plants of WT or the indicated T-DNA insertion line. RT-PCR of *eef1bβ1-2* was performed by Mahsa Nasimi (as part of her lab rotation under my supervision). RT-PCR of *eef1bβ2-1* was performed by Felix Thies (as part of his bachelor thesis under my supervision). Primer sequences are listed in 2.7. *UBIQUITIN* was used as reference gene.

RT-PCR was performed to analyze whether the obtained T-DNA insertion lines still contained full length transcript. To this end, RNA was extracted from leaf tissue of each mutant line and of WT. Primers used for RT-PCR are shown in Fig. 27A as small black triangles below the corresponding gene structure. For analysis of *eEF1Bβ1* transcript, primers spanning from START till STOP codon including the respective T-DNA insertion site were used. As expected, the *eEF1Bβ1* transcript was detected in WT samples (Fig. 27B). No transcript was detected in *eef1bβ1-3* samples showing that the T-DNA insertion successfully disrupted expression of full-length transcript in line *eef1bβ1-3*. But for line *eef1bβ1-2*, two out of three samples still showed a faint band indicating expression of full-length transcript (Fig. 27B). This might indicate that the genotyping of these two samples as homozygous was incorrect or that the primers are binding unspecific. Since *eEF1Bβ1* and *eEF1Bβ2* sequences have 92% similarity, it is difficult to design primers that have no overlap with the other gene. In case of the primers used for

*eEF1Bβ1*, the forward primer contains only three mismatches to the *eEF1Bβ2* sequence. This might be a reason for unspecific binding. Primers binding to *UBIQUITIN* were used for reference excluding an unequal loading of samples.

To circumvent the difficulties with specific primers for transcript analysis and to analyze whether the expression of eEF1Bβ protein was decreased by the T-DNA insertions, the protein levels in the eEF1Bβ T-DNA insertional lines were analyzed by western blotting using an eEF1Bβ-specific antibody. Both protein sequences of eEF1Bβ1 and eEF1Bβ2 share 94% identity, so the obtained polyclonal eEF1Bβ antibody binds both proteins. For loading control, the same membrane was probed with an ACTIN-specific antibody. Four independent experiments were performed with slightly varying results. A representative western blot is shown on the left panel of Fig. 28A. The eEF1Bβ band intensities were quantified and normalized against the ACTIN band intensities for each of the four experiments. The value of WT sample was set to 100%, so that for each T-DNA line a relative percentage compared to WT eEF1Bβ could be calculated. The mean of the four experiments is shown in the graph of Fig. 28A. Line *eef1bβ1-2* and *eef1bβ1-3* displayed significantly reduced eEF1Bβ protein levels, whereas protein levels were slightly, but not significantly reduced in line *eef1bβ2-1*. Surprisingly, no reduced protein levels were detected for the previously published *eef1bβ1-1* line. This was unexpected, since this mutant had been described to display a strong growth phenotype, which was rescued by introduction of an *35S:eEF1Bβ1-YFP* construct (Hossain et al. 2012), implying that a lack of eEF1Bβ1 leads to the phenotype.

Since eEF1Bα and eEF1Bβ share around 58% protein sequence similarity, we hypothesized that the eEF1Bβ-antibody might bind unspecific to eEF1Bα as well. To test antibody specificity, western blot analysis was performed on protein extracts from protoplasts transiently expressing YFP-tagged eEF1Bα2, eEF1Bβ1 or eEF1Bγ2 under a *35S* promoter. Additionally, untransformed protoplasts were used for control. Using an GFP antibody, all three YFP-tagged proteins were detected, while no protein was detected in the untransformed sample (Fig. 28B). The eEF1Bβ antibody strongly detected YFP-eEF1Bβ, but also detected YFP-eEF1Bα2. YFP-eEF1Bγ2 was not detected. In addition, in all samples (including the untransformed sample) native eEF1Bβ was detected. Consequently, the eEF1Bβ antibody does bind unspecific to eEF1Bα, if it is present in excess (expression from *35S*). But the eEF1Bβ antibody apparently does not bind to eEF1Bα at native protein level, since no native eEF1Bα was detected. Native eEF1Bα has a theoretical molecular weight of 24.2 kDa, whereas native eEF1Bβ has a

theoretical molecular weight of 28.8 kDa. If the eEF1B $\beta$  antibody would bind to native eEF1B $\alpha$  a double band would have been detected.

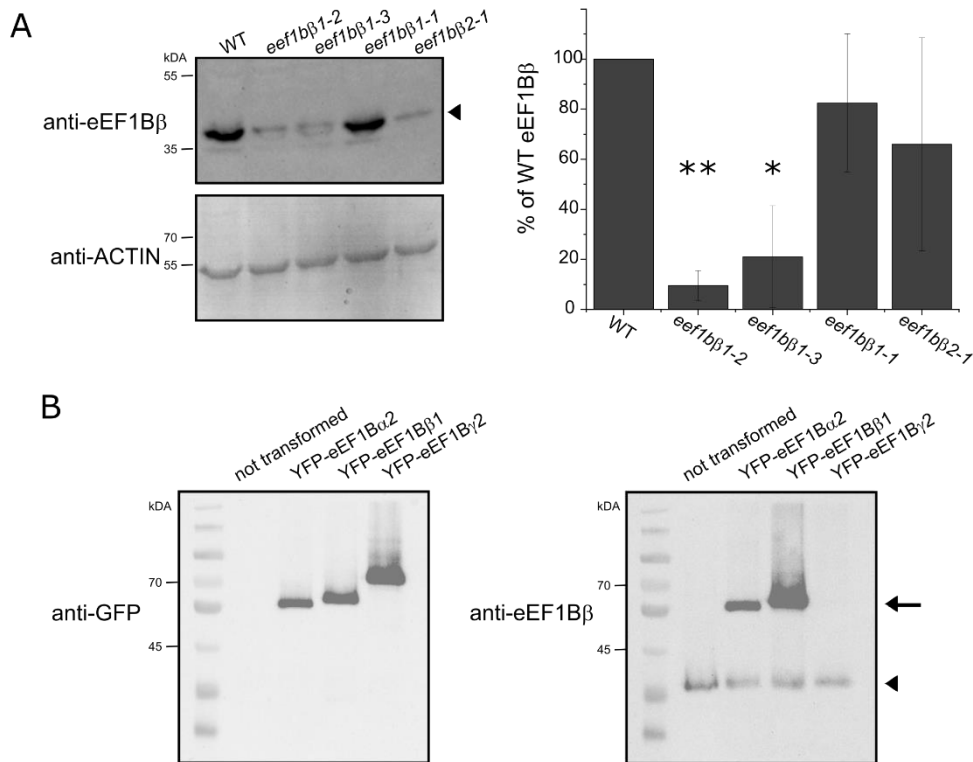


**Figure 28: Protein levels of eEF1B $\beta$  in T-DNA insertion lines. (A)** Immunoblots showing the expression of eEF1B $\beta$  or ACTIN in WT or the indicated mutant lines. Proteins were extracted from seven-days-old seedlings grown in liquid MS cultures. Per sample 15  $\mu$ g of total protein extract were loaded on the SDS gel. Immunoblots were first probed with an eEF1B $\beta$  antibody, stripped and re-probed with an ACTIN antibody for loading control. Quantification shows percentage of eEF1B $\beta$  level compared to WT (with WT set to 1 in each experiment). Data represents means  $\pm$ SE from four independent experiments. **(B)** Specificity test of eEF1B $\beta$  antibody used in (A). Protein extracts from protoplasts transiently expressing YFP-eEF1B $\alpha$ 2, YFP-eEF1B $\beta$ 1 or YFP-eEF1B $\gamma$ 2 from a constitutive 35S promoter were analyzed by immunoblotting using anti-GFP as control or anti-eEF1B $\beta$  for specificity test. As additional negative control, protein extract from untransformed protoplasts were tested. Arrow points towards YFP-tagged eEF1B $\beta$ . Arrowhead marks native eEF1B $\beta$ .

The phenotypes of the different mutant lines of eEF1B $\beta$  were analyzed to find out whether the altered transcript and protein levels lead to phenotypic changes. First, seedlings were grown on vertical placed MS plates and root growth was monitored at 4, 7 and 10 dag (Fig. 29A and 29B). No significant differences between the T-DNA lines and the WT were observed. Also, at later developmental stages, the mutant lines resembled the WT (Fig. 29C and 29D). These results were unexpected for several reasons. First, the WT-like phenotype of *eef1b $\beta$ 1-1* mutant is contradictory to the previously published dwarf phenotype (Hossain et al. 2012). Currently, it

is unknown what the reason for the discrepancy in the observed phenotypes is. Second, at least for the lines with reduced eEF1B $\beta$  protein level (*eef1b $\beta$ 1-2* and *eef1b $\beta$ 1-3*), a phenotypic change would have been expected. Possibly, the remaining eEF1B $\beta$  protein level is sufficient for the cells to fulfill its function. Therefore, in order to study the specific function of eEF1B $\beta$ , crosses between the single mutants of *eEF1B $\beta$ 1* and *eEF1B $\beta$ 2* were performed to generate eEF1B $\beta$  double mutants.

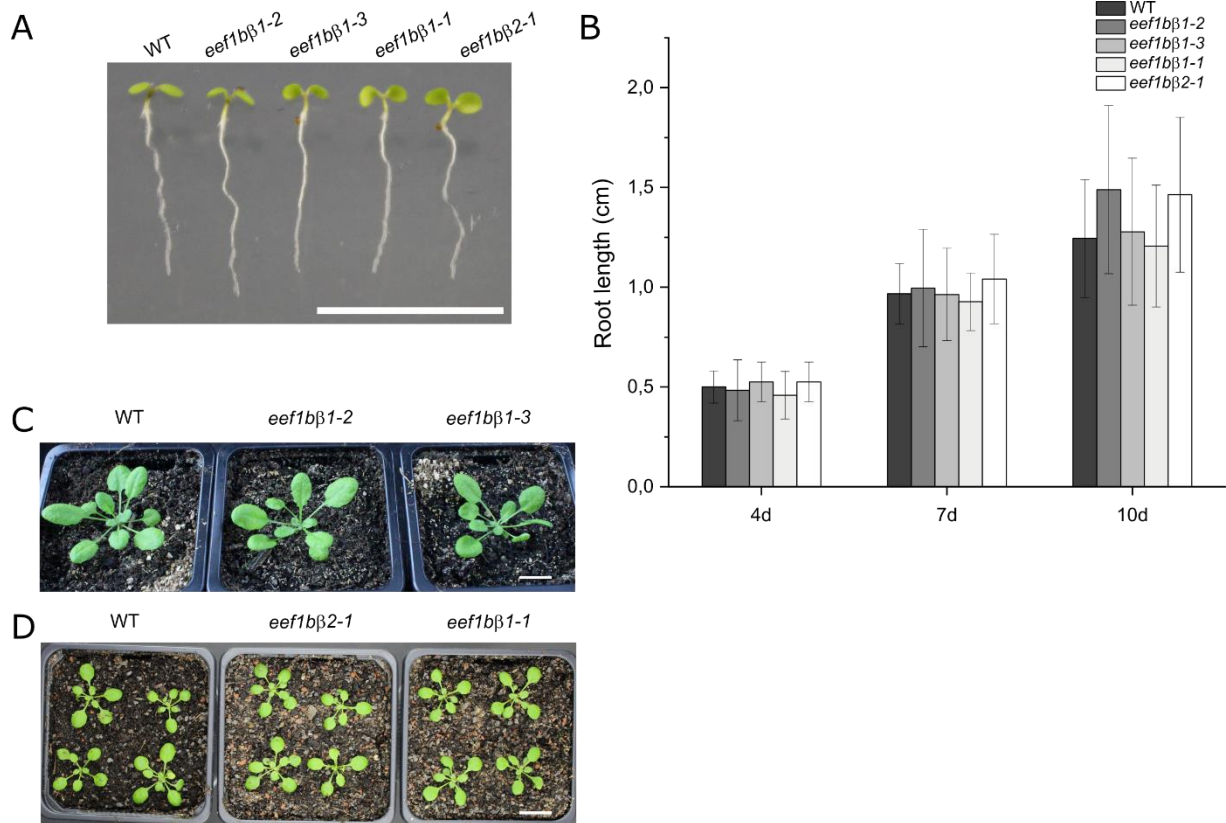


**Figure 29: Phenotype of T-DNA insertion lines of *eEF1B $\beta$ 1* and *eEF1B $\beta$ 2*.** (A) Image of seven-days-old seedlings of WT and the indicated mutant lines grown on vertical MS plates. (B) Root length measurement of WT and the indicated mutant lines grown for 4 d, 7 d or 10 d on solid vertical MS plates. Root length was measured using ImageJ software ( $n \geq 30$ ). Data represent means  $\pm$ SE. (C) Representative pictures of 24 days-old WT, *eef1b $\beta$ 1-2* and *eef1b $\beta$ 1-3* plants grown on soil. Scale bar is 1 cm. (D) Representative pictures of 21 days-old WT, *eef1b $\beta$ 2-1* and *eef1b $\beta$ 1-1* plants grown on soil. Scale bar is 2 cm.

#### 4.2.4 Generation of eEF1B $\beta$ double mutants

For generation of eEF1B $\beta$  double mutants, *eef1b $\beta$ 2-1* was crossed with either *eef1b $\beta$ 1-2* or *eef1b $\beta$ 1-3*. The F1 generation was genotyped and as expected all plants were heterozygous for both genes (crossing and genotyping of F1 was performed by Felix Thies as part of his bachelor thesis under my supervision). F1 generation was self-pollinated and in the F2 generation genotyping was repeated. No double homozygous plants were identified from 63 plants of

*eef1bβ1-2 eef1bβ2-1*. According to Mendelian law, 1 out of 16 plants would be expected to be double homozygous. Six plants were found to be homozygous for *eef1bβ1-2* and heterozygous for *eef1bβ2-1*, whereas no plant was found to be heterozygous for *eef1bβ1-2* and homozygous for *eef1bβ2-1* (Table 3).

**Table 3:** Genotyping results of F2 generation from crossing *eef1bβ1-2*<sup>+/-</sup> with *eef1bβ2-1*<sup>+/-</sup> (+/+ = WT, +/- = heterozygous, -/- = homozygous). Genotyping PCR was performed twice for each plant.

<i>eef1bβ1-2</i>	<i>eef1bβ2-1</i>	Number of plants
+/+	+/+	3
+/-	+/+	9
-/-	+/+	5
+/+	+/-	19
+/+	-/-	7
+/-	+/-	13
+/-	-/-	0
-/-	+/-	7
-/-	-/-	0
Total number of plants genotyped:		63

The *eef1β1-2*<sup>-/-</sup> *eef1β2-1*<sup>+/-</sup> plants showed a dwarf phenotype (Fig. 30A) compared to all plants, which displayed WT genotype for at least one of the *eEF1Bβ* genes. This could lead to the hypothesis that a double homozygous mutant might be lethal and that already *eef1β1-2*<sup>-/-</sup> *eef1β2-1*<sup>+/-</sup> strongly disturbs plant development and leads to the observed phenotype. But also, some *eef1β1-2*<sup>+/-</sup> *eef1β2-1*<sup>+/-</sup> plants displayed a similar phenotype with reduced growth (Fig. 30B), which would rather imply that the observed phenotype is not dependent on the T-DNA insertions. Further analysis will be needed to clarify, whether mutations in both *eEF1Bβ* genes are lethal. This should also include crosses from more independent T-DNA insertion lines to rule out influences of possible second site insertions. Genotyping of 25 F2 plants from the

*eef1bβ1-3 eef1β2-1* crosses did not yield any double homozygous mutants further supporting a possible lethality of a complete loss of eEF1Bβ.

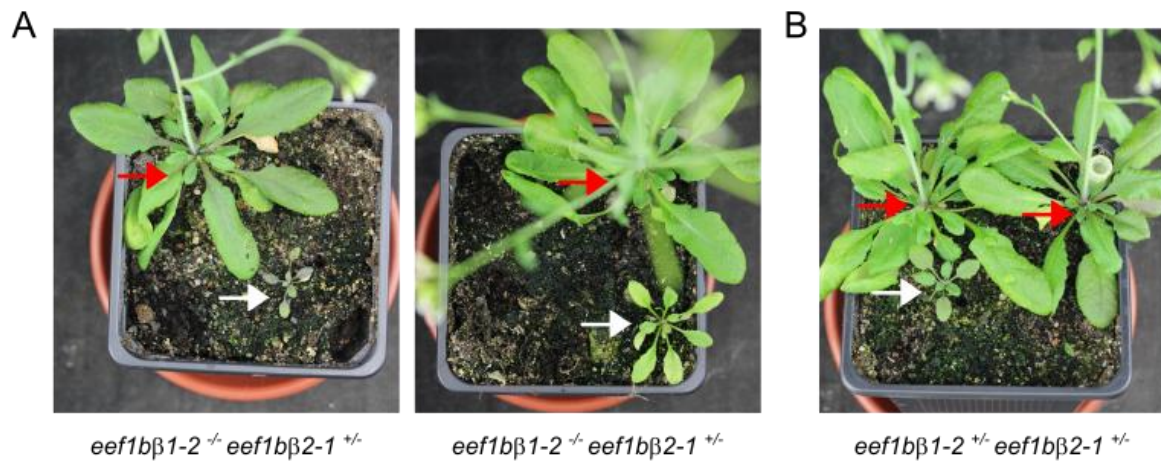


**Figure 30: Phenotype of different genotypes of *eef1bβ1-2 eef1bβ2-1* mutants.** (A) Photograph of 24d-old mutant plants. White arrow marks to a plant of the indicated genotype *eef1bβ1-2<sup>-/-</sup> eef1bβ2-1<sup>+/-</sup>*. Red arrow points to a plant with two WT alleles for *eEF1Bβ1*. (B) Picture of 24d-old mutant plants. White arrow marks a plant of the indicated genotype *eef1bβ1-2<sup>+/-</sup> eef1bβ2-1<sup>+/-</sup>*. Red arrows point to plants, which have both WT alleles for either *eEF1Bβ1* or *eEF1Bβ2* and are heterozygous for the other gene.

### 4.3. Analysis of the eEF1Bγ subunit

#### 4.3.1 Expression of the two eEF1Bγ genes in WT

In Arabidopsis, the eEF1Bγ subunit is encoded by two different genes, *eEF1Bγ1* (AT1G09640) and *eEF1Bγ2* (AT1G57720). Available RNA-Seq data indicate that both genes are ubiquitously expressed in most plant tissues (Klepikova et al. 2016). Fig. 31A shows the comparison of expression levels of *eEF1Bγ1* to *eEF1Bγ2* in different tissues. Yellow color shows an equal expression level of both genes, while red color marks tissues, in which *eEF1Bγ1* is expressed at log<sub>2</sub> fold of 0.93 higher than *eEF1Bγ2*. In most tissues both genes are equally expressed. In young leaves and certain flower stages *eEF1Bγ2* appears to be slightly higher expressed than *eEF1Bγ1*.

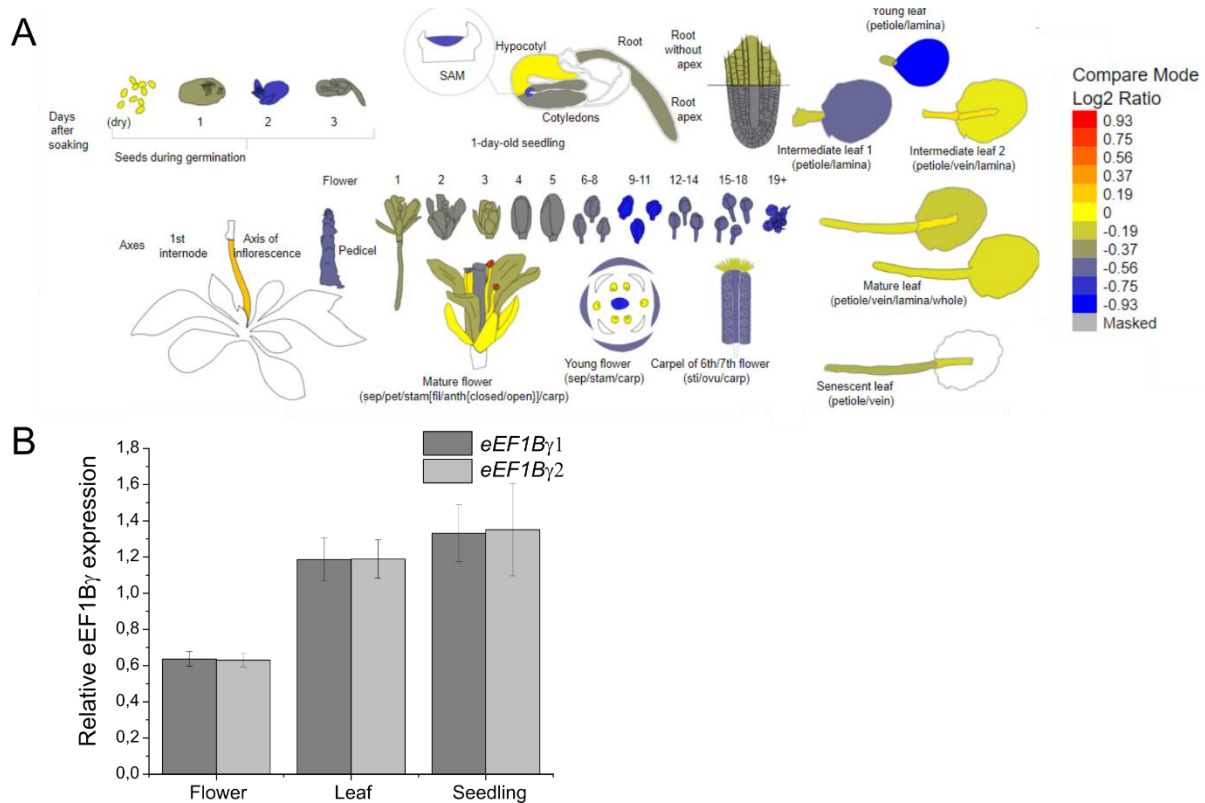


**Figure 31: Expression levels of *eEF1Bγ1* and *eEF1Bγ2* in different WT plant tissues.** (A) Image showing the comparison of *eEF1Bγ1* to *eEF1Bγ2* expression levels in WT plants. The red color demonstrates that *eEF1Bγ1* is expressed log2 ratio of 0.93 higher expressed than *eEF1Bγ2*, while blue color demonstrates a lower expression of *eEF1Bγ1* compared to *eEF1Bγ2*. This image was generated with the Klepikova eFP (RNA-Seq data) at bar.utoronto.ca/eplant by (Waese et al. 2017). (B) Relative transcript levels of *eEF1Bγ1* and *eEF1Bγ2* found in RNA extracted from WT flowers, leaves or seedlings using qRT-PCR. Data represent means from three independent replicates  $\pm$ SE. No significant differences were found between *eEF1Bγ1* and *eEF1Bγ2* expression in any tested tissue using Student's *t*-test ( $P \leq 0.05$ ).

Additionally, transcript levels of both *eEF1Bγ* genes were tested by RT-qPCR. Both genes of *eEF1Bγ* have a cDNA sequence similarity of 86%. Therefore, primers for RT-qPCR have been tested on plasmid DNA for gene-specific binding. Expression levels were analyzed in flowers, leaves and seedlings of WT plants. In all three tissue types, the expression level of *eEF1Bγ1* was similar to *eEF1Bγ2* (Fig. 31B).

#### 4.3.2 N-terminus of eEF1Bγ is necessary for interaction with eEF1Bβ

The compositional analysis of the eEF1B complex using Y2H assays surprisingly revealed that eEF1Bγ is physically interacting with eEF1Bβ, but not with eEF1Bα or itself (Chapter 4.1). To further decipher, which domain of eEF1Bγ is important for the interaction with eEF1Bβ, truncated versions of eEF1Bγ1 and eEF1Bγ2 were generated. The full length eEF1Bγ1 protein

has 414 amino acids, full length eEF1B $\gamma$ 2 has 413 amino acids. Both proteins have two glutathione-S-transferase (GST) domains at the N-terminus coupled via a linker region to the C-terminal eEF1B $\gamma$ -specific protein domain (Fig. 32A). Interestingly, both eEF1B $\gamma$ 1 and eEF1B $\gamma$ 2 contain a conserved phosphorylation site in the N-terminal GST-domain and in the eEF1B $\gamma$ -specific domain (Fig. 32A). To generate truncated versions lacking the C-terminus ( $\Delta$ C), cDNA coding the START codon till base pair 726 (242 aa) of *eEF1B $\gamma$ 1* or cDNA coding the START codon till base pair 669 (223 aa) of *eEF1B $\gamma$ 2* were amplified and an artificial STOP codon was attached. To generate truncated versions lacking the N-terminus ( $\Delta$ N), cDNA from base pair 727 (243aa) till STOP codon of *eEF1B $\gamma$ 1* or from base pair 670 (224 aa) till STOP codon of *eEF1B $\gamma$ 2* were amplified and at N-terminus an artificial START codon was attached. PCR fragments were cloned into yeast expression vectors pGBT9 or pGAD424 using gateway cloning technique. The protein structures of the truncated eEF1B $\gamma$  versions are shown in Fig. 32A.

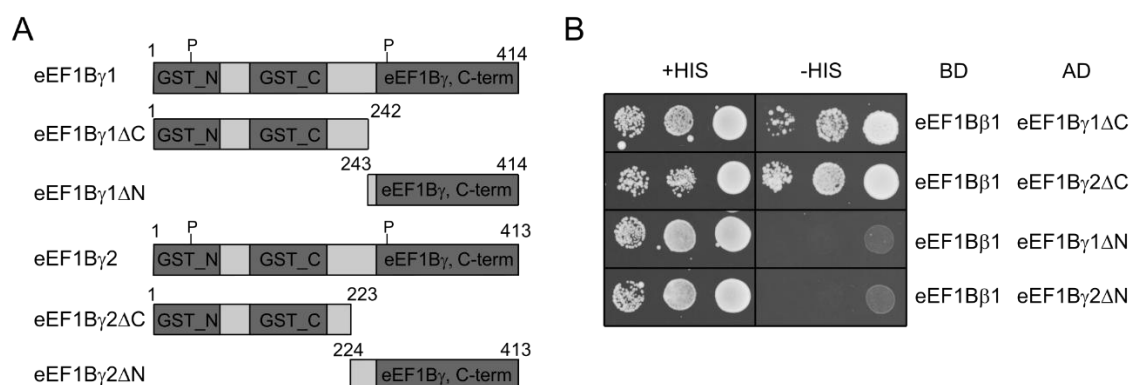


**Figure 32: N-terminal domain of eEF1B $\gamma$  is important for physical interaction with eEF1B $\beta$ 1.** (A) Protein structures with the annotated domains of eEF1B $\gamma$ 1 and eEF1B $\gamma$ 2 (GST\_N: N-terminal glutathione S-transferase-like domain; GST\_C: C-terminal glutathione S-transferase-like domain; eEF1B $\gamma$ , C-term: C-terminal conserved eEF1B $\gamma$ -specific domain) and the generated truncated versions eEF1B $\gamma$ 1 $\Delta$ C, eEF1B $\gamma$ 1 $\Delta$ N, eEF1B $\gamma$ 2 $\Delta$ C and eEF1B $\gamma$ 2 $\Delta$ N. P: phosphorylation site. (B) Y2H assay testing the interaction of the four truncated versions of eEF1B $\gamma$  for interaction with full length eEF1B $\beta$ 1. Dilution series of transformed yeast was spotted on growth control medium (+HIS) and selection medium (-HIS). BD: DNA-binding domain, AD: Activation domain. Data are representative for three independent replicates.

Y2H assays showed that neither eEF1B $\gamma$ 1 $\Delta$ N nor eEF1B $\gamma$ 2 $\Delta$ N is able to interact with eEF1B $\beta$ 1, whereas eEF1B $\gamma$ 1 $\Delta$ C and eEF1B $\gamma$ 2 $\Delta$ C do interact with eEF1B $\beta$ 1 (Fig. 32B). Consequently, the N-terminal domain containing the GST domains is required for the interaction of eEF1B $\gamma$  with

eEF1B $\beta$ 1 in Arabidopsis. This is in accordance with previous studies in mammalian cells, which also showed that the N-terminal domain of eEF1B $\gamma$  is necessary for a physical interaction with eEF1B $\beta$  or eEF1B $\delta$  subunit (Mansilla et al. 2002; Le Sourd et al. 2006). It will be interesting to test whether the interaction of eEF1B $\gamma$  with eEF1B $\beta$  is necessary for the functionality of the whole eEF1B complex.

#### 4.3.2 Characterization of T-DNA insertional lines of eEF1B $\gamma$ 1 and eEF1B $\gamma$ 2

To analyze the function of eEF1B $\gamma$ 1 and eEF1B $\gamma$ 2 *in planta*, two T-DNA insertion lines for each gene were obtained from the Arabidopsis Seed Stock Centre (NASC). Genotyping confirmed that the mutant lines were homozygous for the T-DNA insertions. The exact position of T-DNA was analyzed by sequencing of the sequence flanking the insertion. The T-DNA was positioned in the first intron in line *eef1b $\gamma$ 1-1* and in the seventh exon in *eef1b $\gamma$ 1-2*. In line *eef1b $\gamma$ 2-1*, the T-DNA was inserted in the last exon only a few bases away from the STOP codon. In line *eef1b $\gamma$ 2-2*, the T-DNA was localized in the 3'UTR (Fig. 33A).

The transcript level of *eEF1B $\gamma$ 1* and *eEF1B $\gamma$ 2* in the mutant lines were tested using RT-PCR and RT-qPCR analysis (Fig. 33B and 33C). To this end, RNA was extracted from 7 d-old seedlings of WT and the mutant lines, which had been grown on vertical MS plates, and cDNA was synthesized. Primers amplifying the C-terminal part of *eEF1B $\gamma$ 1* (spanning over the insertion of *eef1b $\gamma$ 1-2*) were used for RT-PCR analyzing *eEF1B $\gamma$ 1* level (Fig. 33A). Primers amplifying *eEF1B $\gamma$ 1* from START until STOP codon could not be used, because these primers contained only two mismatches to the sequence of *eEF1B $\gamma$ 2* and resulted in unspecific binding. RT-PCR analysis revealed that in line *eef1b $\gamma$ 1-1*, the complete C-terminal part of *eEF1B $\gamma$ 1* was still present, whereas it was not expressed in line *eef1b $\gamma$ 1-2* (Fig. 33B). Similar results were obtained by RT-qPCR analysis, which showed a WT-like expression of *eEF1B $\gamma$ 1* in *eef1b $\gamma$ 1-1* and a strongly reduced expression in *eef1b $\gamma$ 1-2* (Fig. 33C).

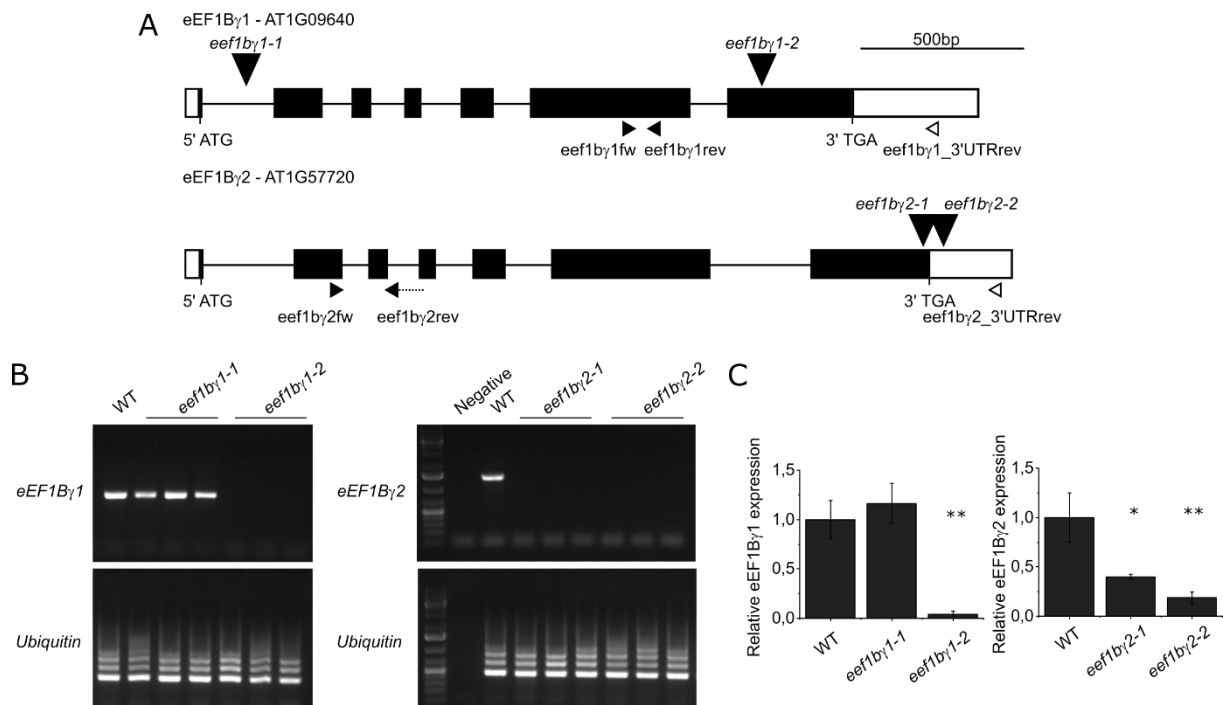


**Figure 33: Analysis of T-DNA insertion lines for eEF1B $\gamma$ 1 and eEF1B $\gamma$ 2.** (A) Gene structure of eEF1B $\gamma$ 1 and eEF1B $\gamma$ 2 showing exons (black boxes), introns (black lines), UTRs (white boxes), T-DNA insertion sites (filled, vertical arrowheads) and the primers used for RT-qPCR (filled, horizontal arrowheads) and RT-PCR (filled and white arrowheads (3'UTRrev)). (B) Agarose gel picture of RT-PCR analysis on RNA isolated from 7 d-old seedlings of WT and the indicated mutant lines. The following primer sets were used: *eef1b $\gamma$ 1fw* and *eef1b $\gamma$ 1\_3'UTRrev* for *eEF1B $\gamma$ 1* expression and *eef1b $\gamma$ 2fw* and *eef1b $\gamma$ 2\_3'UTRrev* for *eEF1B $\gamma$ 2* expression. *UBIQUITIN* was used as reference gene. Negative control contained ddH<sub>2</sub>O instead of cDNA in the PCR reaction. Three biological replicates are shown for each mutant line. RT-PCR was performed by Mahsa Nasimi (as part of her master thesis under my supervision). (C) RT-qPCR analysis examining the transcript level of *eEF1B $\gamma$ 1* and *eEF1B $\gamma$ 2* on RNA isolated from 7-days-old seedlings of WT and mutant lines. Gene-specific primers used for analysis are shown in (A). *FASS* and *SAND* were used as reference genes. WT transcript levels were set to 1 and mutant transcript levels are shown relative to WT. Data represent mean from three biological replicates. Asterisks indicate means differing significantly from WT (two-tail Student's t test; \* P < 0.05; \*\* P < 0.01).

In both lines, *eef1b $\gamma$ 2-1* and *eef1b $\gamma$ 2-2*, no transcript was detected by RT-PCR using primers amplifying from second exon till the 3'UTR (Fig. 33B). The T-DNA insertions of *eef1b $\gamma$ 2-1* and *eef1b $\gamma$ 2-2* are located in the last exon and the 3'UTR. To exclude that the N-terminal part of *eEF1B $\gamma$ 2* was still being expressed, RT-qPCR was performed. It showed that also the expression of the N-terminal region of *eEF1B $\gamma$ 2* was strongly reduced in both mutant lines (Fig. 33C). None of the analyzed T-DNA insertional lines displayed phenotypic alterations compared to WT plants (Fig. 34). Together with the high sequence similarities between both proteins (88%), this could indicate that both proteins are functionally redundant.



**Figure 34: Phenotype of eEF1B $\gamma$  single mutants.** Representative photographs of 24 d-old soil-grown plants of WT and the indicated mutant lines.

#### 4.3.4 Phenotypical analysis of *eef1b $\gamma$ 1/2* double mutants

To further analyze a possible function of eEF1B $\gamma$  in plant development, we crossed the *eef1b $\gamma$ 1* single mutant lines with the *eef1b $\gamma$ 2* single mutant lines. Genotyping of the F1 generation confirmed a successful crossing and resulted in double heterozygous plants. F1 plants were allowed to self-fertilize and F2 generation was again genotyped to find double homozygous mutants. For each of the four generated double mutants (*eef1b $\gamma$ 1-1<sup>+/-</sup>eef1b $\gamma$ 2-1<sup>+/-</sup>*, *eef1b $\gamma$ 1-1<sup>+/-</sup>eef1b $\gamma$ 2-2<sup>+/-</sup>*, *eef1b $\gamma$ 1-2<sup>+/-</sup>eef1b $\gamma$ 2-1<sup>+/-</sup>*, *eef1b $\gamma$ 1-2<sup>+/-</sup>eef1b $\gamma$ 2-2<sup>+/-</sup>*) at least 21 plants were genotyped, but none of them was homozygous for both T-DNA insertions. Therefore, F2 plants, which were homozygous for one gene and heterozygous for the other gene, were again self-fertilized and 50 F3 plants from each double mutant were analyzed (by Mahsa Nasimi as part of her master thesis under my supervision). Only for the combination of *eef1b $\gamma$ 1-2 eef1b $\gamma$ 2-2*, six double homozygous plants were identified from the 50 analyzed plants. This double mutant will further on be named as *eef1b $\gamma$ 1/2* and characterized.

First, the impact of the T-DNA insertions on the eEF1B $\gamma$  protein level was tested. Therefore, a polyclonal eEF1B $\gamma$ -specific antibody (binding both eEF1B $\gamma$ 1 and eEF1B $\gamma$ 2) was used (Agrisera, Sweden). Before use, the specificity of the antibody was determined. To this end, YFP-eEF1B $\beta$ 1 and YFP-eEF1B $\gamma$ 2 were transiently expressed in Arabidopsis protoplasts and protein extracts were probed with the eEF1B $\gamma$ -antibody and an GFP-antibody. In the control western blot using anti-GFP, both YFP-tagged proteins were detected (Fig. 35A). The eEF1B $\gamma$ -antibody specifically bound to the YFP-eEF1B $\gamma$ 2 protein, but not to the YFP-eEF1B $\beta$ 1. Additionally, in both protoplast samples the native eEF1B $\gamma$  protein was detected with the eEF1B $\gamma$ -antibody, but not with anti-GFP. Consequently, the antibody is specifically binding only to the gamma subunit of the eEF1B complex and can be used to quantify the amount of native eEF1B $\gamma$  in the T-DNA insertional lines. To this end, proteins were extracted from 7 d-old seedlings of WT, *eef1b $\gamma$ 1/2*, *eef1b $\gamma$ 1-2* and *eef1b $\gamma$ 2-2* and analyzed by immunoblotting

using the eEF1B $\gamma$ -specific antibody. For loading control, the same membrane was stripped and analyzed again using anti-ACTIN. Three independent experiments showed a strong reduction of eEF1B $\gamma$  protein levels in *eef1b $\gamma$ 1/2* (Fig. 35B). Quantification of the signal intensities from the western blots showed that *eef1b $\gamma$ 1/2* resumed only about 20% of WT protein level, whereas the *eef1b $\gamma$ 1-2* and *eef1b $\gamma$ 2-2* single mutants still contained more than 60% of the native protein level.

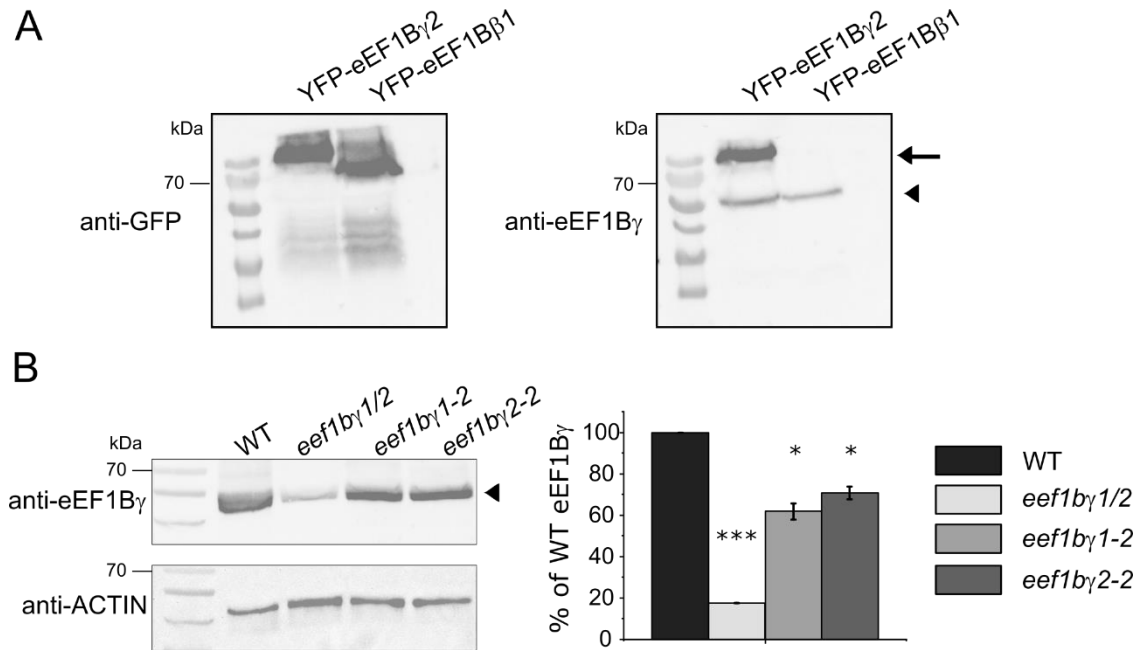


**Figure 35: Protein levels of eEF1B $\gamma$  in single and double mutant lines.** (A) Specificity test of eEF1B $\gamma$ -specific antibody used in (B). Protein extracts from protoplasts transiently expressing YFP-eEF1B $\gamma$ 2 or YFP-eEF1B $\beta$ 1 were analyzed by immunoblotting using anti-GFP as control or anti-eEF1B $\gamma$  for specificity test. Arrow points towards YFP-tagged eEF1B $\gamma$ . Arrowhead marks native eEF1B $\gamma$ . (B) Immunoblots showing the expression of eEF1B $\gamma$  or ACTIN in WT or the indicated mutant lines. Proteins were extracted from seven days-old seedlings grown in liquid MS cultures. For each sample, 40  $\mu$ g of total protein extract were loaded on the SDS gel. Immunoblots were first probed with an eEF1B $\gamma$ -specific antibody, stripped and re-probed with an ACTIN-specific antibody for loading control. Quantification shows percentage of eEF1B $\gamma$  level compared to WT (with WT set to 1 in each experiment). Data represents means  $\pm$ SE from three independent experiments.

Next, the phenotype of *eef1b $\gamma$ 1/2* at seedling stage was observed and compared to WT and both single mutants. Seedlings of *eef1b $\gamma$ 1/2* showed an impaired primary root growth (Fig. 36A and 36B). While the root length of both single mutants did not differ significantly from WT at 4 and 7 dag, the *eef1b $\gamma$ 1/2* was significantly shorter at 4, 7 and 10 dag (Fig. 36A and 36B). Most likely, the observed defects in root development were rather a growth delay than growth arrest. This hypothesis is based on the observation that the root length of *eef1b $\gamma$ 1/2* shows at 10 dag the same length as roots of WT at 7 dag. In addition to defects in primary root length, the

number of lateral roots was significantly reduced in *eef1bγ1/2* at 10 dag compared to WT and both single mutants (Fig. 36C). To find out if this phenotype was due to reduced cell division rates, roots of 4d-old seedlings were stained using propidium iodide (PI) to examine the RAM. In comparison to WT, the *eef1bγ1/2* mutants showed reduced number of dividing cells resulting in a shorter meristematic zone (Fig. 36D and 36E). The analysis of the RAM was performed by Cloe de Luxán-Hernández.

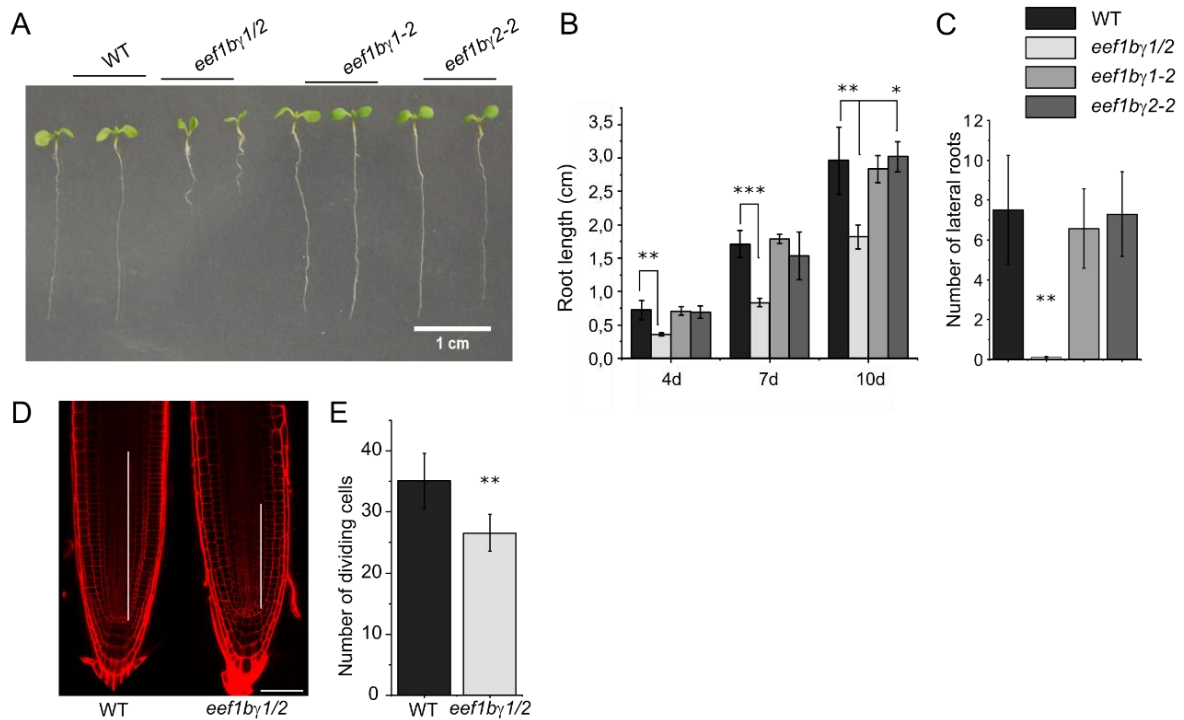


**Figure 36: Root phenotype of *eef1bγ1/2* double mutant compared to WT and single mutant lines. (A)** Photograph of representative 7 d-old seedlings of WT, *eef1bγ1/2*, *eef1bγ1-2* and *eef1bγ2-2* grown on vertical MS plates. **(B)** Measurement of root length of the indicated lines at 4 dag, 7 dag and 10 dag. Data represent mean from three independent experiments  $\pm$ SE. **(C)** Number of lateral roots in 10 d-old seedlings of the indicated genotypes. Data represent mean from three independent experiments  $\pm$ SE. **(D)** Confocal images of PI-stained root tips of 7 d old-seedlings of WT and *eef1bγ1/2*. The white line marks the meristematic zone in the RAM. Scale bar is 60  $\mu$ m. **(E)** Number of dividing cells in the meristematic zone. Values represent mean from four independent experiments  $\pm$ SE (n=30). Asterisks in (B), (C) and (E) indicate means differing significantly from WT (two-tail Student's t test; \* P < 0.05; \*\* P < 0.01; \*\*\* P < 0.001).

Similar to the observed defects in root development, the development of the shoot was delayed in *eef1bγ1/2*. In *eef1bγ1/2*, the number of true leaves was significantly reduced at 7 and 10 dag compared to WT and both single mutants (Fig. 37B). At 13 dag, the difference between the lines is not significant anymore further indicating a growth delay, rather than growth arrest.

Defects in true leaf formation together with the reduced number of dividing cells in the RAM indicate that *eef1b $\gamma$ 1/2* mutants have defects in proper cell division.

The growth phenotype of *eef1b $\gamma$ 1/2* was also observed at later developmental stages (Fig. 37A and 37E). As measure for reduced and delayed growth, the size of the biggest rosette leaf was measured in 28 d-old soil-grown plants. Size of the biggest rosette leaf from WT and both single mutants were similar, whereas the biggest *eef1b $\gamma$ 1/2* leaf was significantly smaller (Fig. 37C and 37D). In contrast, the number of leaves at the flowering timepoint was slightly higher in *eef1b $\gamma$ 1/2* plants compared to WT and both single mutants (Fig. 37E and 37F). This indicates that *eef1b $\gamma$ 1/2* mutants are delayed in flowering.

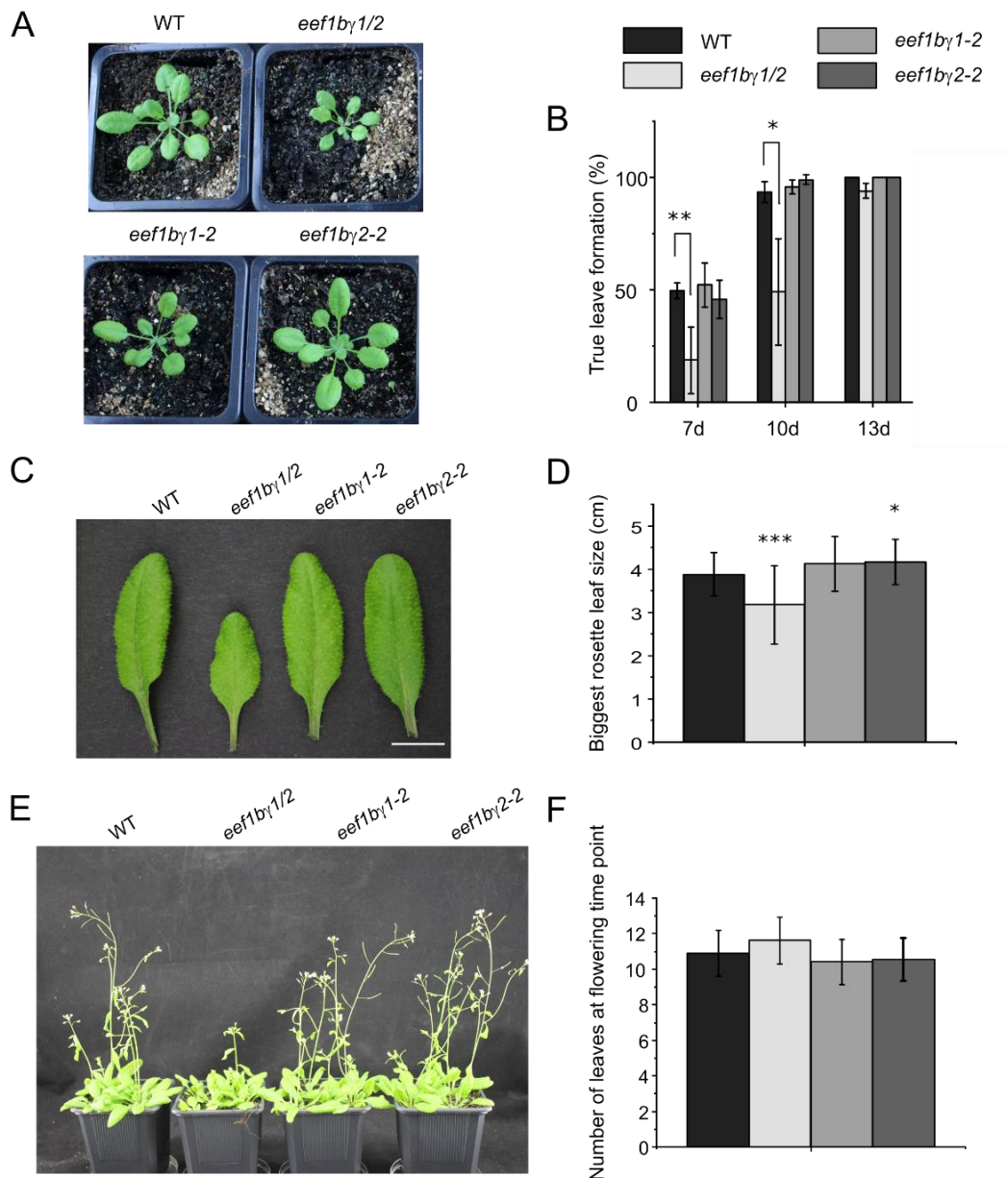


**Figure 37: Shoot phenotype of *eef1bγ1/2* compared to WT and the single mutant lines.** (A) Representative images of 24 d-old soil-grown plants of the indicated genotypes. (B) Percentage of seedlings exhibiting true leaves at 7 dag, 10 dag and 13 dag. Seedlings were grown on horizontal MS plates. Data represent mean  $\pm$ SE from three independent experiments (n=30). Color legend is also used for (D) and (F). (C) Photograph of representative biggest rosette leaves from 28 d-old soil-grown plants of the indicated genotype. Scale bar is 1 cm. (D) Size of the biggest rosette leaf of 26 d-old soil-grown plants of the indicated genotype. The biggest rosette leaf was defined by measurement. The biggest rosette leaf was in each line situated between leaf #9 and leaf #12. Data represent mean from two independent experiments  $\pm$ SE (n=35). (E) Representative photograph of soil-grown WT, *eef1bγ1/2*, *eef1bγ1-2* and *eef1bγ2-2* plants at flowering stage. (F) Number of leaves at flowering time point of plants of the indicated genotype. Data represent mean  $\pm$ SE (n=40). Asterisks in (B) and (D) indicate means differing significantly from WT (two-tail Student's t test; \* P < 0.05; \*\* P < 0.01; \*\*\* P < 0.001).

Lastly, the siliques of the double mutant were analyzed in comparison to WT. Siliques of *eef1bγ1/2* contain overall less seeds than WT and a higher number of 'empty spots' within the siliques (Fig. 38A and 38B). The observed 'empty spots' contained only small white fists, which could result either from unfertilized ovules or collapsed ovules, which were aborted shortly after fertilization. It remains to be examined whether a defect in the male gametophyte is leading to unfertilized ovules in *eef1bγ1/2*. It would be interesting to test the viability of the pollen e.g. with an Alexander staining (Alexander 1969).

To analyze whether the embryos within the produced seeds of *eef1bγ1/2* can develop normally, seeds were extracted from siliques of different ages, de-stained using Hoyer's solution and analyzed using a microscope. The embryo development begins from a single cell and contains distinct stages that can be observed. WT embryos develop from 'globular' stage, to 'heart' stage, in which the embryo already contains around 200 cells. Further the embryo develops into torpedo and bent-cotyledon (or mature) stage, where primordia of cotyledons and organization into root and hypocotyl are already visible (Capron et al. 2009). For both, WT and *eef1bγ1/2* seeds, embryos in every developmental stage, including globular, heart, late heart, torpedo and mature stage, were observed (Fig. 38C). This shows that *eef1bγ1/2* mutants are able to produce fully mature embryos and embryo development is not impaired. Therefore, the enrichment of empty spots in mutant siliques might indicate that the fertility of either the male or female gametophyte might be affected by reduced eEF1B $\gamma$  levels.

In addition to the observed developmental phenotype, we questioned whether the germination of *eef1bγ1/2* seeds might also be affected. To this end, the germination rate of *eef1bγ1/2* was compared to WT. The *eef1bγ1/2* seeds showed a delay of 12 to 24 h in germination (Fig. 38D). Accordingly, the primary root growth delay of about 3 days cannot fully, but partially be

explained by a delayed germination of *eef1b $\gamma$ 1/2* seeds. Overall, the results show that loss of eEF1B $\gamma$  leads to defects in growth and cell division and indicate that eEF1B $\gamma$  is playing an important role in balancing the processes of plant development.

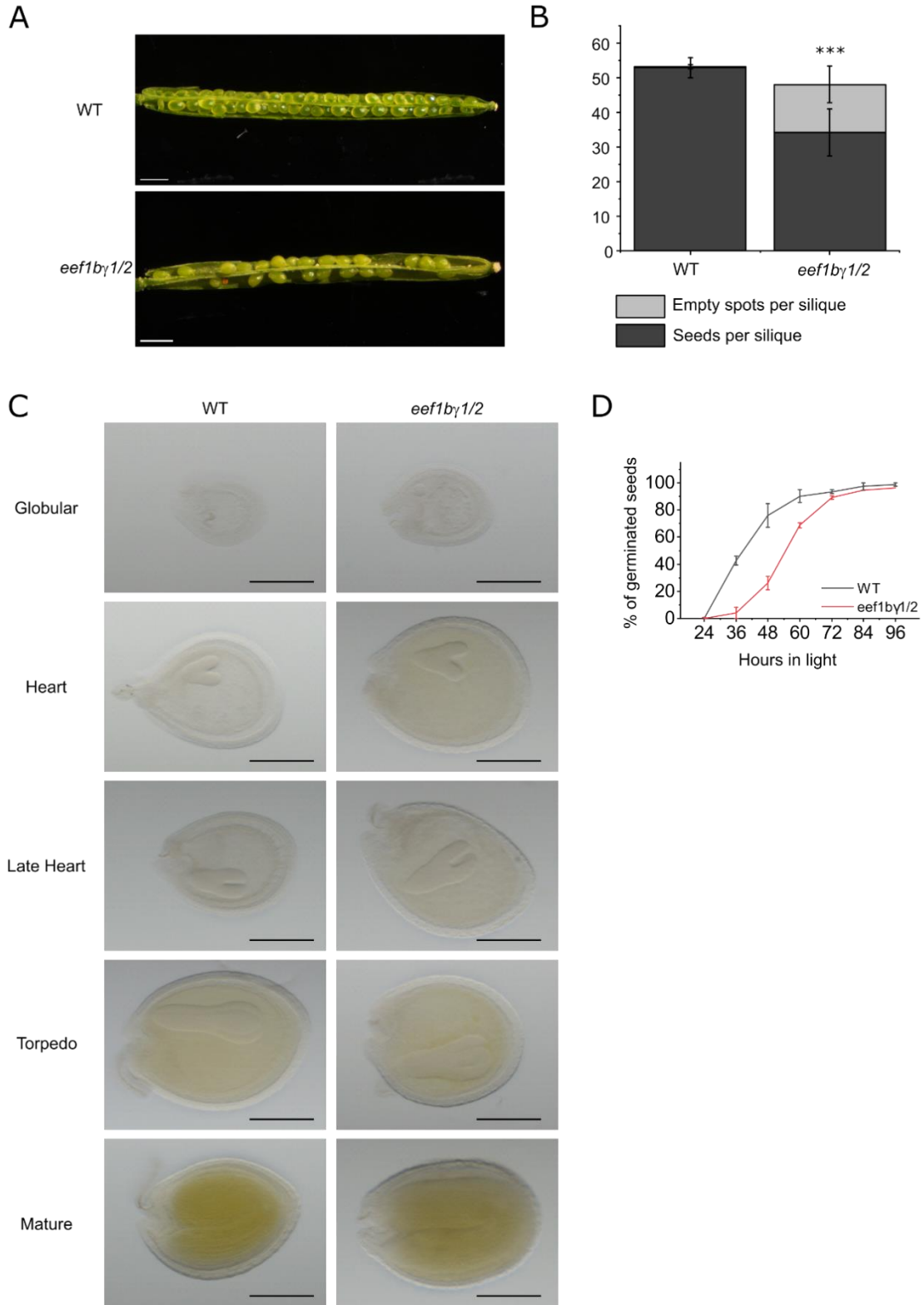


**Figure 38: Silique, embryo and seed germination analysis of *eef1bγ1/2* double mutant.** (A) Siliques of WT and *eef1bγ1/2* mutant. Scale bar is 2 mm. (B) Quantification of number of seeds per silique and empty spots per silique. Data represent mean ±SE (n=30). (C) Representative images of seeds de-stained with Hoyer's solution showing the different developmental stages of embryos. Scale bar is 200 μm. (D) Percentage of germinated seeds of WT and the indicated mutant lines at 24 h until 96 h after transfer of stratified seeds to MS plates in light. Data represent mean ±SE from three independent experiments (n ≥ 25).

#### 4.3.5 Complementation studies in *eef1bγ1/2*

Western blot analysis (Fig. 35) showed that the eEF1Bγ protein levels were strongly reduced in *eef1bγ1/2*. To make sure that the observed phenotype indeed resulted from the reduced protein levels of eEF1Bγ, complementation lines were generated. Therefore, full length eEF1Bγ and the truncated versions of eEF1Bγ used in Y2H (Fig. 32) were N-terminally fused to Yellow Fluorescent protein (YFP) and transformed into *eef1bγ1/2* to be expressed under a constitutive *35S* promoter. The introduced fusion proteins are depicted in Fig. 39A. Unfortunately, no positive transformants were identified for *eef1bγ1/2::YFP-eEF1Bγ1*. For the other five constructs the following number of independent lines were identified by genotyping and optical control for fluorescent signal in seedlings: four lines for *eef1bγ1/2::YFP-eEF1Bγ2*, three lines for *eef1bγ1/2::YFP-eEF1Bγ2ΔN*, one line for *eef1bγ1/2::YFP-eEF1Bγ2ΔC*, three lines for *eef1bγ1/2::YFP-eEF1Bγ1ΔN* and two lines for *eef1bγ1/2::YFP-eEF1Bγ1ΔC*. The full length protein complementation line *eef1bγ1/2::YFP-eEF1Bγ2* rescued the reduced root length phenotype of *eef1bγ1/2* at 4 dag, 7 dag and 10 dag (Fig. 39B and 39C). The reduction of the number of lateral roots observed in *eef1bγ1/2* was partially rescued in 10 d-old seedlings of *eef1bγ1/2::YFP-eEF1Bγ2* (Fig. 39D). Also, the overall stunted growth phenotype was largely rescued in this complementation line (Fig. 39E), verifying that the reduced protein level of eEF1Bγ is in fact responsible for the developmental growth defects in *eef1bγ1/2*.

The truncated versions of eEF1Bγ displayed differential binding capacities towards eEF1Bβ in Y2H. While eEF1BγΔN is unable to bind to eEF1Bβ1, eEF1BγΔC is capable of binding eEF1Bβ1, which appeared to be the central component in the Arabidopsis eEF1B complex (Fig. 23 and 32). If the binding to eEF1Bβ was essential for the function of eEF1Bγ, then it could be hypothesized that eEF1BγΔN would not be able to complement the *eef1bγ1/2* phenotype. Consequently, it would be expected that introduction of eEF1BγΔC would rescue the developmental defects. Overall, none of the truncated versions of eEF1Bγ1 or eEF1Bγ2, neither ΔN nor ΔC versions, was able to complement the phenotype in contrast to the full length

eEF1B $\gamma$ 2. Instead root lengths and number of lateral roots of each truncated version complementation line were still significantly reduced compared to WT (Fig. 39B and 39C).

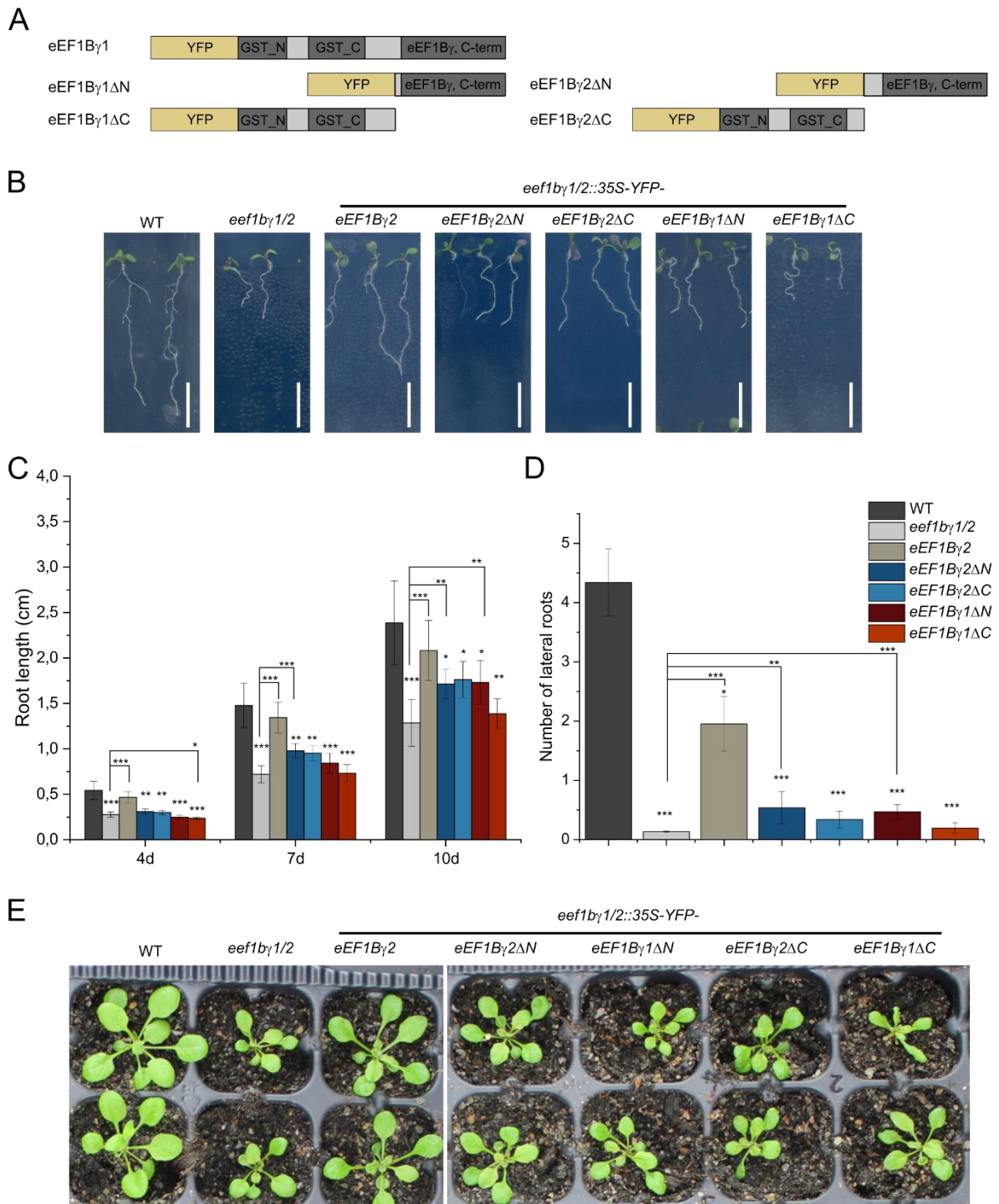


**Figure 39: Full length eEF1B $\gamma$ 2 complements the growth phenotype of *eef1bγ1/2* double mutants. (A)** Structures of full length and truncated versions of YFP-fusion proteins that were introduced into *eef1bγ1/2* under an *35S* promoter for complementation studies. **(B)** Representative photographs of 10d-old T2 seedlings of the indicated lines grown on vertical MS plates. Presence of the transgene in the complementation lines was verified

by checking for YFP-fluorescence of the seedlings. Scale bar is 1 cm. (C) Root length measurements of seedlings of the indicated lines at 4 dag, 7 dag and 10 dag. Figure legend shown in (D) is also valid for (C). (D) Quantification of lateral roots from 10d-old seedlings of the indicated lines. (C+D) Data represent means from at least two independent experiments from the following amount of independent transgenic lines (eEF1B $\gamma$ 2 = 4; eEF1B $\gamma$ 2 $\Delta$ N = 3; eEF1B $\gamma$ 2 $\Delta$ C = 1; eEF1B $\gamma$ 1 $\Delta$ N = 3; eEF1B $\gamma$ 1 $\Delta$ C = 2) with  $n \geq 20$  for each experiment and line. Asterisks mark significant compared to WT (unless otherwise indicated) using two-tailed student's t test (\* P < 0.05; \*\* P < 0.01; \*\*\* P < 0.001). (E) Representative photographs of plants of the indicated lines grown for 10 days on MS plates and after transfer for 10d on soil.

Nonetheless, there were slight differences observed between the eEF1B $\gamma$  $\Delta$ N and eEF1B $\gamma$  $\Delta$ C complementation lines. At 7 dag, seedlings of *eef1bg1/2::YFP-eEF1B $\gamma$ 1 $\Delta$ N*, and at 10 dag, seedlings of *eef1bg1/2::YFP-eEF1B $\gamma$ 2 $\Delta$ N*, had significantly longer roots than *eef1bg1/2* (Fig. 39C). Similarly, at 10 dag seedlings of both eEF1B $\gamma$  $\Delta$ N complementation lines had significantly more lateral roots in comparison to *eef1bg1/2* (Fig. 39D). This effect was not observed for eEF1B $\gamma$  $\Delta$ C complementation lines and is therefore contradicting the previously discussed hypothesis of interaction of eEF1B $\beta$  and eEF1B $\gamma$  being important for the functionality of the eEF1B complex and leading to developmental defects in *eef1bg1/2*. These results rather indicate a similarly important function of the conserved C-terminal eEF1B $\gamma$  domain for plant development.

Several points have to be considered, when drawing conclusions from this data. First, only one line has been analyzed for *eef1bg1/2::YFP-eEF1B $\gamma$ 2 $\Delta$ C* and only two lines for *eef1bg1/2::YFP-eEF1B $\gamma$ 1 $\Delta$ C*. Since the insertion of the transgene happens coincidentally, it is feasible that genes are disrupted by the insertion and lead to undesired side effects. Also, it is possible that the transgene is inserted several times and leads to strongly varying expression levels. Therefore, several independent lines should be analyzed and ideally be analyzed by southern and western blotting to characterize the number of inserted transgenes and the protein levels.

Additionally, it has to be considered that the linker region between both domains contains IDRs, which were only partially maintained in the truncated versions. These IDRs might also have important functions in protein stability and/or intracellular localization. Therefore, the localization of the proteins was observed. Protoplasts were transiently transformed with constructs harboring the CDS under an 35S promotor and N-terminally tagged with YFP. For both full-length proteins, eEF1B $\gamma$ 1 and eEF1B $\gamma$ 2, a fluorescent signal was observed in the cytoplasm and in some cells additionally in the nucleus. All truncated versions displayed a similar localization pattern as the full-length proteins (Fig. 40). This indicates that the proteins

are at least expressed in the expected subcellular localization. Nonetheless, it might be of interest to generate additional truncated versions, which keep the linker region intact and analyze their localization pattern and ability to complement the *eef1bγ1/2* mutant phenotype.

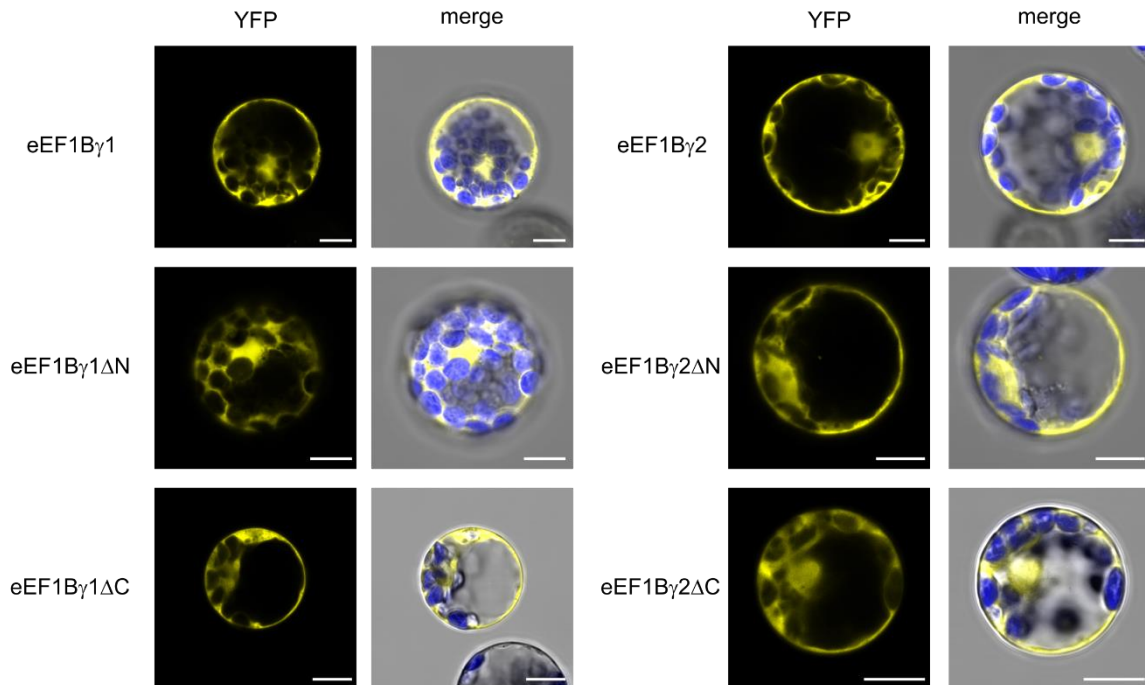


**Figure 40: Truncated versions of eEF1B $\gamma$  localize to the cytoplasm and partially in the nucleus.** Representative confocal images of Arabidopsis protoplasts transiently expressing N-terminally YFP-tagged eEF1B $\gamma$ 1, eEF1B $\gamma$ 1 $\Delta$ N, eEF1B $\gamma$ 1 $\Delta$ C, eEF1B $\gamma$ 2, eEF1B $\gamma$ 2 $\Delta$ N or eEF1B $\gamma$ 2 $\Delta$ C under a constitutive 35S promoter. Merged images show an overlap of YFP signal (yellow), autofluorescence of chlorophyll (blue) and bright field image. Scale bar is 10  $\mu$ m.

#### 4.3.6 The role of eEF1B $\gamma$ in translation regulation

The canonical function of the eEF1B complex is the support of delivery of aminoacyl-tRNA to the ribosome by GDP/GTP exchange on the eEF1A complex, so universally spoken the promotion of protein synthesis. Although eEF1A can bind to GTP by itself, eEF1B enhances the exchange rate of eEF1A-GDP to eEF1A-GTP by a factor of 1000 in wheat embryos (Lanzani et al. 1976). Nonetheless, a direct influence of the eEF1B $\gamma$  subunit on protein synthesis and translational fidelity in plants remains unsure. In mammalian cells, it was shown that RNAi-mediated silencing of *eEF1B $\gamma$*  impairs translation (Kim, Kellner, et al. 2007). Contrarily, loss of both eEF1B $\gamma$ -encoding genes did not lead to changes in protein synthesis or translational fidelity in *Saccharomyces cerevisiae* (Kinzy, Ripmaster, and Woolford 1994; Esposito and Kinzy 2010).

To find out whether translation was affected in *eef1bγ1/2* mutants and whether the observed phenotypes can be explained by reduced protein synthesis several assays were performed.

First, the sensitivity of WT and *eef1bγ* mutants towards different translation inhibitors was tested. Two common translation inhibitors, cycloheximide (CHX) and hygromycin B (HYG) were chosen. Both have already been applied to Arabidopsis and were shown to lead to reduced plant growth and developmental defects (Duan et al. 2011; Kurepa et al. 2010). CHX inhibits translation elongation by binding to the ribosomal E-site and stopping eEF2-mediated translocation (Schneider-Poetsch et al. 2010). This mechanism allows one full translational cycle to be completed before elongation is blocked. HYG is an aminoglycoside that binds closely to the A-site of the small ribosomal subunit and thereby inhibits eEF2-mediated tRNA translocation from the A site to the P site (Moazed and Noller 1987; Gonzalez et al. 1978).

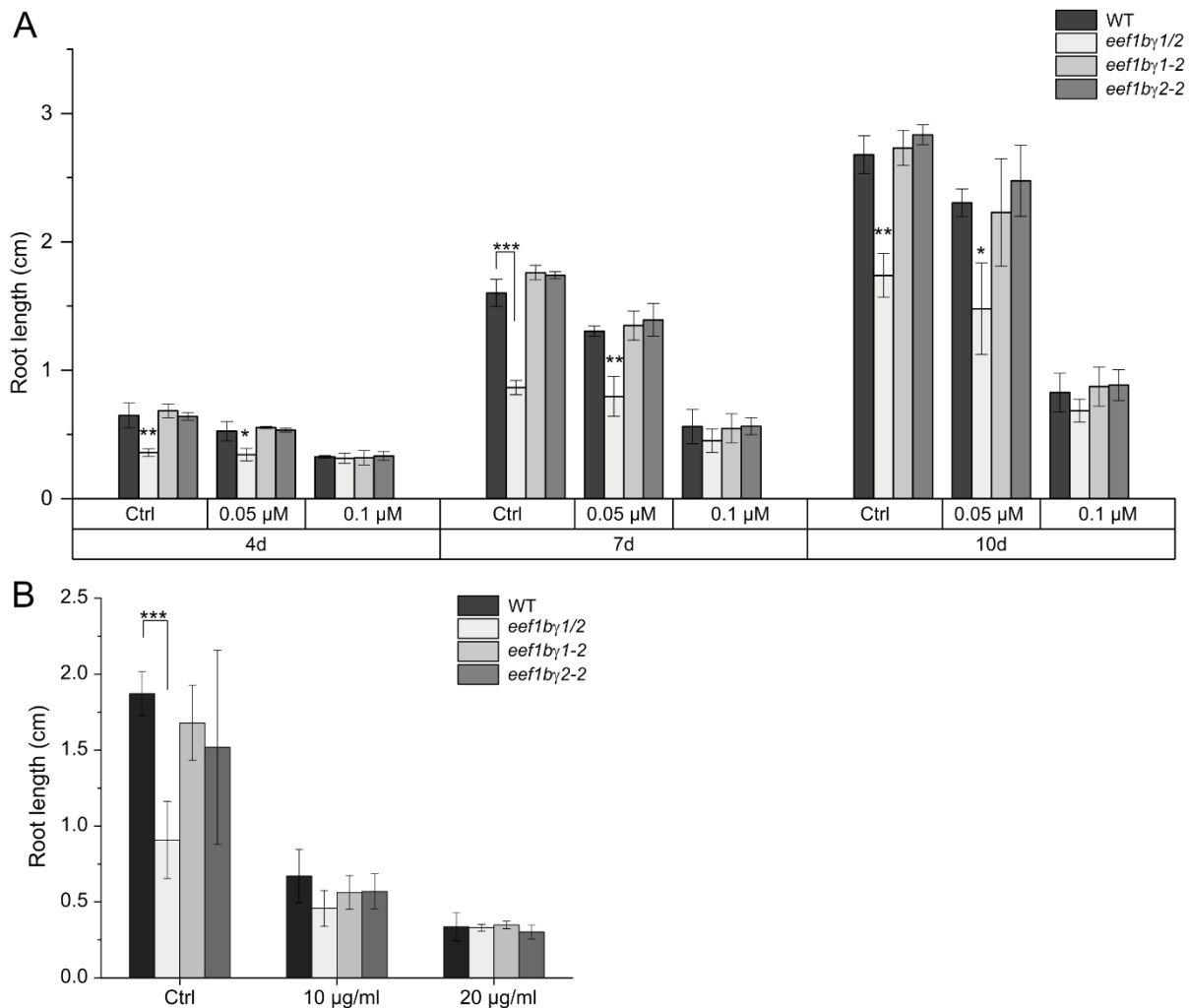


**Figure 41: *eef1bγ1/2* mutants are more tolerant towards translation inhibitors.** (A) Root length measurements of 4 dag, 7 dag and 10 dag seedlings of WT, *eef1bγ1/2*, *eef1bγ1-2* and *eef1bγ2-2*, which were germinated and grown on vertically placed MS plates (Ctrl) or MS plates supplemented with 0.05 μM or 0.1 μM cycloheximide

(CHX). Data represent means  $\pm$ SE from 3 independent experiments ( $n \geq 20$ ). **(B)** Root length measurements of seedlings of the indicated genotypes at 7 dag, which were germinated and grown on vertically placed MS plates (Ctrl) or MS plates supplemented with 10  $\mu$ g/ml or 20  $\mu$ g/ml hygromycin B (HYG). Data represent means  $\pm$ SE from 3 independent experiments ( $n \geq 20$ ). Asterisks indicate means differing significantly from WT at the indicated timepoint and condition (two-tail *t*-test; \*\*\* $P < 0.001$ ; \*\*  $P < 0.01$ ; \*  $P < 0.05$ ).

For sensitivity assays, seeds of WT, *eef1b $\gamma$ 1/2* double mutant and both single mutants were germinated on control MS plates or on MS plates containing 0.05  $\mu$ M or 0.1  $\mu$ M CHX. Root length was measured at 4 dag, 7 dag and 10 dag. As expected, root length of WT plants was strongly affected by increasing CHX concentration. The growth inhibition of WT roots was amplified with increasing seedling age (Fig. 41A). No significant difference was observed between WT and *eef1b $\gamma$ 1-2* and *eef1b $\gamma$ 2-2*. Both single mutant lines showed similar responses to CHX as the WT. This is in line with the yeast eEF1B $\gamma$  double mutant, which also reacted to CHX treatment comparable to WT (Olarewaju et al. 2004).

Similar to the phenotype described in Chapter 4.3.4, the root length of *eef1b $\gamma$ 1/2* was significantly reduced under control conditions compared to WT. Interestingly, *eef1b $\gamma$ 1/2* roots were not significantly shorter than WT roots, when plants were grown on 0.1  $\mu$ M CHX at 4 dag, 7 dag or 10 dag (Fig. 41A). The difference to WT length was already reduced on 0.05  $\mu$ M CHX, but *eef1b $\gamma$ 1/2* roots were still significantly shorter on this lower concentration of CHX. This means that the *eef1b $\gamma$ 1/2* mutant is less sensitive towards translation inhibition through CHX.

The same assay was performed using HYG and root length was measured at 7 dag. Length of WT roots grown on 10  $\mu$ g/ml HYG was reduced to one third of WT root length under control conditions (Fig. 41B). Root length was even further impaired on 20  $\mu$ g/ml HYG. Again, both single mutant lines reacted similar to the WT, whereas *eef1b $\gamma$ 1/2* mutants reacted less strongly to HYG treatment. On 10  $\mu$ g/ml and 20  $\mu$ g/ml HYG, no significant difference between WT and *eef1b $\gamma$ 1/2* mutant was observed (Fig. 41B). These results indicate that *eef1b $\gamma$ 1/2* might indeed be impaired in translation. In the double mutant, root growth would already be adapted and reduced due to translational slow down as consequence of loss of eEF1B $\gamma$ . Therefore, an additional reduction of translation rate by translation inhibitors would not lead to an equally strong reaction as in fully translating plants. Since the reduced sensitivity towards translation inhibitors is an indirect method to detect defects in translation and it has to be taken into consideration that CHX does not only affect translation elongation, but also several other

cellular processes (Ellis and Macdonald 1970; McMahon 1975), we next thought to measure translational efficiency and global protein synthesis rates more directly.

A high number of ribosomes being associated with an mRNA defines an active translation. An actively translating mRNA, that is bound by several ribosomes simultaneously, is named polysome. Assuming that all mRNAs are transcribed with the same speed and efficiency, one can define the ratio of polysome-bound RNA to monosome-bound RNA as measure for translational efficiency. Polysome profiling is an established method, which uses a sucrose gradient to identify ribosomal subunits and ribosomes (monosomes, disomes or polysomes) that are bound to mRNA (reviewed in (Mazzoni-Putman and Stepanova 2018)). The polysome profiles of WT and *eef1bγ1/2* mutant plants were generated by Yang Gao and Reimo Zoschke at MPI Potsdam and are shown in Fig. 42A. For both WT and *eef1bγ1/2*, RNA bound to 40S ribosomal subunit, 60S ribosomal subunits, monosomes, disomes and polysomes was identified, but the amount of each ribosome type differed between both lines. To compare translational efficiency, the ratio of polysome-bound RNA to monosome-bound RNA was calculated. Surprisingly, the ratio was slightly higher for the *eef1bγ1/2* mutant compared to WT. This was unexpected because initially a reduction of translational efficiency was suspected for *eef1bγ1/2*.

Another even more direct way to analyze global protein synthesis rates in vivo is the SUnSET method (Schmidt et al. 2009; Van Hoewyk 2016). It makes use of the antibiotic puromycin, which is an analog of tyrosal-tRNA and can be incorporated into the elongating polypeptide chain instead of tyrosal-tRNA. Consequently, plants can be treated with puromycin and actively translating cells will label freshly synthesized proteins with puromycin. Puromycylation of a polypeptide chain will lead to a halt in translation elongation because the chain cannot be further elongated after the puromycin. This leads to a variety of different lengths of actively transcribed proteins. Proteins can then be extracted, separated by SDS-PAGE and puromycylated proteins can be identified in immunoblots using a puromycin-specific antibody. WT and *eef1bγ1/2* mutant were analyzed with the SUnSET method (Fig. 42C). As proof of concept, we used untreated plants, which showed no signal in the puromycin blot. As expected, a large pattern of different sized puromycylated proteins were detected in WT and *eef1bγ1/2* mutants that had been treated for 2 h with 100 μM puromycin. An additional control for the correct performance of the SUnSET method was the treatment with CHX before treatment with puromycin. CHX will stop translation elongation, thus no proteins should be labeled during puromycin incubation. No puromycylated proteins were detected in CHX-treated samples by

immunoblotting. The comparison between WT and *eef1bγ1/2* mutant yielded no obvious difference in the amount of puromycylated proteins (Fig. 42C). To quantify the ‘optical’ and thereby subjective evaluation of the western blot, band intensities from three independent experiments were quantified using ImageJ software and normalized to ACTIN. Similar to the ‘optical’ observation, no significant difference was observed between the amount of puromycylated proteins in WT and *eef1bγ1/2*. This indicates that global protein synthesis rates, similar to the translational efficiency calculated from the polysome profiling, is not impaired by loss-of-function of eEF1Bγ.

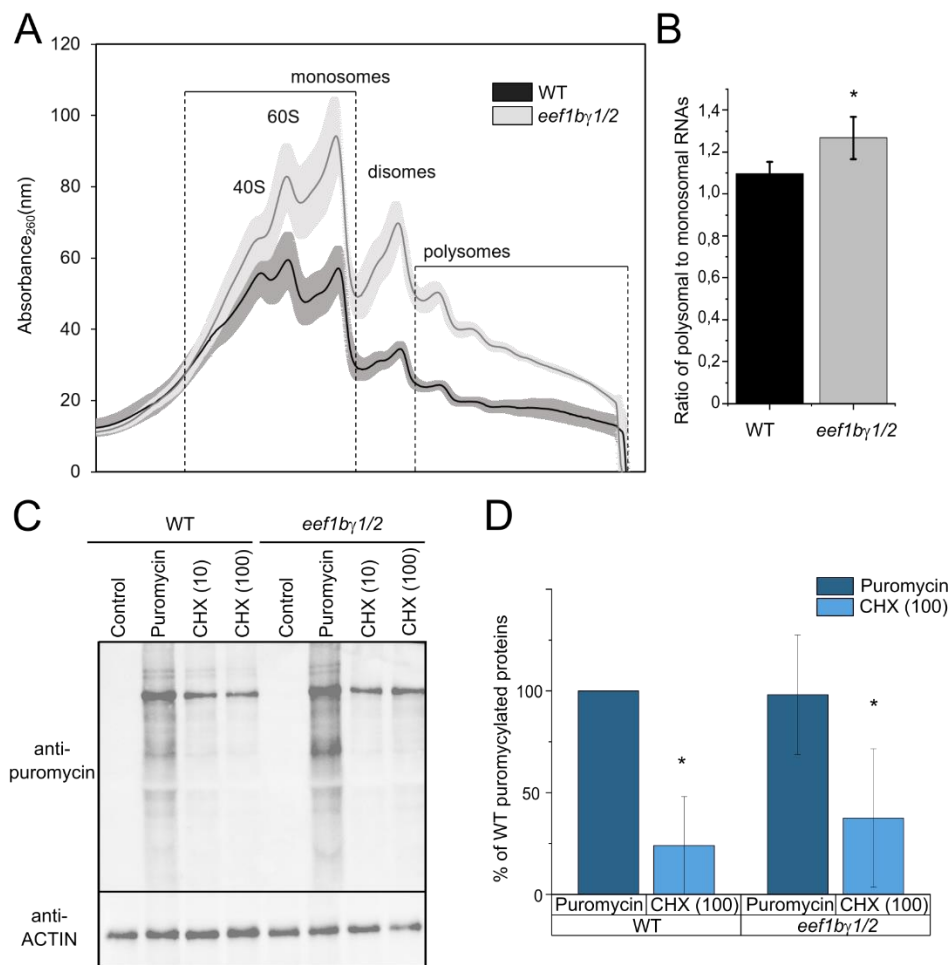


**Figure 42: Global protein synthesis rate is not reduced in *eef1bγ1/2*.** (A) Polysome profiling analysis of leaves from 24 d-old soil-grown WT or *eef1bγ1/2* plants. Cell lysates were fractionated using sucrose gradient sedimentation and the absorbance at 254 nm was documented for each fraction. Data represent means from three experiments  $\pm$ SD (SD shown as shading of the line). (B) Ratio of polysomal to monosomal RNAs (shown in between dashed lines in (A)) was calculated as approximation of translational efficiency. Data represent means from three experiments  $\pm$ SD. (C) Immunoblots showing puromycylated proteins as approximation for global protein synthesis rate using SUNSET method. Proteins were extracted from 7 d-old seedlings, which were untreated (control), treated with 100  $\mu$ M puromycin for 2 h (puromycin), treated with 10  $\mu$ M CHX for 4 h and then with 100

$\mu\text{M}$  puromycin for 2 h (CHX (10)) or treated with 100  $\mu\text{M}$  CHX for 4 h and then with 100  $\mu\text{M}$  puromycin for 2 h (CHX (100)). Immunoblotting was performed using a puromycin-specific antibody and for loading control an ACTIN-specific antibody was used. Data are representative for three independent experiments. (D) Quantification of immunoblots shown in (C). Graph represents percentage of puromycylated proteins compared to WT (with WT set to 1 in each experiment) and values normalized to ACTIN levels. Data represents means  $\pm$ SE from three independent experiments.

But how can plants that are lacking an important and highly conserved elongation factor keep protein synthesis rates to a normal level? Another look at the polysome profiles reveals that the total amount of all ribosomes (40S ribosomal subunits, 60S ribosomal subunits, monosomes, disomes and polysomes taken together) appears to be higher in the *eef1b $\gamma$ 1/2* mutant compared to WT (Fig. 43A and 43B).

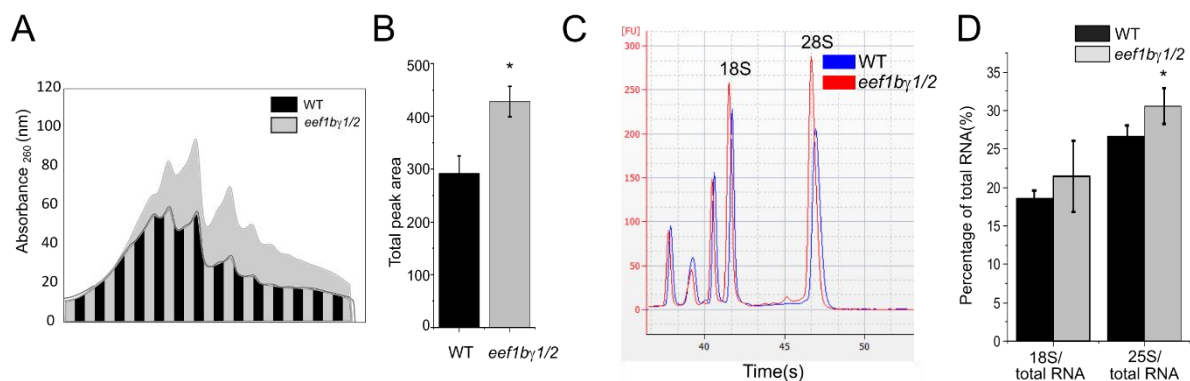


**Figure 43: *eef1b $\gamma$ 1/2* mutant has an enriched number of ribosomes.** (A) Polysome profiles shown in Fig. 42A with new markings to exemplify area used for calculations of total peak area shown in (B). (B) Total peak area used as approximation of total ribosome content of samples analyzed in Fig. 42A. (C) Representative electropherograms of RNA extracted from samples used for polysome profiling in Fig. 42A. (D) Ratios showing 18S rRNA and 25S rRNA content compared to total RNA. Data represent means  $\pm$ SE from four independent biological replicates.

To verify that *eef1b $\gamma$ 1/2* mutants contain in total more RNA-bound ribosomes than WT, total RNA was extracted from the same leaf samples that were used for the polysome profiling. The characteristics of the total RNAs were analyzed with an Agilent BioAnalyzer (with the help of Dr. Steffen Ostendorp, AG Kehr, IPM). Representative electropherograms of WT RNA compared to *eef1b $\gamma$ 1/2* RNA are shown in Fig. 43C. There are slight differences in the peak size of the 18S rRNA and the 25S rRNA. In plant cytosolic ribosomes, the 18S rRNA is included in the small ribosomal subunit (40S) and the 25S rRNA is in the large ribosomal subunit (60S) (Martinez-Seidel et al. 2020). Both small and large subunit together form a ribosome. Hence, the amount of 18S rRNA and 25S rRNA can be viewed as measures for total ribosome amount.

The 18S and 25S rRNA peaks were evaluated from four independent samples for each line and the percentage of 18S or 25S rRNA to the total RNA was calculated (Fig. 43D). 18S rRNA ratio is slightly, but not significantly enriched in *eef1bγ1/2* compared to WT. The 25S rRNA ratio is significantly higher in the *eef1bγ1/2*. Thus, *eef1bγ1/2* mutants could accumulate more ribosomes than WT. This could be a mechanism to compensate for loss of the elongation factor subunit eEF1Bγ and enable the double mutants to keep translation and protein synthesis rates at standard level.

To exclude the possibility that the enrichment of ribosomes in *eef1bγ1/2* results from smaller and thereby more cells in *eef1bγ1/2* instead of more ribosomes per cell, the number of cells in 1 mm<sup>2</sup> of adaxial leaf epidermis cells were quantified in WT and *eef1bγ1/2*. Leaves of 7 d-old seedlings were stained with FM4-64 (Fig. 44).

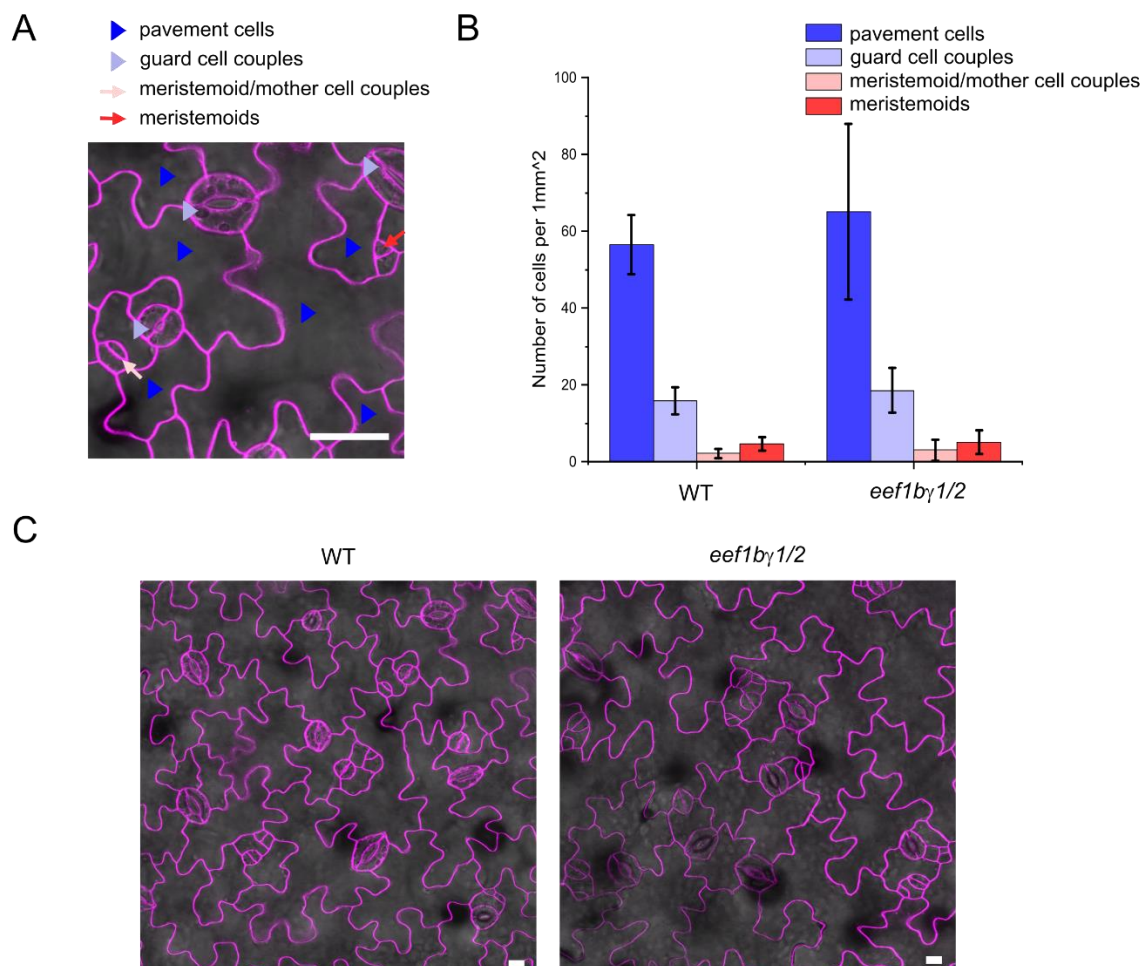


**Figure 44: Number of cells per 1 mm<sup>2</sup> in *eef1bγ1/2* epidermal leaves is similar to WT.** (A) Confocal image of adaxial epidermal leaf cells from 7d-old WT seedlings stained with FM4-64. The four different cell types are marked in this image to exemplify the categorization and counting shown in (B). Scale bar is 10 μm. (B) Number of cells counted in 1 mm<sup>2</sup> of adaxial epidermal leaves of 7d-old WT or *eef1bγ1/2* mutants. Data represent means

± SE from ten individual seedlings per line (n=30). (C) Representative confocal images of FM4-64 stained, adaxial epidermal leaf cells from 7d-old seedlings from WT or *eef1bγ1/2*. Scale bar is 10 μm.

FM4-64 is a lipophilic styryl dye, that stains the plasma membrane (Rigal, Doyle, and Robert 2015) and thereby reveals the cells. On the adaxial epidermis, different types of cells can be found. Pavement cells and fully developed stomatal guard cells are easily detected. During the differentiation of the guard cells, several stages are passed. First, a mother cell builds a meristemoid, which are often observed as meristemoid/mother cell couple. The meristemoid further on diverges from the mother cell and can be identified as single meristemoid. The categorization of the cells is exemplified in Fig. 44A. No significant difference was measured between WT and *eef1bγ1/2* in any of the numbers of the four cell types (pavement, guard cell couples, meristemoid/mother cell couple or meristemoid); (Fig. 44B and 44C). This means that *eef1bγ1/2* has a similar number of cells per mm<sup>2</sup> as WT. Consequently, the observed accumulation of ribosomes in *eef1bγ1/2* is due to higher numbers of ribosomes per cell and supports the hypothesis that increased numbers of ribosomes could be a mechanism to compensate translational defects resulting from the absence of eEF1Bγ.

#### 4.3.7 eEF1Bγ does not influence heat stress response

The ability of plants to cope with increased temperatures is becoming more important in times of global warming. Plants have innate abilities to respond to heat stress. These mechanisms allow plants to survive short periods of above-optimal temperatures. This innate ability to survive is called basal thermotolerance (BT). Additionally, plants have the ability to acquire tolerance to otherwise lethal temperatures when pre-exposed to a mild temperature increase. This ability is called acquired thermotolerance (Larkindale et al. 2005; Larkindale and Vierling 2008). Acquired thermotolerance has further been classified in short-term acquired thermotolerance (SAT; defined by a ‘short’ recovery phase of few hours between mild pre-heat treatment and severe heat stress) and long-term acquired thermotolerance (LAT; defined by a ‘long’ recovery phase of several days between mild pre-heat treatment and severe heat stress);(Yeh et al. 2012). Different heat treatments lead to partially overlapping and partially unique stress responses and phenotypes, therefore several publications emphasize the importance of thorough phenotyping to identify possible heat sensitivity phenotypes (Yeh et al. 2012; Silva-Correia et al. 2014; Kim et al. 2017).

Translational regulation is one of the major mechanisms in heat stress response of plants (Matsuura et al. 2010; Yanguéz et al. 2013; Echevarria-Zomeno et al. 2016). A critical role of translation factors in heat stress response in *Arabidopsis* has been shown for the translation

initiation factor eIF5B (Zhang, Liu, et al. 2017; Salome 2017) and the plastidial EF-Tu RABE1B (Li et al. 2018). Arabidopsis eEF1B $\gamma$  protein was shown to accumulate in heat-induced aggregates and was suggested to be required for recovery of translation after heat stress relief (McLoughlin et al. 2016; McLoughlin et al. 2019). Here, a possible role of eEF1B $\gamma$  in heat stress response was deciphered by analyzing the ability of *eef1b $\gamma$ 1/2* mutants to respond to heat in several different assays aiming at the above mentioned different thermotolerance types. As positive control for the heat treatment, the heat sensitive *hsp101* mutant was used (Hong and Vierling 2001; McLoughlin et al. 2019).

First, the BT was assessed by examining the seed germination under control conditions or after 3,5 h at 45°C. Under control conditions, WT and *hsp101* seeds showed similar germination rates, whereas *eef1b $\gamma$ 1/2* seed germination was slightly delayed (Fig. 45) as already observed in Fig. 38. After heat stress, seed germination of *hsp101* mutant was strongly impaired with only 18 % germinated seeds 7 days after transfer to light (Fig. 45). WT seed germination was less severely affected with 70 % germinated seeds after 7 days. Seed germination of *eef1b $\gamma$ 1/2* was comparable to WT indicating that basal thermotolerance was not affected by reduced eEF1B $\gamma$  protein levels.

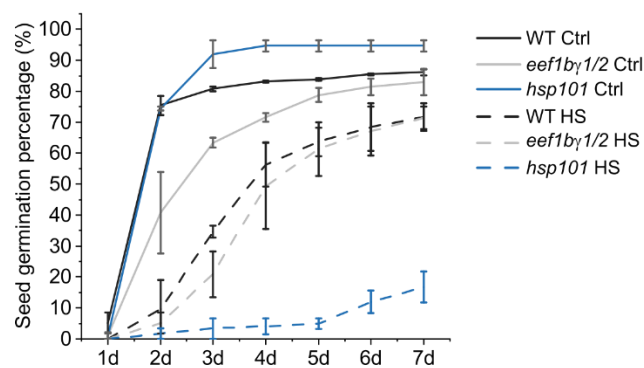


**Figure 45: Basal thermotolerance is not impaired in *eef1b $\gamma$ 1/2* mutants.** Seed germination of WT, *eef1b $\gamma$ 1/2* mutants and the heat-sensitive *hsp101* mutants seeds was documented under control condition (Ctrl) and after 3,5 h at 45°C (HS). HS was applied to imbibed seeds and seeds were afterwards directly sown on MS plates. Germination was observed every 24h after transfer to light. Data represent means  $\pm$ SE of two biological replicates (n=50).

Next, the SAT of *eef1b $\gamma$ 1/2* was analyzed using hypocotyl elongation, root growth and seedling survival as phenotypical traits to be observed. For hypocotyl elongation assay, seedlings were grown for 2,5 d on vertical MS plates in the dark. Then, a mild pre-heat treatment for 90 min at 38°C was applied, seedlings were recovered for 120 min at 22°C and consequent severe heat

stress was applied for 180 min at 45°C. The hypocotyl elongation was measured 2,5 d after heat stress (Fig. 46A). Hypocotyl elongation was strongly reduced after heat stress compared to control conditions in WT, *eef1bγ1/2* and *hsp101* mutants (Fig. 46B). To compare if all lines were similarly affected, the ratio of heat stress to control condition was calculated for each line. The hypocotyl growth ratio of WT and *eef1bγ1/2* were not significantly different from each other, while hypocotyl growth of *hsp101* was significantly reduced (Fig. 46C).

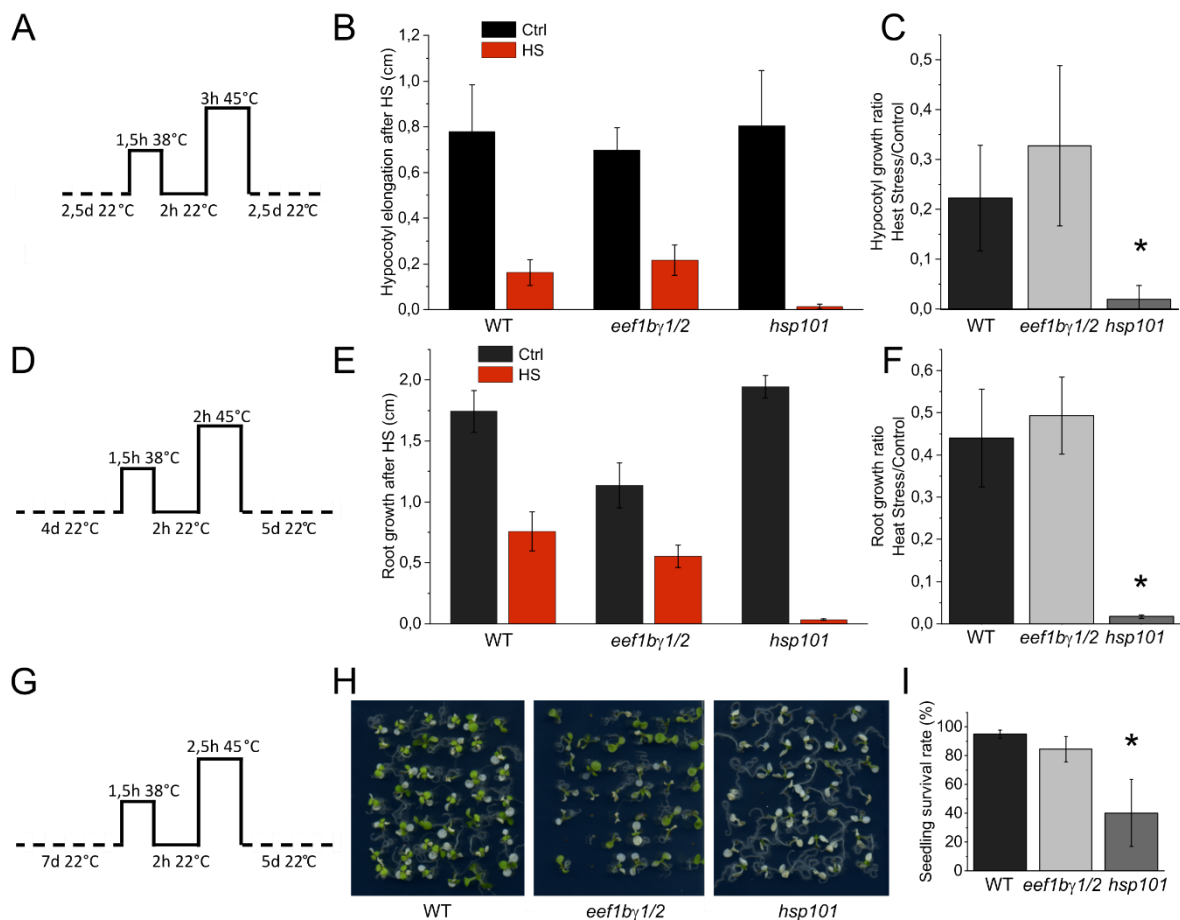


**Figure 46: Short-term acquired thermotolerance of *eef1bγ1/2* mutants is similar to WT.** (A), (D) and (G) show schemes of the applied heat stress for experiments shown in (B) and (C), (E) and (F), (H) and (I), respectively. Seedlings of WT, *eef1bγ1/2* and *hsp101* lines were grown on vertically oriented MS plates in the dark in (A), on vertically oriented MS plates in light in (D) and on horizontal MS plates in light in (G). (B) Hypocotyl elongation measurement under control conditions or after HS described in (A). Data show means  $\pm$ SE of three biological replicates ( $n \geq 20$ ). (C) Hypocotyl growth ratio calculated from data shown in (B). (E) Root growth measurement under control conditions or after HS as shown in (D). Values are representative for means  $\pm$ SE from three independent experiments ( $n \geq 15$ ). (F) Root growth ratio from HS/control from data shown in (E). (H) Representative photographs of seedlings after HS as shown in (G). (I) Quantification of seedling survival after HS as shown in (G). Seedling survival was defined by development of green leaves. Values are representative for

means  $\pm$ SE from three independent experiments ( $n \geq 30$ ). Asterisks indicate means differing significantly from the WT (two-tail t-test; \* $P < 0.05$ ).

Root growth was examined from WT, *eef1b $\gamma$ 1/2* and *hsp101* seedlings, which were grown for 4 d at 22°C before applying the following heat treatment: pre-treatment for 90 min at 38°C, recovered for 2 h at 22°C, heat stressed for 2 h at 45°C. The root length was measured 5 days after the heat treatment (Fig. 46D). Similar to the results of hypocotyl elongation, primary root length was strongly reduced in all lines compared to control conditions (Fig. 46E). The root growth ratio of *hsp101* was significantly reduced compared to WT, while *eef1b $\gamma$ 1/2* growth ratio was not different to WT (Fig. 46F).

Seedling survival is another phenotypical trait that is often used to determine heat stress responses in plants (Yeh et al. 2012). Seedlings grown for 7 days on horizontal MS plates were subjected to 90 min at 38°C, 120 min at 22°C, 150 min at 45°C and were subsequently analyzed after 5 d at 22°C (Fig. 46G). Photographs were taken and seedlings, which had developed green leaves were determined as survivors. Again, WT and *eef1b $\gamma$ 1/2* were significantly less affected than *hsp101* mutants (Fig. 46H and 46I). Overall, none of the three assays indicated an impaired SAT in *eef1b $\gamma$ 1/2*.

The mild pre-heat treatment and subsequent recovery time allows the plant to initiate signaling and stress response mechanisms. Part of the first responses to heat stress is the downregulation of global translation, meanwhile an increased expression of HEAT SHOCK PROTEINS (HSPs), which are supporting protein re-/folding and act as chaperones (Vierling 1991; Al-Whaibi 2011). Two of the most prominent HSPs known to be induced upon heat stress are HSP90 and HSP70. Mutants impaired in thermotolerance can have decreased ability to accumulate HSPs in response to stress, e.g. *elf5b* mutant accumulates less HSP101, HSP70 and HSP21 than WT (Zhang, Liu, et al. 2017). In order to test, if *eef1b $\gamma$ 1/2* was impaired in HSP expression upon heat stress, immunoblotting using specific antibodies for HSP90 and HSP70 were used. 10 d-old seedlings were incubated at control conditions or heat-treated with the following conditions: 90 min at 38°C, 120 min at 22°C, 90 min at 45° (Fig. 47A). Seedlings were immediately snap-frozen in liquid nitrogen, proteins were extracted and subjected to immunoblotting. HSP90 was strongly induced upon HS and HSP70 was slightly induced after HS in WT and in *eef1b $\gamma$ 1/2* (Fig. 47B). So, *eef1b $\gamma$ 1/2* mutants are able to produce WT-like amounts of HSPs when confronted with heat stress.

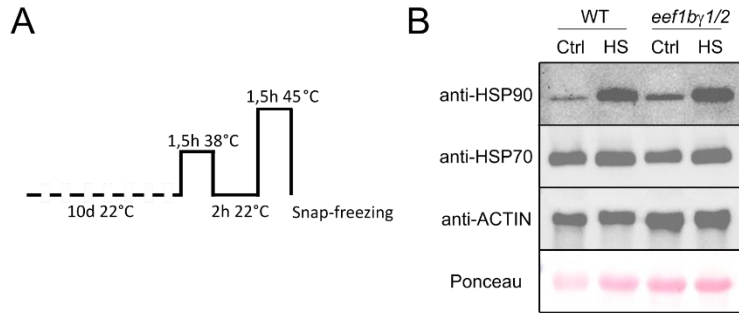


**Figure 47: Induction of HSPs after heat stress.** (A) Scheme of heat treatment applied to seedlings before protein extraction and western blotting shown in (B). 10d-old seedlings grown on MS plates were pre-heat treated for 90 min at 38°C, allowed to recover for 120 min at 22°C before second heat treatment for 90 min at 45°C. Seedlings were immediately snap-frozen in liquid nitrogen after HS. (B) Immunoblotting of protein extracts from seedlings grown under control conditions (Ctrl) or after heat stress (HS) as described in (A). Specific antibodies for HSP90 and HSP70 were used for analysis of HSP induction. Specific antibody for ACTIN and ponceau staining was used for loading control. Immunoblots are representative for three independent experiments.

Some factors important for acquired thermotolerance are not required to induce SAT, but are rather playing a role in sustaining the heat stress response. Plants lacking HSA32 protein do not show a phenotype after a short time of recovery as in SAT, but show strong defects in sustaining heat stress response after long recovery time as in LAT (Charng et al. 2006). To test whether *eef1bγ1/2* mutants were defective in acquiring long-term heat stress resistance, seedlings were grown for 6 d on MS plates, then treated for 90 min at 38°C and allowed to recover for 2 d at 22°C before severe heat stress for 100 min at 45°C (Fig. 48A). The number of green leaves per plant was counted 7 days after the severe heat stress. The number of green leaves per WT plant at control condition was set to 1 and relative amounts were calculated for *eef1bγ1/2* mutants and *hsp101* mutants. *eef1bγ1/2* mutants and WT plants had similar numbers of green leaves after HS, which were not significantly different to control conditions. The number of green leaves on *hsp101* mutants was significantly less after HS than under control conditions (Fig. 48B and 48C). Consequently, the *eef1bγ1/2* mutant is able to acquire long-term thermotolerance.

All previously described experiments included a severe heat stress of 45°C, which is just rarely occurring in nature. More realistic is an ambient increase of temperature for longer time periods. Therefore, the response of plants to ambient temperature changes has become an important research field of interest (Wigge 2013; Hayes et al. 2021). To analyze whether the thermosensing and response to ambient temperature increase was affected by reduction of

eEF1B $\gamma$  level, *eef1b $\gamma$ 1/2* mutants were grown for 7 d at 22°C for control conditions or at 27°C for increased ambient temperature.

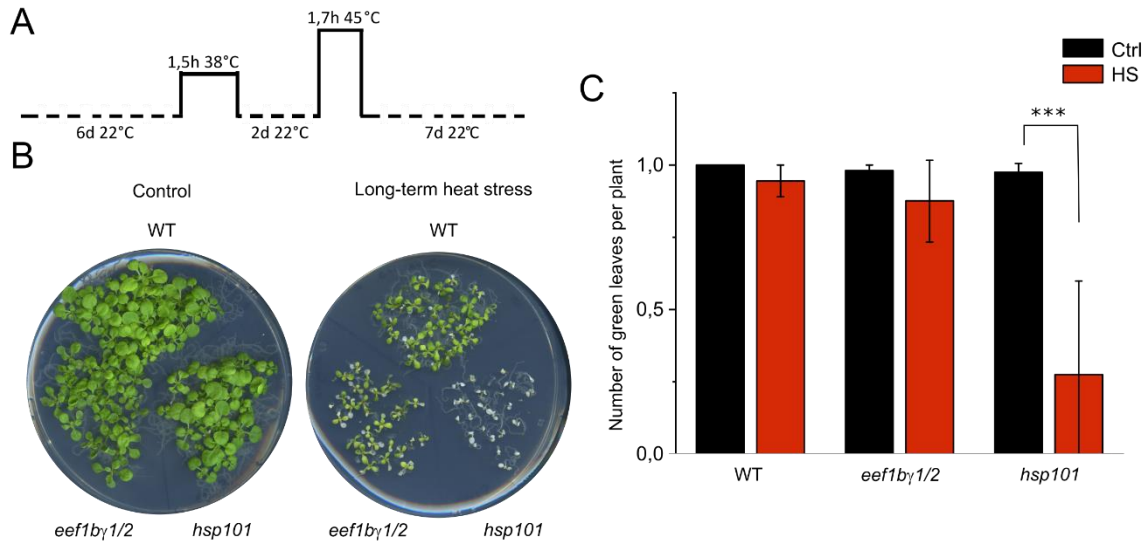


**Figure 48: *eef1b $\gamma$ 1/2* mutants display similar long-term acquired thermotolerance as WT plants.** (A) Scheme of heat treatment applied to seedlings shown in (B) and (C). Seedlings were grown on horizontal MS plates for 6d before pre-heat treatment for 90 min at 38°C. Recovery was performed for 2 d at 22°C before second heat stress for 100 min at 45°C. Seedlings were grown for another 7 days before analysis. (B) Representative photographs of WT, *eef1b $\gamma$ 1/2* and *hsp101* seedlings grown under control conditions or after long-term heat stress as described in (A). (C) Quantification of the number of green leaves of seedlings grown under control conditions (Ctrl) or after heat treatment (HS) as described in (A). The number of green leaves per WT plant at control conditions was set to 1 and relative amounts were calculated, respectively. Values represent means  $\pm$  SE from three independent experiments ( $n \geq 30$ ). Asterisks indicate means differing significantly from control conditions (two-tail t-test; \*\*\* $P < 0.001$ ).

The root length and the hypocotyl elongation of WT, *eef1b $\gamma$ 1/2* and *hsp101* seedlings was assessed. The experiments were performed by Cloe de Luxán-Hernández. All three lines showed a slight increase in root length and hypocotyl elongation at 27°C compared to 22°C (Fig. 49A and 49B). This elongation effect of increased ambient temperature has been described previously (Gray et al. 1998). Interestingly, calculation of root length ratio and hypocotyl length ratio of 27°C to 22°C showed no significant difference between WT, *eef1b $\gamma$ 1/2* and *hsp101*, indicating that none of the lines was defective in ambient temperature response. Overall, all tested conditions and experiments showed that *eef1b $\gamma$ 1/2* behaved similar to WT regarding different temperature treatments. The reduction of eEF1B $\gamma$  level did not influence the thermotolerance of the plants.

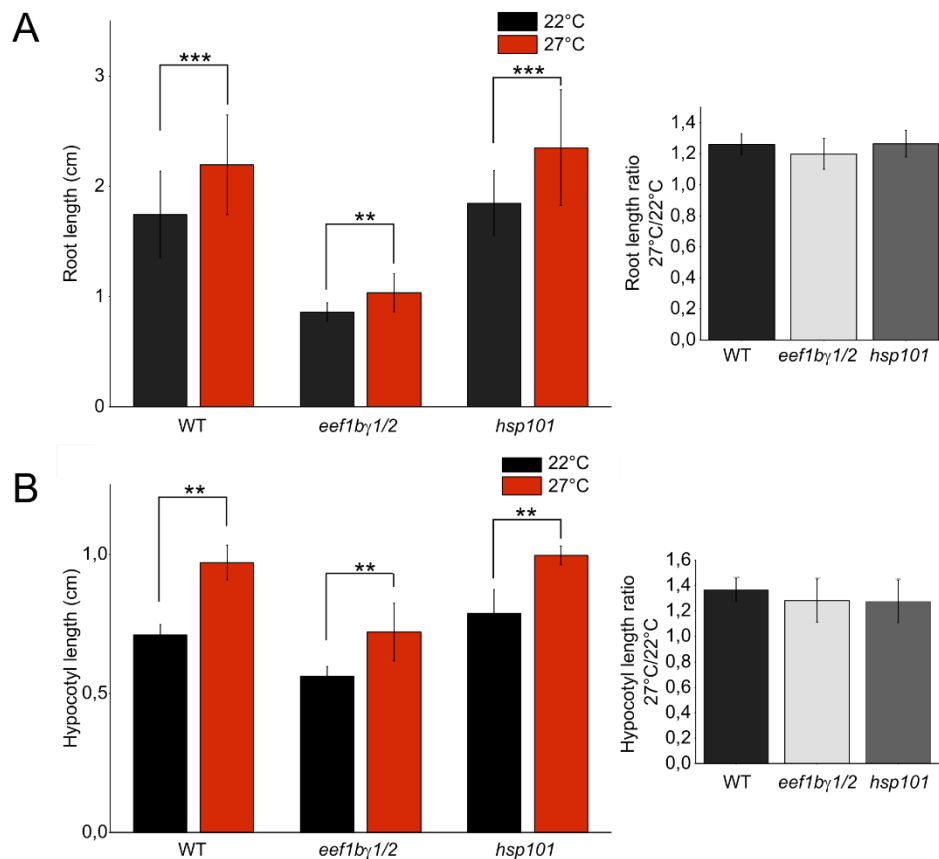


**Figure 49: Ambient temperature response of WT, *eef1bγ1/2* and *hsp101* is comparable. (A)** Root length measurements of WT, *eef1bγ1/2* and *hsp101* mutants grown for 7 days on vertical MS plates at control conditions (22°C) or at increased ambient temperature (27°C). To emphasize differences between the ambient temperature response between the three lines, the root length ratio (27°C/22°C) was calculated. Values are representative for means  $\pm$ SE from three independent experiments ( $n \geq 30$ ). **(B)** Measurement of hypocotyl length of WT, *eef1bγ1/2* and *hsp101* mutants grown for 7 days on vertical MS plates at control conditions (22°C) or at increased ambient temperature (27°C). Additionally, the hypocotyl length ratio was calculated. Values are representative for means  $\pm$ SE from three independent experiments ( $n \geq 30$ ). Asterisks indicate means differing significantly from control conditions (two-tail t-test; \*\*\* $P < 0.001$ ).

#### 4.3.8 eEF1B $\gamma$ has an influence on the oxidative stress level in plants

Several studies indicated that eEF1B $\gamma$  might be inflicted in response to oxidative stress. Loss of eEF1B $\gamma$  in yeast results in constitutive resistance to oxidative stress (Olarewaju et al. 2004) and accumulation of oxidized proteins inside the cells (Esposito and Kinzy 2010). As shown in Fig. 32, Arabidopsis eEF1B $\gamma$  contains two putative glutathione S-transferase (GST) domains. GST activity has not been proven in Arabidopsis yet, but GST activity has been shown for rice eEF1B $\gamma$  (Kobayashi, Kidou, and Ejiri 2001). Additionally, independent studies showed that

overexpression of different GSTs in *Arabidopsis* led to increased tolerance to methylviologen-induced oxidative stress (Sharma et al. 2014; Xu et al. 2016; Ugalde et al. 2021). These results prompted us to test, if *Arabidopsis* eEF1B $\gamma$  played a role in oxidative stress response.

For phenotypical analysis, the fresh weight and root length of the established *eef1b $\gamma$ 1/2* mutant line was compared to WT on MS plates with or without methylviologen (MV). MV, which is also known as paraquat, is a non-selective and soil-inactivated herbicide. MV leads to formation of reactive oxygen species (ROS) by diverting electrons from the photosystem I to molecular oxygen (Hawkes 2014). For WT plants, it is known that fresh weight and root length are reduced upon MV treatment (He et al. 2021). As expected, rosette sizes and fresh weight of WT plants were slightly reduced (-28%), when grown for 21 d on MS containing 25 nM MV, and were strongly reduced (-81%) upon growth on 50 nM MV (Figure 50A and 50B) compared to control conditions. Fresh weight was also reduced in *eef1b $\gamma$ 1/2* mutants upon MV treatment. *eef1b $\gamma$ 1/2* mutants weighed 22% less on 25 nM MV and 78% less on 50 nM MV. There was no significant difference between WT and *eef1b $\gamma$ 1/2* in the reduction of fresh weight (Fig. 50B). Additionally, a line overexpressing YFP-eEF1B $\gamma$ 2 under a constitutive 35S-promotor in WT background (OE-eEF1B $\gamma$ 2) was analyzed. The overexpression line showed a similar reduction of fresh weight upon growth on MV as the WT (Figure 50B).

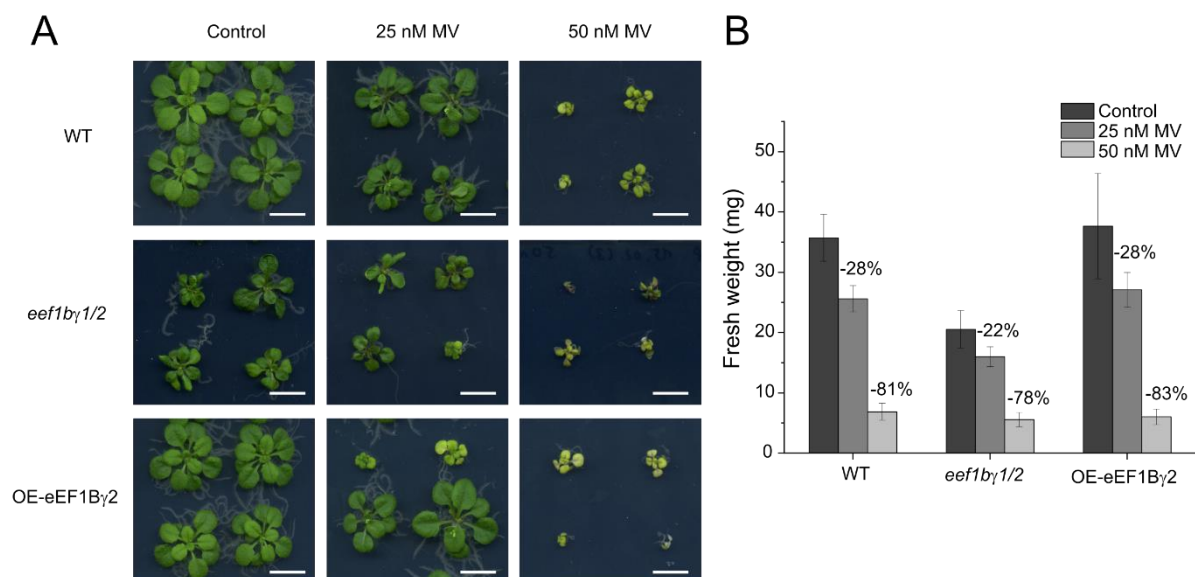


**Figure 50: Methylviologen-treatment reduces growth and fresh weight of plants.** WT, *eef1b $\gamma$ 1/2* mutants and WT plants overexpressing an 35S:YFP-eEF1B $\gamma$ 2 construct were germinated and grown on horizontally placed MS plates (Control) or MS plates containing methylviologen (25 nM or 50 nM MV). Plants were photographed and fresh weight was measured at 21 dag. Data represents mean  $\pm$ SE from three independent experiments ( $n \geq 25$ ).

As second phenotypic trait, root length of WT and *eef1bγ1/2* mutants was measured at 7 dag, 10 dag and 14 dag grown on vertically placed MS plates (Control) or with 100 nM MV. As anticipated, root length of WT plants was strongly reduced, when seeds were germinated and grown on MS plates containing MV compared to control conditions (Fig. 51A). The reduction of WT root length was between -70% to -72% at 7 dag, 10 dag and 14 dag (Fig. 51B). Similarly, the root length of *eef1bγ1/2* mutant was firmly diminished at each of the tested time points. Interestingly, the reduction of root length of *eef1bγ1/2* on MV increased with increasing age of plants. At 7 dag, *eef1bγ1/2* roots were 65% shorter, at 10 dag they were 78% shorter and at 14 dag 84% compared to control conditions (Fig. 51B). This indicates that *eef1bγ1/2* mutants could at first respond to the MV similar to the WT, but were not able to endure growth for longer times under constant oxidative stress. Since no difference in response to MV was observed at fresh weight level, this could point to a slightly disturbed ROS homeostasis in the root of *eef1bγ1/2* mutants.

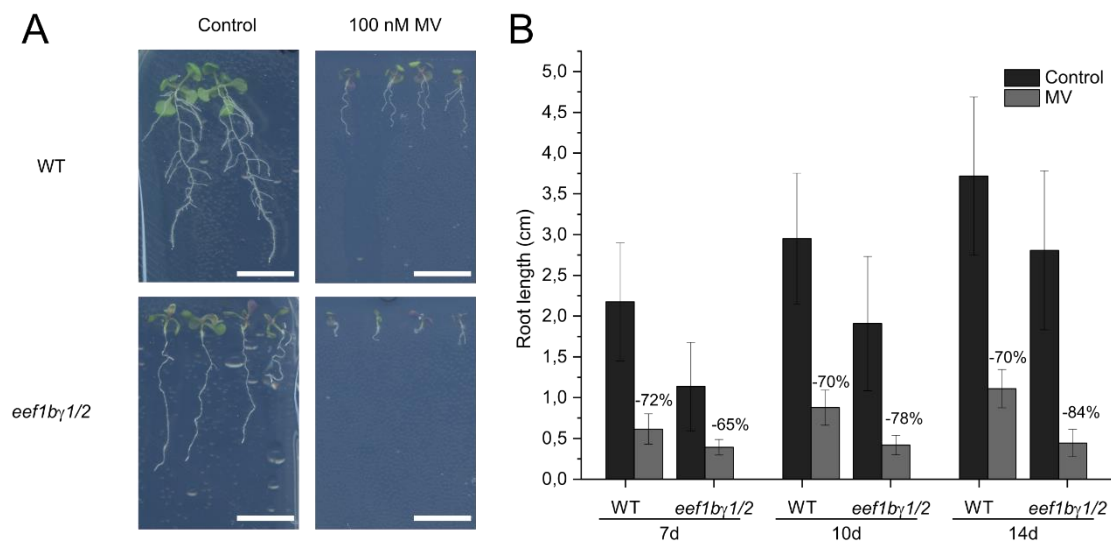


**Figure 51: Root growth of WT and *eef1bγ1/2* mutants is strongly impaired by MV treatment.** (A) WT and *eef1bγ1/2* seeds were germinated and grown on MS plates containing sucrose (Control) or MS plates containing sucrose and 100 nM MV. Representative seedlings are shown at 10 dag. (B) Root length of seedlings described in (A) was measured at 7 dag, 10 dag and 14 dag. Numbers above graphs show reduction of root length under MV treatment compared to control conditions of the same line at the same dag. Scale bar is 1 cm. Graphs represent mean ± SE from three independent experiments (n ≥ 60).

In addition to the described root growth inhibition, it was also observed that leaves of WT and *eef1bγ1/2* seedlings showed a strong purple coloration on the abaxial leaf surface. A mild purple coloration was already detectable for *eef1bγ1/2* mutants at control conditions, which intensified

after MV treatment. A purple coloration is usually resulting from an increased anthocyanin content in the cells. Anthocyanins are belonging to the flavonoid group of pigment, which also have a function as antioxidants and scavengers of ROS (Brunetti et al. 2013). This led us to hypothesize that the *eef1bγ1/2* might have a constant enhanced level of oxidative stress leading them to produce higher levels of anthocyanins. The hypothesis was tested by performing a 3,3'-Diaminobenzidine (DAB)-staining of WT and *eef1bγ1/2* seedlings for in situ detection of hydrogen peroxide. In presence of peroxidases, DAB is oxidized by hydrogen peroxide leading to precipitation and color changing to dark brown (Daudi and O'Brien 2012).

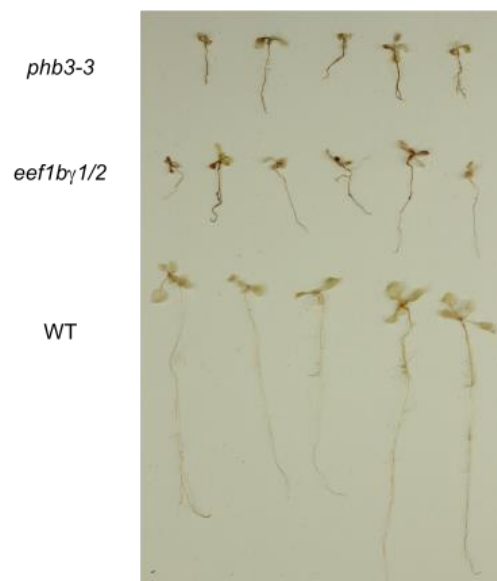


**Figure 52: Detection of hydrogen peroxide in Arabidopsis seedlings with DAB staining.** Seedlings of the indicated lines were grown on vertical MS plates and DAB staining was performed at 8 dag. Seedlings were photographed after overnight staining and following destaining. Photograph is representative for three independent experiments.

DAB staining is only a qualitative method, so that lines of interest have to be compared directly. As positive control, a *phb3-3* mutant was used. PHB3 is required for root stem cell niche maintenance and ROS homeostasis in the root, and it was published that *phb3-3* mutants show an overaccumulation of hydrogen peroxide in the root tips (Kong et al. 2018). In comparison to the WT, *phb3-3* showed a stronger accumulation of dark brown DAB precipitate in the roots and in the cotyledons (Fig. 52). The *eef1bγ1/2* seedlings showed a similar staining pattern as *phb3-3* indicating an increased amount of hydrogen peroxide in both mutants. This could be another hint that *eef1bγ1/2* mutants have a disturbed ROS homeostasis. Nonetheless, hydrogen peroxide is only one of several ROS and the observed differences are slight. Additional methods

should be used to verify the increased ROS levels in the cells. In the course of his master thesis in our lab, Christoph Kittel tried to establish ROS measurement in purified plant extracts with a potassium iodide or Amplex Red method. The results of both methods (data not shown) displayed a high variability between replicates implying difficulties with the reproducibility. This is in accordance with strongly varying absolute ROS values between different papers and the many different techniques used for ROS measurements (Kaurilind, Xu, and Brosche 2015; Liu et al. 2010; Lee et al. 2022).

#### 4.4 Subcellular localization of the three plant eEF1B subunits

##### 4.4.1 eEF1B subunits accumulate in cytoplasmic condensates after heat stress

The subcellular localization of proteins is an important factor for defining the function of a protein in the cell. Mammalian eEF1B subunits mainly localize to the cytoplasm, fitting to their designated function in cytoplasmic protein translation. Additionally, mammalian eEF1B subunits localize to the nucleus and putative functions inside the nucleus are still being unraveled (Kapustian et al. 2019; Kapustian, Dadlez, and Negrutskii 2017; Negrutskii 2020). Here, the localization of eEF1B subunits in plant cells was analyzed using fluorescently tagged-fusion proteins. First, eEF1B $\alpha$ 2, eEF1B $\beta$ 1, eEF1B $\gamma$ 1 and eEF1B $\gamma$ 2 were N-terminally-tagged with YFP and transiently expressed in *Arabidopsis* protoplasts under an 35S promotor. All eEF1B subunits were found evenly distributed in the cytoplasm (Fig. 53A). In few protoplasts, eEF1B subunits were also detected in the nucleus (data not shown). As control, YFP-Citrine was expressed, which localized to the cytoplasm and the nucleus. The correct expression of the fusion proteins was verified using immunoblotting. Therefore, proteins were extracted from the protoplasts. All four fusion proteins were detected using an GFP antibody at their corresponding molecular weight (Fig. 53C). Unfortunately, also free YFP was detected in each sample indicating that truncated versions of the fusion proteins might be expressed. Free YFP in the protoplasts might lead to wrong assumption about the localization of the fusion proteins. This problem was tried to be circumvented by analyzing C-terminally tagged GFP-fusion proteins.

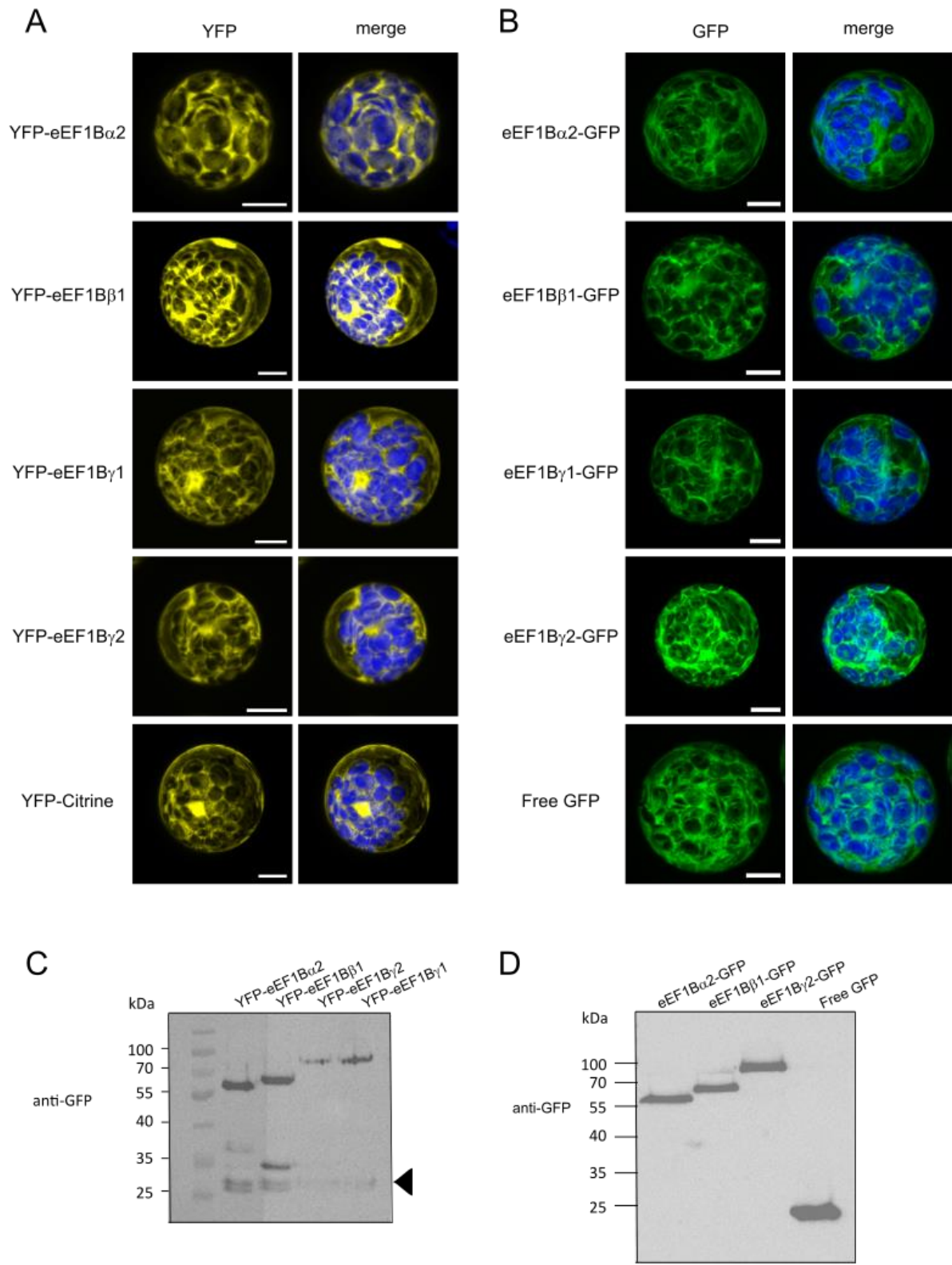


**Figure 53: Subcellular localization of eEF1B subunits in Arabidopsis protoplasts.** (A) Representative confocal images of Arabidopsis protoplasts transiently expressing N-terminally YFP-tagged eEF1B $\alpha$ 2, eEF1B $\beta$ 1, eEF1B $\gamma$ 1, eEF1B $\gamma$ 2 or negative control Citrine under 35S promoter. Merged images show YFP signal in yellow and chlorophyll autofluorescence in blue. Scale bar is 10  $\mu$ m. (B) Representative confocal images of Arabidopsis

protoplasts transiently expressing C-terminally GFP-tagged eEF1B $\alpha$ 2, eEF1B $\beta$ 1, eEF1B $\gamma$ 1, eEF1B $\gamma$ 2 or negative control free GFP under 35S promotor. Merged images show GFP signal in green and chlorophyll autofluorescence in blue. Scale bar is 10  $\mu$ m. (C) Immunoblot of protein extract from protoplasts transiently expressing N-terminally YFP-tagged eEF1B $\alpha$ 2, eEF1B $\beta$ 1, eEF1B $\gamma$ 2 or eEF1B $\gamma$ 1. Analysis was performed using an GFP antibody. Arrowhead points to free YFP. (D) Immunoblot of protein extract from protoplasts transiently expressing C-terminally GFP-tagged eEF1B $\alpha$ 2, eEF1B $\beta$ 1, eEF1B $\gamma$ 2 or free GFP. Analysis was performed using an GFP antibody.

To this end, cDNA of eEF1B subunits were cloned into pABind117 vector, which allows expression of C-terminally tagged GFP fusion proteins under an estradiol inducible 35S promotor. Plasmids were again expressed in Arabidopsis protoplasts and localization was analyzed using confocal laser-scanning microscopy. Similar, to the YFP-tagged versions, the GFP-tagged eEF1B proteins localized in the cytoplasm and for few protoplasts fluorescent signal was observed in the nucleus (Fig. 53B). Proteins were extracted from protoplasts expressing eEF1B $\alpha$ 2-GFP, eEF1B $\beta$ 1-GFP, eEF1B $\gamma$ 2-GFP and free GFP and were examined by immunoblotting. All GFP fusion proteins were detected at the expected sizes without additional free GFP in the sample (Fig. 53D). Free GFP was detected in the corresponding sample at around 27 kDa. No difference in subcellular localization was observed between N-terminally and C-terminally tagged proteins, but N-terminally tagged YFP-fusion proteins contained the free YFP in each sample, whereas no free GFP was found in samples with GFP-fusion proteins. Therefore, the GFP-tagged eEF1B subunits were used for further localization studies in Arabidopsis protoplasts.

Subcellular localization can change in response to environmental cues and upon stress conditions. Many different cytoplasmic proteins have been found to assemble in distinct cytoplasmic condensates after different stresses including heat, drought, osmotic or oxidative stress (Jang, Jang, and Wu 2020; Glauninger et al. 2022; Emenecker, Holehouse, and Strader 2020). McLoughlin et al. has examined the localization of eEF1B $\beta$  and eEF1B $\gamma$  with immunostaining under control conditions and after heat stress. Both eEF1B subunits localized to the cytoplasm under control conditions, but assembled in cytoplasmic condensates together with HSP101 after heat stress (McLoughlin et al. 2016).

To test whether cytoplasmic condensates containing the eEF1B subunits are formed in protoplasts after heat stress, transiently transformed protoplasts were subjected to 42°C for 60 min. eEF1B $\alpha$ 2-, eEF1B $\beta$ 1-, eEF1B $\gamma$ 1- and eEF1B $\gamma$ 2-GFP fusion proteins localized in cytoplasmic condensates after heat stress (Fig. 54). As negative control, protoplasts expressing free GFP were exposed to the same heat treatment. Free GFP did not change localization and

was still evenly distributed in the cytoplasm after heat stress. This indicates that the change of subcellular localization is specific to the eEF1B proteins and is in accordance with the observations published by (McLoughlin et al. 2016).

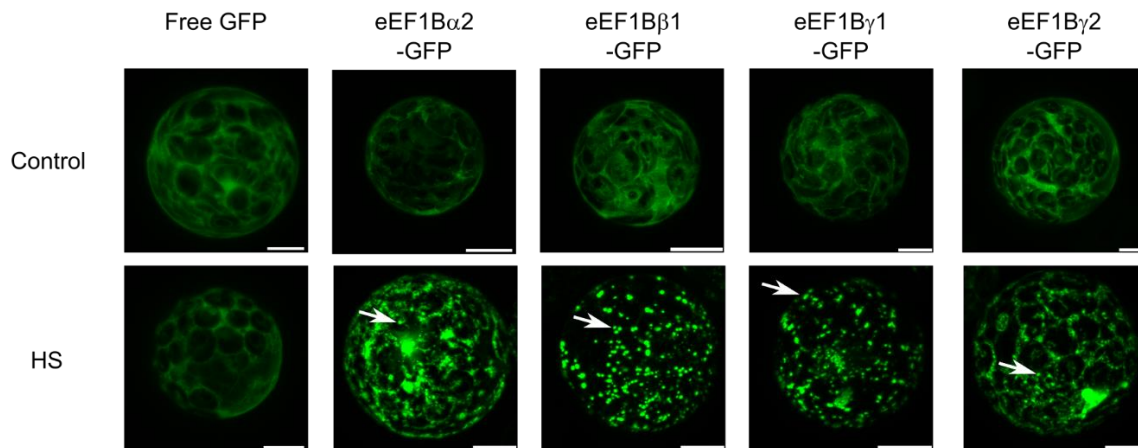


**Figure 54: eEF1B subunits accumulate in heat-induced cytoplasmic condensates.** Representative confocal images of Arabidopsis protoplasts transiently expressing free GFP (under constitutive 35S promoter), or eEF1B $\alpha$ 2-GFP, eEF1B $\beta$ 1-GFP, eEF1B $\gamma$ 1-GFP or eEF1B $\gamma$ 2-GFP (under an estradiol-inducible 35S promoter). Scale bar is 10  $\mu$ m. Free GFP remains evenly distributed in the cytoplasm after heat stress, but all three eEF1B subunits accumulate in cytoplasmic condensates. White arrows mark cytoplasmic condensates.

Since the two isoforms, eEF1B $\gamma$ 1 and eEF1B $\gamma$ 2, showed similar localization patterns, in the following only eEF1B $\gamma$ 2 was analyzed as representative for the eEF1B $\gamma$  subunit.

#### 4.4.2 eEF1B-containing condensates are partially overlapping with stress granules after heat stress

Different kinds of cytoplasmic condensates have been described for plant cells. The most prominent and most described membrane-less cytoplasmic condensates are stress granules (SGs) and processing bodies (PBs); (Kearly et al. 2022). Both of them are RNA-protein assemblies, which are formed via liquid-liquid phase separation (Kim et al. 2021). PBs are condensates, which contain translationally repressed mRNAs and proteins and the machinery for mRNA degradation including e.g. factors involved in deadenylation, decapping or non-sense mediated decay (reviewed in (Chantarachot and Bailey-Serres 2018)). Consequently, these factors are defined as marker proteins for PBs. One of these marker proteins is the mRNA decapping enzyme 1, DCP1 (Xu et al. 2006; Maldonado-Bonilla 2014; van Dijk et al. 2002). PBs are present in the cytoplasm under non-stress conditions, but change their dynamics, size and conformation upon different stresses.

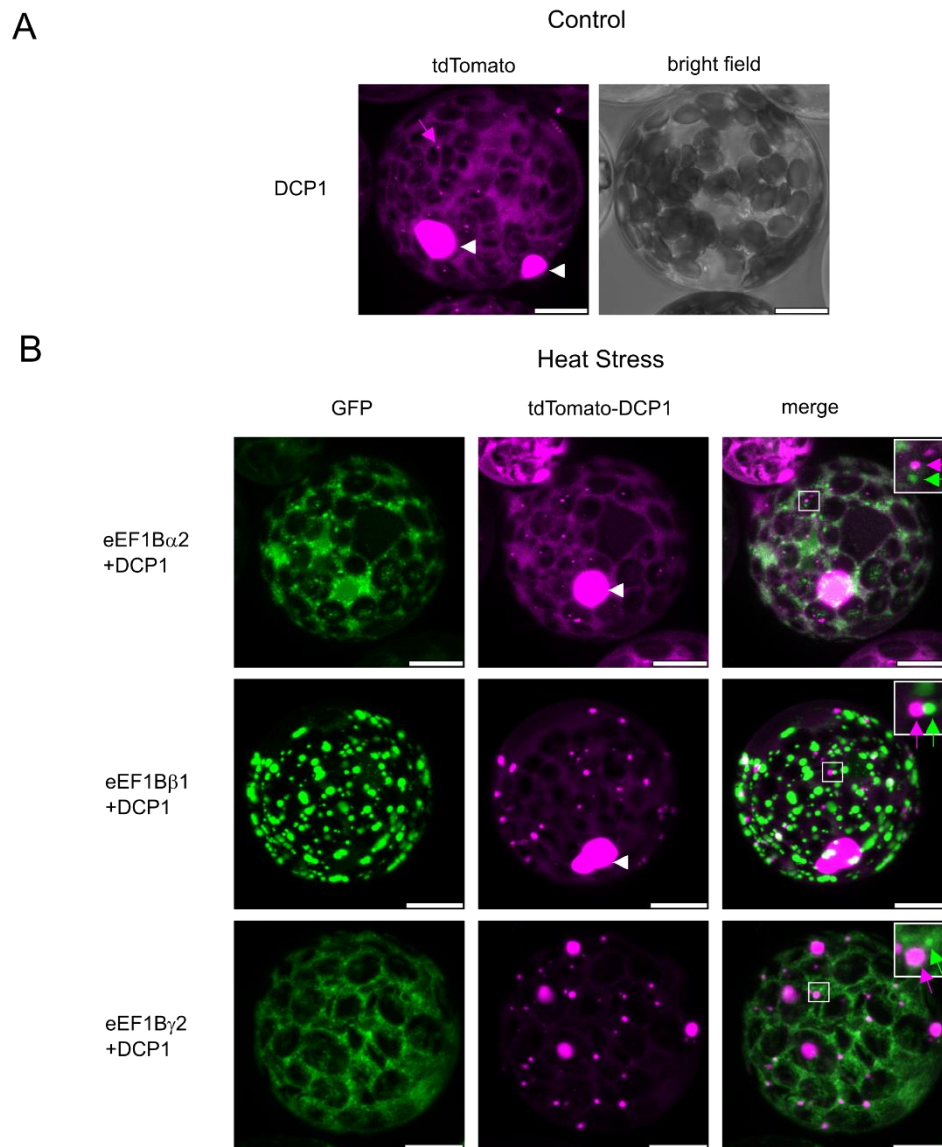


**Figure 55: Co-localization of eEF1B subunits with processing body marker DCP1.** (A) Representative confocal image of Arabidopsis protoplast transiently expressing *35S:tdTomato-Dcp1* under control conditions. White arrowheads indicate large aggregates formed by DCP1. Magenta arrow indicates processing bodies. Scale bar is 10  $\mu$ m. (B) Representative confocal images of protoplasts co-expressing eEF1B $\alpha$ 2-GFP, eEF1B $\beta$ 1-GFP or eEF1B $\gamma$ 2-GFP with tdTomato-DCP1 after 60 min at 42°C. Magenta arrows indicate processing bodies, green arrows indicate eEF1B subunit-containing condensates. eEF1B-containing condensates mostly do not co-localize with DCP1-processing bodies. Scale bar is 10  $\mu$ m.

To find out, whether the observed heat-induced eEF1B-containing condensates might be processing bodies, we obtained a tdTomato-DCP1 marker construct with a constitutive *35S* promoter from Markus Fauth (Weber, Nover, and Fauth 2008). The construct was transiently expressed in Arabidopsis protoplasts and observed under control conditions. tdTomato-DCP1 localizes to the cytoplasm, in few small condensates (marked by a magenta-colored arrow) and

in large aggregates (marked by a white arrowhead); (Fig. 55A). The small condensates were expected to be processing bodies. The large aggregates were unexpected, but after consultation with Markus Fauth, we know that the tdTomato-DCP1 tends to form aggregates, when it is overexpressed. To reduce the formation of large aggregates, the amount of plasmid DNA used for protoplast transformation was reduced, but still some large aggregates remained. Nonetheless, td-Tomato-DCP1 was co-expressed with the three GFP-tagged eEF1B subunits in protoplasts and co-localization was analyzed. Interestingly, there was little to no co-localization between any of the eEF1B-GFP subunits with DCP1 (Fig. 55B). This indicates that eEF1B-containing condensates are unlikely processing bodies.

The other most studied cytoplasmic condensates are SGs. SGs are not present in the cell under non-stress conditions and are only formed after different stimuli. The composition of SGs is partially dependent on the applied stress condition, but the main components include polyadenylated RNA, RNA-binding proteins, translation initiation factors and specific ribosomal proteins (Chantarachot and Bailey-Serres 2018). Analysis of the SG proteome in Arabidopsis has revealed the presence of eEF1B subunits in SGs (Kosmacz et al. 2019; Gutierrez-Beltran et al. 2021). To analyze the presence of eEF1B subunits in SGs, the proteins were co-expressed with the known marker protein for SGs, POLY-A-BINDING PROTEIN 8 (PAB8). A pUBN::RFP-PAB8 plasmid was kindly provided by Dr. Justin Lee (Tabassum et al. 2020). To make sure that we have similar expression levels of eEF1B subunits and PAB8, the PAB8 CDS was cloned into the pAB118, which is the same vector as the previously used GFP-containing pAB117 vector, but pAB118 allows expression with a C-terminal mCherry tag. Correct expression of the full-length fusion protein PAB8-mCherry (99,4 kDa) was verified by western blot analysis (Fig. 56D). PAB8-mCherry and each of the eEF1B-GFP subunits localized with an evenly distributed signal in the cytoplasm under control conditions. After 60 min at 42°C, each of the three eEF1B-GFPs co-localized with PAB8-mCherry in cytoplasmic condensates (Fig. 56A). To quantify the degree of co-localization two methods were used. First, the Pearson correlation value and the Spearman's rank correlation value were calculated. Both values can range from -1 to +1, with -1 representing no co-localization and +1 representing full co-localization. The correlation values for the three eEF1B-GFP subunits with PAB8-mCherry were all above +0,8, indicating a strong co-localization (Fig. 56B). Second, the number of condensates showing both GFP and mCherry fluorescence, and the total number of condensates (only GFP, only mCherry and both) were counted per cell. The percentage of condensates showing both fluorescent signals compared to the total number of condensates per cell was calculated and shown as frequency of co-localization. Each of the eEF1B-GFP subunits showed

at least 40 % overlap with the PAB8-mCherry (Fig. 56C). All together, these experiments showed a high degree of co-localization of eEF1B-containing condensates and PAB8-containing SGs, indicating that eEF1Bs are part of SGs.

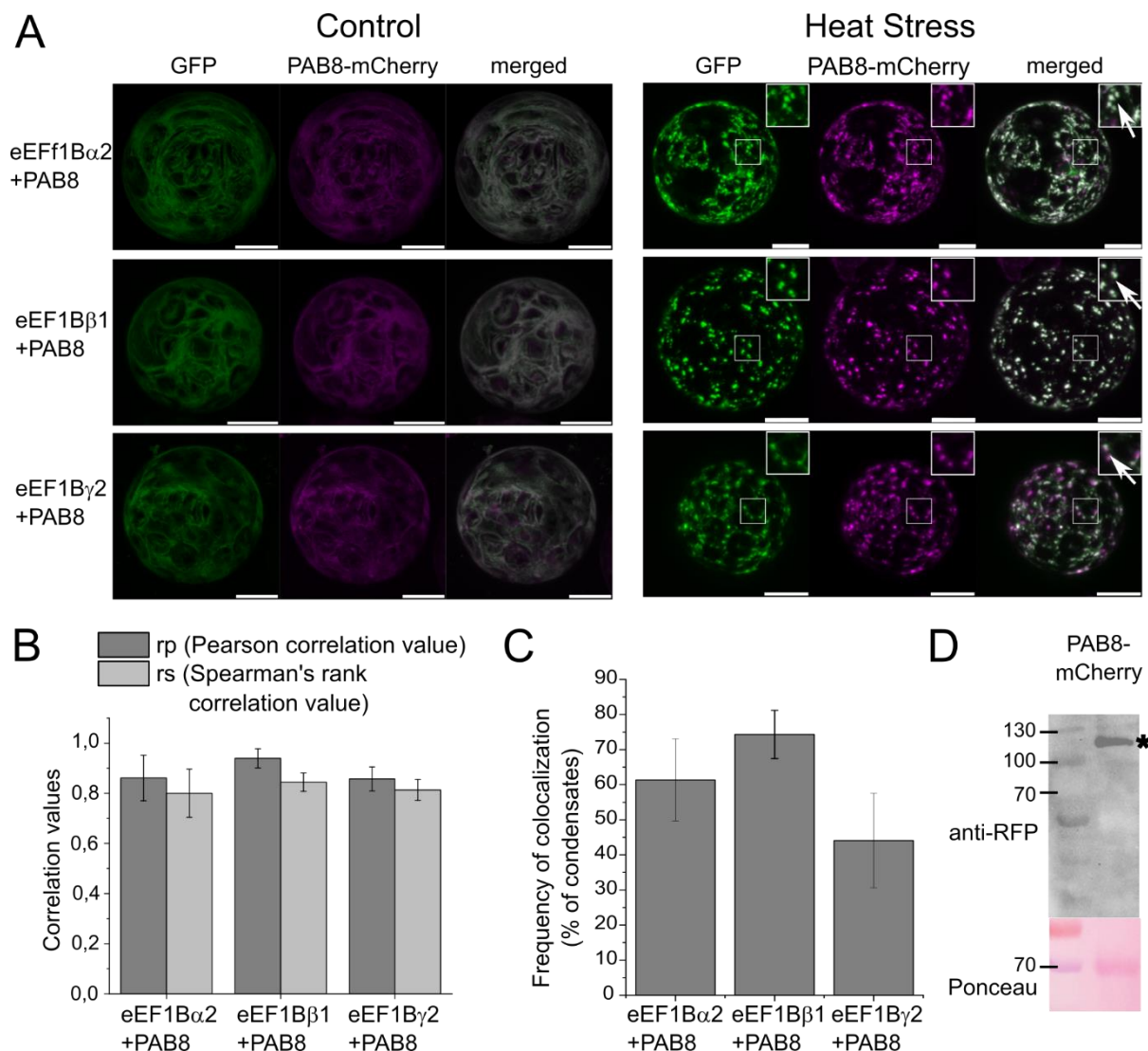


**Figure 56: Co-localization of eEF1B subunits with SG marker PAB8.** (A) Representative confocal images of Arabidopsis protoplasts co-expressing either eEF1B $\alpha$ 2-GFP, eEF1B $\beta$ 1-GFP or eEF1B $\gamma$ 2-GFP with PAB8-mCherry from an estradiol-inducible 35S promoter. All three eEF1B subunits perfectly co-localize with PAB8 under control condition, where each protein is equally distributed among the cytoplasm. After heat stress (60 min at 42°C), eEF1B subunits and PAB8 co-localize in cytoplasmic condensates. Scale bar is 10  $\mu$ m. Insets show 2x magnification of the small box indicated. Arrows point at condensates. (B) Pearson correlation value and Spearman's rank correlation value to quantify the co-localization between eEF1B subunits and PAB8. Correlation values can vary between +1 (positive correlation) and -1 (negative correlation). All three eEF1B subunits show a positive correlation with PAB8 indicating a high degree of co-localization (n=25). (C) Frequency of co-localization between eEF1B subunits and PAB8 is showing the ratio of co-localizing condensate (showing GFP and mCherry fluorescence) to the total number of condensates (only GFP, only mCherry or both). eEF1B $\beta$  subunit show the highest frequency of co-localization (n=25). Data represent means  $\pm$ SE from three independent

experiments. **(D)** Immunoblot of protein extract from protoplasts transiently expressing C-terminally mCherry-tagged PAB8. Analysis was performed using an RFP antibody. Asterisk marks PAB8-mCherry.

To further analyze if eEF1B condensates are SGs, another SG feature was examined. SG assembly is induced by stress conditions and after stress relief SGs are disassembled (Hofmann et al. 2021). To analyze whether observed eEF1B condensates are able to disassemble after stress relief, stably transformed lines overexpressing 35S:YFP-eEF1B $\beta$ 1 or 35S:YFP-eEF1B $\gamma$ 2 were generated. Using stably transformed lines simplifies the observation of the same cells after stress relief. Protoplasts are often too sensitive and might burst after longer incubation time. Root cells of 4 dag seedlings were observed at control conditions, immediately after 20 min at 42°C (Heat Stress) or after 12 h at 22°C after the heat stress (Recovery). This analysis was performed by Dr. Magdalena Weingartner. In root cells of eEF1B $\beta$ 1- and eEF1B $\gamma$ 2-expressing cells cytoplasmic condensates were observed after heat stress (Fig. 57). No condensates were observed in a 35S:GFP line, which was used as negative control. The observed eEF1B $\beta$ 1 and eEF1B $\gamma$ 2 condensates were fully disassembled 12 h after recovery from heat stress. This shows that eEF1B condensates show another SG-defining feature, in addition to co-localizing with the SG marker PAB8.

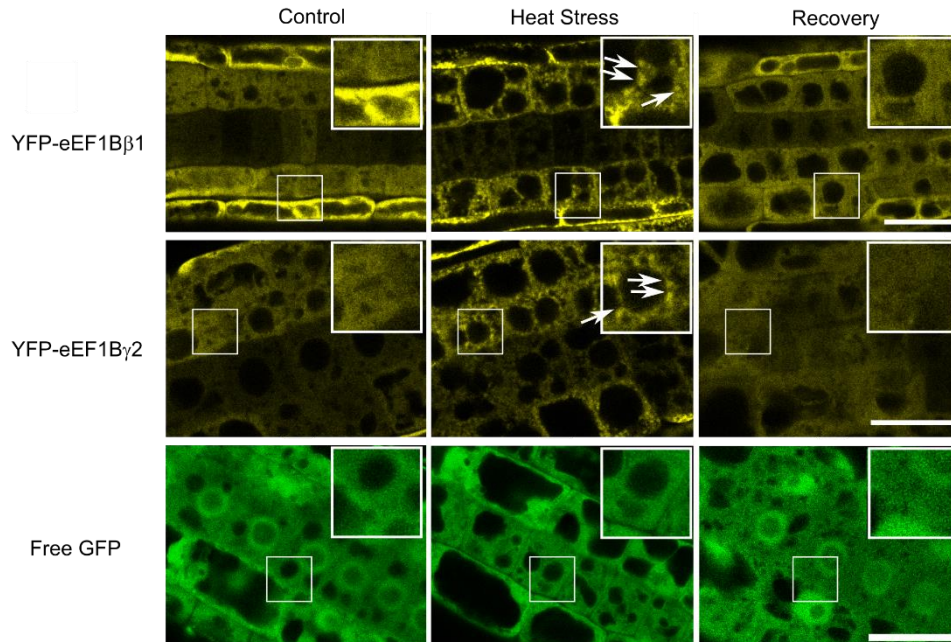


**Figure 57: Condensate assembly and disassembly in Arabidopsis root cells.** Confocal images of Arabidopsis root cells from 4 dag seedlings stably transformed with 35S:YFP-eEF1B $\beta$ 1 (n=35), 35S:YFP-eEF1B $\gamma$ 2 (n=32) or 35S:GFP (n=32). Roots were imaged under control conditions, after heat stress (20 min at 42°C) and after recovery (12 h at 22°C after heat stress). In root cells expressing YFP-eEF1B $\beta$ 1 or YFP-eEF1B $\gamma$ 2 cytoplasmic condensates

were observed after heat stress, which were disassembled after recovery. No condensates were observed in cells expressing GFP after heat stress. Scale bar is 23  $\mu\text{m}$ .

Formation of SGs is strongly dependent on presence of mRNAs. In presence of CHX, which hinders the release of mRNAs from polysomes, SG assembly is inhibited (Kedersha et al. 2000; Weber, Nover, and Fauth 2008). We analyzed the assembly of eEF1B-containing condensates in presence of CHX. Therefore, protoplasts transiently expressing eEF1B $\alpha$ 2-GFP, eEF1B $\beta$ 1-GFP or eEF1B $\gamma$ 2-GFP were either treated with 100  $\mu\text{M}$  CHX and then heat treated for 60 min at 42°C (CHX + HS) or directly heat stressed for 60 min at 42°C (HS). As positive control for the CHX treatment, we also analyzed the PAB8-GFP condensate formation. It was expected that significantly less PAB8-containing SGs were being formed. After HS, around 70 PAB8-GFP condensates were present per cell. As anticipated, if pre-treated with CHX the number of PAB8-GFP condensates was significantly reduced to about 45 condensates (Fig. 58A and 58B). Similarly, the number of eEF1B $\alpha$ 2- and eEF1B $\gamma$ 2-GFP-containing condensates was significantly reduced by CHX pre-treatment, indicating that they behave similar to PAB8-associated condensates. In contrast, the number of eEF1B $\beta$ 1-GFP-containing condensates was slightly, but not significantly reduced. This indicates that accumulation of eEF1B $\beta$ 1-GFP in condensates is less dependent on the presence of free mRNAs compared to PAB8-associated condensates. It might be concluded that although eEF1B $\beta$ 1-GFP condensates are partially overlapping with SGs (Fig. 56), eEF1B $\beta$ 1 is also present in other forms of condensates or aggregates that are not dependent on the presence of free mRNAs.

Interestingly, the eEF1B $\beta$ 1-GFP-containing condensates are not only different from the other two eEF1B subunit-containing condensates by being able to form despite the CHX treatment, but show overall a higher number of condensates after heat stress. More than 130 eEF1B $\beta$ 1-GFP condensates are formed per cell after heat stress, while only about 50 eEF1B $\alpha$ 2- or eEF1B $\gamma$ 2-GFP condensates are assembled. The number of eEF1B $\beta$ 1-GFP condensates is even higher than the number of PAB8-containing stress granules (Fig. 58B). The observed differences in condensation behavior of eEF1B $\beta$ 1-GFP compared to other eEF1B-GFP subunits have not been described in any organism so far and therefore it was examined in more detail in the following. Before, I would like to shortly digress and explain the methods used to quantify the condensates.

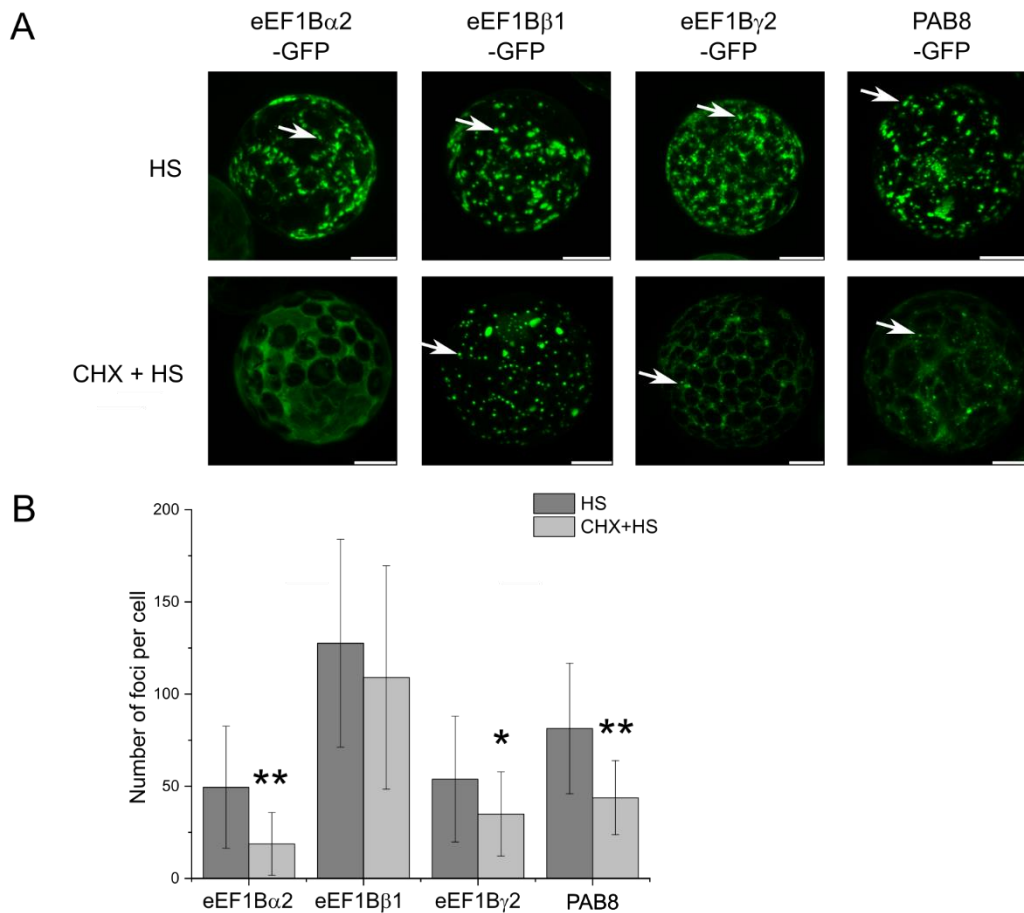


**Figure 58: eEF1B $\beta$ 1-condensates are distinct from eEF1B $\alpha$ 2- and eEF1B $\gamma$ 2 condensates.** (A) Representative confocal images of Arabidopsis protoplasts transiently expressing eEF1B $\alpha$ 2-GFP, eEF1B $\beta$ 1-GFP, eEF1B $\gamma$ 2-GFP or stress granule marker PAB8-GFP from an estradiol-inducible *35S* promoter. Protoplasts were either heat stressed for 60 min at 42°C (HS) or first treated with 100  $\mu$ M CHX for 120 min and then heat stressed for 60 min at 42°C (CHX+HS). Cytoplasmic condensates are marked by arrows. Scale bar is 10  $\mu$ m. (B) Number of cytoplasmic condensates per cell counted from confocal images taken in the experiment shown in (A) using ImageJ software. Values show means  $\pm$ SE from two or three independent experiments (n=20-50). Asterisks indicate significant difference between HS and CHX+HS (two-tail t-test; \*\*P<0.01 and \*P<0.05).

#### 4.4.3 Short digression: Quantification of condensates – possibilities and disadvantages

The quantification of condensates is important to demonstrate differences in the condensation behavior of various proteins. Although all three eEF1B subunits were found in cytoplasmic condensates after heat stress, a different number of condensates per cell has been found (Fig. 58B). The quantification of condensates was performed using ImageJ software. To this end, a certain number of protoplasts was imaged with the exact same microscopic settings (e.g. laser intensity) and z-stacks were evaluated using the ‘Analyze Particles’ function in ImageJ. This method allows an automated counting of number and size of the condensates. But there are also certain withdrawals to this method. The automated recognition of particles often leads to poor

coverage, which is the case when several condensates are in close proximity, have different fluorescent signal intensities or there is a lot of cytoplasmic ‘background’ signal. An example showing the automatic recognition and coverage of condensates using ‘Analyze Particles’ function of two different protoplasts is shown in Fig. 59.

Evaluation with the eye leads to the observation that the upper protoplast has few condensates with much cytoplasmic ‘background’ signal, while the lower protoplast has many distinct condensates (Fig. 59). But the automatic counting of condensates results in contradicting numbers of 82 condensates for the upper protoplast and 53 condensates for the lower protoplast. This leads to the necessity of manual adjustment of the coverage for each protoplast.

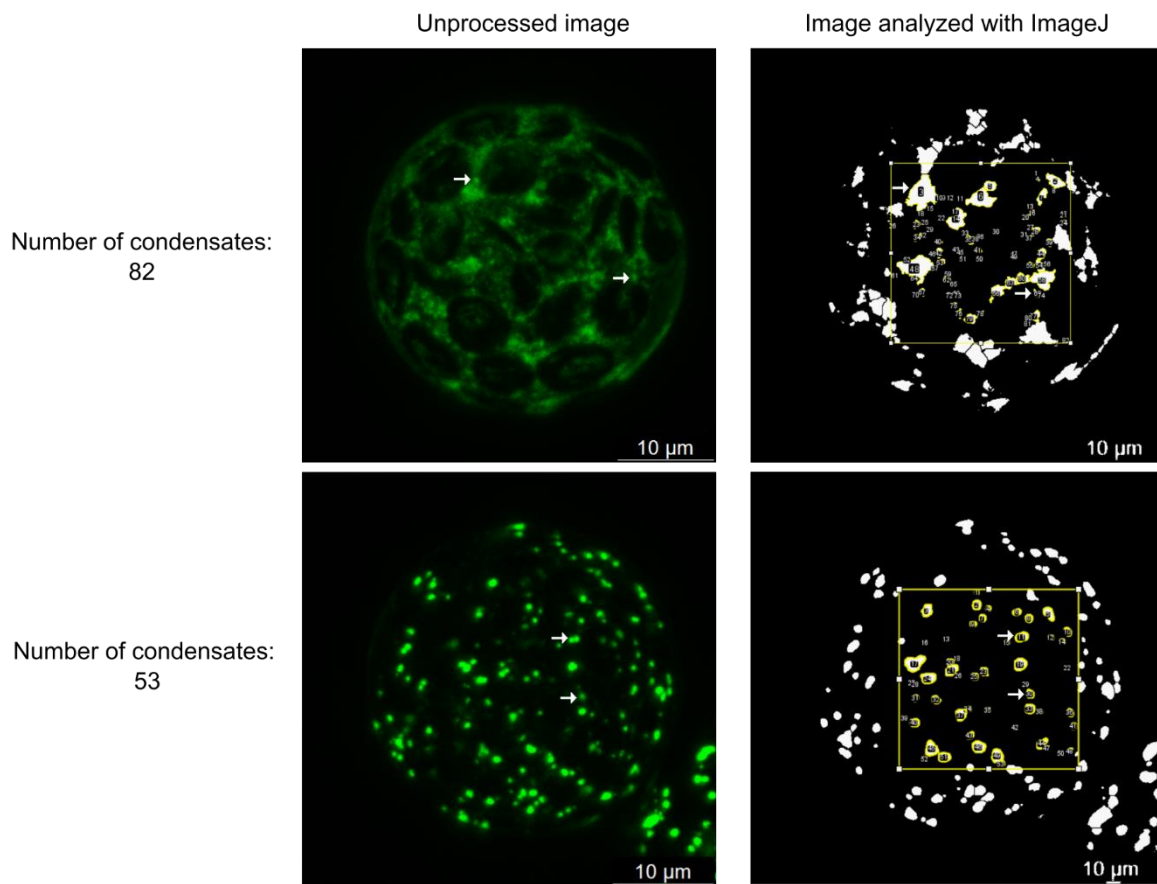


**Figure 59: Quantification of condensates – possibilities and disadvantages.** Representative confocal images transiently expressing eEF1B $\alpha$ 2-GFP (top) or eEF1B $\beta$ 1-GFP (bottom) to illustrate quantification of condensates using ImageJ ‘Analyze Particles’ function. Left images show Z-stacks of further unprocessed images taken with same confocal settings. Right images show the same images after preparation for and use of ‘Analyze particles’ function. White color represents every fluorescent signal recognized by ImageJ with the chosen ‘Intermediates’ filter. Yellow color shows particles were counted for the quantification by the ‘Particles Analyzer’, for top image 82 condensates were counted, for bottom image 53 condensates were counted.

Another withdrawal to this automatic quantification method is that the decision, which protoplasts are being imaged, is still subjectively taken by the microscopist. This can be challenging since there are differences within each protoplast population that is transformed with the same construct. Not all protoplasts that were transformed with an eEF1B construct showed exactly the same condensate pattern. Representative images of different protoplasts from the same transformation showing these diverging condensate patterns are shown in Figure 60.

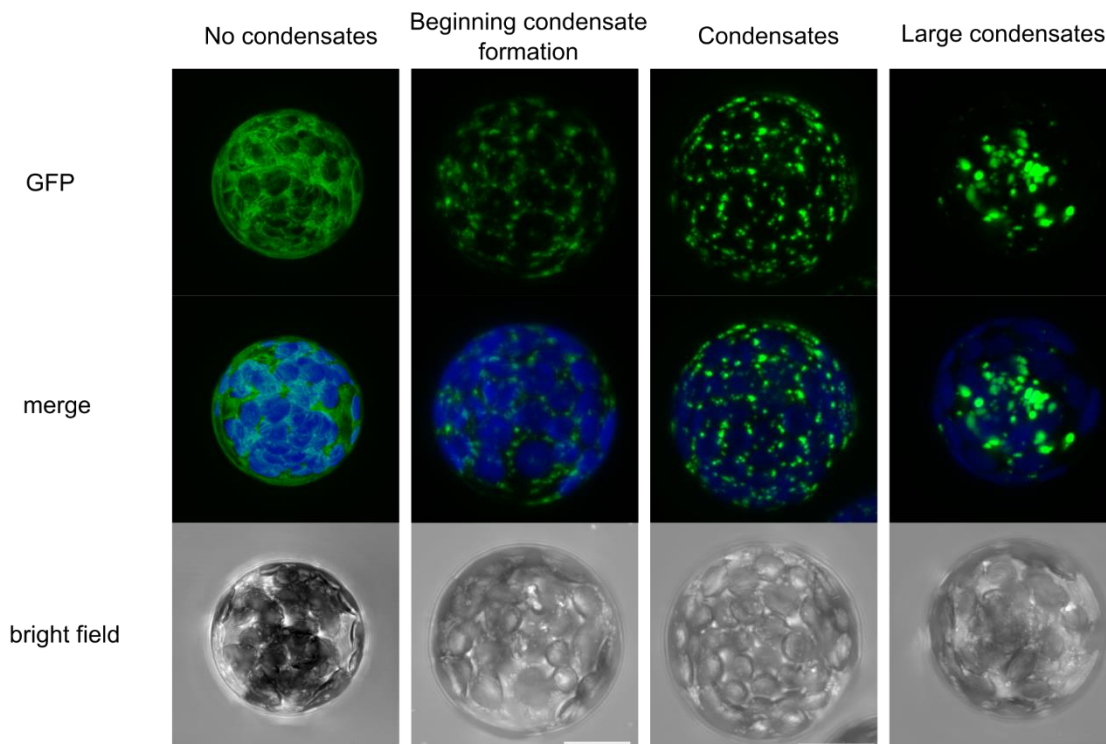


**Figure 60: Quantification of condensates.** Representative confocal images of protoplasts transiently expressing eEF1B $\beta$ 1-GFP to explain the semi-quantitative quantification of condensates shown in Fig. 61. Protoplasts were classified in four categories based on observation at the confocal microscope and counted: No condensates (even cytoplasmic fluorescent signal), beginning condensate formation (small condensates formed, but still a lot of cytoplasmic signal), condensates (small and medium-sized condensates formed with non or very little cytoplasmic signal) or large condensates (large condensates with no cytoplasmic signal). Scale bar is 10  $\mu$ m.

The explained disadvantages led us to use another semi-quantitative evaluation method to analyze condensate formation. Three independent experiments were performed and in each experiment 50-60 protoplasts for each construct were observed. The protoplasts were sorted in four categories according to the condensate pattern: ‘no condensates’, ‘beginning condensate formation’, ‘condensates’ or ‘large condensates’. The category ‘beginning condensate

formation' defines protoplasts having most fluorescent signal in the cytoplasm with only very small condensates. Protoplasts of the category 'condensates' accumulate most fluorescent signal in condensates with little to no cytoplasmic signal. Protoplasts with 'large condensates' show no cytoplasmic signal and few condensates, which were larger in size. Categories are exemplified in Fig. 60. This method considers the relative differences that derive from protoplast transformation. Nonetheless, this method of evaluation is dependent on the subjective categorization of the microscopist as well. Consequently, both methods used in this study have advantages and disadvantages. Optimal evaluation of confocal condensates requires careful and thoughtful imaging and an optimized automatic pipeline for image analysis. Lately, several groups have developed such pipelines and thereby drastically improved the reliability of condensate characterization from live cell imaging (Baggett et al. 2022).

#### 4.4.4 eEF1B $\beta$ shows a different condensation behavior than the other eEF1B subunits

First, this semi-quantitative evaluation was used to decipher differences between the three eEF1B subunits upon different temperature stress conditions. Protoplasts transformed with eEF1B $\alpha$ 2-GFP, eEF1B $\beta$ 1-GFP or eEF1B $\gamma$ 2-GFP were subjected to 30°C, 34°C or 38°C for 60 min. Interestingly, eEF1B $\beta$ -GFP derived fluorescence was observed in condensates or large condensates in about 30% of protoplasts that were incubated at 30°C. Condensate formation further increased after incubation at 34°C, and 88% of protoplasts showed condensates or large condensates after incubation at 38°C (Fig. 61A and 61B).

In contrast, protoplasts expressing eEF1B $\alpha$ 2-GFP or eEF1B $\gamma$ 2-GFP showed almost no cytoplasmic condensates after incubation at 30°C and 34°C. At 38°C, about 30% of protoplasts expressing eEF1B $\alpha$ 2-GFP or eEF1B $\gamma$ 2-GFP were in the category of beginning condensate formation (Fig. 61A and 61B). In conclusion, this experiment further underlined that eEF1B $\beta$ 1-GFP showed a different pattern of condensate formation than the two other eEF1B subunits.

Next, we wanted to find out, whether the presence of eEF1B $\beta$ 1 has an influence on the accumulation of the other two subunits in cytoplasmic condensates. Therefore, eEF1B $\beta$ 1 was co-expressed with eEF1B $\alpha$ 2 or eEF1B $\gamma$ 2 in protoplasts. As controls, eEF1B $\alpha$ 2 was co-expressed with eEF1B $\gamma$ 2 and additionally eEF1B $\gamma$ 2 was co-expressed with eEF1B $\gamma$ 1. In general, more eEF1B $\alpha$ 2- and eEF1B $\gamma$ 2-containing condensates were detected in presence of eEF1B $\beta$ 1 (Fig. 62A).

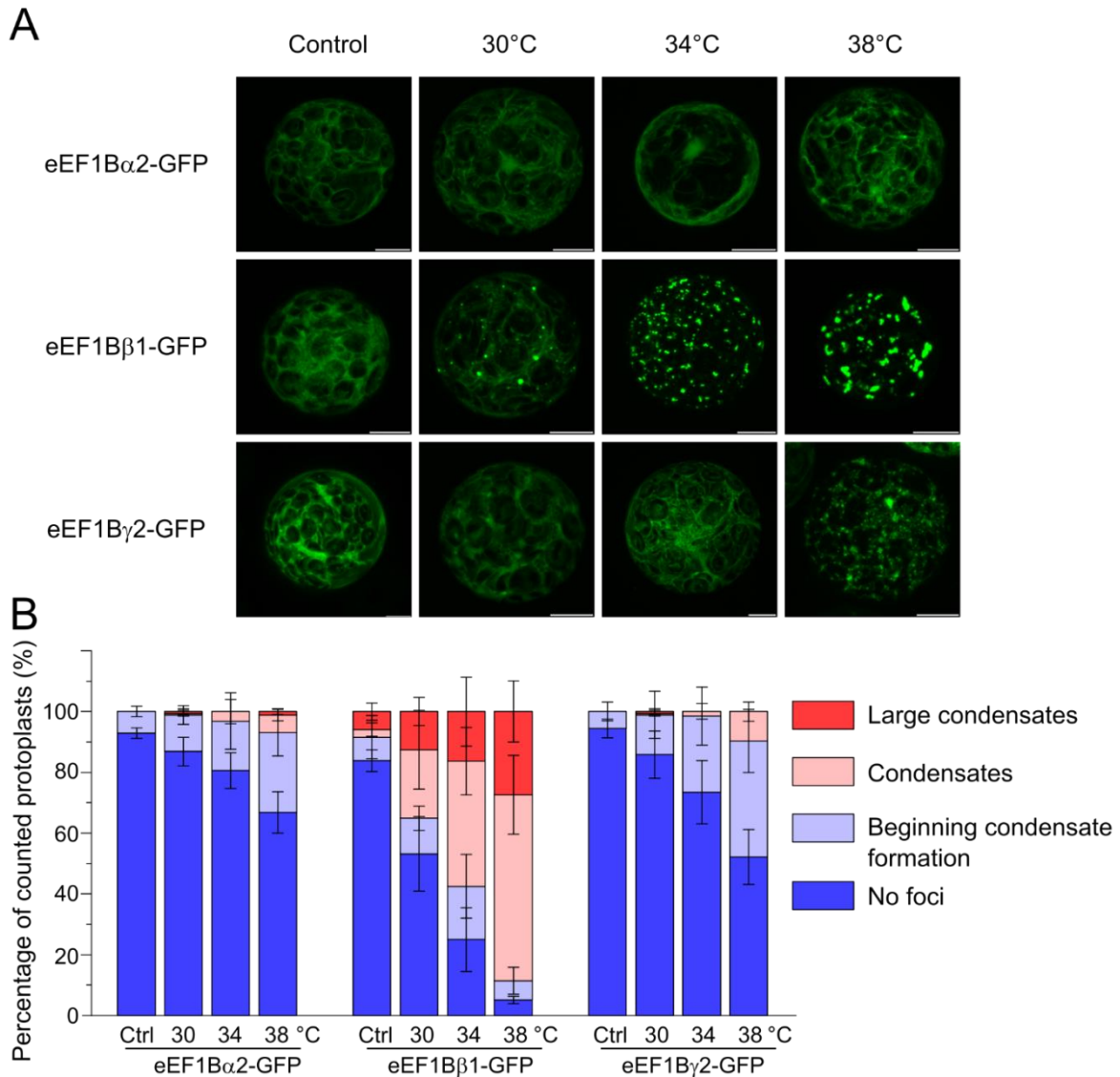


**Figure 61: eEF1B $\beta$  subunit accumulates in cytoplasmic condensates at lower temperatures compared to eEF1B $\alpha$  or eEF1B $\gamma$ .** (A) Representative confocal images of Arabidopsis protoplasts transiently expressing eEF1B $\alpha$ 2-GFP, eEF1B $\beta$ 1-GFP or eEF1B $\gamma$ 2-GFP from an estradiol-inducible 35S promoter. Protoplasts were imaged at 22°C for control or after 60 min at 30°C, 34°C or 38°C. Scale bar is 10  $\mu$ m. (B) Semi-quantitative evaluation of protoplasts transformed and heat-stressed as described in (A). Data show means  $\pm$ SE from three independent experiments with at least 60 protoplasts being counted for each construct at each condition and each experiment.

Both above mentioned quantification methods were used to evaluate this observation. First, the quantification with ImageJ was used to count all condensates per cell, which either showed only GFP fluorescence, only mCherry fluorescence or both. More than 90 eEF1B $\alpha$ 2-containing condensates were counted when co-expressed with eEF1B $\beta$ 1, whereas only 30 eEF1B $\alpha$ 2-condensates were detected, if co-expressed with eEF1B $\gamma$ 2 (Fig. 62B). Second, the influence of eEF1B $\beta$ 1 co-expression was evaluated using the semi-quantitative categorization of

protoplasts. Similar to the automatic counting did this underline that presence of eEF1B $\beta$ 1 increases the number of eEF1B $\alpha$ 2- or eEF1B $\gamma$ 2-containing condensates (Fig. 62C). The number of protoplasts showing ‘condensates’ increased drastically, if eEF1B $\beta$ 1 was present in addition to eEF1B $\alpha$ 2 or eEF1B $\gamma$ 2.

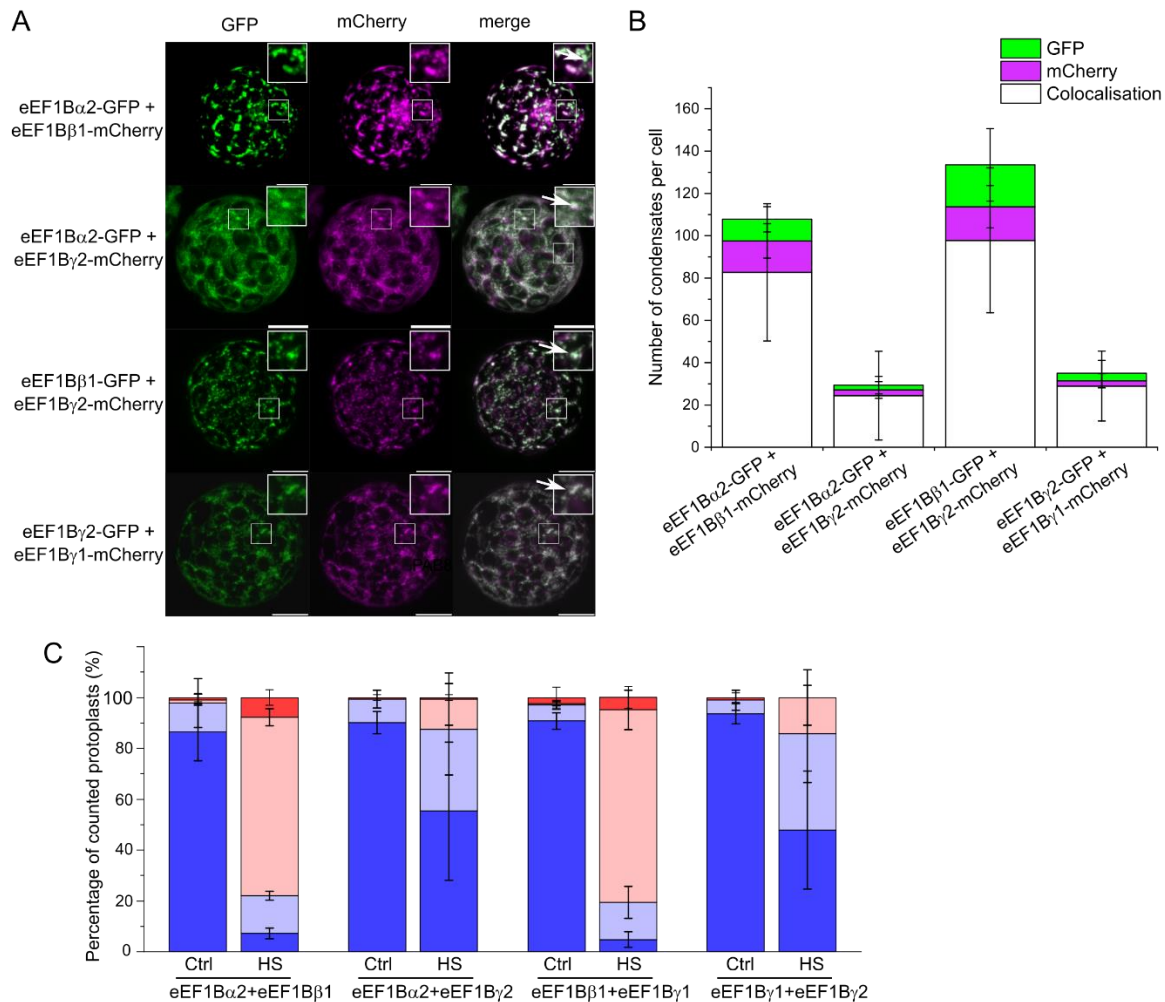


**Figure 62: Expression of eEF1B $\beta$  influences the assembly of both other eEF1B subunits in cytoplasmic condensates.** (A) Representative confocal images of protoplasts transiently co-expressing the following combinations: eEF1B $\alpha$ 2-GFP + eEF1B $\beta$ 1-mCherry; eEF1B $\alpha$ 2-GFP + eEF1B $\gamma$ 2-mCherry; eEF1B $\beta$ 1-GFP + eEF1B $\gamma$ 2-mCherry; eEF1B $\gamma$ 2-GFP + eEF1B $\beta$ 1-mCherry from an estradiol-inducible 35S promoter after 60 min at 42°C. White arrows indicate co-localizing proteins in cytoplasmic condensates. Scale bar is 10  $\mu$ m. (B) Quantification of cytoplasmic condensates from confocal images of protoplasts as described in (A). Condensates showing only GFP fluorescence, only mCherry or both were counted using ImageJ software. Values show means  $\pm$ SE from three independent experiments (n=25 per construct). (C) Semi-quantitative evaluation of protoplast populations as described in (A). Protoplasts were counted under control conditions or after heat stress (60 min at 42°C; HS). Values show means  $\pm$ SE from three independent experiments (n  $\geq$  60 per construct).

In conclusion, both quantification methods indicated the same result: eEF1B condensate formation is strongly influenced by the presence of eEF1B $\beta$ . Y2H analysis has shown that eEF1B $\beta$  is the central component in the eEF1B complex (Fig. 23). Together with the localization results this could lead to the hypothesis that eEF1B $\beta$  plays an important role for accumulation of translation elongation factors in cytoplasmic condensates in response to stress. This could be a mechanism supporting the translational downregulation upon stress conditions. The next consecutive experiment to prove the role of eEF1B $\beta$  in enhancing condensate assembly after heat stress would be the analysis of condensate assembly in *eef1b $\beta$*  knock-out mutants. If eEF1B $\beta$  is crucial for condensate formation, the knock-out mutant would be defective in condensate assembly as it has been shown for e.g. *tsn1 tsn2* mutants (Gutierrez-Beltran et al. 2015). As described in 4.2.4, no *eef1b $\beta$*  knock-out mutant was available at the moment.

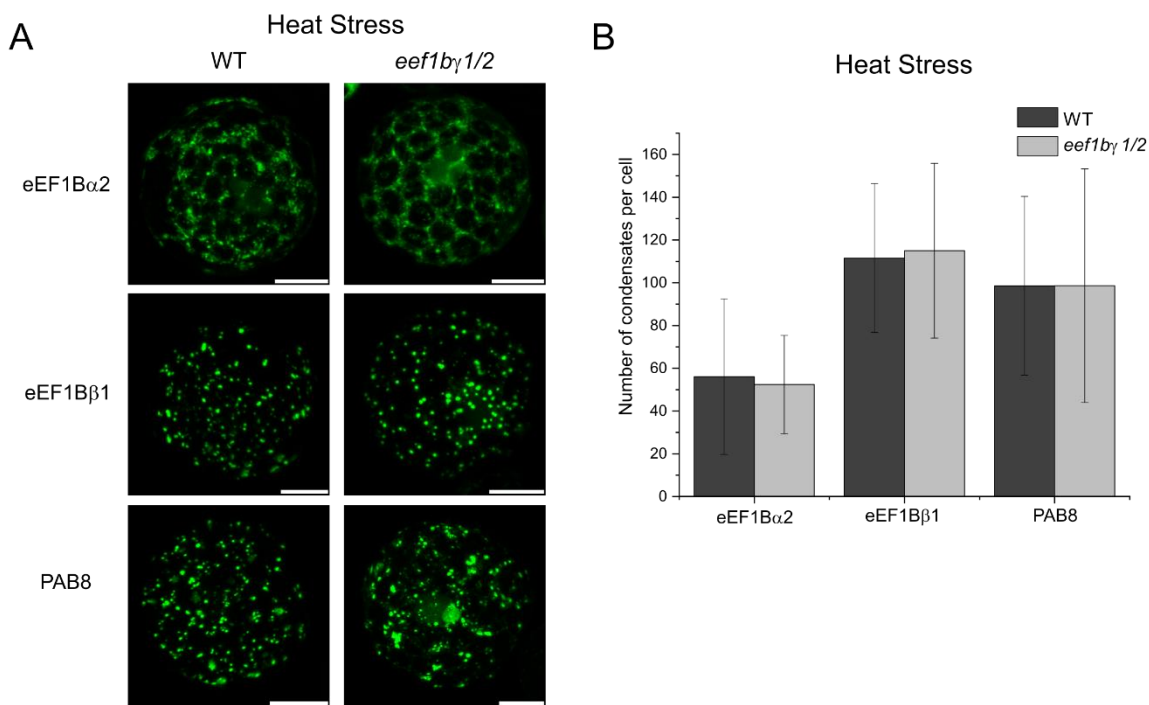


**Figure 63: Loss of eEF1B $\gamma$  does not influence cytoplasmic condensate formation.** (A) Representative confocal images of WT or *eef1b $\gamma$ 1/2* protoplasts expressing eEF1B $\alpha$ 2-GFP, eEF1B $\beta$ 1-GFP or PAB8-GFP from an estradiol-inducible *35S* promoter. Protoplasts were imaged after 60 min at 42°C. (B) Quantification of condensates per cell in protoplasts as described in (A). Values represent means  $\pm$ SE from at least two independent experiments (n=20-30).

To analyze whether loss of any eEF1B subunit does already have an effect on condensate assembly, the *eef1b $\gamma$ 1/2* double mutant was analyzed. Protoplasts were isolated from WT plants

or *ee1b $\gamma$ 1/2* plants and transformed with eEF1B $\alpha$ 2-GFP, eEF1B $\beta$ 1-GFP or PAB8-GFP. The number of condensates per cell was counted using ImageJ software. No significant difference was observed for any of the three proteins in the number of condensates between WT and *ee1b $\gamma$ 1/2* protoplasts (Fig. 63A and 63B). Consequently, eEF1B $\gamma$  subunit is not required for condensate assembly.

#### 4.5 Interaction networks of eEF1B $\beta$ and eEF1B $\gamma$

Our subcellular localization studies indicated that the eEF1B subunits are part of heat-induced condensates, which are partially co-localizing with SG components. Additionally, we found significant differences in the localization changes of the eEF1B $\beta$  subunit compared to eEF1B $\gamma$  after heat stress. To analyze the interaction networks of eEF1B $\beta$  and eEF1B $\gamma$  in more depth, we used the stably transformed *35S:YFP-eEF1B $\beta$ 1* and *35S:YFP-eEF1B $\gamma$ 2* lines to perform immunoaffinity purification followed by mass spectrometry analysis (IP-MS). Seedlings were grown for seven days in liquid MS medium to generate large amounts of plant material. Initially, it was planned to analyze both lines of interest under control conditions and after heat stress. Before the IP-MS analysis, we performed pre-experiments to decide for the best experimental conditions. First, we tested whether cytoplasmic condensates could be observed after the seedlings were exposed to heat stress at 42°C for 30 min in a water bath. Indeed, both fluorescently tagged proteins localized in cytoplasmic condensates after the heat stress (Fig. 64A). Second, we tested whether both proteins could be extracted from leaf material with the chosen standard extraction buffer. Therefore, grinded snap-frozen leaf material was resuspended in the extraction buffer and centrifuged once to obtain a supernatant and a pellet fraction. YFP-eEF1B $\beta$ 1 and YFP-eEF1B $\gamma$ 2, which localize in the cytosol, were expected to be extracted into the supernatant fraction. Under control conditions, both proteins, YFP-eEF1B $\beta$ 1 and YFP-eEF1B $\gamma$ 2 could be detected by immunoblotting using an GFP-antibody. After heat stress, only YFP-eEF1B $\gamma$ 2, but not YFP-eEF1B $\beta$ 1 could be detected in the supernatant of the protein extract (Fig. 64B). A second experiment verified this result and showed that a large amount of YFP-eEF1B $\beta$ 1 protein retained in the pellet fraction (Fig. 64C). Therefore, we chose to analyze YFP-eEF1B $\beta$ 1 only under control conditions and YFP-eEF1B $\gamma$ 2 under both, control and heat stress, conditions in IP/MS assays. As negative control, a *35S:GFP* expressing line was used under control and heat stress condition. Three samples of 3 g frozen plant material for each line and condition were sent to Dominique Eeckhout and Geert Persiau at VIB-UGent Center for Systems Biology (Ghent, Belgium), who performed the protein extraction and IP/MS analysis.

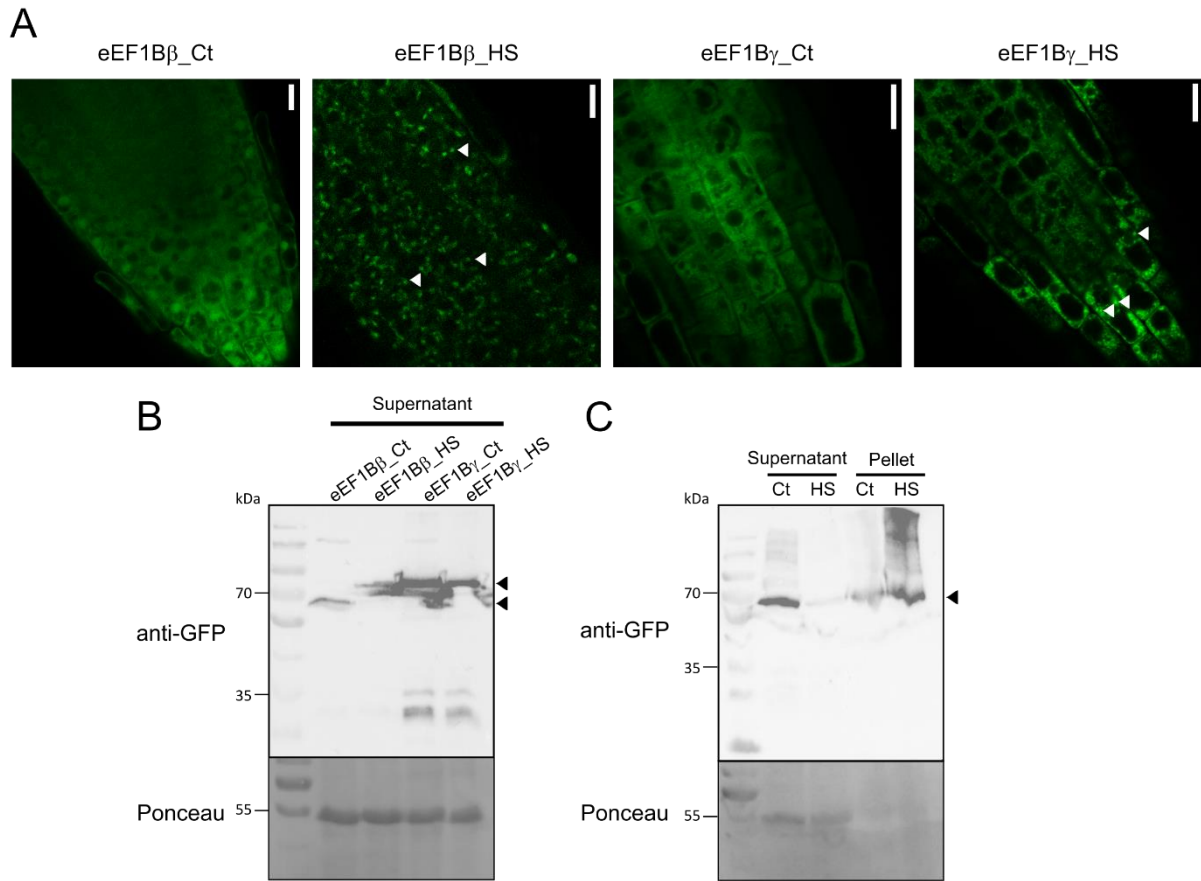


**Figure 64: eEF1B $\beta$  protein remains in pellet fraction after heat stress.** (A) Representative confocal images of Arabidopsis roots of seven days-old seedlings grown in liquid culture under control conditions (Ct) or after 30 min at 42°C (HS) from stably transformed lines expressing 35S:YFP-eEF1B $\beta$ 1 or 35S:YFP-eEF1B $\gamma$ 2. Scale bar is 10  $\mu$ m. (B) Immunoblot of supernatants from protein extracts of seedlings shown in (A). Immunoblotting was performed using GFP-antibody. Nitrocellulose membrane was stained with Ponceau S for loading control. Arrowheads point at YFP-eEF1B $\beta$  and YFP-eEF1B $\gamma$  protein bands. (C) Immunoblots of supernatant and pellet fraction of protein extracts of YFP-eEF1B $\beta$  expressing lines at control conditions (Ct) or after 30 min at 42°C (HS). Arrowhead points at YFP-eEF1B $\beta$ . For each supernatant sample 15  $\mu$ g protein was loaded onto the SDS gel.

Label-free mass spectrometric measurements were performed on a Q Exactive (Thermo Fisher) and searches were done with MaxQuant. MaxQuant LFQ intensities (Cox et al. 2014) were used for quantitative analysis in Perseus (Tyanova et al. 2016). In the following, a preliminary analysis of the generated data was performed. The identified interactions will have to be verified in independent experiments. To select specific interactors of eEF1B $\beta$  or eEF1B $\gamma$  under control conditions, the identified protein pools were compared to GFP pool under control conditions. Similarly, the eEF1B $\gamma$  protein pool after heat stress was compared to the GFP pool after heat stress. Pairwise comparisons were done via Students *t*-test. All enriched proteins of the three comparisons are shown as volcano plots in Fig. 65A, 65B and 65C. Significantly enriched

proteins from each comparison with a False Discovery Rate (FDR) below 0.01 are marked in red. Interestingly, a higher number of proteins was identified as significantly enriched in eEF1B $\gamma$ \_HS vs. GFP\_HS (119 proteins) compared to control conditions (eEF1B $\beta$ \_Ct vs. GFP\_Ct (13 proteins); eEF1B $\gamma$ \_Ct vs. GFP\_Ct (16 proteins)). Hereafter, the protein lists will be shortly named eEF1B $\gamma$ \_HS, eEF1B $\beta$ \_Ct and eEF1B $\gamma$ \_Ct, which will correspond to above mentioned GFP controls (unless stated otherwise).

In order to get an overview of the biological processes that the eEF1B interactors are involved in, a Gene Ontology (GO) enrichment analysis was performed using a combination of Panther, Revigo and R as previously described (Bonnot, Gillard, and Nagel 2019). The identified enriched biological processes of eEF1B $\beta$  and eEF1B $\gamma$  under control conditions were very similar (Fig. 65D). Several metabolic and biosynthetic processes were enriched as well as 'gene expression'. The highest fold enrichment was notified for 'translation elongation'. This confirms that the IP/MS experiment was successfully performed, since the strongest interactions of eEF1B subunits were expected to be with other translation elongation factor subunits. After heat stress, 'translation elongation' was still enriched, but the fold change was less than under control conditions. This comparably reduced enrichment of 'translation elongation' after heat stress might either indicate that translational activity is reduced by less interactions of eEF1B $\gamma$  with other translation elongation factors or it might be an artefact from the differing numbers of proteins that have been taken into consideration for the GO analysis. As mentioned above 119 proteins were identified as enriched for eEF1B $\gamma$ \_HS, while only 13 proteins were identified for eEF1B $\beta$ \_Ct and 16 proteins for eEF1B $\gamma$ \_Ct .

In contrast to control conditions, metabolic and biosynthetic processes were not enriched among eEF1B $\gamma$ -interacting proteins after heat stress, instead several processes involved in photosynthesis were identified. Additionally, an enrichment of 'COP9 signalosome assembly' and 'protein deneddylation' were observed. Also, 'protein refolding', 'ER body organization' and 'endoplasmic reticulum (ER) to Golgi vesicle-mediated transport' were enriched after heat stress. This analysis showed that the applied heat stress significantly changed the interactome of eEF1B $\gamma$ .

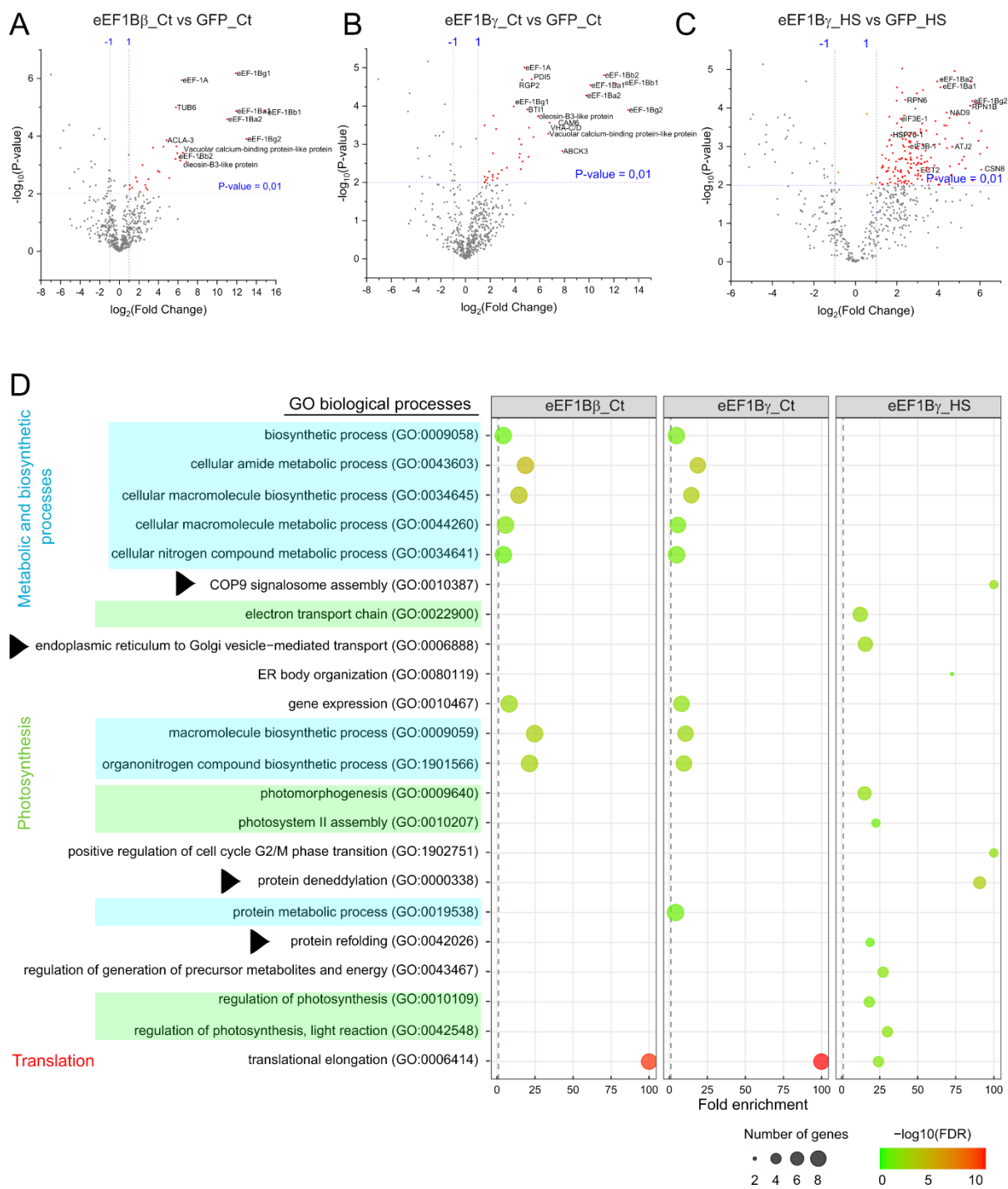


**Figure 65: GO term enrichment analysis of biological processes.** (A) Volcano plots showing enriched proteins among eEF1B $\beta$ -interactors (eEF1B $\beta$ \_Ct) under control conditions compared to GFP under control conditions (GFP\_Ct). Significantly enriched proteins are marked in red and were used for GO enrichment analysis shown in (D). Pairwise comparisons were performed via t-tests in Perseus. Correction for multiple testing was done by permutation based False Discovery Rate (FDR). FDR=0.01 was used for all comparisons shown in this figure. (B) Volcano plot showing enriched proteins among eEF1B $\gamma$ -interactors under control condition (eEF1B $\gamma$ \_Ct) compared to GFP under control condition (GFP\_Ct). (C) Volcano plot showing enriched proteins among eEF1B $\gamma$ -interactors after heat stress (eEF1B $\gamma$ \_HS) compared to GFP after heat stress (GFP\_HS). (D) Gene Ontology (GO) enrichment analysis of the significantly enriched proteins indicated in (A, B, C) to identify the connected biological processes. Size of dots resembles the number of genes that have been identified in the

corresponding biological process. Color of dots describes the FDR with green color representing  $FDR = -\log_{10}(0)$  and red color representing  $FDR = -\log_{10}(10)$ . Higher FDR (green color) resembles enhanced probability of false positives. The fold enrichment is demonstrated on the x-axis of the diagram and describes how much the proteins found in the corresponding biological process are enriched in comparison to the whole Arabidopsis proteome. Black triangles highlight biological processes that are specifically enriched after heat stress and later on discussed in more detail (Fig. 67).

GO enrichment analysis was similarly performed to observe the molecular function of eEF1B $\beta$  and eEF1B $\gamma$  interactors (Fig. 66).

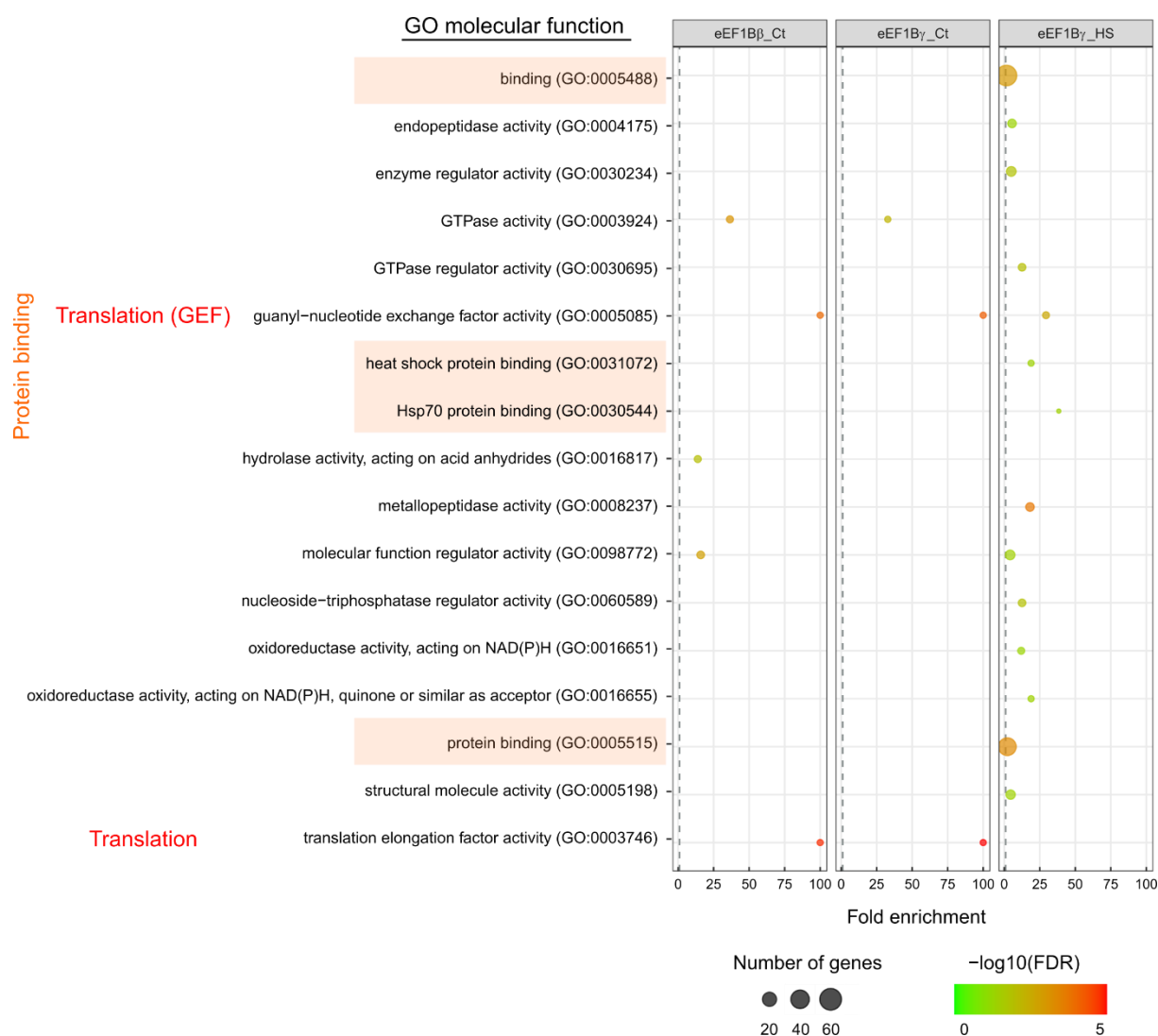


**Figure 66: GO term enrichment of molecular function.** Gene Ontology (GO) enrichment analysis of the significantly enriched proteins indicated in (Fig. 59A, 59B, 59C) to identify the connected molecular functions. Size of dots resembles the number of genes that have been identified in the corresponding molecular function. Color of dots describes the FDR with green color representing  $FDR = -\log_{10}(0)$  and red color representing  $FDR = -\log_{10}(5)$ . Higher FDR (green color) resembles enhanced probability of false positives. The fold enrichment is demonstrated on the x-axis of the diagram and describes how much the proteins found in the corresponding molecular function are enriched in comparison to the whole Arabidopsis proteome.

Again, eEF1B $\beta$  and eEF1B $\gamma$  interactors were very similar under control conditions, being mainly enriched in translation factor activity and guanyl-nucleotide exchange factor activity (Fig. 66). Strikingly, after heat stress eEF1B $\gamma$  interactome was enriched in ‘binding’, ‘protein binding’ and ‘heat shock protein binding’, which fits to the presence of eEF1B $\gamma$  in cytoplasmic condensates, which rely on many interactions between RNA and protein molecules. Also, expression of heat shock protein is a typical response to heat stress, since HSPs are needed for binding to proteins and act as chaperones.

To get a better insight into which proteins are heat-sensitive, heat-insensitive or heat-dependent interactors, the overlap between the three data sets eEF1B $\beta$ \_Ct, eEF1B $\gamma$ \_Ct and eEF1B $\gamma$ \_HS (each compared to its GFP control) were calculated and are shown in a Venn diagram (Fig. 67). Heat-sensitive interactors are only expected to be found under control conditions. Proteins interacting with both, eEF1B $\beta$  and eEF1B $\gamma$  under control conditions, but not after heat stress, are an Oleosin-B3-like protein (AT1G13930) and eEF1A (AT5G60390). The Oleosin-B3-like protein is a constitutively expressed protein, which is important for salt stress tolerance (Du et al. 2008). It would be interesting to investigate whether this protein plays a role in the connection between translation regulation and stress response. It is very interesting that eEF1A is only found in the interaction network of eEF1B $\gamma$  under control conditions, but not after heat stress. This might be a mechanism to reduce translational efficiency in stress conditions.

Heat-stress-independent interactors can be found under control and heat stress conditions. There is a total of six proteins, which are binding to both eEF1B $\beta$  and eEF1B $\gamma$  independent of applied conditions. These include all eEF1B subunits and a Vacuolar calcium-binding protein-like protein (AT1G62480), which has so far been described as calcium-binding mediator in response to continuous dark (Ide et al. 2007). Presence of all eEF1B subunits indicates that the eEF1B complex components stay in close proximity to each other, independent of the environmental conditions.

The 119 heat-dependent interactors of eEF1B $\gamma$  are a diverse group of proteins. Subcellular localization analysis of the 119 proteins using SUBA5 (Hooper et al. 2017) revealed that 35 proteins were mainly localized in chloroplasts or mitochondria. These proteins were excluded from the subsequent analysis. The GO enrichment analysis of biological processes performed in Panther (shown in Fig. 65) showed an enrichment of certain processes. To underline the results with an independent algorithm, a STRING network of the remaining 84 proteins was generated in Cytoscape (Shannon et al. 2003) and searched for clusters using MCODE app

(Bader and Hogue 2003). Clusters with related functions are shown in Fig. 67. The identified clusters largely resemble the identified enriched biological processes (Fig. 65). Several proteins of the COP9 signalosome were identified (COP9, COP8, CSN5A, COP13, RBX1 and FUS5), which are shown as red cluster. The COP9 signalosome is a multiprotein-complex which plays an important role in the ubiquitin-proteasome pathway (Schwechheimer and Isono 2010; Qin et al. 2020). It regulates activity of specific E3 ligases through protein deneddylation (Merlet et al. 2009) and was shown to be important for cell cycle progression and genome stability (Dohmann et al. 2008). Loss of different CSNs lead to developmental defects (Gusmaroli et al. 2007). Few lines of evidence also indicate a role of CSN subunits in high temperature response (Delker et al. 2014; Zhang, Lei, et al. 2017; Singh et al. 2019). The subunits of the COP9 signalosome are homologous to the lid subcomplex subunits of the 26S proteasome, which led even to the (so far unproven) hypothesis that COP9 can act as alternative lid of the 26S proteasome (Qin et al. 2020). A cluster of the 26S proteasome proteins (e.g. RPN1A, RPN1B, and RPT5A) were found as heat-dependent interactors of eEF1B $\gamma$ . The orange ‘proteasome’ cluster is strongly connected with the red ‘COP9’ signalosome cluster (Fig. 67). Loss of proteasomal subunit RPN1A leads to developmental defects and decreased heat stress tolerance (Wang, Kurepa, and Smalle 2009) showing that a functional proteostasis is needed for correct plant growth and development (Silverblatt-Buser et al. 2018). A link between translation elongation and proteasomal degradation might add another layer to the regulation of plant development and stress response.

Another, rather expected, cluster of proteins was identified as ‘protein folding’ (violet), which included chaperones as HSP70-2, J2 or J3. All three proteins are known to be upregulated upon heat stress and to play a role in plant heat stress response (Li et al. 2005; Wu et al. 2019; Wang et al. 2021; Tiwari, Khungar, and Grover 2020; Leng et al. 2017).

Interestingly, many proteins involved in intracellular transport, specifically ER-to-Golgi and vesicle-mediated transport were identified in another cluster (blue), as well as vacuolar ATPases (green cluster). A study in human cells have demonstrated that COPII coat proteins are recruited to SGs and thereby trafficking along early secretory pathway is inhibited (Zappa et al. 2019). In Arabidopsis, the recruitment of Golgi-localized PARP12 to SGs upon stress is also associated with changes in the structure of the Golgi apparatus and block of anterograde membrane traffic (Catara et al. 2017). Consequently, the recruitment of ER-to-Golgi transport proteins to SGs or other membrane-less condensates might be a mechanism to reduce cellular trafficking.

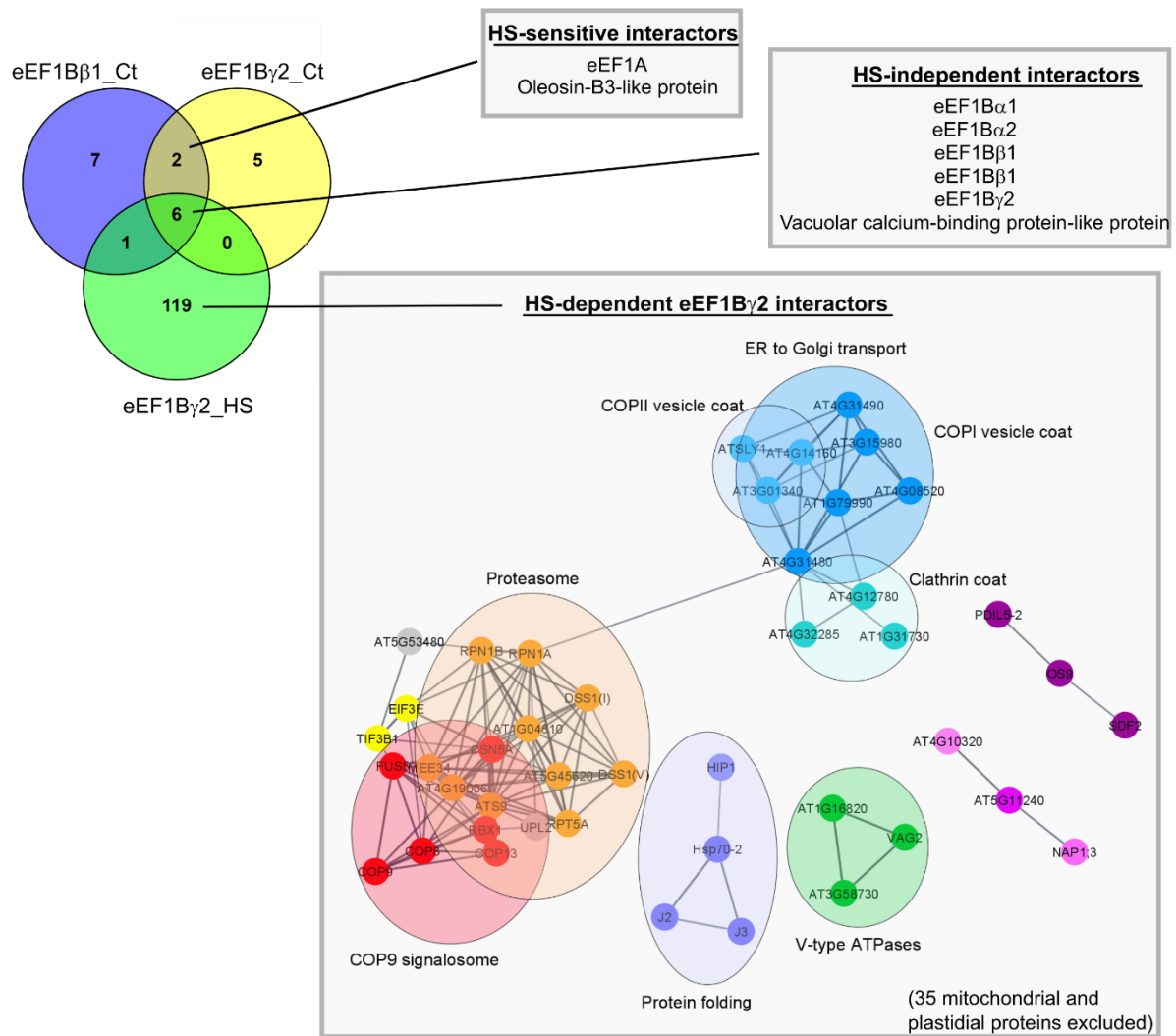


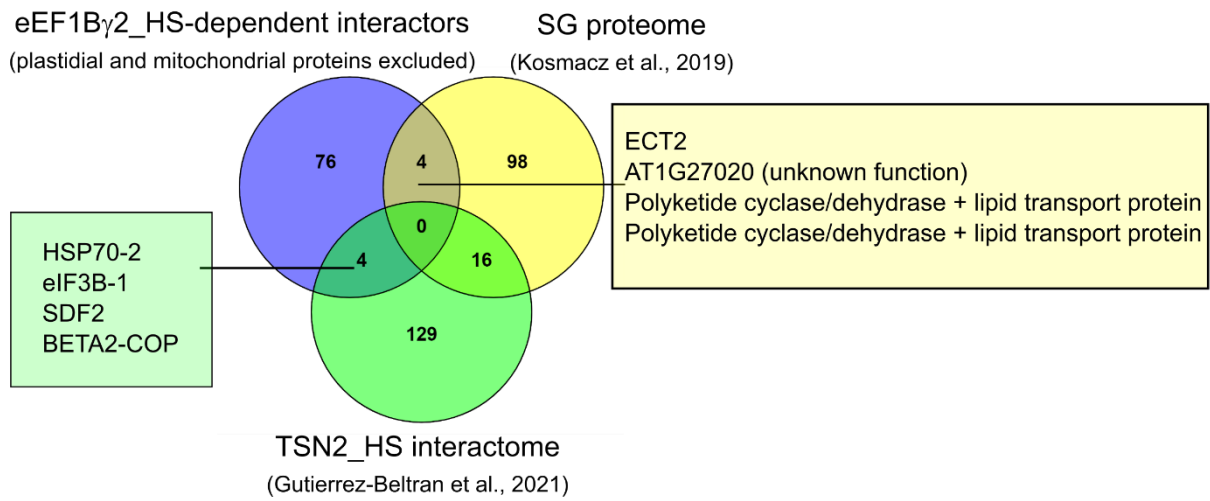
**Figure 67: List of heat-sensitive, heat-independent and heat-dependent interactors of eEF1B $\beta$  and eEF1B $\gamma$ .** A Venn diagram showing the overlap between eEF1B $\beta$ \_Ct, eEF1B $\gamma$ \_Ct and eEF1B $\gamma$ \_HS (each compared to the corresponding GFP control). HS-dependent interactors localized to mitochondria or plastids were excluded from the network analysis. A network of 84 HS-dependent interactors was generated using STRING database search in Cytoscape. Proteins were clustered using MCODE app. Proteins that were not found in clusters are not shown. Function of clusters were assigned using STRING enrichment.

Since eEF1B $\gamma$  was found to localize at least partially in stress granules upon heat stress, the heat-dependent eEF1B $\gamma$  interactome was compared to the previously published Arabidopsis stress granule proteome (Kosmacz et al. 2019). SG proteome was identified from an enrichment of stress granule fraction through differential centrifugation and subsequent immunoaffinity-enrichment of interactors of the stress granule marker RNA-binding-protein 47 (RBP47). In the SG proteome, several known stress granule components like Poly-A-binding proteins (PAB2 and PAB8), TSN1 and TSN2 and ECT2 were identified. Our eEF1B $\gamma$ \_HS pool had an overlap of four proteins with the SG proteome (Fig. 68A). These four proteins included ECT2, for which

localization to stress granule had already been shown previously (Scutenaire et al. 2018). The other three overlapping proteins have not been analyzed so far. It is a protein of unknown function and two proteins that have been annotated as polyketide cyclase/dehydrase and lipid transport superfamily protein. Each subunit of the eEF1B subunit has been identified as part of the RBP47-associated SG proteome, but reciprocally we did not find RBP47 in the eEF1B $\gamma$ \_HS pool. Likewise, eEF1B $\gamma$ \_HS pool did not include the established SG proteins TSN1 or TSN2, although eEF1B subunits have been identified as heat-sensitive interactors of TSN2 (Gutierrez-Beltran et al. 2021). Comparison of heat-dependent TSN2\_HS and eEF1B $\gamma$ \_HS pools resulted in an overlap of four proteins (Fig. 68A). One of the proteins included in the overlap is the translation initiation factor eIF3B-1. Translation initiation factors are known as typical stress granule components (Anderson and Kedersha 2006). Moreover, two chaperones were shared between heat-dependent TSN2\_HS and eEF1B $\gamma$ \_HS pool, the cytosolic HSP70-2 and the ER-localized SDF2, which is also playing a role in ER to plasma membrane transport. The fourth shared protein was BETA-COP2, which is a vesicle coatomer. Overall, only a small overlap was found for eEF1B $\gamma$ \_HS pool with known SG markers.

The SG proteome of plants and also of yeast and human cells contains typically many RNA binding proteins (RBPs), proteins with prion-like domains (PRLDs) or ATPase activity (Jain et al. 2016; Gutierrez-Beltran et al. 2021). Therefore, the amount of RBPs, PRLDs and ATPases was compared between eEF1B $\gamma$ \_HS pool, Arabidopsis SG proteome (Kosmacz et al. 2019) and TSN2\_HS pool (Gutierrez-Beltran et al. 2021); (Fig. 68B). Similar to the other two studies, a high amount (44%) of RBPs were identified in eEF1B $\gamma$ \_HS pool. This fits to the enriched molecular function 'binding' (Fig. 66). Also, the amount of ATPases was comparable between all three studies. Only 6% of eEF1B $\gamma$ \_HS pool were proteins containing prion-like domains, which was comparable to the amount found for TSN2\_HS pool (8%); (Gutierrez-Beltran et al. 2021). In contrast, the Arabidopsis SG proteome contained a higher amount of PRLDs (15%); (Kosmacz et al. 2019). Prion-like domains are contributing to recruitment of proteins to SGs (Fomicheva and Ross 2021). While SGs were enriched in Arabidopsis SG proteome analysis by differential centrifugation, the whole protein extracts were analyzed in our and in the TSN2 study. In the whole protein extracts, it could be possible to find a mixture of cytoplasmic localized protein and SG-localized protein. This might explain, why the percentage of PRLDs might be higher in SG-enriched fractions.

**A**



**B**

Dataset	RNA-binding proteins	Prion-like domains	ATPase activity
eEF1B $\gamma$ 2_HS (84)	37 (44%)	5 (6%)	3 (4%)
SG_proteome (118)	55 (47%)	18 (15%)	3 (3%)
TSN2_HS (149)	79 (55%)	12 (8%)	6 (4%)

**Figure 68: Comparison of heat-dependent eEF1B $\gamma$ 2-interactome with previously published proteomics data for Arabidopsis stress granule proteome and heat-dependent TSN2 interactome. (A)** Venn diagram comparing 84 heat-specific eEF1B $\gamma$ 2-interactors to 118 RBP47-interactors in the stress granule enriched protein fractions (Kosmacz et al. 2019) and 149 heat-dependent TSN2-interactors (Gutierrez-Beltran et al. 2021). **(B)** Identification of number of RNA binding proteins, proteins with prion-like domains and ATPase activity in the above-mentioned datasets.

## 5 Discussion

### 5.1 PP7L as part of MAIN-MAIL1-PP7L interaction complex

The plant mobile domain (PMD) proteins MAIN and MAIL1 act redundantly and play important roles in two distinct biological processes. The first process, that MAIN and MAIL1 are essential for, is primary root growth associated with genome stability in the stem cell niche of the root apical meristem. Both mutants show strong developmental defects and accumulation of dead cells in the root stem cell niche (Wenig et al. 2013; Uhlken et al. 2014). The second process, that MAIN and MAIL1 are involved in, is silencing of transposable elements associated with condensation of heterochromatin (Ikeda et al. 2017). Whether both processes are functionally connected via MAIN-MAIL1 signaling is currently unknown. With identification of PP7L as interaction partner of MAIN and MAIL1 (de Luxan-Hernandez et al. 2020; Nicolau et al. 2020), a third protein has been identified, which acts in the same signaling pathway. *pp7l* mutants share both described phenotypes, defects in development and TE silencing, with *main* and *mail1* mutants. Besides the two mentioned processes, PP7L has also been connected to chloroplast biogenesis in developing seeds, seedlings and adult plants. *pp7l* mutants show reduced maximum quantum yield of PSII. Also, PP7L was shown to play a role in response to abiotic stress including salt, high light and cold stress response (Xu et al. 2019; Xu, Leister, and Kleine 2019). These traits have so far not been analyzed in *main* or *mail1* mutants. It would be interesting to see, whether these are PP7L-specific traits or whether these are shared within the MAIN-MAIL1-PP7L complex.

MAIN and MAIL1 are exclusively localized to the nucleus, whereas PP7L localizes to the nucleus and the cytoplasm (de Luxan-Hernandez et al. 2020). It is intriguing to hypothesize that the subcellular localization plays a role for the signaling pathway that is affected and the resultant phenotype displayed by PP7L. Could the interaction of MAIN and MAIL1 with PP7L be responsible for the nuclear localization of PP7L? In this study, the domains that are necessary for the interaction between MAIL1 and PP7L were specified. Y2H studies with truncated protein versions indicated that the N-terminus of MAIL1 interacts with the N-terminus of PP7L. The N-terminus of PP7L contains the NLS and is required for the nuclear localization of PP7L. The nuclear localization of PP7L is not dependent on the interaction of PP7L with MAIL1, because PP7L still localized to the nucleus in the absence of MAIN and MAIL1. Analysis of *pp7l* mutants complemented with truncated versions of PP7L (e.g. lacking the NLS or the N-terminus), would help to understand whether the nuclear localization of PP7L is essential for its function in primary root growth, genome stability and TE silencing.

TE silencing is regulated by a multitude of factors and silencing pathways including DNA methylation, MICRORCHIDIA (MORC) ATPases, histone modifications and non-coding RNA (reviewed in (Nicolau, Picault, and Moissiard 2021)). A highly conserved epigenetic methylation mark is the methylation of the 5<sup>th</sup> carbon of cytosines (5-methylcytosine - 5mC). Among other factors, DOMAINS REARRANGED METHYLTRANSFERASE 1 and 2 (DRM1 and DRM2), DNA METHYLTRANSFERASE 1 (MET1) and CHROMO-METHYLASE 2 and 3 (CMT2 and CMT3) are required for various de novo 5mC and maintenance of 5mC marks. Although genome-wide methylation levels and global methylation patterns of TEs are unchanged in *mail1* mutants compared to WT (Ikeda et al. 2017), synergistic effects have been reported for MAIN and 5mC pathways. It was suggested that the MAIN-MAIL1-PP7L complex might cooperate with DRM2- and CMT3-mediated 5mC to silence TEs (Nicolau et al. 2020; Nicolau, Picault, and Moissiard 2021).

MORC ATPases are part of DNA-methylation-independent TE silencing. MORC ATPases, including MORC1 and MORC6, have been associated with maintenance of heterochromatin condensation (Moissiard et al. 2012). RNA-sequencing of *main*, *mail1* and *pp7l* single mutants as well as higher order mutants revealed 26 genes that are commonly down-regulated in all genetic backgrounds. Among these down-regulated genes is *MORC1* (Jarry et al. 2023). Re-introducing MORC1 in *main*, *mail1* or *pp7l* background could restore the silencing of several TEs. Possibly, MAIN-MAIL1-PP7L maintains the expression of MORC1 protein, which ensures the silencing of specific TEs together with other MORC proteins (Jarry et al. 2023).

Nevertheless, double mutant analysis showed that MORC1 down-regulation is not responsible for the developmental phenotypes of *main*, *mail1* or *pp7l* mutants (Jarry et al. 2023). Thus, the signaling pathway and interaction partners involved in primary root growth and genome stability are still elusive. Mutants that show highly similar phenotypes compared to *main* and *mail1* are mutants of chromatin modifiers. Chromatin modification highly impacts processes like DNA replication, DNA repair and gene transcription. Both *m56-Ifas2-4* triple mutant and *fas1-4hira1* double mutant showed comparable phenotypes to *mail1* or *main* mutants. *m56-Ifas2-4* triple mutant almost completely stopped primary root elongation after 5 dag and displayed reduced numbers of cells in the root apical meristem. In distal stem cells in the meristematic zone of *m56-Ifas2-4* mutants cell death occurred and was accompanied by increased DNA repair gene expression (Ma et al. 2018). *m56-Ifas2-4* mutants lack factors of two important histone chaperone complexes. CHROMATIN ASSEMBLY FACTOR-1 (CAF-1) is a trimeric complex and acts as histone H3/H4 chaperone. FASCIATA1 (FAS1), FAS2 and

MULTICOPY SUPPRESSOR OF IRA1 (MSI1) belong to the CAF1 complex (Exner et al. 2006). NAP1 acts as H2A/H2B histone chaperone. The NAP1-RELATED PROTEINS 1 and 2 (NPR1 and NPR2) are mutated in *m56-1* mutants (Zhu et al. 2006). The *m56-1fas2-4* showed increased  $\gamma$ -H2AX levels, which correlates with the occurrence of DNA double strand breaks (Friesner et al. 2005). Similarly, the *fas1-4hira1* double mutant shows a severe dwarf phenotype (Duc et al. 2015). *fas1-4hira1* double mutant lacks besides FAS1, also HISTONE REGULATOR A (HIRA), which promotes histone deposition (Ray-Gallet et al. 2002). Loss of HIRA leads to the reduction of extractable histone H3 protein levels and is associated with reduced nucleosome occupancy at heterochromatic targets (Duc et al. 2015). Thus, modification of chromatin can lead to developmental defects comparable to *main*, *mail1* or *pp7l* mutants. Whether MAIN, MAIL1 or PP7L are able to interact with chromatin is currently unknown. Based on the nuclear localization and the similarity to phenotypes of chromatin modifier mutants, a possible influence of loss of MAIN, MAIL1 or PP7L on histone levels should be examined.

In contrast to MAIN and MAIL1, PP7L does not contain a PMD domain. Instead PP7L belongs to the subclass of plant-specific PP7 protein phosphatases and contains a protein phosphatase domain (PPD) (Bheri et al. 2021). The PP7 subclass includes PP7L as well as protein phosphatase PP7 and MAIN-LIKE3 (MAIL3). Interestingly, MAIL3 contains a PMD at its N-terminus and a PPD domain at its C-terminus (Andreeva and Kutuzov 2009). Phylogenetic analysis suggested partially convergent evolutionary processes between the PMD and PPD domains (Nicolau et al. 2020). It was proposed that fusion of PMD and PPD proteins might allow for neofunctionalization of this protein module (Nicolau et al. 2020). But so far, the function of MAIL3 is unknown. Analysis of *mail3* mutants showed a WT-like phenotype (Uhlken et al. 2014). Further research is required to define the function of a PMD-PPD protein module.

It is note worth mentioning that the PPD of PP7L has been described as inactive because of specific alterations in the amino acid sequence of the PPD domain compared to the active protein phosphatase PP7 (Farkas et al. 2007). Here, we aimed at finding out whether these alterations in the PPD domain of PP7L are required for PP7L's function. Based on sequence alignments, a specific amino-acid motif in the catalytic center of the PPD of PP7L was mutated and the resultant "active" version of PP7L was analyzed. PP7L (active) interacted with MAIL1 and showed a subcellular localization similar to the PP7L. This is in line with the identification of the N-terminus of PP7L as being essential for interaction with MAIL1 and nuclear

localization of PP7L. It will be necessary to analyze *pp7l* mutants complemented with PP7L (active) to examine an influence of the introduced mutations on plant development, TE silencing or chloroplast biogenesis. It has to be considered that the mutation of two amino acids is not sufficient for changing the activity of PPD in PP7L. Potentially, more amino acids have to be modified in order to generate an active version of PP7L. As control, the phosphatase (in)activity of PP7L and the phosphatase activity of PP7L (active) should be determined.

It remains an open question: what is the function of PP7L as inactive phosphatase? Inactive phosphatases, also named pseudophosphatases, were suggested to have regulatory functions as signaling molecules via several mechanisms. Most often, pseudophosphatases are described as competitors of phosphatases. By binding to potential substrates of active phosphatases, pseudophosphatases hinder dephosphorylation of these substrates. Additionally, pseudophosphatases could act as integrators by interaction with multiple pathways, as modulators, when pseudophosphatases dimerize with the active enzyme to change its enzymatic activity or as anchors, where the pseudophosphatase binds to a substrate and thereby restricts its subcellular localization (Hinton 2019). It is tempting to speculate that PP7L binds to MAIN and MAIL1 as competitor of phosphatases. Binding of PP7L to MAIN and MAIL1 could hinder de-phosphorylation of MAIN and MAIL1 and thereby ensure the correct downstream signaling. In turn, loss of PP7L could lead to dephosphorylation of MAIN and MAIL1, which then negatively affects downstream signaling leading to the described *pp7l* phenotypes. Currently, no experimental data are available, which demonstrate the phosphorylation status of MAIN and MAIL1. Phosphorylation prediction tool Phosphat4.0 indicates a potential phosphorylation site at the C-terminus of MAIN (<https://phosphat.uni-hohenheim.de/phosphat.html>; (Durek et al. 2010). It would be interesting to test whether the phosphorylation status of MAIN and MAIL1 is changed in the absence of PP7L.

Overall, the signaling pathways that PP7L is involved in remain unknown. As part of this thesis, two attempts have been followed to identify PP7L interactors or proteins in the PP7L signaling pathway. Co-immunoprecipitation of PP7L yielded a list of potential protein interactors. The highest peptide count was identified for MAIN and MAIL1, which indicated a successful co-immunoprecipitation experiment. Unfortunately, none of the other interactors could be verified by independent methods. A suppressor screen aimed at the identification of proteins acting in the same signaling pathway as PP7L. Several suppressor candidates display an improved root growth phenotype. It remains to be analyzed whether the release of TEs is also suppressed in these suppressor candidates and which genes are affected by the suppressing mutation. An

overview of the current knowledge of the function of the MAIN-MAIL1-PP7L complex is illustrated in Fig. 69.

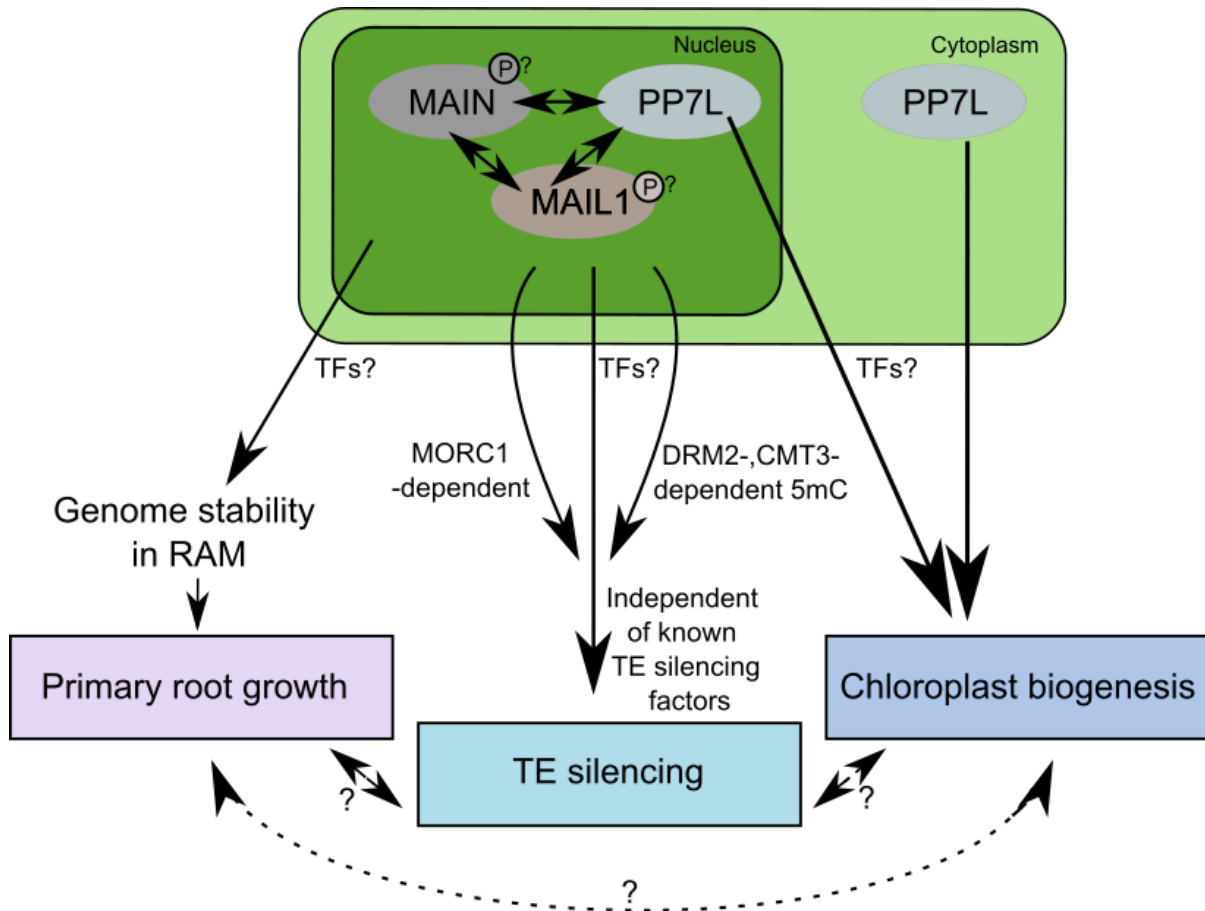


**Figure 69: Overview of MAIN-MAIL1-PP7L functions.** Within the nucleus, MAIN interacts with MAIL1 and PP7L. The complex is involved in genome stability of the RAM and primary root growth. The downstream targets of MAIN-MAIL1-PP7L in this signaling pathway are currently unknown. MAIN-MAIL1-PP7L is additionally involved in TE silencing. Partially MAIN-MAIL1-PP7L mediate TE-silencing via MORC1 and DRM2-/CMT3-dependent pathways. The majority of TEs that are silenced by MAIN-MAIL1-PP7L are silenced via an unknown pathway. Additionally, PP7L is present in the cytoplasm. PP7L has been associated with chloroplast biogenesis.

## 5.2 eEF1B $\beta$ is central to the plant eEF1B complex

Studies on the eEF1 complex began already in the 1960's and 1970's, when large macromolecular complexes were purified during the search for tRNA transferring factors (reviewed in (Le Sourd et al. 2006)). Since then numerous studies revealed the structures and compositions of the eEF1 complex in different organisms. While the presence of eEF1A as aminoacyl-tRNA transferase and an eEF1B complex for GDP/GTP exchange on eEF1A is conserved among all species in prokaryotes and eukaryotes, the conformation of the macrocomplex eEF1 differs between organisms (Sasikumar, Perez, and Kinzy 2012). In 2003, a model has been proposed for the architecture of the yeast eEF1 complex. Using X-ray

structures and gel-filtration studies, a complex composed of [eEF1A:eEF1B $\alpha$ :eEF1B $\gamma$ ]<sub>2</sub> was suggested (Jeppesen et al. 2003). The C-terminal domain of eEF1B $\alpha$  interacts with eEF1A for GDP/GTP exchange, while the N-terminal domain interacts with the N-terminal domain of eEF1B $\gamma$ . A stable dimerization of the eEF1B $\gamma$  subunit was identified. The proposed model of yeast eEF1 complex is displayed in Fig. 70. Much effort has been performed to model and elucidate the structure of human eEF1 complex. An extensive Y2H study showed the interactions between the human eEF1 subunits and clarified that the N-terminal domains of the eEF1B proteins are necessary for interactions within the complex (Mansilla et al. 2002). Bondarchuk et al. showed that human eEF1B $\delta$  forms a stable trimer with an elongated shape by analyzing sedimentation velocity during ultracentrifugation (Bondarchuk et al. 2022). This analysis was extended by Hydrogen-Deuterium Exchange Mass Spectrometry (HDX-MS). The central leucine zipper domain of eEF1B $\delta$  was suggested to be responsible for trimerization. A full structure of human eEF1 complex was proposed by Negrutskii et al. (Negrutskii et al. 2023). A simplified model of this suggested structure is displayed in Fig. 70. Each subunit of trimerized eEF1B $\delta$  can interact with an eEF1A at its C-terminus and with eEF1B $\gamma$  at its N-terminus. In turn, each eEF1B $\gamma$  interacts with one eEF1B $\alpha$  that can each bind an eEF1A. So, one heterotrimeric eEF1B( $\alpha\delta\gamma$ )<sub>3</sub> can possibly perform guanine exchanges on six eEF1A proteins (Bondarchuk et al. 2022).

In plants, little research had been performed on the structure of the eEF1B complex. Interactions within the complex had solely been proposed based on studies from other organisms. In this study, a first overview of interactions of Arabidopsis eEF1B subunits with each other was provided by using Y2H assays (Fig. 70). We found that plant-specific eEF1B $\beta$  is able to interact with both, eEF1B $\gamma$  and eEF1B $\alpha$ . Similar to human eEF1B, we found that the N-terminal domain of Arabidopsis eEF1B $\gamma$  is required for the interaction with eEF1B $\beta$ . Human eEF1B $\delta$ 1 (Uniprot P29692) and Arabidopsis eEF1B $\beta$ 1 share 64 % protein sequence identity, which could suggest a similar mode of action for both proteins. Nonetheless, the idea of eEF1B $\beta$  or eEF1B $\delta$  being the central component of the eEF1B complex is rather new, because previously eEF1B $\gamma$  has been regarded as structural component (Le Sourd et al. 2006; Sasikumar, Perez, and Kinzy 2012). For Arabidopsis eEF1B $\gamma$  we did not identify an interaction with eEF1B $\alpha$  suggesting that eEF1B $\beta$  is the central component in Arabidopsis eEF1B complex. Possibly, eEF1B $\gamma$  might connect the eEF1B complex to the cytoskeleton as it was shown for yeast and human eEF1B $\gamma$  through an interaction with keratin (Kim, Wong, and Coulombe 2006; Kim, Kellner, et al. 2007).

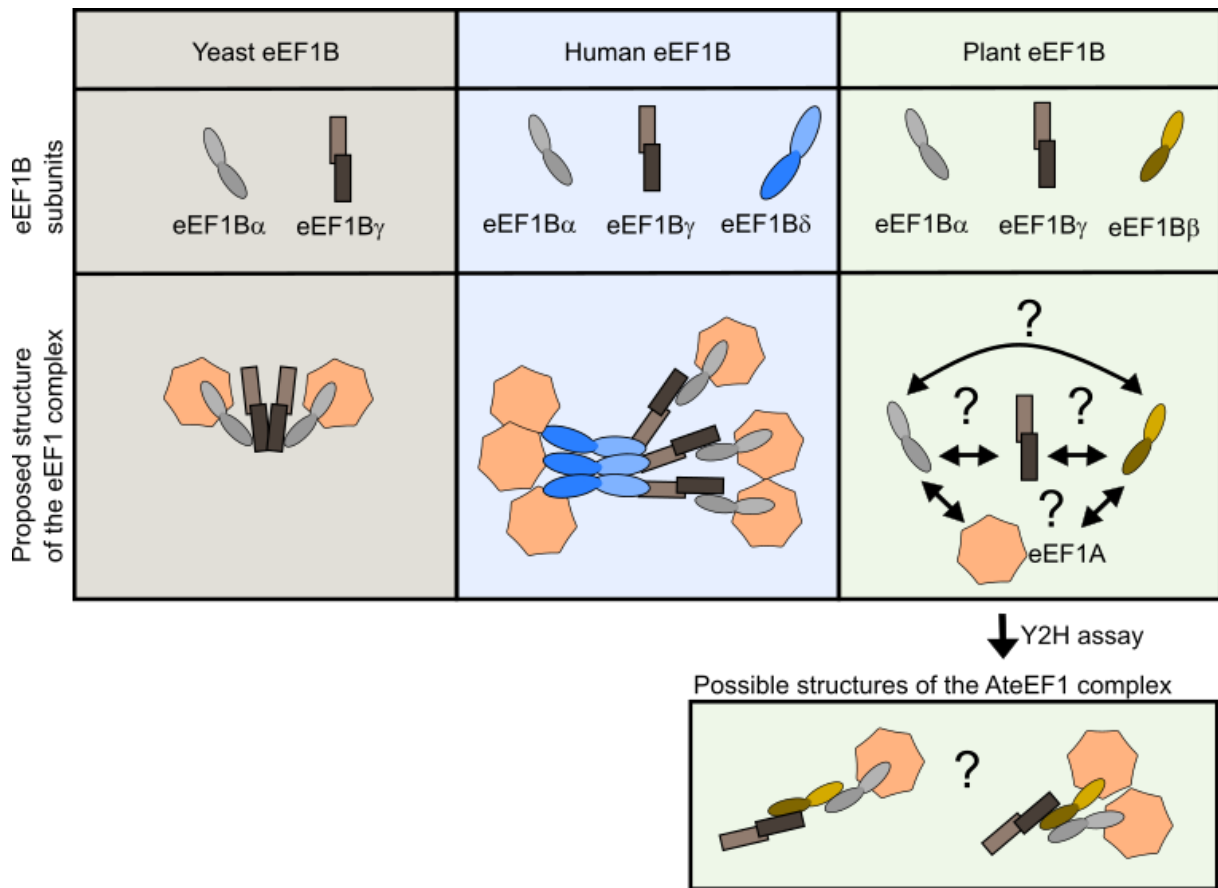


**Figure 70: Models for eEF1 complex in different organisms.** Models for yeast and human eEF1 complex have been described previously (Sasikumar, Perez, and Kinzy 2012; Bondarchuk et al. 2022; Negrutskii et al. 2023). Structural data of the eEF1 complex in plants is not available so far. Here, the current understanding of the plant eEF1 complex based on our Y2H data is shown.

In contrast to yeast and human eEF1, no self-association of any of the Arabidopsis eEF1B subunits was detected in this study. Thus, based on our current knowledge no dimerization or trimerization is supported by eEF1B subunits in Arabidopsis. To verify this finding, an independent method testing for direct protein-protein interactions, like pull down, microscale thermophoresis or surface plasmon resonance should be performed. Since the interaction of eEF1B subunits with eEF1A was not analyzed here, we cannot propose a complete model for Arabidopsis eEF1 complex yet. It is conceivable that the C-terminus of eEF1B $\gamma$  connects the eEF1B complex to the cell. The N-terminus of eEF1B $\gamma$  binds to eEF1B $\beta$ . eEF1B $\beta$  can either bind to eEF1B $\alpha$ , which interacts with eEF1A for guanine exchange, or eEF1B $\beta$  might in addition to eEF1B $\alpha$  binding also directly interact with eEF1A to allow for a second GDP/GTP exchange mediated by one eEF1B complex. This second option is supported by the finding that both, eEF1B $\alpha$  and eEF1B $\beta$ , are able to interact with eEF1A in potato (Hwang et al. 2015). The proposed modes of action of Arabidopsis eEF1B subunits are shown in Fig. 70.

Many questions about the architecture of the Arabidopsis eEF1B complex remain open. Some questions could be answered by extending our Y2H assay including: Is the eEF1B $\beta$  subunit binding to eEF1B $\alpha$  and eEF1B $\gamma$  by its N-terminus? Which domains are responsible for eEF1A binding? Is eEF1B $\gamma$  connecting eEF1B to the cytoskeleton? Other interesting questions will require extensive research including different methods like structural analysis, ultracentrifugation sedimentation velocity or HDX-MS. Thereby, the following questions could help to understand the eEF1B architecture in plants: Are eEF1B $\alpha$  and eEF1B $\gamma$  competing to bind to the same binding site of eEF1B $\beta$ ? Is there indeed no dimerization or trimerization? Can one Arabidopsis eEF1B complex perform GEF on several eEF1A proteins simultaneously?

### 5.3 The canonical function of Arabidopsis eEF1B in translation elongation and its influence on general translation efficiency

The rate of translation is mainly determined by translation initiation (Shah et al. 2013). But also, translation elongation and termination can have an influence on protein synthesis (Negrutskii et al. 2018; Xu, Liu, and Song 2021). Different steps within translation elongation have been identified to be decisive for elongation speed. Additionally, features of the mRNA, tRNA and the encoded protein can determine elongation rates. These steps and features are marked with a small clock in Fig. 71, which shows an overview of translation elongation and its regulation. As early as 1984, it was shown in *E. coli* that tRNA availability corresponding to the mRNA sequence is crucial for translation elongation rates (Varenne et al. 1984). Highly available tRNAs are translated more efficiently. Thus, codon usage highly regulates overall translation rates (Sørensen, Kurland, and Pedersen 1989; Tuller et al. 2010). Aminoacyl-tRNAs are bound and transported to the ribosome by eEF1A. After GTP-dependent transfer of the aminoacyl-tRNA to the ribosomal A-site, eEF1A-GDP needs to dissociate from the ribosome. Based on the fact that the affinity of different tRNAs to eEF1A\*GDP varies, this tRNA-dependent dissociation step has been described as rate-limiting for overall elongation speed in human cells (Negrutskii et al. 2018). Besides tRNA availability and codon usage, also global features of the encoded protein like the charge and the isoelectric point (pI) have an influence on the translation elongation rate. It was shown that for example yeast ribosomal proteins (RPs), which are positively charged, have low elongation rates compared to RPs with a negative charge (Riba et al. 2019). Another translation factor that regulates translation elongation is eEF2. Phosphorylation of eEF2 leads to its inactivation and thereby a drastic inhibition of translation (Ryazanov, Shestakova, and Natapov 1988). Interestingly, slowdown of translation elongation through inactivity of eEF2 kinase and consequent dephosphorylation of eEF2 does not lead to

reduction of overall protein synthesis, but enhances translational fidelity and accuracy of elongation in *Caenorhabditis elegans* (Xie et al. 2019).

One important research question of this thesis was, which influence Arabidopsis eEF1B has on translation elongation and thereby on general protein biosynthesis. Using the SunSET method, it was found that the overall protein biosynthesis rate of the double mutant of eEF1B $\gamma$  is comparable to WT plants. This is in line with results from *S. cerevisiae*, where eEF1B $\gamma$ -deleted strains showed no significant difference in total translation compared to WT (Olarewaju et al. 2004). Nonetheless, polysome profiling revealed that Arabidopsis *eef1b $\gamma$ 1/2* double mutants contain a significantly higher number of overall mRNA-bound ribosomes compared to WT. The increase in mRNA-bound ribosomes resulted from a higher number of ribosomes per cell. This could indicate a mechanism, in which plants that are impaired in translation elongation attempt to compensate this defect with an increased expression of ribosomal subunits. Most likely, this hypothetical mechanism is dosage-dependent. A slight reduction of translation elongation speed, e.g. resulting from reduced eEF1B $\gamma$  levels, could be compensated by higher ribosome density on the mRNAs and higher expression of ribosomal subunits. This slight translational slowdown might even lead to improved translational accuracy, as it has been shown for *C. elegans* (Riba et al. 2019). In contrast, a drastic decrease of elongation would rather lead to inhibition of global protein synthesis. The strongly increased number of ribosomes per mRNA could lead to a roadblock, meaning that too many simultaneously translating ribosomes hinder each other, and prolong the time that ribosomes stay on the mRNA. Together with a higher density of ribosomes on the mRNA, this would decrease the pools of free ribosomes that are necessary for translation initiation. Ultimately, this would resume in a feedback loop down-regulating translation initiation in response to reduced translation elongation. Such a mechanism differentiating between mild slowdown of translation and a complete block translation elongation has been suggested previously (Urquidi Camacho, Lokdarshi, and von Arnim 2020) and it is outlined in Fig. 71. A complete translation elongation stop could e.g. occur during extreme stress conditions like strong heat or oxidative stress. Overall, the data obtained in this thesis indicate that eEF1B subunits do play a role in regulation of translation levels. It remains to be analyzed whether the three different eEF1B subunits, eEF1B $\alpha$ , eEF1B $\beta$  and eEF1B $\gamma$ , have different impacts on translation.

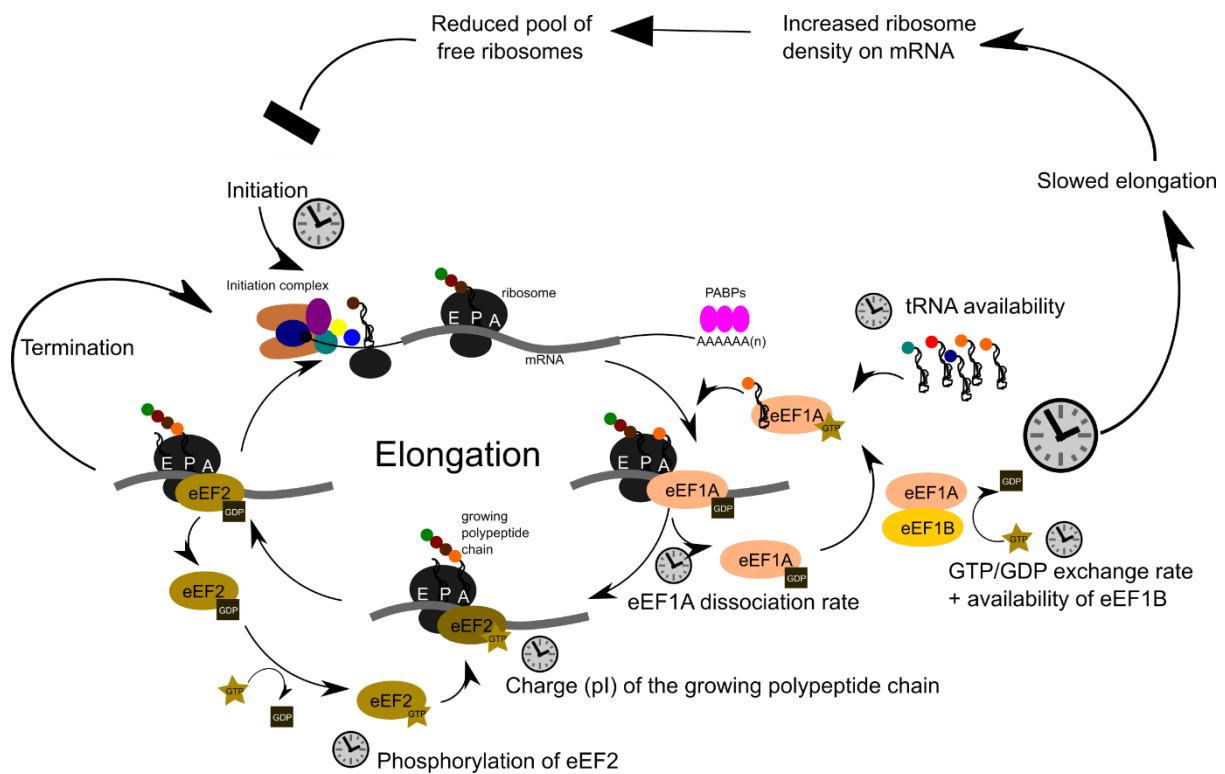


**Figure 71: Rate-limiting steps of translation elongation and the feedback to translation initiation.** Steps and features that are limiting the speed of translation are marked with a clock. Translation initiation is mainly regarded as rate-limiting, but there are several steps within elongation that can vary the speed of translation. Translation elongation relies strongly on tRNA availability to be able to find the correct codon:anticodon pairing. The eEF1A complex delivers the tRNA to the ribosome and the dissociation rate of eEF1A can influence elongation speed. Based on this study, a mechanism modulating and compensating for elongation slowdown through eEF1B was suggested. The charge of the encoded protein and the activity of eEF2 also play a role in translational elongation rates.

#### 5.4 Translation factor complex eEF1B impacts plant development

Translation is a major process within cells, which has large impact on the health and fitness of plants. Here, it was tried to decipher, whether the translation elongation factor complex has an influence on plant growth and development. Several studies showed that translation undergoes dynamic changes during plant development. Already during seed germination, translation is of utmost importance. Dry seeds contain mRNAs that were transcribed during seed development and are stored associated with monosomes (Bai et al. 2020). During seed hydration, a translational shift occurs and allows active translation of these mRNAs. A second translational shift occurs before root protrusion and initiates active translation of mRNAs required for rRNA processing and lipid metabolism (Bai et al. 2017; Urquidi Camacho, Lokdarshi, and von Arnim 2020). A genome-wide study of polysome-bound mRNAs during different stages of plant growth showed that the translational status strongly changes during growth. For example, the

shift from expanding to expanded leaves is associated with a change in distribution of polysome-associated mRNAs from repressed to activated mRNAs (Yamasaki et al. 2015).

Accordingly, it is not surprising that previous studies showed that loss or knockdown of specific translation factors can lead to defects in plant growth and development (Castellano and Merchante 2021). Several translation initiation and elongation factor mutants have been analyzed. While some mutations are lethal, others result in little to severe effects on plant development (Castellano and Merchante 2021). In this study, it was aimed at elucidating the influence of the translation elongation factor complex eEF1B on plant development by analyzing T-DNA insertion lines of the two subunits eEF1B $\beta$  and eEF1B $\gamma$ . Both proteins are encoded by two genes. Neither *eef1b $\beta$*  nor *eef1b $\gamma$*  single mutants did show any developmental defects in this study. Both proteins are encoded by two genes implying that knockout of both genes could be necessary to observe a phenotype. Our double mutant analysis for eEF1B $\beta$  and eEF1B $\gamma$  indicated two different impacts.

#### 5.4.1 Loss of eEF1B $\beta$ might be lethal

For eEF1B $\beta$ , no double homozygous mutants were identified. Although further experiments are required to confirm this result, the non-Mendelian segregation of alleles might indicate that eEF1B $\beta$  is essential for seed development or seed germination and a full knockout could be lethal. A comparable phenotype has been observed for translation initiation factors eIF4E and eIFiso4E, which are required for binding of the 5' cap of mRNAs. Knockout mutants of only eIFiso4E show a phenotype comparable to WT, but display increased expression of eIF4E, which might be able to compensate a possible defect in mRNA translation (Duprat et al. 2002). Later on, it was shown that both eIF4E and eIFiso4E act redundantly in male gametophyte development. Therefore, double mutants of eIF4E and eIFiso4E are lethal (Callot and Gallois 2014). To clarify, whether *eef1b $\beta$*  double mutants are indeed also affected in gametophyte development, it will be necessary to perform several backcrosses to WT. First, to ensure that the single mutations do not affect male or female transmission, single mutants should be backcrossed to WT and the segregation needs to be analyzed. Second, to find out whether the double mutants are defective in gametophyte development, F1 plants that are heterozygous for both mutations need to be back-crossed to WT reciprocally and progenies analyzed regarding the transmitted gamete genotypes (Callot and Gallois 2014).

A previously published study is contradicting the hypothesis that eEF1B $\beta$ 1 and eEF1B $\beta$ 2 act redundantly. Phenotypical analysis of the single mutant line *eef1b $\beta$ 1-1* by Hossain et al.

revealed a severe dwarf phenotype at later developmental stages. Histochemical analysis demonstrated a reduced total lignin content in *eef1bβ1-1*, which correlated with decreased vasculature and interfascicular fibers. Together with a reduction of the cellulose level, it was suggested that the secondary cell thickening is impaired in *eef1bβ1-1* plants. The phenotype could be rescued by introduction of an *35S::eEF1Bβ1* construct (Hossain et al. 2012). This would imply that both eEF1B isoforms cannot complement each other's function. Another possibility could be that eEF1Bβ1 and eEF1Bβ2 act only redundant in their canonical function during translation elongation, but eEF1Bβ1 has additional non-canonical functions in secondary cell wall thickening. So far, the impact of loss-of-function of eEF1Bβ on translation elongation has not been studied in plants.

In this thesis, the same T-DNA insertional line *eef1bβ1-1* was obtained from SALK institute, but we did not observe a difference between *eef1bβ1-1* and WT neither at seedling stage (similar to Hossain et al.) nor at later developmental stages (in contrast to (Hossain et al. 2012)). The discrepancy between the observed phenotypes is a so far unsolved conundrum. Like previously described, a backcross of the single mutant *eef1bβ1-1* with WT with consequent analysis of the segregation could reveal whether the line that was obtained for the experiments in this thesis segregates according to mendelian law.

#### 5.4.2 Reduction of eEF1Bγ levels delays plant development and disturbs cell division

For the first time, a double mutant line for eEF1Bγ in plants was successfully established in this study. The line *eef1bγ1/2* showed strongly reduced eEF1Bγ protein levels, but retained about 20% residual eEF1Bγ protein. Knockdown of eEF1Bγ1 and eEF1Bγ2 in Arabidopsis led to a distinct delay in germination and plant growth at seedling and later developmental stages. An increased number of rosette leaves at flowering time point indicated a delayed flowering in *eef1bγ1/2*. Also, *eef1bγ1/2* mutants produced smaller siliques with fewer seeds. Since the overall protein synthesis rate is not reduced in *eef1bγ1/2* mutants, the developmental defects are most likely not a direct consequence of impaired general protein biosynthesis. It appears rather likely that the expression of a few specific genes that are required for regulatory mechanisms in plant development are disturbed due to the loss of eEF1Bγ.

One other translation elongation factor mutant has been analyzed previously in Arabidopsis based on its role in conferring cold tolerance. At standard conditions, the elongation factor mutant *eef2* (*los1-1* in the original publication) showed a slight delay in flowering, but no other developmental defects, nor any change in protein synthesis rates (Guo et al. 2002). The

observed growth phenotype of *eef1bγ1/2* mutants is therefore more comparable to phenotypes of other previously described translation initiation factor mutants, like *eif4g* or *eif3h* mutants. The plant specific translation initiation factor eIF4G, which is a scaffold protein facilitating interactions with other initiation factors, is encoded by two genes in Arabidopsis. While *eif4g* single mutants also did not show large variation to WT phenotype, the double mutant showed developmental defects in germination, growth rate, chloroplast gene expression and fertility. Also, the transition to flowering was delayed in *eif4g* double mutants. The general protein synthesis rate determined by [<sup>35</sup>S]-methionine incorporation was unchanged compared to WT (Lellis et al. 2010). Mutants of eIF3h show defects in postembryonic growth including delayed root growth and flowering. Similar to other non-lethal translation factor mutants the *eif3h* mutants did not show a reduction in overall protein synthesis rates. Instead the translation of specific mRNAs containing an upstream open reading frame (uORF) in their 5' sequence was changed in *eif3h* mutants. One example of affected genes was *LATE ELONGATED HYPOCOTYL (LHY)*, which is a regulator of the circadian clock (Kim et al. 2004). So similar to *eef1bγ1/2*, both translation initiation factor mutants show a developmental defect combined with unchanged general protein biosynthesis.

In *eef1bγ1/2* mutants, we observed an increase in polysome-associated mRNA and overall ribosome content per cell, which indicated that translation kinetics could be shifted due to knockdown of eEF1Bγ. In accordance, microarray data of polysomal and non-polysomal samples revealed a translational stimulation for small and large ribosomal proteins in *eif3h* mutants (Kim, Cai, et al. 2007). Based on current knowledge, the most intriguing hypothesis is that loss of each translation factor changes translation kinetics. These changes lead to differential expression of specific mRNAs involved in plant development, which consequently lead to the observed developmental defects. It would be very interesting to test on the one hand which mRNAs are differentially expressed by RNA sequencing and on the other hand which mRNAs are actively translated in *eef1bγ1/2* compared to WT by ribosome sequencing. This would help to understand which signaling pathways are affected by the translation elongation factor subunit eEF1Bγ. An interesting future research question would be whether any of the observed phenotypical traits of *eef1bγ1/2* is specific for the eEF1Bγ subunit or whether the developmental defects are a result of the impaired function of the complex eEF1B or as discussed above the impaired translation kinetics in general.

Another interesting phenotypical trait of the *eef1bγ1/2* mutant is the defect in cell division, especially in the RAM. *eef1bγ1/2* mutants showed a reduced size of the meristematic zone in

the RAM combined with a decreased number of meristematic cells. Additionally, the development of true leaves was delayed, which taken together hints at a disturbed cell division in *eef1bγ1/2*. At least to my knowledge, the root phenotype of *eif4g* or *eif3h* has not been investigated in detail. Nonetheless, it was shown that eIF3h is necessary for patterning and functionality of the SAM. *eif3h* mutants showed an enlarged meristematic zone in the SAM, which resulted from mis-expression of the main SAM regulators, WUSCHEL and CLAVATA3 at the translational level (Zhou et al. 2014). This indicates that developmental regulators can be controlled through translational regulation (Raabe, Honys, and Michailidis 2019). Furthermore, analysis of the translation initiation factor, eIF4E, demonstrated its regulatory function in embryogenesis and root growth. Both single mutants, *eif4e1* and *eif4e2*, exhibited reduced primary root growth combined with a reduced number of cells in the meristematic zone. Since no difference in the cell size has been observed, it was suggested that the mutants display a defect in cell division. Interestingly, also similar to *eef1bγ1/2*, *eif4e1* mutants were less sensitive to CHX than WT. Reduced auxin maxima and reduced abundance of PIN3 and PIN7 at the protein level were reasoned to lead to the defects in root development in *eif4e1* mutants. Reduced auxin maxima and reduced abundance of PIN3 and PIN7 might be mediated through the interaction of eIF4E with RAC/ROP GTPase activator, RopGEF7, which is an important factor for RAM maintenance (Liu et al. 2022). It remains to be analyzed which root-specific developmental regulators are mis-regulated in *eef1bγ1/2* mutants. Additionally, it might be interesting to analyze the SAM of *eef1bγ1/2* in more detail to test for parallelisms with other translation factor mutants and possibly unravel a connection of translation and meristem development.

### 5.5 eEF1B $\gamma$ does play a role for specific stress responses

Translation also plays an important role in the stress response of plants. Inhibition of global protein synthesis rates is as important as induction of stress-specific gene expression for plant survival. Many translation factors were shown to be involved in regulating stress responses. Functions of the subunits of translation elongation factor complex eEF1B in stress responses had not been analyzed in Arabidopsis so far. Based on previous studies in other organisms, possible functions of eEF1B $\gamma$  in oxidative stress and heat stress response have been examined in this thesis using the established *eef1bγ1/2* double mutant. Subcellular localization studies of all three eEF1B subunits demonstrated the sequestration into heat-induced stress granules, which could indicate a role of eEF1B in stress adaption.

### 5.5.1 eEF1B $\gamma$ modulates ROS homeostasis in Arabidopsis

In nature, oxidative stress is often a result of other stress conditions that lead to the production of ROS, e.g. drought, salt, heavy metals or UV light. An important factor in detoxification of ROS is glutathione, which can bind, solubilize and facilitate the removal of toxic ROS. Glutathione-S-transferases support the reduction of glutathione and its transfer to ROS. eEF1B $\gamma$  belongs to the family of GSTs as it contains an N-terminal and C-terminal GST domain (Liu et al. 2012). To analyze the ability of Arabidopsis *eef1b $\gamma$ 1/2* mutants to cope with oxidative stress, the plants were treated with methylviologen (MV) which directly induces the production of ROS. While the percentual decrease in fresh weight upon MV treatment was similar between WT and *eef1b $\gamma$ 1/2* mutants, the root growth of *eef1b $\gamma$ 1/2* was slightly more repressed upon MV treatment with increasing age of the plants compared to WT. Together with an observed increase in H<sub>2</sub>O<sub>2</sub> levels in *eef1b $\gamma$ 1/2* seedlings, it indicates that eEF1B $\gamma$  might play a role in maintaining ROS homeostasis in Arabidopsis, but it is likely to be a subtle effect.

These results are partially overlapping and partially contradicting with results from studies that have been performed on eEF1B $\gamma$  in other organisms. Arguing in favor of a function of eEF1B $\gamma$  in ROS maintenance in Arabidopsis, *eef1b $\gamma$ 1/2* mutants might lack the GST activity, which is supporting ROS detoxification. In consequence, the ROS levels would be increased, which was observed by the DAB staining. An increased number of oxidized proteins has also been observed in yeast *eef1b $\gamma$*  double mutants (Esposito and Kinzy 2010). So far, the GST activity of eEF1B $\gamma$  has not been tested in Arabidopsis. Recombinant rice eEF1B $\gamma$  has a low GST activity. Interestingly, the GST activity of rice eEF1B $\gamma$  has only been detected, when the recombinant protein has been produced in stabilizing conditions (Kobayashi, Kidou, and Ejiri 2001). In combination with other studies showing no GST activity of recombinant eEF1B $\gamma$  proteins without the presence of other eEF1B subunits, it was suggested that GST activity of eEF1B $\gamma$  is dependent on stability and/or conformation of the protein (Vickers and Fairlamb 2004; Renou et al. 2022). Arguing against a function of AteEF1B $\gamma$  as GST is that the overexpression line of eEF1B $\gamma$  did not show any difference compared to WT in response to MV. Overexpression of other GSTs in Arabidopsis have previously been shown to increase the tolerance to MV treatment, for example overexpression of rice GSTU4 or AtGSTU19 (Sharma et al. 2014; Xu et al. 2016). It would be interesting to test for a possible GST activity of recombinant AteEF1B $\gamma$ , but it might necessary to reconstitute the complete eEF1B complex *in vitro*.

In yeast, recombinant eEF1B $\gamma$  did not show GST activity. Nonetheless, yeast eEF1B $\gamma$  was shown to be important for ROS maintenance. In contrast to the *Ateef1b $\gamma$ 1/2* mutants, which show a slightly higher sensitivity to MV compared to WT, the yeast *eef1b $\gamma$*  double mutant was more resistant to H<sub>2</sub>O<sub>2</sub> and CdSO<sub>4</sub> (Olarewaju et al. 2004). It was additionally shown that the lack of catalytic activity of eEF1B $\alpha$  is required for conferring the resistance to oxidative stress. It was concluded that the reduction of GDP/GTP exchange on eEF1A in *eef1b* mutants helps to regulate translation rates during oxidative stress and thereby support yeast survival (Olarewaju et al. 2004). This would imply that rather the regulation of translation rates through the whole eEF1B complex than an GST activity of eEF1B $\gamma$  is important for oxidative stress tolerance. Several lines of evidence are supporting that translation elongation and response to oxidative stress are strongly connected. Studies in yeast showed that increased ROS levels downregulate translation elongation rates through decreased ribosomal run-off from mRNAs (Shenton et al. 2006). The ribosome density was especially increased on short uORFs and at the 5'UTR of ORFs upon oxidative stress in yeast cells, which elongated the transit time of ribosomes on mRNAs (Gerashchenko, Lobanov, and Gladyshev 2012). *Ateef1b $\gamma$ 1/2* mutants did already under control conditions show an increased number of ribosomes and an increased ribosome density on mRNA. Regardless *Ateef1b $\gamma$ 1/2* mutants did not display higher resistance to oxidative stress, which might indicate that the role of eEF1B $\gamma$  for oxidative stress response in Arabidopsis is considerably minor compared to its role in yeast.

### 5.5.2 eEF1B $\gamma$ is not directly involved in heat stress response

Adaption to heat stress is one of the most important traits of plants to secure survival during times of climate change. Translation is tightly regulated upon heat stress to inhibit general protein biosynthesis and thereby prevent damage or incorrect folding of nascent polypeptide chains. Additionally, translation of heat stress-specific genes is continued and secured. Translation factors have been shown to be connected to heat stress responses. Here, it was analyzed if eEF1B $\gamma$  is mediating heat stress response in Arabidopsis. Initially, it was expected that the *eef1b $\gamma$ 1/2* double mutant would show a higher sensitivity towards heat stress compared to WT. On the one hand, yeast eEF1B $\gamma$  double mutants showed additive sensitivity to heat stress (Olarewaju et al. 2004). On the other hand, an Arabidopsis translation initiation factor mutant, *eif5b1*, has previously been identified as heat sensitive mutant. In control conditions, *eif5b1* mutant and *eef1b $\gamma$ 1/2* double mutants display similar phenotypes. Loss of eIF5B1 leads to retarded germination, reduced primary and lateral root growth and an overall delayed development (Zhang, Liu, et al. 2017), which is very similar to *eef1b $\gamma$ 1/2* double mutants. In

response to acclimated heat stress, the *EIF5B1* mutant showed reduced hypocotyl elongation and reduced seedling survival. But seedlings of the eEF1B $\gamma$  double mutant did not show altered thermotolerance towards different heat stress conditions including basal, acquired (short-term or long-term acquired) or ambient temperature stress compared to WT. Also, the seed germination rate was similar to WT after heat treatment of seeds. So, in contrast to yeast eEF1B $\gamma$  and Arabidopsis eIF5B1, eEF1B $\gamma$  does not play a significant role in heat stress response. Further analysis comprehensively explained the difference between *EIF5B1* and *eef1b $\gamma$ 1/2* mutants in heat stress response. The heat sensitivity of *EIF5B1* mutants resulted from a delayed recovery of polysomes to mRNA after heat stress relief (Zhang, Liu, et al. 2017), which was caused by a reduced abundance of mature 18S rRNA in *EIF5B1* mutants. Without mature 18S rRNA, 80S ribosomes are genome-wide stalled at the start codon (Hang et al. 2023). In contrast, *eef1b $\gamma$ 1/2* double mutants displayed a slightly higher content of 18S and 25S rRNAs under control conditions, consequently the ribosome assembly is not disturbed and polysomes are available for re-initiation of translation after heat stress relief. Clearly, it is necessary to confirm the correct re-initiation of translation after heat stress relief by analyzing the polysome profiles of *eef1b $\gamma$ 1/2* double mutants during heat stress and after stress relief.

A connection between translational regulation and heat stress through a translation factor has been established in plants at the initiation step (Salome 2017). A first link between a translation elongation factor and heat stress resistance has been established for the plastid translation elongation factor EF-Tu, RABE1b. The aggregation-prone RABE1b is required to confer thermotolerance and to ensure translation under heat stress conditions. Loss-of-function of RABE1b leads to heat-sensitivity and downregulated translation in plastids during heat conditions (Li et al. 2018). In human cells, the translation elongation factor complex eEF1A mediates the transcription and translation of HSP70 and thereby confers thermotolerance. HSF1 is recruited to the HSP70 promoter through eEF1A. Then, eEF1A binds to RNA polymerase II and the 3'UTR of HSP70 to stabilize the HSP70 transcript and mediate its transport to actively translating ribosomes (Vera et al. 2014). The ability to synthesize HSPs is especially important for heat stress resistance since HSPs are required for proper protein folding of nascent polypeptide chains. Elevated temperatures lead to increased numbers of misfolded proteins. HSC/HSP70 complexes are not only required as chaperones, but also play a role in protein triage decisions and help to target misfolded proteins for degradation together with HSP70/HSP90 interacting protein (Zhang and Qian 2011). If the number of misfolded proteins exceeds the number of available HSC/HSP70 complexes, a feedback loop leads to ribosome

pausing at the elongation step, which has been shown for mammalian cells (Liu, Han, and Qian 2013; Shalgi et al. 2013) and for plants cells (Merret et al. 2015). Whether human eEF1B is important for induction of HSP synthesis and heat stress resistance has not been elucidated yet. Here, it was shown that the knockdown of eEF1B $\gamma$  subunit does not affect heat stress sensitivity in *Arabidopsis*. *eef1b $\gamma$ 1/2* double mutants are able to produce HSP70 and HSP90 under heat stress similar to WT levels. It remains to be analyzed whether the other two subunits, eEF1B $\alpha$  and eEF1B $\beta$ , or other translation elongation factors, like eEF1A or eEF2, might play a more important role in heat stress response in plants.

Lately, it has also been discussed that heat stress experiments in the lab are unrealistic. In nature, heat stress would also occur in combination of with other stresses or wind. Furthermore, the temperature changes are subtle and graduate (Plessis 2023). There is a big difference between the temperature changes through climate change, heat shock and heat waves (Jagadish, Way, and Sharkey 2021). Another interesting point regarding application of heat stress in the lab is exactness of applied temperatures. There is a growing need to associate plant responses to tissue temperatures. This would be possible through infrared thermometers (Jagadish, Way, and Sharkey 2021). Since the ultimate goal of understanding the heat stress response in plants would most certainly be the engineering of more resistant plants for agricultural use, it would be of great relevance to implement these considerations in further studies of the heat stress response in plants.

## 5.6 eEF1B subunits accumulate in heat-induced stress granules

Biomolecular condensates have become a field of large and intensive research. Stress granules are especially of interest since they have been associated with different important stress response processes in plants and other organisms. In the beginning of stress granule research, the accumulation of translation initiation factors and untranslated mRNAs in stress granules had been reasoned to be responsible for general translational arrest during stress (Nover, Scharf, and Neumann 1989; Kedersha et al. 1999). Early research did neither identify 60S ribosomal subunits (Kimball et al. 2003), translation elongation factors, translation termination factors, nor heat-stress induced transcripts like *HSP90* mRNA as components of stress granules. These findings led to the assumption that the inhibition of translation initiation is mediated by SG assembly and that no active translation is occurring within SGs. But recent research has shown that stress granule formation and translational regulation are intertwined in a highly specific and complex interaction network (reviewed in (Mateju and Chao 2022; Adjibade and Mazroui 2023)). While the translation of specific factors can be based on their accumulation in SGs

(Adjibade and Mazroui 2023; Moon et al. 2019), the downregulation of translation in response to stress is still able to occur in SG-deficient cells (Buchan, Muhlrad, and Parker 2008; Mokaš et al. 2009; Kedersha et al. 2016). The re-initiation of translation after stress relief can also occur independently of SG disassembly (Hofmann et al. 2012). In human cells, it was shown that full cycles of translation of specific transcripts can occur within stress granules (Mateju et al. 2020). For complete translation cycles within SGs, it is necessary that translation elongation and termination factors are at least transiently present within SGs.

Indeed, several studies demonstrated the presence of translation elongation and/or termination factors in stress granules within different organisms. Arsenite stress-induced mammalian SGs contain translation elongation factor eIF5A, translation termination factors eRF1 and eRF3, and even ribosome recycling factors ABCE1, MCT1 and eIF2D. eRF1 and eRF3 are required for correct translation termination. Loss of eRF1 and eRF3 leads to elevated stop-codon readthrough, which results in production of proteins with C-terminal extensions (Janzen and Geballe 2004). Elevated stop-codon readthrough is also observed in mammalian cells during arsenite stress. Since arsenite stress simultaneously leads to elevated stop-codon readthrough as well as sequestration of eRF1 and eRF3 to SGs, it was suggested that the compartmentalization of eRF1 and eRF3 in SGs contributes to the regulation of translation termination (Makeeva et al. 2023). In yeast, two translation elongation factors, eEF1B $\gamma$ /Tef4 and eEF3/Yef3, as well as two translation termination factors, eRF1/Sup45 and eRF3/Sup35, were identified as components of heat-induced stress granules. It was discussed that the translation elongation factors, which aggregated and co-localized with SG markers already at mild temperatures, could have a function as nucleation sites for formation of SGs (Grousl et al. 2013; Wallace et al. 2015).

Here, it was shown that all three subunits of the Arabidopsis eEF1B complex do accumulate in stress granules after heat stress. This is in accordance with the identification of all three eEF1B subunits in the heat-induced stress granule proteome (Kosmacz et al. 2019), the co-localization of eEF1B subunits with HSP101 in cytoplasmic foci after heat stress (McLoughlin et al. 2016) and the identification of eEF1B subunits as heat-dependent interactors of SG core protein TSN2 in Arabidopsis (Gutierrez-Beltran et al. 2021). To find out whether eEF1B $\gamma$  is a SG scaffold or a SG client protein, the ability of SG assembly was analyzed in the *eef1b $\gamma$ 1/2* double mutant. Since the *eef1b $\gamma$ 1/2* double mutant was not deficient in SG assembly, it can be concluded that eEF1B $\gamma$  is neither a scaffold protein nor a nucleation site for SG assembly, but rather a SG client protein. This could explain the relatively small overlap between the heat-induced

interactome of eEF1B $\gamma$  with heat-induced interactomes of the SG scaffold proteins TSN2 or RBP47 found in the coimmunoprecipitation experiment. The overlap between the heat-induced interactome of eEF1B $\gamma$  with TSN2 or RBP47 heat-induced interactomes was restricted to four proteins each. As SG client protein eEF1B $\gamma$  localizes to the outer shell of SGs, while TSN2 and RBP47 as SG scaffold proteins are located within the core of SGs. Additionally, SG assembly and disassembly is a highly dynamic process, which does allow a high number of transient interactions between cytosolic proteins and SG components.

It would be of high interest to test eEF1B $\alpha$ - or eEF1B $\beta$ -deficient plants for SG assembly, in order to determine whether these proteins could act as nucleation site for SGs. This applies especially to eEF1B $\beta$ , because eEF1B $\beta$  did show a different SG accumulation pattern than eEF1B $\alpha$  and eEF1B $\gamma$ . Overexpressed eEF1B $\beta$ -GFP forms heat-induced stress granules in higher numbers, in larger sizes and at lower temperatures than eEF1B $\alpha$  and eEF1B $\gamma$ . In addition, the presence of eEF1B $\beta$  enhances the recruitment of eEF1B $\alpha$  or eEF1B $\gamma$  to heat-induced stress granules. What could be the reason of the increased SG accumulation of eEF1B $\beta$  in heat-induced stress granules compared to the other eEF1B subunits?

An important feature of proteins, which strongly accumulate in SGs, is the presence of an intrinsically disordered region (IDR). IDRs of proteins can be essential and/or sufficient to re-localize proteins to stress granules *in vivo* or to lead to phase separation into liquid droplets *in vitro* (Protter et al. 2018; Lin et al. 2015). Analysis of the protein sequence of eEF1B $\alpha$ , eEF1B $\beta$  and eEF1B $\gamma$  using IUPred3 prediction tool revealed that all three proteins contain an IDR in their linker domain, which connects two functional domains (Erdős, Pajkos, and Dosztányi 2021). Thus, the presence of an IDR cannot be the sole reason for the observed unique SG accumulation pattern behavior of eEF1B $\beta$ . To elucidate the molecular basis, it would be useful to analyze the aggregation of eEF1B $\beta$  *in vitro*. Also, the biomolecular condensate formation of eEF1B $\beta$  should be analyzed when it is expressed under its native promotor. In this study, all three eEF1B subunits have been expressed under a constitutive 35S promotor or an estradiol-inducible 35S promotor. The overexpression from 35S promotor could lead to results that are not reflecting the natural biological condition within the cells.

Another indication for an extended aggregation behavior of eEF1B $\beta$  was that some protoplasts transformed with eEF1B $\beta$ -GFP from 35S promotor did show an accumulation of microscopically observable condensates already at room temperature. In accordance, Hossain et al. observed in some cells the accumulation of overexpressed eEF1B $\beta$  in cytoplasmic

condensates at room temperature in stable transgenic lines (Hossain et al. 2012). A small amount of eEF1B $\beta$  condensates did also appear in the presence of cycloheximide (CHX). CHX blocks the release of untranslated mRNAs from ribosomes and thus inhibits formation of SGs and PBs (Kedersha et al. 2000). The CHX-insensitive eEF1B $\beta$  condensates are consequently neither SGs nor PBs, but most likely protein aggregates. Although SG and PB assembly and disassembly are dynamic and reversible processes (Anderson and Kedersha 2008), under certain conditions, SGs can transition from a liquid state to a solid state. Such “solid” SGs cannot be disassembled after stress relief and form protein aggregates that are permanent and possibly toxic for the cell. In human cells, such aggregates are associated with diseases like motor neuron diseases, Huntington’s (Pesket et al. 2018) Alzheimer’s (Vanderweyde et al. 2012) or amyotrophic lateral sclerosis (Taylor, Brown, and Cleveland 2016; Wolozin and Ivanov 2019). Intracellular aggregation of an abnormally long polyglutamine stretch in the huntingtin protein is responsible for Huntington’s disease (Pesket et al. 2018). Long polyglutamine stretches are typical for intrinsically disordered proteins. Interestingly, the overexpression of a polyglutamine-containing protein that is causative for toxic protein aggregation in human cells, does not lead to protein aggregation in plant cells under standard conditions (Llamas et al. 2023). This indicates that plants have an efficient system to cope with protein aggregation (Alberti and Hyman 2021). Among the heat-induced interactors of eEF1B $\gamma$  are members of the COP9 signalosome and the proteasome. It would be interesting to know, whether these are similarly interactors of eEF1B $\beta$  upon heat stress and play a role for degradation of CHX-insensitive aggregates of eEF1B $\beta$ . Currently, it remains unknown whether the CHX-insensitive aggregates of eEF1B $\beta$  are toxic for the plant cells or if they might fulfil a specific function and are efficiently degraded afterwards.

Overall, one outstanding research question, resulting from the data in this thesis, is: does the accumulation of eEF1Bs in heat-induced SGs have a specific function in translational regulation during heat stress? An interesting observation from the co-immunoprecipitation experiment with eEF1B is that eEF1A does interact with eEF1B $\gamma$  under control conditions, but it is not found among the eEF1B $\gamma$  interactors after heat stress. eEF1A has also not been identified as SG component in the heat-induced interactome of TSN2 or the SG proteome based on the interactome of RBP47 in plants (Gutierrez-Beltran et al. 2021; Kosmacz et al. 2019). Similarly, in a study in human cells, eEF1A has not been identified in heat-induced G3BP1- or CAPRIN1-interactomes (Hu et al. 2023). Both proteins are known as SG scaffold proteins in human SGs (Kedersha et al. 2016). It is intriguing to hypothesize that the absence of eEF1A in heat-induced

SGs, the increased aggregation of eEF1B $\beta$  and the sequestration of the eEF1B subunits in SGs are part of a mechanism to regulate the level of translation during stress. Under standard conditions, eEF1A and eEF1B are present in the cytosol. mRNAs are loaded with polysomes and eEF1A delivers aminoacyl-tRNAs to the ribosome. Under GTP hydrolysis, the aminoacyl-tRNAs are loaded onto the elongating polypeptide chain. eEF1B exchanges GDP for GTP on eEF1A and translation is occurring efficiently. Upon stress conditions, eEF1B $\beta$  is starting to aggregate and thereby localizing to SGs together with eEF1B $\alpha$  and eEF1B $\gamma$ . Reduced availability of eEF1B could reduce translation elongation rates in the cytosol. As discussed for the *eef1b $\gamma$ 1/2* double mutant, it is possible that the alteration of translation rates might be dosage dependent. At mild stress conditions, a part of eEF1B subunits could remain cytosolic and could allow for compensation of translational slow down. With increasing stress levels, a higher number of eEF1B $\beta$  protein aggregates forms. Concurrently, eEF1B $\beta$  subunits are not present in the cytosol, but either in SGs (together with eEF1B $\alpha$  and eEF1B $\gamma$ ) or in "solid" eEF1B $\beta$  protein aggregates. The SG localization is reversible. Upon stress relief, the eEF1B subunits can be released and help to restart translation initiation. In contrast, "solid" protein aggregates need to be degraded, thus eEF1B subunits aggregated in "solid" protein aggregates cannot be re-introduced to the translation cycle. During severe heat stress, translation of stress-specific transcript is essential for plant survival. Independent of stress conditions, eEF1A remains in the cytoplasm. Thus, cytoplasmic eEF1A could ensure the required translation of stress-specific transcripts. Although eEF1B highly increases the GDP/GTP exchange rate, eEF1A is able to perform GDP/GTP exchange without eEF1B. In yeast cells, it was shown that overexpression of eEF1A is able to compensate for loss of eEF1B $\alpha$  (Kinzy and Woolford 1995). A scheme of the described hypothesis for a mechanism of translational regulation at the elongation step through sequestration of eEF1B into SGs is shown in Fig. 72.

In conclusion, it was shown that eEF1B $\gamma$  in Arabidopsis has a conserved function in translation elongation in Arabidopsis. Reduced eEF1B $\gamma$  levels were associated with developmental defects and affected the ribosome occupancy of RNAs. Although, no direct role of eEF1B $\gamma$  was detected in heat stress response, the sequestration of the three eEF1B subunits in heat-induced stress granules allows for a potential role of eEF1B in translational regulation during heat stress. Highly interesting research questions regarding the exact regulation of eEF1B sequestration and downstream effects on translation levels remain to be answered.

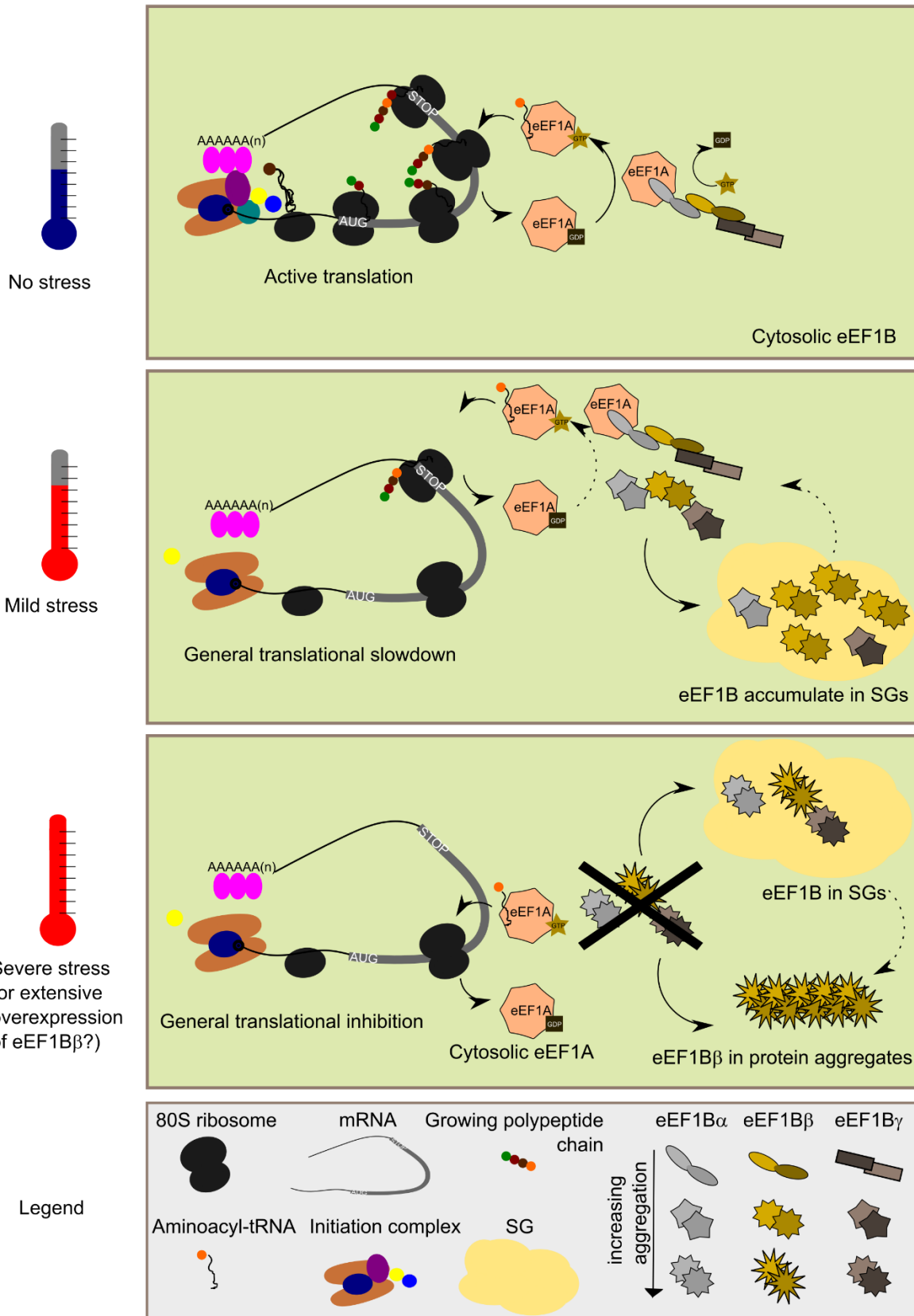


**Figure 72: Hypothesis for a regulatory role of eEF1B sequestration in stress granules during heat stress.** During standard conditions, mRNAs are actively translated with the support of eEF1A, whose GDP/GTP exchange is conducted by soluble, cytosolic eEF1B. During mild heat stress, eEF1B $\beta$  starts to aggregate and thereby supports

the sequestration of all three eEF1B subunits into heat-induced stress granules. Partially, eEF1B subunits still remain in the cytosol, which allows for specific translation. Overall, sequestration of eEF1B slows down translation elongation rates. Even during severe stress, eEF1A stays cytosolic, which could allow the necessary translation of stress-specific genes. eEF1B subunits are completely removed from the cytosol. Strong aggregation of eEF1B $\beta$  leads to accumulation of microscopically visible protein aggregates, which might be toxic to the cell and cannot be solubilized after stress removal. Grey: eEF1B $\alpha$ ; ochre: eEF1B $\beta$ ; brown: eEF1B $\gamma$ .

## 6 Summary

Growth and development of plants, as sessile organisms, are dependent on many internal signaling factors and on external environmental cues. Coordinated root growth is required for an optimal supply with nutrients and water. Undifferentiated stem cells within the root apical meristem regulate cell division and thereby coordinate continuous replenishment of root cells. DNA integrity is of utmost importance in stem cells to hinder damaged DNA from being passed onto the next generation of cells. A heteroprotein complex consisting of (at least) three proteins plays an important role for genome stability and primary root growth. MAINTENANCE OF MERISTEMS (MAIN), MAINTENANCE OF MERISTEMS-LIKE1 (MAIL1) and PROTEIN PHOSPHATASE 7-LIKE (PP7L) interact with each other and are acting within the same signaling pathway. T-DNA insertional of each of these three proteins show similar phenotypes with drastically reduced primary root growth, accumulation of dead cells within the root apical meristem and the release of transposable elements from silencing. Currently, it is unknown in which signaling pathway the MAIN-MAIL1-PP7L complex is active. In the first part of this thesis, different approaches were utilized to characterize the MAIN-MAIL1-PP7L complex. On the one hand, a suppressor screen was performed on *pp7l* mutants to identify suppressor mutations that reverse the short root phenotype. Potential suppressor lines were isolated. Identification of the affected genes will give insight about the potential signaling pathway. On the other hand, protein interaction partners of PP7L were identified using co-immunoprecipitation coupled with mass spectroscopy.

Environmental cues strongly influence plant development. Climate change including increasing temperatures challenge plants to constant adaption. Protein biosynthesis and a balanced protein homeostasis are essential for plant growth. Both processes have a high energy consumption and are therefore tightly regulated. Upon stress conditions, global protein biosynthesis is inhibited and solely translation of stress-specific proteins is performed. Translation rates are mostly regulated at the translation initiation step, but recently a regulation at the translation elongation step has been considered. The second part of this thesis focused on the characterization of the translation elongation factor complex eEF1B. eEF1B has a conserved GDP/GTP exchange function on the translation elongation factor complex eEF1A. eEF1A transports aminoacyl-tRNAs to the translating ribosomes at the mRNA and translocates the aminoacyl-tRNAs onto the growing polypeptide chain under GTP hydrolysis. The Arabidopsis eEF1B complex consists of three subunits, whose function have scarcely been analyzed. Here, a function of the Arabidopsis eEF1B $\gamma$  subunit for efficient translation and for plant development has been

identified. Mutants with reduced eEF1B $\gamma$  protein levels show a delayed plant development with defects in cell division. The global protein biosynthesis rates are similar to WT, but an increased number of total ribosomes indicate a compensation of reduced translation elongation rates in *eef1b $\gamma$ 1/2* mutant. A direct function of eEF1B $\gamma$  in plant heat stress response has not been identified. Nonetheless, all three eEF1B subunits were found to localize to heat-induced stress granules. Stress granules are stress-induced accumulations of mRNA and proteins in the cytoplasm, which are formed via liquid-liquid phase separation. The eEF1B $\beta$  subunit shows an increased accumulation within stress granules and is able to enhance the accumulation of the other two eEF1B subunits to stress granules upon heat stress. The accumulation of eEF1B subunits might be a mechanism to finetune the regulation of protein biosynthesis during stress conditions.

## 6.1 Zusammenfassung

Das Wachstum und die Entwicklung von Pflanzen als sessile Organismen sind von diversen Faktoren innerhalb und außerhalb der Pflanze abhängig. Innerhalb der Pflanze ist ein koordiniertes Wurzelwachstum essenziell um die optimale Versorgung der Pflanze mit Nährstoffen und Wasser sicherzustellen. Die fortlaufende Bildung neuer Wurzelzellen findet im apikalen Wurzelmeristem statt. Nicht-differenzierte Stammzellen im Meristem regulieren die Zellteilung und können neue Zellen ausbilden. Die Integrität der DNA in den Stammzellen ist besonders wichtig, damit keine beschädigte DNA an Tochterzellen weitergegeben wird. Der Verlust der Genomstabilität in der Stammzellnische verhindert das korrekte Ausbilden neuer Wurzelzellen. Ein Heteroproteinkomplex bestehend aus (mindestens) drei Proteinen spielt eine wichtige Rolle in der Aufrechterhaltung der Genomstabilität und somit für die gesamte Entwicklung der Pflanze. ‚MAINTENANCE OF MERISTEMS‘ (MAIN), ‚MAINTENANCE OF MERISTEMS-LIKE‘ (MAIL1) und ‚PROTEIN PHOSPHATASE 7-LIKE‘ (PP7L) interagieren miteinander und agieren im gleichen Signalweg. T-DNA Insertionslinien für jede Komponente dieses Proteinkomplexes zeigen einen ähnlichen Phänotyp mit einem drastisch verkürzten Wurzelwachstum und der Akkumulation toter Zellen im Wurzelmeristem. Außerdem ist das ‚Silencing‘ von Transposablen Elementen (TE) in den Mutanten gestört. Der Signalweg durch welchen MAIN, MAIL1 und PP7L zur Genomstabilität und zum ‚TE silencing‘ beitragen, ist bislang unbekannt. Daher wurde im ersten Teil dieser Arbeit begonnen einen Suppressorscreen durchzuführen. Hierbei sollte mittels einer EMS-Mutagenese von Samen der *pp7l*-Mutante, eine Suppressor-Mutation eingeführt werden, die den kurzen Wurzel-Phänotyp revidiert. Es wurden potenzielle Kandidaten identifiziert, deren weitere Analyse zum

Identifizieren der zugrunde liegenden Gene notwendig ist. Des Weiteren wurden in dieser Arbeit potenzielle Protein-Interaktionspartner von PP7L mittels einer Koimmunopräzipitations-Massenspektrometrie-Analyse identifiziert.

Klimatische Veränderungen, insbesondere erhöhte Temperaturen, haben einen großen Einfluss auf die pflanzliche Entwicklung und erfordern eine stetige Anpassung der Pflanzen. Die Biosynthese neuer Proteine und eine ausgeglichene Protein-Homöostase sind Voraussetzung für ein optimales Wachstum. Die Proteinbiosynthese hat einen hohen Energieverbrauch und wird deshalb stark reguliert. Unter Stressbedingungen wird die globale Proteinbiosynthese inhibiert und lediglich eine Translation von spezifischen Proteinen für die Stressantwort ermöglicht. Die Translationsrate wird hauptsächlich am ersten Schritt der Translation, der Initiation, reguliert. Kürzlich wurde auch eine Beteiligung des zweiten Schrittes der Translation, der Elongation, festgestellt. Im zweiten Teil dieser Arbeit wurde der Translations-Elongationsfaktor-Komplex eEF1B analysiert. eEF1B hat eine konservierte Funktion im Austausch von GDP zu GTP am Translations-Elongationsfaktorkomplex eEF1A. eEF1A transportiert Aminoacyl-tRNAs zu den translatierenden Ribosomen an der mRNA und transferiert diese unter GTP-Verbrauch auf die wachsende Polypeptidkette. Der pflanzliche eEF1B-Komplex besteht aus drei Untereinheiten, deren Funktionen in Arabidopsis bisher kaum untersucht wurden. In Rahmen dieser Arbeit wurde eine Rolle der eEF1B $\gamma$ -Untereinheit in der Translation und in der pflanzlichen Entwicklung nachgewiesen. Mutanten mit stark reduziertem eEF1B $\gamma$ -Proteinlevel zeigen ein verzögertes Wachstum mit Defekten in der Zellteilung. Die generelle Proteinsynthese ist unverändert im Vergleich zum Wildtyp, aber eine erhöhte Anzahl an Ribosomen deutet auf eine Kompensation einer reduzierten Translations-Elongationsrate hin. Eine direkte Funktion von eEF1B $\gamma$  in der pflanzlichen Hitzestressantwort wurde nicht nachgewiesen. Trotz dessen wurden alle drei eEF1B-Untereinheiten in hitze-induzierten, zytoplasmatischen ‚Stress granules‘ nachgewiesen. Stress granules sind Akkumulationen von mRNA und Proteinen, die im Zytoplasma unter Stressbedingungen durch eine Flüssig-Flüssig-Phasenseparation entstehen. Nach Beendigung des Stresses lösen sich die Stress granules auf. Hier wurde untersucht, welche eEF1B-Untereinheiten in zytoplasmatischen Kondensaten während verschiedener Hitzestressbedingungen akkumulieren. Die eEF1B $\beta$ -Untereinheit zeigt eine besonders ausgeprägte Akkumulation in Stress granules, welches auch die Lokalisation der anderen beiden Untereinheiten in Stress Granules verstärkt. Die verstärkte Akkumulation von eEF1B $\beta$  in Stress granules mit den anderen eEF1B-Untereinheiten wird als möglicher Mechanismus zur Inhibierung der generellen Translationsrate unter Hitzestress diskutiert.

## 7 References

- Adachi, S., K. Minamisawa, Y. Okushima, S. Inagaki, K. Yoshiyama, Y. Kondou, E. Kaminuma, M. Kawashima, T. Toyoda, M. Matsui, D. Kurihara, S. Matsunaga, and M. Umeda. 2011. 'Programmed induction of endoreduplication by DNA double-strand breaks in Arabidopsis', *Proc Natl Acad Sci U S A*, 108: 10004-9.
- Adjibade, Pauline, and Rachid Mazroui. 2023. 'Stress granules: stress-induced cytoplasmic mRNPs compartments linked to mRNA translational regulatory pathways', *Frontiers in RNA Research*, 1.
- Advani, Vivek M., and Pavel Ivanov. 2019. 'Translational Control under Stress: Reshaping the Translatome', *BioEssays*, 41: 1900009.
- Aida, Mitsuhiro, Dimitris Beis, Renze Heidstra, Viola Willemsen, Ikram Blilou, Carla Galinha, Laurent Nussaume, Yoo-Sun Noh, Richard Amasino, and Ben Scheres. 2004. 'The PLETHORA Genes Mediate Patterning of the Arabidopsis Root Stem Cell Niche', *Cell*, 119: 109-20.
- Aizer, Adva, Alon Kalo, Pinhas Kafri, Amit Shraga, Rakefet Ben-Yishay, Avi Jacob, Noa Kinor, and Yaron Shav-Tal. 2014. 'Quantifying mRNA targeting to P-bodies in living human cells reveals their dual role in mRNA decay and storage', *Journal of Cell Science*, 127: 4443-56.
- Al-Whaibi, Mohamed H. 2011. 'Plant heat-shock proteins: A mini review', *Journal of King Saud University - Science*, 23: 139-50.
- Alberti, Simon, and Anthony A. Hyman. 2021. 'Biomolecular condensates at the nexus of cellular stress, protein aggregation disease and ageing', *Nature Reviews Molecular Cell Biology*, 22: 196-213.
- Alexander, M. P. 1969. 'Differential staining of aborted and nonaborted pollen', *Stain Technol*, 44: 117-22.
- Alonso, J. M., A. N. Stepanova, T. J. Leisse, C. J. Kim, H. Chen, P. Shinn, D. K. Stevenson, J. Zimmerman, P. Barajas, R. Cheuk, C. Gadrinab, C. Heller, A. Jeske, E. Koesema, C. C. Meyers, H. Parker, L. Prednis, Y. Ansari, N. Choy, H. Deen, M. Geralt, N. Hazari, E. Hom, M. Karnes, C. Mulholland, R. Ndubaku, I. Schmidt, P. Guzman, L. Aguilar-Henonin, M. Schmid, D. Weigel, D. E. Carter, T. Marchand, E. Risseuw, D. Brogden, A. Zeko, W. L. Crosby, C. C. Berry, and J. R. Ecker. 2003. 'Genome-wide insertional mutagenesis of Arabidopsis thaliana', *Science*, 301: 653-7.
- Anderson, P., and N. Kedersha. 2006. 'RNA granules', *J Cell Biol*, 172: 803-8.
- . 2008. 'Stress granules: the Tao of RNA triage', *Trends Biochem Sci*, 33: 141-50.
- Andreeva, A. V., and M. A. Kutuzov. 2009. 'PPEF/PP7 protein Ser/Thr phosphatases', *Cell Mol Life Sci*, 66: 3103-10.
- Armenta-Medina, Alma, C. Stewart Gillmor, Peng Gao, Javier Mora-Macias, Leon V. Kochian, Daoquan Xiang, and Raju Datla. 2021. 'Developmental and genomic architecture of plant embryogenesis: from model plant to crops', *Plant Communications*, 2.
- Bader, G. D., and C. W. Hogue. 2003. 'An automated method for finding molecular complexes in large protein interaction networks', *BMC Bioinformatics*, 4: 2.
- Baggett, D. W., A. Medyukhina, S. Tripathi, H. K. Shirnekhi, H. Wu, S. B. Pounds, K. Khairy, and R. Kriwacki. 2022. 'An Image Analysis Pipeline for Quantifying the Features of Fluorescently-Labeled Biomolecular Condensates in Cells', *Front Bioinform*, 2: 897238.
- Bai, B., A. Peviani, S. van der Horst, M. Gamm, B. Snel, L. Bentsink, and J. Hanson. 2017. 'Extensive translational regulation during seed germination revealed by polysomal profiling', *New Phytol*, 214: 233-44.

- Bai, B., S. van der Horst, J. H. G. Cordewener, Tahp America, J. Hanson, and L. Bentsink. 2020. 'Seed-Stored mRNAs that Are Specifically Associated to Monosomes Are Translationally Regulated during Germination', *Plant Physiol*, 182: 378-92.
- Banani, S. F., H. O. Lee, A. A. Hyman, and M. K. Rosen. 2017. 'Biomolecular condensates: organizers of cellular biochemistry', *Nat Rev Mol Cell Biol*, 18: 285-98.
- Baradaran-Heravi, Y., C. Van Broeckhoven, and J. van der Zee. 2020. 'Stress granule mediated protein aggregation and underlying gene defects in the FTD-ALS spectrum', *Neurobiol Dis*, 134: 104639.
- Barkan, A. 1998. 'Approaches to investigating nuclear genes that function in chloroplast biogenesis in land plants', *Photosynthesis: Molecular Biology of Energy Capture*, 297: 38-57.
- Bascos, N. A. D., and S. J. Landry. 2019. 'A History of Molecular Chaperone Structures in the Protein Data Bank', *Int J Mol Sci*, 20.
- Bchini, R., J. M. Girardet, R. Sormani, E. Gelhaye, and M. Morel-Rouhier. 2020. 'Oxidized glutathione promotes association between eukaryotic translation elongation factor 1B gamma and Ure2p glutathione transferase from *Phanerochaete chrysosporium*', *Febs Journal*.
- Bhasin, H., and M. Hülskamp. 2017. 'ANGUSTIFOLIA, a Plant Homolog of CtBP/BARS Localizes to Stress Granules and Regulates Their Formation', *Front Plant Sci*, 8: 1004.
- Bheri, Malathi, Swati Mahiwal, Sibaji K. Sanyal, and Girdhar K. Pandey. 2021. 'Plant protein phosphatases: What do we know about their mechanism of action?', *The FEBS Journal*, 288: 756-85.
- Bleckmann, A., S. Weidtkamp-Peters, C. A. Seidel, and R. Simon. 2010. 'Stem cell signaling in Arabidopsis requires CRN to localize CLV2 to the plasma membrane', *Plant Physiol*, 152: 166-76.
- Bondarchuk, T. V., V. F. Shalak, D. M. Lozhko, A. Fatal'ska, R. H. Szczepanowski, V. Liudkovska, O. Y. Tsuvariev, M. Dadlez, A. V. El'skaya, and B. S. Negrutskii. 2022. 'Quaternary organization of the human eEF1B complex reveals unique multi-GEF domain assembly', *Nucleic Acids Res*, 50: 9490-504.
- Bonnot, Titouan, Morgane B. Gillard, and Dawn H. Nagel. 2019. 'A Simple Protocol for Informative Visualization of Enriched Gene Ontology Terms', *Bio-protocol*, 9: e3429.
- Browning, K. S., and J. Bailey-Serres. 2015. 'Mechanism of cytoplasmic mRNA translation', *Arabidopsis Book*, 13: e0176.
- Brunetti, C., M. Di Ferdinando, A. Fini, S. Pollastri, and M. Tattini. 2013. 'Flavonoids as antioxidants and developmental regulators: relative significance in plants and humans', *Int J Mol Sci*, 14: 3540-55.
- Bruns, A. N., S. Li, G. Mohannath, and D. M. Bisaro. 2019. 'Phosphorylation of Arabidopsis eIF4E and eIFiso4E by SnRK1 inhibits translation', *Febs Journal*, 286: 3778-96.
- Buchan, J. Ross, Denise Muhlrud, and Roy Parker 2008. 'P bodies promote stress granule assembly in *Saccharomyces cerevisiae*', *Journal of Cell Biology*, 183: 441-55.
- Cairns, Narelle G., Maciej Pasternak, Andreas Wachter, Christopher S. Cobbett, and Andreas J. Meyer. 2006. 'Maturation of Arabidopsis Seeds Is Dependent on Glutathione Biosynthesis within the Embryo', *Plant Physiology*, 141: 446-55.
- Callot, Caroline, and Jean-Luc Gallois. 2014. 'Pyramiding resistances based on translation initiation factors in Arabidopsis is impaired by male gametophyte lethality', *Plant Signaling & Behavior*, 9: e27940.
- Campos-Melo, Danae, Zachary C. E. Hawley, Cristian A. Droppelmann, and Michael J. Strong. 2021. 'The Integral Role of RNA in Stress Granule Formation and Function', *Frontiers in Cell and Developmental Biology*, 9.
- Capron, A., S. Chatfield, N. Provart, and T. Berleth. 2009. 'Embryogenesis: pattern formation from a single cell', *Arabidopsis Book*, 7: e0126.

- Castellano, M. M., and C. Merchante. 2021. 'Peculiarities of the regulation of translation initiation in plants', *Curr Opin Plant Biol*, 63: 102073.
- Catara, G., G. Grimaldi, L. Schembri, D. Spano, G. Turacchio, M. Lo Monte, A. R. Beccari, C. Valente, and D. Corda. 2017. 'PARP1-produced poly-ADP-ribose causes the PARP12 translocation to stress granules and impairment of Golgi complex functions', *Sci Rep*, 7: 14035.
- Chantarachot, T., and J. Bailey-Serres. 2018. 'Polysomes, Stress Granules, and Processing Bodies: A Dynamic Triumvirate Controlling Cytoplasmic mRNA Fate and Function', *Plant Physiol*, 176: 254-69.
- Chang, Yee-yung, Hsiang-chin Liu, Nai-yu Liu, Fu-chiun Hsu, and Swee-suak Ko. 2006. 'Arabidopsis Hsa32, a Novel Heat Shock Protein, Is Essential for Acquired Thermotolerance during Long Recovery after Acclimation', *Plant Physiology*, 140: 1297-305.
- Clark, N. M., A. P. Fisher, B. Berckmans, L. Van den Broeck, E. C. Nelson, T. T. Nguyen, E. Bustillo-Avendano, S. G. Zebell, M. A. Moreno-Risueno, R. Simon, K. L. Gallagher, and R. Sozzani. 2020. 'Protein complex stoichiometry and expression dynamics of transcription factors modulate stem cell division', *Proc Natl Acad Sci U S A*, 117: 15332-42.
- Considine, Michael J, and Christine H Foyer. 2021. 'Stress effects on the reactive oxygen species-dependent regulation of plant growth and development', *Journal of Experimental Botany*, 72: 5795-806.
- Cox, J., M. Y. Hein, C. A. Luber, I. Paron, N. Nagaraj, and M. Mann. 2014. 'Accurate proteome-wide label-free quantification by delayed normalization and maximal peptide ratio extraction, termed MaxLFQ', *Mol Cell Proteomics*, 13: 2513-26.
- Cui, Y., S. Lu, Z. Li, J. Cheng, P. Hu, T. Zhu, X. Wang, M. Jin, X. Wang, L. Li, S. Huang, B. Zou, and J. Hua. 2020. 'CYCLIC NUCLEOTIDE-GATED ION CHANNELs 14 and 16 Promote Tolerance to Heat and Chilling in Rice', *Plant Physiol*, 183: 1794-808.
- Curtis, M. D., and U. Grossniklaus. 2003. 'A gateway cloning vector set for high-throughput functional analysis of genes in planta', *Plant Physiol*, 133: 462-9.
- Daudi, A., and J. A. O'Brien. 2012. 'Detection of Hydrogen Peroxide by DAB Staining in Arabidopsis Leaves', *Bio Protoc*, 2.
- de Luxan-Hernandez, C., J. Lohmann, W. Hellmeyer, S. Seanpong, K. Woltje, Z. Magyar, A. Pettko-Szandtner, T. Pelissier, G. De Jaeger, S. Hoth, O. Mathieu, and M. Weingartner. 2020. 'PP7L is essential for MAIL1-mediated transposable element silencing and primary root growth', *Plant J*, 102: 703-17.
- Delker, C., L. Sonntag, G. V. James, P. Janitza, C. Ibanez, H. Ziermann, T. Peterson, K. Denk, S. Mull, J. Ziegler, S. J. Davis, K. Schneeberger, and M. Quint. 2014. 'The DET1-COP1-HY5 pathway constitutes a multipurpose signaling module regulating plant photomorphogenesis and thermomorphogenesis', *Cell Rep*, 9: 1983-9.
- Dello Ioio, Raffaele, Francisco Scaglia Linhares, Emanuele Scacchi, Eva Casamitjana-Martinez, Renze Heidstra, Paolo Costantino, and Sabrina Sabatini. 2007. 'Cytokinins Determine Arabidopsis Root-Meristem Size by Controlling Cell Differentiation', *Current Biology*, 17: 678-82.
- Di Mambro, Riccardo, and Raffaele Dello Ioio. 2020. 'Root stem cells: how to establish and maintain the eternal youth', *Rendiconti Lincei. Scienze Fisiche e Naturali*, 31: 223-30.
- Dohmann, E. M., M. P. Levesque, L. De Veylder, I. Reichardt, G. Jurgens, M. Schmid, and C. Schwechheimer. 2008. 'The Arabidopsis COP9 signalosome is essential for G2 phase progression and genomic stability', *Development*, 135: 2013-22.
- Dolan, Liam, Kees Janmaat, Viola Willemsen, Paul Linstead, Scott Poethig, Keith Roberts, and Ben Scheres. 1993. 'Cellular organisation of the Arabidopsis thaliana root', *Development*, 119: 71-84.

- Doskocilova, A., L. Kohoutova, J. Volc, H. Kourova, O. Benada, J. Chumova, O. Plihal, B. Petrovska, P. Halada, L. Bogre, and P. Binarova. 2013. 'NITRILASE1 regulates the exit from proliferation, genome stability and plant development', *New Phytol*, 198: 685-98.
- Du, J., Y. P. Huang, J. Xi, M. J. Cao, W. S. Ni, X. Chen, J. K. Zhu, D. J. Oliver, and C. B. Xiang. 2008. 'Functional gene-mining for salt-tolerance genes with the power of Arabidopsis', *Plant J*, 56: 653-64.
- Duan, Hongying, Xiaosheng Ding, Zhiqing Wei, Chune Zhou, and Yanqing Zhou. 2011. 'The influences of Hygromycin B on growth of Arabidopsis thaliana cotyledon and leaf', *African Journal of Biotechnology*, 10: 17742-47.
- Duc, Céline, Matthias Benoit, Samuel Le Goff, Lauriane Simon, Axel Poulet, Sylviane Cotterell, Christophe Tatout, and Aline V. Probst. 2015. 'The histone chaperone complex HIR maintains nucleosome occupancy and counterbalances impaired histone deposition in CAF-1 complex mutants', *The Plant Journal*, 81: 707-22.
- Duprat, Anne, Carole Caranta, Frédéric Revers, Benoît Menand, Karen S. Browning, and Christophe Robaglia. 2002. 'The Arabidopsis eukaryotic initiation factor (iso)4E is dispensable for plant growth but required for susceptibility to potyviruses', *The Plant Journal*, 32: 927-34.
- Durek, P., R. Schmidt, J. L. Heazlewood, A. Jones, D. MacLean, A. Nagel, B. Kersten, and W. X. Schulze. 2010. 'PhosPhAt: the Arabidopsis thaliana phosphorylation site database. An update', *Nucleic Acids Res*, 38: D828-34.
- Earley, K. W., J. R. Haag, O. Pontes, K. Opper, T. Juehne, K. Song, and C. S. Pikaard. 2006. 'Gateway-compatible vectors for plant functional genomics and proteomics', *Plant J*, 45: 616-29.
- Echevarria-Zomeno, S., L. Fernandez-Calvino, A. B. Castro-Sanz, J. A. Lopez, J. Vazquez, and M. M. Castellano. 2016. 'Dissecting the proteome dynamics of the early heat stress response leading to plant survival or death in Arabidopsis', *Plant Cell Environ*, 39: 1264-78.
- Ellis, R. J., and I. R. Macdonald. 1970. 'Specificity of cycloheximide in higher plant systems', *Plant Physiol*, 46: 227-32.
- Emenecker, Ryan J., Alex S. Holehouse, and Lucia C. Strader. 2020. 'Emerging Roles for Phase Separation in Plants', *Developmental Cell*, 55: 69-83.
- Erdős, Gábor, Mátyás Pajkos, and Zsuzsanna Dosztányi. 2021. 'IUPred3: prediction of protein disorder enhanced with unambiguous experimental annotation and visualization of evolutionary conservation', *Nucleic Acids Research*, 49: W297-W303.
- Esposito, A. M., and T. G. Kinzy. 2010. 'The Eukaryotic Translation Elongation Factor 1B gamma Has a Non-guanine Nucleotide Exchange Factor Role in Protein Metabolism', *Journal of Biological Chemistry*, 285: 37995-8004.
- Exner, V., P. Taranto, N. Schönrock, W. Gruissem, and L. Hennig. 2006. 'Chromatin assembly factor CAF-1 is required for cellular differentiation during plant development', *Development*, 133: 4163-72.
- Farkas, I., V. Dombradi, M. Miskei, L. Szabados, and C. Koncz. 2007. 'Arabidopsis PPP family of serine/threonine phosphatases', *Trends Plant Sci*, 12: 169-76.
- Fernández-Bautista, Nuria, Lourdes Fernández-Calvino, Alfonso Muñoz, René Toribio, Hans P. Mock, and M. Mar Castellano. 2018. 'HOP family plays a major role in long-term acquired thermotolerance in Arabidopsis', *Plant, Cell & Environment*, 41: 1852-69.
- Fomicheva, A., and E. D. Ross. 2021. 'From Prions to Stress Granules: Defining the Compositional Features of Prion-Like Domains That Promote Different Types of Assemblies', *Int J Mol Sci*, 22.
- Forzani, Celine, Ernst Aichinger, Emily Sornay, Viola Willemsen, Thomas Laux, Walter Dewitte, and James A H. Murray. 2014. 'WOX5 Suppresses *CYCLIN D*

- Activity to Establish Quiescence at the Center of the Root Stem Cell Niche', *Current Biology*, 24: 1939-44.
- Franklin, K. A., S. H. Lee, D. Patel, S. V. Kumar, A. K. Spartz, C. Gu, S. Ye, P. Yu, G. Breen, J. D. Cohen, P. A. Wigge, and W. M. Gray. 2011. 'Phytochrome-interacting factor 4 (PIF4) regulates auxin biosynthesis at high temperature', *Proc Natl Acad Sci U S A*, 108: 20231-5.
- Friesner, J. D., B. Liu, K. Culligan, and A. B. Britt. 2005. 'Ionizing radiation-dependent gamma-H2AX focus formation requires ataxia telangiectasia mutated and ataxia telangiectasia mutated and Rad3-related', *Mol Biol Cell*, 16: 2566-76.
- Fulcher, N., and R. Sablowski. 2009. 'Hypersensitivity to DNA damage in plant stem cell niches', *Proc Natl Acad Sci U S A*, 106: 20984-8.
- Furukawa, T., M. J. Curtis, C. M. Tominey, Y. H. Duong, B. W. L. Wilcox, D. Aggoune, J. B. Hays, and A. B. Britt. 2010. 'A shared DNA-damage-response pathway for induction of stem-cell death by UVB and by gamma irradiation', *DNA Repair*, 9: 940-48.
- Galinha, Carla, Hugo Hofhuis, Marijn Luijten, Viola Willemsen, Ikram Blilou, Renze Heidstra, and Ben Scheres. 2007. 'PLETHORA proteins as dose-dependent master regulators of Arabidopsis root development', *Nature*, 449: 1053-57.
- Gallie, D. R., H. Le, C. Caldwell, R. L. Tanguay, N. X. Hoang, and K. S. Browning. 1997. 'The phosphorylation state of translation initiation factors is regulated developmentally and following heat shock in wheat', *J Biol Chem*, 272: 1046-53.
- Genoud, T., M. T. Santa Cruz, T. Kulisic, F. Sparla, C. Fankhauser, and J. P. Mettraux. 2008. 'The protein phosphatase 7 regulates phytochrome signaling in Arabidopsis', *PLoS One*, 3: e2699.
- Gerashchenko, Maxim V., Alexei V. Lobanov, and Vadim N. Gladyshev. 2012. 'Genome-wide ribosome profiling reveals complex translational regulation in response to oxidative stress', *Proceedings of the National Academy of Sciences*, 109: 17394-99.
- Gietz, R. D., B. Triggs-Raine, A. Robbins, K. C. Graham, and R. A. Woods. 1997. 'Identification of proteins that interact with a protein of interest: applications of the yeast two-hybrid system', *Mol Cell Biochem*, 172: 67-79.
- Glauninger, H., C. J. Wong Hickernell, J. A. M. Bard, and D. A. Drummond. 2022. 'Stressful steps: Progress and challenges in understanding stress-induced mRNA condensation and accumulation in stress granules', *Mol Cell*, 82: 2544-56.
- Goldberg, J., H. B. Huang, Y. G. Kwon, P. Greengard, A. C. Nairn, and J. Kuriyan. 1995. 'Three-dimensional structure of the catalytic subunit of protein serine/threonine phosphatase-1', *Nature*, 376: 745-53.
- Gonzalez, A, A Jimenez, D Vazquez, JE Davies, and D Schindler. 1978. 'Studies on the mode of action of hygromycin B, an inhibitor of translocation in eukaryotes', *Biochimica et Biophysica Acta (BBA)-Nucleic Acids and Protein Synthesis*, 521: 459-69.
- Gray, W. M., A. Ostin, G. Sandberg, C. P. Romano, and M. Estelle. 1998. 'High temperature promotes auxin-mediated hypocotyl elongation in Arabidopsis', *Proc Natl Acad Sci U S A*, 95: 7197-202.
- Grousl, T., P. Ivanov, I. Malcova, P. Pompach, I. Frydlova, R. Slaba, L. Senohrabkova, L. Novakova, and J. Hasek. 2013. 'Heat Shock-Induced Accumulation of Translation Elongation and Termination Factors Precedes Assembly of Stress Granules in *S. cerevisiae*', *PLoS One*, 8.
- Gultekin, H., and K. H. Heermann. 1988. 'The use of polyvinylidenedifluoride membranes as a general blotting matrix', *Anal Biochem*, 172: 320-9.
- Guo, Yan, Liming Xiong, Manabu Ishitani, and Jian-Kang Zhu. 2002. 'An Arabidopsis mutation in translation elongation factor 2 causes superinduction of CBF/DREB1 transcription factor genes but blocks the induction of their

- downstream targets under low temperatures', *Proceedings of the National Academy of Sciences*, 99: 7786-91.
- Gusmaroli, G., P. Figueroa, G. Serino, and X. W. Deng. 2007. 'Role of the MPN subunits in COP9 signalosome assembly and activity, and their regulatory interaction with Arabidopsis Cullin3-based E3 ligases', *Plant Cell*, 19: 564-81.
- Gutierrez-Beltran, E., P. H. Elander, K. Dalman, G. W. Dayhoff, 2nd, P. N. Moschou, V. N. Uversky, J. L. Crespo, and P. V. Bozhkov. 2021. 'Tudor staphylococcal nuclease is a docking platform for stress granule components and is essential for SnRK1 activation in Arabidopsis', *EMBO J*, 40: e105043.
- Gutierrez-Beltran, Emilio, Panagiotis N. Moschou, Andrei P. Smertenko, and Peter V. Bozhkov. 2015. 'Tudor Staphylococcal Nuclease Links Formation of Stress Granules and Processing Bodies with mRNA Catabolism in Arabidopsis', *The Plant Cell*, 27: 926-43.
- Haecker, Achim, Rita Groß-Hardt, Bernd Geiges, Ananda Sarkar, Holger Breuninger, Marita Herrmann, and Thomas Laux. 2004. 'Expression dynamics of WOX genes mark cell fate decisions during early embryonic patterning in Arabidopsis thaliana', *Development*, 131: 657-68.
- Hanahan, D. 1983. 'Studies on transformation of Escherichia coli with plasmids', *J Mol Biol*, 166: 557-80.
- Hang, R., Y. Xu, X. Wang, H. Hu, N. Flynn, C. You, and X. Chen. 2023. 'Arabidopsis HOT3/eIF5B1 constrains rRNA RNAi by facilitating 18S rRNA maturation', *Proc Natl Acad Sci U S A*, 120: e2301081120.
- Hawkes, T. R. 2014. 'Mechanisms of resistance to paraquat in plants', *Pest Manag Sci*, 70: 1316-23.
- Hayes, S., J. Schachtschabel, M. Mishkind, T. Munnik, and S. A. Arisz. 2021. 'Hot topic: Thermosensing in plants', *Plant Cell Environ*, 44: 2018-33.
- He, H., J. Denecker, K. Van Der Kelen, P. Willems, R. Pottie, S. Y. Phua, M. A. Hannah, D. Vertommen, F. Van Breusegem, and A. Mhamdi. 2021. 'The Arabidopsis mediator complex subunit 8 regulates oxidative stress responses', *Plant Cell*, 33: 2032-57.
- Heino, Matias, Pekka Kinnunen, Weston Anderson, Deepak K. Ray, Michael J. Puma, Olli Varis, Stefan Siebert, and Matti Kumm. 2023. 'Increased probability of hot and dry weather extremes during the growing season threatens global crop yields', *Scientific Reports*, 13: 3583.
- Hellemans, J., G. Mortier, A. De Paepe, F. Speleman, and J. Vandesompele. 2007. 'qBase relative quantification framework and software for management and automated analysis of real-time quantitative PCR data', *Genome Biol*, 8: R19.
- Heyman, Jefri, Toon Cools, Balkan Canher, Sviatlana Shavialenka, Jan Traas, Ilse Vercauteren, Hilde Van den Daele, Geert Persiau, Geert De Jaeger, Keiko Sugimoto, and Lieven De Veylder. 2016. 'The heterodimeric transcription factor complex ERF115–PAT1 grants regeneration competence', *Nature Plants*, 2: 16165.
- Heyman, Jefri, Toon Cools, Filip Vandenbussche, Ken S. Heyndrickx, Jelle Van Leene, Ilse Vercauteren, Sandy Vanderauwera, Klaas Vandepoele, Geert De Jaeger, Dominique Van Der Straeten, and Lieven De Veylder. 2013. 'ERF115 Controls Root Quiescent Center Cell Division and Stem Cell Replenishment', *Science*, 342: 860 - 63.
- Hinton, Shantá D. 2019. 'The role of pseudophosphatases as signaling regulators', *Biochimica et Biophysica Acta (BBA) - Molecular Cell Research*, 1866: 167-74.
- Hofmann, Sarah, Valeria Cherkasova, Peter Bankhead, Bernd Bukau, and Georg Stoecklin. 2012. 'Translation suppression promotes stress granule formation and cell survival in response to cold shock', *Molecular Biology of the Cell*, 23: 3786-800.

- Hofmann, Sarah, Nancy Kedersha, Paul Anderson, and Pavel Ivanov. 2021. 'Molecular mechanisms of stress granule assembly and disassembly', *Biochimica et Biophysica Acta (BBA) - Molecular Cell Research*, 1868: 118876.
- Hong, S. W., and E. Vierling. 2001. 'Hsp101 is necessary for heat tolerance but dispensable for development and germination in the absence of stress', *Plant J*, 27: 25-35.
- Hooper, C. M., I. R. Castleden, S. K. Tanz, N. Aryamanesh, and A. H. Millar. 2017. 'SUBA4: the interactive data analysis centre for Arabidopsis subcellular protein locations', *Nucleic Acids Res*, 45: D1064-D74.
- Hossain, Z., L. Amyot, B. McGarvey, M. Gruber, J. Jung, and A. Hannoufa. 2012. 'The translation elongation factor eEF-1Bbeta1 is involved in cell wall biosynthesis and plant development in Arabidopsis thaliana', *PLoS One*, 7: e30425.
- Hu, Shuyao, Yufeng Zhang, Qianqian Yi, Cuiwei Yang, Yanfen Liu, and Yun Bai. 2023. 'Time-resolved proteomic profiling reveals compositional and functional transitions across the stress granule life cycle', *Nature Communications*, 14: 7782.
- Huang, Honglin, Farhan Ullah, Dao-Xiu Zhou, Ming Yi, and Yu Zhao. 2019. 'Mechanisms of ROS Regulation of Plant Development and Stress Responses', *Frontiers in Plant Science*, 10.
- Hwang, JeeNa, Seonhee Lee, Joung-Ho Lee, Won-Hee Kang, Jin-Ho Kang, Min-Young Kang, Chang-Sik Oh, and Byoung-Cheorl Kang. 2015. 'Plant Translation Elongation Factor 1Bβ Facilitates Potato Virus X (PVX) Infection and Interacts with PVX Triple Gene Block Protein 1', *PLoS One*, 10: e0128014.
- Ide, Y., R. Tomioka, Y. Ouchi, T. Kamiya, and M. Maeshima. 2007. 'Transcriptional Induction of Two Genes for CCaPs, Novel Cytosolic Proteins, in Arabidopsis thaliana in the Dark', *Plant Cell Physiol*, 48: 54-65.
- Ikeda, Y., T. Pelissier, P. Bourguet, C. Becker, M. N. Pouch-Pelissier, R. Pogorelnik, M. Weingartner, D. Weigel, J. M. Deragon, and O. Mathieu. 2017. 'Arabidopsis proteins with a transposon-related domain act in gene silencing', *Nature Communications*, 8: 15122.
- Iwasaki, S., and N. T. Ingolia. 2017. 'The Growing Toolbox for Protein Synthesis Studies', *Trends Biochem Sci*, 42: 612-24.
- Jagadish, S.V. Krishna, Danielle A. Way, and Thomas D. Sharkey. 2021. 'Plant heat stress: Concepts directing future research', *Plant, Cell & Environment*, 44: 1992-2005.
- Jain, S., J. R. Wheeler, R. W. Walters, A. Agrawal, A. Barsic, and R. Parker. 2016. 'ATPase-Modulated Stress Granules Contain a Diverse Proteome and Substructure', *Cell*, 164: 487-98.
- James, P., J. Halladay, and E. A. Craig. 1996. 'Genomic libraries and a host strain designed for highly efficient two-hybrid selection in yeast', *Genetics*, 144: 1425-36.
- Jang, G. J., J. C. Jang, and S. H. Wu. 2020. 'Dynamics and Functions of Stress Granules and Processing Bodies in Plants', *Plants (Basel)*, 9.
- Janzen, D. M., and A. P. Geballe. 2004. 'The effect of eukaryotic release factor depletion on translation termination in human cell lines', *Nucleic Acids Res*, 32: 4491-502.
- Jarry, Lucas, Julie Descombin, Melody Nicolau, Ange Dussutour, Nathalie Picault, and Guillaume Moissiard. 2023. 'Plant mobile domain proteins ensure Microrhizobia 1 expression to fulfill transposon silencing', *Life Science Alliance*, 6: e202201539.
- Jeppesen, M. G., P. Ortiz, W. Shepard, T. G. Kinzy, J. Nyborg, and G. R. Andersen. 2003. 'The crystal structure of the glutathione S-transferase-like domain of elongation factor 1B gamma from Saccharomyces cerevisiae', *Journal of Biological Chemistry*, 278: 47190-98.
- Jiang, Keni, and Lewis J. Feldman. 2005. 'REGULATION OF ROOT APICAL MERISTEM DEVELOPMENT', *Annual Review of Cell and Developmental Biology*, 21: 485-509.

- Jones, K. H., and J. A. Senft. 1985. 'An improved method to determine cell viability by simultaneous staining with fluorescein diacetate-propidium iodide', *J Histochem Cytochem*, 33: 77-9.
- Jung, J. H., M. Domijan, C. Klose, S. Biswas, D. Ezer, M. Gao, A. K. Khattak, M. S. Box, V. Charoensawan, S. Cortijo, M. Kumar, A. Grant, J. C. Locke, E. Schäfer, K. E. Jaeger, and P. A. Wigge. 2016. 'Phytochromes function as thermosensors in Arabidopsis', *Science*, 354: 886-89.
- Jurgens, G., R. A. Torres Ruiz, T. Laux, U. Mayer, and T. Berleth. 1994. 'Early events in apical-basal pattern formation in Arabidopsis', *NATO ASI series. Series H, Cell biology*, 81: 95-103.
- Kapustian, LM, M Dadlez, and BS Negrutskii. 2017. 'Protein partners of the eEF1B $\beta$  subunit of the translation elongation complex eEF1B in the nuclear fraction of human lung carcinoma cells', *Biopolymers and Cell*.
- Kapustian, LM, IL Lysetsky, TV Bondarchuk, OV Novosylina, and BS Negrutskii. 2019. 'Analysis of eEF1B $\gamma$  interactome in the nuclear fraction of A549 human lung adenocarcinoma cells', *Biopolymers and Cell*, 35: 268-87.
- Kaurilind, E., E. Xu, and M. Brosche. 2015. 'A genetic framework for H<sub>2</sub>O<sub>2</sub> induced cell death in Arabidopsis thaliana', *BMC Genomics*, 16: 837.
- Kearly, A., A. D. L. Nelson, A. Skirycz, and M. Chodasiewicz. 2022. 'Composition and function of stress granules and P-bodies in plants', *Semin Cell Dev Biol*.
- Kedersha, N., M. R. Cho, W. Li, P. W. Yacono, S. Chen, N. Gilks, D. E. Golan, and P. Anderson. 2000. 'Dynamic shuttling of TIA-1 accompanies the recruitment of mRNA to mammalian stress granules', *J Cell Biol*, 151: 1257-68.
- Kedersha, N. L., M. Gupta, W. Li, I. Miller, and P. Anderson. 1999. 'RNA-binding proteins TIA-1 and TIAR link the phosphorylation of eIF-2 alpha to the assembly of mammalian stress granules', *J Cell Biol*, 147: 1431-42.
- Kedersha, Nancy, Marc D. Panas, Christopher A. Achorn, Shawn Lyons, Sarah Tisdale, Tyler Hickman, Marshall Thomas, Judy Lieberman, Gerald M. McInerney, Pavel Ivanov, and Paul Anderson. 2016. 'G3BP–Caprin1–USP10 complexes mediate stress granule condensation and associate with 40S subunits', *Journal of Cell Biology*, 212.
- Kedersha, Nancy, Georg Stoecklin, Maranatha Ayodele, Patrick Yacono, Jens Lykke-Andersen, Marvin J. Fritzler, Donalyn Scheuner, Randal J. Kaufman, David E. Golan, and Paul Anderson 2005. 'Stress granules and processing bodies are dynamically linked sites of mRNP remodeling', *Journal of Cell Biology*, 169: 871-84.
- Kim, Byung-Hoon, Xue Cai, Justin N. Vaughn, and Albrecht G. von Arnim. 2007. 'On the functions of the h subunit of eukaryotic initiation factor 3 in late stages of translation initiation', *Genome Biology*, 8: R60.
- Kim, J., H. Lee, H. G. Lee, and P. J. Seo. 2021. 'Get closer and make hotspots: liquid-liquid phase separation in plants', *EMBO Rep*, 22: e51656.
- Kim, Minsoo, Fionn McLoughlin, Eman Basha, and Elizabeth Vierling. 2017. 'Assessing Plant Tolerance to Acute Heat Stress', *Bio-protocol*, 7: e2405.
- Kim, S., J. Kellner, C. H. Lee, and P. A. Coulombe. 2007. 'Interaction between the keratin cytoskeleton and eEF1B $\gamma$  affects protein synthesis in epithelial cells', *Nat Struct Mol Biol*, 14: 982-3.
- Kim, S., P. Wong, and P. A. Coulombe. 2006. 'A keratin cytoskeletal protein regulates protein synthesis and epithelial cell growth', *Nature*, 441: 362-5.
- Kim, T. H., B. H. Kim, A. Yahalom, D. A. Chamovitz, and A. G. von Arnim. 2004. 'Translational regulation via 5' mRNA leader sequences revealed by mutational analysis of the Arabidopsis translation initiation factor subunit eIF3h', *Plant Cell*, 16: 3341-56.

- Kimball, Scot R., Rick L. Horetsky, David Ron, Leonard S. Jefferson, and Heather P. Harding. 2003. 'Mammalian stress granules represent sites of accumulation of stalled translation initiation complexes', *American Journal of Physiology-Cell Physiology*, 284: C273-C84.
- Kinzy, T. G., T. L. Ripmaster, and J. L. Woolford. 1994. 'Multiple Genes Encode the Translation Elongation-Factor Ef-1-Gamma in *Saccharomyces-Cerevisiae*', *Nucleic Acids Research*, 22: 2703-07.
- Kinzy, T. G., and J. L. Woolford, Jr. 1995. 'Increased expression of *Saccharomyces cerevisiae* translation elongation factor 1 alpha bypasses the lethality of a TEF5 null allele encoding elongation factor 1 beta', *Genetics*, 141: 481-9.
- Klepikova, A. V., A. S. Kasianov, E. S. Gerasimov, M. D. Logacheva, and A. A. Penin. 2016. 'A high resolution map of the *Arabidopsis thaliana* developmental transcriptome based on RNA-seq profiling', *Plant J*, 88: 1058-70.
- Kobayashi, S., S. Kidou, and S. Ejiri. 2001. 'Detection and characterization of glutathione S-transferase activity in rice EF-1betabeta'gamma and EF-1gamma expressed in *Escherichia coli*', *Biochem Biophys Res Commun*, 288: 509-14.
- Koncz, Csaba, and Jeff Schell. 1986. 'The promoter of TL-DNA gene 5 controls the tissue-specific expression of chimaeric genes carried by a novel type of *Agrobacterium* binary vector', *Molecular and General Genetics MGG*, 204: 383-96.
- Kong, X., H. Tian, Q. Yu, F. Zhang, R. Wang, S. Gao, W. Xu, J. Liu, E. Shani, C. Fu, G. Zhou, L. Zhang, X. Zhang, and Z. Ding. 2018. 'PHB3 Maintains Root Stem Cell Niche Identity through ROS-Responsive AP2/ERF Transcription Factors in *Arabidopsis*', *Cell Rep*, 22: 1350-63.
- Kosmacz, M., M. Gorka, S. Schmidt, M. Luzarowski, J. C. Moreno, J. Szlachetko, E. Leniak, E. M. Sokolowska, K. Sofroni, A. Schnittger, and A. Skiryecz. 2019. 'Protein and metabolite composition of *Arabidopsis* stress granules', *New Phytol*, 222: 1420-33.
- Kumar, M., M. M. Gromiha, and G. P. Raghava. 2011. 'SVM based prediction of RNA-binding proteins using binding residues and evolutionary information', *J Mol Recognit*, 24: 303-13.
- Kurepa, J., C. Karangwa, L. S. Duke, and J. A. Smalle. 2010. 'Arabidopsis sensitivity to protein synthesis inhibitors depends on 26S proteasome activity', *Plant Cell Rep*, 29: 249-59.
- Laemmli, U. K. 1970. 'Cleavage of structural proteins during the assembly of the head of bacteriophage T4', *Nature*, 227: 680-5.
- Lancaster, A. K., A. Nutter-Upham, S. Lindquist, and O. D. King. 2014. 'PLAAC: a web and command-line application to identify proteins with prion-like amino acid composition', *Bioinformatics*, 30: 2501-2.
- Lanzani, G. A., E. Caldiroli, L. A. Manzocchi, R. Bollini, and LDe Albertie. 1976. 'The translational system from wheat embryos: some properties of the polypeptides associated in EF1H', *FEBS Lett*, 64: 102-6.
- Larkin, John C., Matt L. Brown, and John Schiefelbein. 2003. 'How Do Cells Know What They Want to Be When They Grow Up? Lessons from Epidermal Patterning in *Arabidopsis*', *Annual Review of Plant Biology*, 54: 403-30.
- Larkindale, J., J. D. Hall, M. R. Knight, and E. Vierling. 2005. 'Heat stress phenotypes of *Arabidopsis* mutants implicate multiple signaling pathways in the acquisition of thermotolerance', *Plant Physiol*, 138: 882-97.
- Larkindale, J., and E. Vierling. 2008. 'Core genome responses involved in acclimation to high temperature', *Plant Physiol*, 146: 748-61.
- Le Sourd, F., S. Boulben, R. Le Bouffant, P. Cormier, J. Morales, R. Belle, and O. Mulner-Lorillon. 2006. 'eEF1B: At the dawn of the 21st century', *Biochim Biophys Acta*, 1759: 13-31.

- Lee, J., H. H. Nguyen, Y. Park, J. X. Lin, and I. Hwang. 2022. 'Spatial regulation of RBOHD via AtECA4-mediated recycling and clathrin-mediated endocytosis contributes to ROS accumulation during salt stress response but not flg22-induced immune response', *Plant Journal*, 109: 816-30.
- Lee, Yew, Woo Sung Lee, and Soo-Hwan Kim. 2012. 'Hormonal regulation of stem cell maintenance in roots', *Journal of Experimental Botany*, 64: 1153-65.
- Lellis, Andrew D, M Leah Allen, Alice W Aertker, Jonathan K Tran, David M Hillis, Courtney R Harbin, Christian Caldwell, Daniel R Gallie, and Karen S Browning. 2010. 'Deletion of the eIFiso4G subunit of the Arabidopsis eIFiso4F translation initiation complex impairs health and viability', *Plant molecular biology*, 74: 249-63.
- Leng, L., Q. Liang, J. Jiang, C. Zhang, Y. Hao, X. Wang, and W. Su. 2017. 'A subclass of HSP70s regulate development and abiotic stress responses in Arabidopsis thaliana', *J Plant Res*, 130: 349-63.
- Li, G. L., B. Li, H. T. Liu, and R. G. Zhou. 2005. '[The responses of AtJ2 and AtJ3 gene expression to environmental stresses in Arabidopsis]', *Zhi Wu Sheng Li Yu Fen Zi Sheng Wu Xue Xue Bao*, 31: 47-52.
- Li, X., C. Cai, Z. Wang, B. Fan, C. Zhu, and Z. Chen. 2018. 'Plastid Translation Elongation Factor Tu Is Prone to Heat-Induced Aggregation Despite Its Critical Role in Plant Heat Tolerance', *Plant Physiol*, 176: 3027-45.
- Lin, Yuan, David SW Protter, Michael K Rosen, and Roy Parker. 2015. 'Formation and maturation of phase-separated liquid droplets by RNA-binding proteins', *Molecular Cell*, 60: 208-19.
- Liu, B. T., Y. Han, and S. B. Qian. 2013. 'Cotranslational Response to Proteotoxic Stress by Elongation Pausing of Ribosomes', *Molecular Cell*, 49: 453-63.
- Liu, H. C., H. T. Liao, and Y. Y. Charng. 2011. 'The role of class A1 heat shock factors (HSFA1s) in response to heat and other stresses in Arabidopsis', *Plant Cell Environ*, 34: 738-51.
- LIU, HONG-TAO, GUO-LIANG LI, HUI CHANG, DA-YE SUN, REN-GANG ZHOU, and BING LI. 2007. 'Calmodulin-binding protein phosphatase PP7 is involved in thermotolerance in Arabidopsis', *Plant, Cell & Environment*, 30: 156-64.
- Liu, Taibo, Qianyu Liu, Zhen Yu, Chunling Wang, Huafu Mai, Guolan Liu, Ruijing Li, Gang Pang, Dingwu Chen, Huili Liu, Jiangyi Yang, and Li-Zhen Tao. 2022. 'eIF4E1 Regulates Arabidopsis Embryo Development and Root Growth by Interacting With RopGEF7', *Frontiers in Plant Science*, 13.
- Liu, Y., N. Ye, R. Liu, M. Chen, and J. Zhang. 2010. 'H<sub>2</sub>O<sub>2</sub> mediates the regulation of ABA catabolism and GA biosynthesis in Arabidopsis seed dormancy and germination', *J Exp Bot*, 61: 2979-90.
- Liu, Yan-Jing, Xue-Min Han, Lin-Ling Ren, Hai-Ling Yang, and Qing-Yin Zeng. 2012. 'Functional Divergence of the Glutathione S-Transferase Supergene Family in Physcomitrella patens Reveals Complex Patterns of Large Gene Family Evolution in Land Plants', *Plant Physiology*, 161: 773-86.
- Llamas, Ernesto, Seda Koyuncu, Hyun Ju Lee, Markus Wehrmann, Ricardo Gutierrez-Garcia, Nick Dunken, Nyasha Charura, Salvador Torres-Montilla, Elena Schlimgen, Amrei M. Mandel, Erik Boelen Theile, Jan Grossbach, Prerana Wagle, Jan-Wilm Lackmann, Bernhard Schermer, Thomas Benzing, Andreas Beyer, Pablo Pulido, Manuel Rodriguez-Concepcion, Alga Zuccaro, and David Vilchez. 2023. 'In planta expression of human polyQ-expanded huntingtin fragment reveals mechanisms to prevent disease-related protein aggregation', *Nature Aging*, 3: 1345-57.
- Londoño Vélez, Violeta, Fatema Alquraish, Ibrahim Tarbiyyah, Fareena Rafique, Duruo Mao, and Monika Chodasiewicz. 2022. 'Landscape of biomolecular condensates in heat stress responses', *Frontiers in Plant Science*, 13.

- Lu, Linrong, An-Ping Han, and Jane-Jane Chen. 2001. 'Translation Initiation Control by Heme-Regulated Eukaryotic Initiation Factor 2 $\alpha$  Kinase in Erythroid Cells under Cytoplasmic Stresses', *MOLECULAR AND CELLULAR BIOLOGY*, 21: 7971-80.
- Ma, Jing, Yuhao Liu, Wangbin Zhou, Yan Zhu, Aiwu Dong, and Wen-Hui Shen. 2018. 'Histone chaperones play crucial roles in maintenance of stem cell niche during plant root development', *The Plant Journal*, 95: 86-100.
- Mähönen, Ari Pekka, Kirsten ten Tusscher, Riccardo Siligato, Ondřej Smetana, Sara Díaz-Triviño, Jarkko Salojärvi, Guy Wachsman, Kalika Prasad, Renze Heidstra, and Ben Scheres. 2014. 'PLETHORA gradient formation mechanism separates auxin responses', *Nature*, 515: 125-29.
- Makeeva, Desislava S., Claire L. Riggs, Anton V. Burakov, Pavel A. Ivanov, Artem S. Kushchenko, Dmitri A. Bykov, Vladimir I. Popenko, Vladimir S. Prassolov, Pavel V. Ivanov, and Sergey E. Dmitriev. 2023. 'Relocalization of Translation Termination and Ribosome Recycling Factors to Stress Granules Coincides with Elevated Stop-Codon Readthrough and Reinitiation Rates upon Oxidative Stress', *Cells*, 12: 259.
- Maldonado-Bonilla, L. D. 2014. 'Composition and function of P bodies in *Arabidopsis thaliana*', *Front Plant Sci*, 5: 201.
- Mansilla, F., I. Friis, M. Jadidi, K. M. Nielsen, B. F. Clark, and C. R. Knudsen. 2002. 'Mapping the human translation elongation factor eEF1H complex using the yeast two-hybrid system', *Biochem J*, 365: 669-76.
- Martinez-Seidel, Federico, Olga Beine-Golovchuk, Yin-Chen Hsieh, and Joachim Kopka. 2020. 'Systematic Review of Plant Ribosome Heterogeneity and Specialization', *Frontiers in Plant Science*, 11.
- Maruri-Lopez, I., N. E. Figueroa, I. E. Hernandez-Sanchez, and M. Chodasiewicz. 2021. 'Plant Stress Granules: Trends and Beyond', *Front Plant Sci*, 12: 722643.
- Mateju, D., and J. A. Chao. 2022. 'Stress granules: regulators or by-products?', *Febs Journal*, 289: 363-73.
- Mateju, D., B. Eichenberger, F. Voigt, J. Eglinger, G. Roth, and J. A. Chao. 2020. 'Single-Molecule Imaging Reveals Translation of mRNAs Localized to Stress Granules', *Cell*, 183: 1801-12.e13.
- Matsuura, H., Y. Ishibashi, A. Shinmyo, S. Kanaya, and K. Kato. 2010. 'Genome-wide analyses of early translational responses to elevated temperature and high salinity in *Arabidopsis thaliana*', *Plant Cell Physiol*, 51: 448-62.
- Mazzoni-Putman, Serina M., and Anna N. Stepanova. 2018. 'A Plant Biologist's Toolbox to Study Translation', *Frontiers in Plant Science*, 9.
- McLoughlin, F., E. Basha, M. E. Fowler, M. Kim, J. Bordowitz, S. Katiyar-Agarwal, and E. Vierling. 2016. 'Class I and II Small Heat Shock Proteins Together with HSP101 Protect Protein Translation Factors during Heat Stress', *Plant Physiol*, 172: 1221-36.
- McLoughlin, F., M. Kim, R. S. Marshall, R. D. Vierstra, and E. Vierling. 2019. 'HSP101 Interacts with the Proteasome and Promotes the Clearance of Ubiquitylated Protein Aggregates', *Plant Physiol*, 180: 1829-47.
- McMahon, D. 1975. 'Cycloheximide is not a specific inhibitor of protein synthesis in vivo', *Plant Physiol*, 55: 815-21.
- Merlet, J., J. Burger, J. E. Gomes, and L. Pintard. 2009. 'Regulation of cullin-RING E3 ubiquitin-ligases by neddylation and dimerization', *Cell Mol Life Sci*, 66: 1924-38.
- Merret, R., M. C. Carpentier, J. J. Favory, C. Picart, J. Descombin, C. Bousquet-Antonelli, P. Tillard, L. Lejay, J. M. Deragon, and Y. Y. Charng. 2017. 'Heat Shock Protein HSP101 Affects the Release of Ribosomal Protein mRNAs for Recovery after Heat Shock', *Plant Physiol*, 174: 1216-25.
- Merret, R., V. K. Nagarajan, M. C. Carpentier, S. Park, J. J. Favory, J. Descombin, C. Picart, Y. Y. Charng, P. J. Green, J. M. Deragon, and C. Bousquet-Antonelli. 2015. 'Heat-

- induced ribosome pausing triggers mRNA co-translational decay in *Arabidopsis thaliana*', *Nucleic Acids Research*, 43: 4121-32.
- Merret, Rémy, Julie Descombin, Yu-ting Juan, Jean-Jacques Favory, Marie-Christine Carpentier, Cristian Chaparro, Yee-yung Charng, Jean-Marc Deragon, and Cécile Bousquet-Antonelli. 2013. 'XRN4 and LARP1 Are Required for a Heat-Triggered mRNA Decay Pathway Involved in Plant Acclimation and Survival during Thermal Stress', *Cell Reports*, 5: 1279-93.
- Millar, Sean R., Jie Qi Huang, Karl J. Schreiber, Yi-Cheng Tsai, Jiyun Won, Jianping Zhang, Alan M. Moses, and Ji-Young Youn. 2023. 'A New Phase of Networking: The Molecular Composition and Regulatory Dynamics of Mammalian Stress Granules', *Chemical Reviews*, 123: 9036-64.
- Mittler, Ron. 2002. 'Oxidative stress, antioxidants and stress tolerance', *trends in plant science*, 7: 405-10.
- Miyazaki, Masazumi, Masahiro Uritani, Katsuya Fujimura, Hirohisa Yamakatsu, Takashi Kageyama, and Kenji Takahashi. 1988. 'Peptide Elongation Factor 1 from Yeasts: Purification and Biochemical Characterization of Peptide Elongation Factors  $\alpha$  and  $1\beta(\alpha)$  from *Saccharomyces carlsbergensis* and *Schizosaccharomyces pombe*1', *The Journal of Biochemistry*, 103: 508-21.
- Moazed, Danesh, and Harry F Noller. 1987. 'Interaction of antibiotics with functional sites in 16S ribosomal RNA', *Nature*, 327: 389-94.
- Moissiard, G., S. J. Cokus, J. Cary, S. Feng, A. C. Billi, H. Stroud, D. Husmann, Y. Zhan, B. R. Lajoie, R. P. McCord, C. J. Hale, W. Feng, S. D. Michaels, A. R. Frand, M. Pellegrini, J. Dekker, J. K. Kim, and S. E. Jacobsen. 2012. 'MORC family ATPases required for heterochromatin condensation and gene silencing', *Science*, 336: 1448-51.
- Mokas, S., J. R. Mills, C. Garreau, M. J. Fournier, F. Robert, P. Arya, R. J. Kaufman, J. Pelletier, and R. Mazroui. 2009. 'Uncoupling stress granule assembly and translation initiation inhibition', *Mol Biol Cell*, 20: 2673-83.
- Moon, Stephanie L., Tatsuya Morisaki, Anthony Khong, Kenneth Lyon, Roy Parker, and Timothy J. Stasevich. 2019. 'Multicolour single-molecule tracking of mRNA interactions with RNP granules', *Nature Cell Biology*, 21: 162-68.
- Moore, M., N. Gossmann, and K. J. Dietz. 2016. 'Redox Regulation of Cytosolic Translation in Plants', *Trends Plant Sci*, 21: 388-97.
- Negrutskii, B. 2020. 'Non-translational Connections of eEF1B in the Cytoplasm and Nucleus of Cancer Cells', *Frontiers in Molecular Biosciences*, 7.
- Negrutskii, B. S., V. F. Shalak, O. V. Novosylina, L. V. Porubleva, D. M. Lozhko, and A. V. El'skaya. 2023. 'The eEF1 family of mammalian translation elongation factors', *BBA Adv*, 3: 100067.
- Negrutskii, B., D. Vlasenko, M. Mirande, P. Futernyk, and A. El'skaya. 2018. 'mRNA-Independent way to regulate translation elongation rate in eukaryotic cells', *Iubmb Life*, 70: 192-96.
- Nguyen, C. C., K. Nakaminami, A. Matsui, S. Kobayashi, Y. Kurihara, K. Toyooka, M. Tanaka, and M. Seki. 2016. 'Oligouridylylate Binding Protein 1b Plays an Integral Role in Plant Heat Stress Tolerance', *Front Plant Sci*, 7: 853.
- Nianiou-Obeidat, Irini, Panagiotis Madesis, Christos Kissoudis, Georgia Voulgari, Evangelia Chronopoulou, Athanasios Tsiftaris, and Nikolaos E. Labrou. 2017. 'Plant glutathione transferase-mediated stress tolerance: functions and biotechnological applications', *Plant Cell Reports*, 36: 791-805.
- Nicolau, M., N. Picault, J. Descombin, Y. Jami-Alahmadi, S. Feng, E. Bucher, S. E. Jacobsen, J. M. Deragon, J. Wohlschlegel, and G. Moissiard. 2020. 'The plant mobile domain proteins MAIN and MAIL1 interact with the phosphatase PP7L to regulate gene

- expression and silence transposable elements in *Arabidopsis thaliana*', *PLoS Genet*, 16: e1008324.
- Nicolau, Melody, Nathalie Picault, and Guillaume Moissiard. 2021. 'The Evolutionary Volte-Face of Transposable Elements: From Harmful Jumping Genes to Major Drivers of Genetic Innovation', *Cells*, 10: 2952.
- Niehaus, T. D., J. A. Patterson, D. C. Alexander, J. S. Folz, M. Pyc, B. S. MacTavish, S. D. Bruner, R. T. Mullen, O. Fiehn, and A. D. Hanson. 2019. 'The metabolite repair enzyme Nit1 is a dual-targeted amidase that disposes of damaged glutathione in *Arabidopsis*', *Biochem J*, 476: 683-97.
- Nisa, Maher-Un, Ying Huang, Moussa Benhamed, and Cécile Raynaud. 2019. 'The Plant DNA Damage Response: Signaling Pathways Leading to Growth Inhibition and Putative Role in Response to Stress Conditions', *Frontiers in Plant Science*, 10.
- Niu, Xin, Lei Zhang, Yuchen Wu, Zhi Zong, Bin Wang, Jisheng Liu, Long Zhang, and Fangfang Zhou. 2023. 'Biomolecular condensates: Formation mechanisms, biological functions, and therapeutic targets', *MedComm*, 4: e223.
- Noctor, Graham, and Christine H. Foyer. 1998. 'ASCORBATE AND GLUTATHIONE: Keeping Active Oxygen Under Control', *Annual Review of Plant Physiology and Plant Molecular Biology*, 49: 249-79.
- Nover, L., K. D. Scharf, and D. Neumann. 1989. 'Cytoplasmic heat shock granules are formed from precursor particles and are associated with a specific set of mRNAs', *Mol Cell Biol*, 9: 1298-308.
- Nukarinen, Ella, Thomas Nägele, Lorenzo Pedrotti, Bernhard Wurzinger, Andrea Mair, Ramona Landgraf, Frederik Börnke, Johannes Hanson, Markus Teige, Elena Baena-Gonzalez, Wolfgang Dröge-Laser, and Wolfram Weckwerth. 2016. 'Quantitative phosphoproteomics reveals the role of the AMPK plant ortholog SnRK1 as a metabolic master regulator under energy deprivation', *Scientific Reports*, 6: 31697.
- O'Keeffe, G., C. Jochl, K. Kavanagh, and S. Doyle. 2013. 'Extensive proteomic remodeling is induced by eukaryotic translation elongation factor 1Bgamma deletion in *Aspergillus fumigatus*', *Protein Sci*, 22: 1612-22.
- Olarewaju, O., P. A. Ortiz, W. Q. Chowdhury, I. Chatterjee, and T. G. Kinzy. 2004. 'The translation elongation factor eEF1B plays a role in the oxidative stress response pathway', *RNA Biol*, 1: 89-94.
- Ortiz-Bobea, Ariel, Haoying Wang, Carlos M. Carrillo, and Toby R. Ault. 2019. 'Unpacking the climatic drivers of US agricultural yields', *Environmental Research Letters*, 14.
- Pace, H. C., and C. Brenner. 2001. 'The nitrilase superfamily: classification, structure and function', *Genome Biol*, 2: REVIEWS0001.
- Perilli, Serena, Riccardo Di Mambro, and Sabrina Sabatini. 2012. 'Growth and development of the root apical meristem', *Current Opinion in Plant Biology*, 15: 17-23.
- Peskett, T. R., F. Rau, J. O'Driscoll, R. Patani, A. R. Lowe, and H. R. Saibil. 2018. 'A Liquid to Solid Phase Transition Underlying Pathological Huntingtin Exon1 Aggregation', *Mol Cell*, 70: 588-601.e6.
- Pi, Limin, Ernst Aichinger, Eric van der Graaff, Cristina I Llavata-Peris, Dolf Weijers, Lars Hennig, Edwin Groot, and Thomas Laux. 2015. 'Organizer-Derived WOX5 Signal Maintains Root Columella Stem Cells through Chromatin-Mediated Repression of CDF4 Expression', *Developmental Cell*, 33: 576-88.
- Piotrowski, M. 2008. 'Primary or secondary? Versatile nitrilases in plant metabolism', *Phytochemistry*, 69: 2655-67.
- Pisarev, Andrey V., Maxim A. Skabkin, Vera P. Pisareva, Olga V. Skabkina, Aurélie M. Rakotondrafara, Matthias W. Hentze, Christopher U. T. Hellen, and Tatyana V. Pestova. 2010. 'The Role of ABCE1 in Eukaryotic Posttermination Ribosomal Recycling', *Molecular Cell*, 37: 196-210.

- Plessis, Anne. 2023. 'Abiotic stress experiments need a reality check to improve translation to the field', *Journal of Experimental Botany*, 74: 1741-44.
- Protter, David S. W., Bhalchandra S. Rao, Briana Van Treeck, Yuan Lin, Laura Mizoue, Michael K. Rosen, and Roy Parker. 2018. 'Intrinsically Disordered Regions Can Contribute Promiscuous Interactions to RNP Granule Assembly', *Cell Reports*, 22: 1401-12.
- Qin, N., D. Xu, J. Li, and X. W. Deng. 2020. 'COP9 signalosome: Discovery, conservation, activity, and function', *J Integr Plant Biol*, 62: 90-103.
- Raabe, Karel, David Honys, and Christos Michailidis. 2019. 'The role of eukaryotic initiation factor 3 in plant translation regulation', *Plant Physiology and Biochemistry*, 145: 75-83.
- Ray-Gallet, Dominique, Jean-Pierre Quivy, Christine Scamps, Emmanuelle M. D. Martini, Marc Lipinski, and Geneviève Almouzni. 2002. 'HIRA Is Critical for a Nucleosome Assembly Pathway Independent of DNA Synthesis', *Molecular Cell*, 9: 1091-100.
- Rayman, J. B., and E. R. Kandel. 2017. 'TIA-1 Is a Functional Prion-Like Protein', *Cold Spring Harb Perspect Biol*, 9.
- Renou, Julien, Rodnay Sormani, Eric Gelhaye, Claude Didierjean, and Mélanie Morel-Rouhier. 2022. 'Genomic and functional insights into the diversification of the elongation factor eEF1B $\gamma$  in fungi', *Fungal Biology Reviews*, 42: 74-84.
- Riba, Andrea, Noemi Di Nanni, Nitish Mittal, Erik Arhné, Alexander Schmidt, and Mihaela Zavolan. 2019. 'Protein synthesis rates and ribosome occupancies reveal determinants of translation elongation rates', *Proceedings of the National Academy of Sciences*, 116: 15023-32.
- Rigal, A., S. M. Doyle, and S. Robert. 2015. 'Live cell imaging of FM4-64, a tool for tracing the endocytic pathways in Arabidopsis root cells', *Methods Mol Biol*, 1242: 93-103.
- Ryazanov, Alexey G., Elena A. Shestakova, and Pavel G. Natapov. 1988. 'Phosphorylation of elongation factor 2 by EF-2 kinase affects rate of translation', *Nature*, 334: 170-73.
- Sabatini, S., R. Heidstra, M. Wildwater, and B. Scheres. 2003. 'SCARECROW is involved in positioning the stem cell niche in the Arabidopsis root meristem', *Genes Dev*, 17: 354-8.
- Salome, P. A. 2017. 'Some Like It HOT: Protein Translation and Heat Stress in Plants', *Plant Cell*, 29: 2075.
- Sander, H., S. Wallace, R. Plouse, S. Tiwari, and A. V. Gomes. 2019. 'Ponceau S waste: Ponceau S staining for total protein normalization', *Anal Biochem*, 575: 44-53.
- Sangwan, V., B. L. Orvar, J. Beyerly, H. Hirt, and R. S. Dhindsa. 2002. 'Opposite changes in membrane fluidity mimic cold and heat stress activation of distinct plant MAP kinase pathways', *Plant J*, 31: 629-38.
- Sarkar, Ananda K., Marijn Lijten, Shunsuke Miyashima, Michael Lenhard, Takashi Hashimoto, Keiji Nakajima, Ben Scheres, Renze Heidstra, and Thomas Laux. 2007. 'Conserved factors regulate signalling in Arabidopsis thaliana shoot and root stem cell organizers', *Nature*, 446: 811-14.
- Sasikumar, A. N., W. B. Perez, and T. G. Kinzy. 2012. 'The many roles of the eukaryotic elongation factor 1 complex', *Wiley Interdiscip Rev RNA*, 3: 543-55.
- Scarpin, M. Regina, Samuel Leiboff, and Jacob O. Brunkard. 2020. 'Parallel global profiling of plant TOR dynamics reveals a conserved role for LARP1 in translation', *Elife*, 9: e58795.
- Scheres, Ben. 2007. 'Stem-cell niches: nursery rhymes across kingdoms', *Nature Reviews Molecular Cell Biology*, 8: 345-54.
- Schmidt, Enrico K., Giovanna Clavarino, Maurizio Ceppi, and Philippe Pierre. 2009. 'SUnSET, a nonradioactive method to monitor protein synthesis', *Nature Methods*, 6: 275-77.

- Schneider-Poetsch, T., J. Ju, D. E. Eyler, Y. Dang, S. Bhat, W. C. Merrick, R. Green, B. Shen, and J. O. Liu. 2010. 'Inhibition of eukaryotic translation elongation by cycloheximide and lactimidomycin', *Nat Chem Biol*, 6: 209-17.
- Schwechheimer, C., and E. Isono. 2010. 'The COP9 signalosome and its role in plant development', *Eur J Cell Biol*, 89: 157-62.
- Scutenaire, J., J. M. Deragon, V. Jean, M. Benhamed, C. Raynaud, J. J. Favory, R. Merret, and C. Bousquet-Antonelli. 2018. 'The YTH Domain Protein ECT2 Is an m(6)A Reader Required for Normal Trichome Branching in Arabidopsis', *Plant Cell*, 30: 986-1005.
- Sega, G. A. 1984. 'A review of the genetic effects of ethyl methanesulfonate', *Mutat Res*, 134: 113-42.
- Shah, P., Y. Ding, M. Niemczyk, G. Kudla, and J. B. Plotkin. 2013. 'Rate-limiting steps in yeast protein translation', *Cell*, 153: 1589-601.
- Shalgi, R., J. A. Hurt, I. Krykbaeva, M. Taipale, S. Lindquist, and C. B. Burge. 2013. 'Widespread regulation of translation by elongation pausing in heat shock', *Mol Cell*, 49: 439-52.
- Shannon, P., A. Markiel, O. Ozier, N. S. Baliga, J. T. Wang, D. Ramage, N. Amin, B. Schwikowski, and T. Ideker. 2003. 'Cytoscape: a software environment for integrated models of biomolecular interaction networks', *Genome Res*, 13: 2498-504.
- Sharma, R., A. Sahoo, R. Devendran, and M. Jain. 2014. 'Over-expression of a rice tau class glutathione s-transferase gene improves tolerance to salinity and oxidative stresses in Arabidopsis', *PLoS One*, 9: e92900.
- Shenton, D., J. B. Smirnova, J. N. Selley, K. Carroll, S. J. Hubbard, G. D. Pavitt, M. P. Ashe, and C. M. Grant. 2006. 'Global translational responses to oxidative stress impact upon multiple levels of protein synthesis', *J Biol Chem*, 281: 29011-21.
- Silva-Correia, J., S. Freitas, R. M. Tavares, T. Lino-Neto, and H. Azevedo. 2014. 'Phenotypic analysis of the Arabidopsis heat stress response during germination and early seedling development', *Plant Methods*, 10: 7.
- Silva, Jerson L., Debora Foguel, Vitor F. Ferreira, Tuane C. R. G. Vieira, Mayra A. Marques, Giulia D. S. Ferretti, Tiago F. Outeiro, Yraima Cordeiro, and Guilherme A. P. de Oliveira. 2023. 'Targeting Biomolecular Condensation and Protein Aggregation against Cancer', *Chemical Reviews*, 123: 9094-138.
- Silverblatt-Buser, E. W., M. A. Frick, C. Rabeler, and N. J. Kaplinsky. 2018. 'Genetic Interactions Between BOB1 and Multiple 26S Proteasome Subunits Suggest a Role for Proteostasis in Regulating Arabidopsis Development', *G3 (Bethesda)*, 8: 1379-90.
- Singh, A. K., B. S. Yadav, S. Dhanapal, M. Berliner, A. Finkelshtein, and D. A. Chamovitz. 2019. 'CSN5A Subunit of COP9 Signalosome Temporally Buffers Response to Heat in Arabidopsis', *Biomolecules*, 9.
- Solis-Miranda, Jorge, Monika Chodasiewicz, Aleksandra Skiryicz, Alisdair R Fernie, Panagiotis N Moschou, Peter V Bozhkov, and Emilio Gutierrez-Beltran. 2023. 'Stress-related biomolecular condensates in plants', *The Plant Cell*, 35: 3187-204.
- Son, Seungmin, and Sang Ryeol Park. 2023. 'Plant translational reprogramming for stress resilience', *Frontiers in Plant Science*, 14.
- Sørensen, M. A., C. G. Kurland, and S. Pedersen. 1989. 'Codon usage determines translation rate in Escherichia coli', *J Mol Biol*, 207: 365-77.
- Sorenson, R., and J. Bailey-Serres. 2014. 'Selective mRNA sequestration by OLIGOURIDYLATE-BINDING PROTEIN 1 contributes to translational control during hypoxia in Arabidopsis', *Proc Natl Acad Sci U S A*, 111: 2373-8.
- Stael, S., L. P. Miller, A. D. Fernandez-Fernandez, and F. Van Breusegem. 2022. 'Detection of Damage-Activated Metacaspase Activity by Western Blot in Plants', *Methods Mol Biol*, 2447: 127-37.

- Stellberger, T., R. Hauser, A. Baiker, V. R. Pothineni, J. Haas, and P. Uetz. 2010. 'Improving the yeast two-hybrid system with permutated fusions proteins: the Varicella Zoster Virus interactome', *Proteome Sci*, 8: 8.
- Strotmann, Vivien I, and Yvonne Stahl. 2021. 'At the root of quiescence: function and regulation of the quiescent center', *Journal of Experimental Botany*, 72: 6716-26.
- Supek, F., M. Bosnjak, N. Skunca, and T. Smuc. 2011. 'REVIGO summarizes and visualizes long lists of gene ontology terms', *PLoS One*, 6: e21800.
- Tabassum, N., L. Eschen-Lippold, B. Athmer, M. Baruah, M. Brode, L. D. Maldonado-Bonilla, W. Hoehenwarter, G. Hause, D. Scheel, and J. Lee. 2020. 'Phosphorylation-dependent control of an RNA granule-localized protein that fine-tunes defence gene expression at a post-transcriptional level', *Plant J*, 101: 1023-39.
- Tauber, Devin, Gabriel Tauber, and Roy Parker. 2020. 'Mechanisms and Regulation of RNA Condensation in RNP Granule Formation', *Trends in Biochemical Sciences*, 45: 764-78.
- Taylor, J. P., R. H. Brown, Jr., and D. W. Cleveland. 2016. 'Decoding ALS: from genes to mechanism', *Nature*, 539: 197-206.
- Teixeira, D., U. Sheth, M. A. Valencia-Sanchez, M. Brengues, and R. Parker. 2005. 'Processing bodies require RNA for assembly and contain nontranslating mRNAs', *RNA*, 11: 371-82.
- Tiwari, L. D., L. Khungar, and A. Grover. 2020. 'AtHsc70-1 negatively regulates the basal heat tolerance in Arabidopsis thaliana through affecting the activity of HsfAs and Hsp101', *Plant J*, 103: 2069-83.
- Tiwari, Lalit Dev, Ritesh Kumar, Vijyesh Sharma, Alok Kumar Sahu, Balram Sahu, Subhash Chandra Naithani, and Anil Grover. 2021. 'Stress and development phenotyping of Hsp101 and diverse other Hsp mutants of Arabidopsis thaliana', *Journal of Plant Biochemistry and Biotechnology*, 30: 889-905.
- Torrent, Marc, Guilhem Chalancon, Natalia S. de Groot, Arthur Wuster, and M. Madan Babu. 2018. 'Cells alter their tRNA abundance to selectively regulate protein synthesis during stress conditions', *Science Signaling*, 11: eaat6409.
- Towbin, H., T. Staehelin, and J. Gordon. 1979. 'Electrophoretic transfer of proteins from polyacrylamide gels to nitrocellulose sheets: procedure and some applications', *Proc Natl Acad Sci U S A*, 76: 4350-4.
- Tuller, Tamir, Asaf Carmi, Kalin Vestsigian, Sivan Navon, Yuval Dorfan, John Zaborske, Tao Pan, Orna Dahan, Itay Furman, and Yitzhak Pilpel. 2010. 'An Evolutionarily Conserved Mechanism for Controlling the Efficiency of Protein Translation', *Cell*, 141: 344-54.
- Tyanova, S., T. Temu, P. Sinitcyn, A. Carlson, M. Y. Hein, T. Geiger, M. Mann, and J. Cox. 2016. 'The Perseus computational platform for comprehensive analysis of (prote)omics data', *Nat Methods*, 13: 731-40.
- Ueda, M., E. Aichinger, W. Gong, E. Groot, I. Verstraeten, L. D. Vu, I. De Smet, T. Higashiyama, M. Umeda, and T. Laux. 2017. 'Transcriptional integration of paternal and maternal factors in the Arabidopsis zygote', *Genes Dev*, 31: 617-27.
- Ugalde, J. M., L. Lamig, A. Herrera-Vasquez, P. Fuchs, M. Homagk, S. Kopriva, S. J. Muller-Schussele, L. Holuigue, and A. J. Meyer. 2021. 'A dual role for glutathione transferase U7 in plant growth and protection from methyl viologen-induced oxidative stress', *Plant Physiol*, 187: 2451-68.
- Uhlken, C., B. Horvath, R. Stadler, N. Sauer, and M. Weingartner. 2014. 'MAIN-LIKE1 is a crucial factor for correct cell division and differentiation in Arabidopsis thaliana', *Plant J*, 78: 107-20.
- Uhlken, C., S. Hoth, and M. Weingartner. 2014. 'MAIL1 is essential for development of the primary root but not of anchor roots', *Plant Signal Behav*, 9: e976477.

- Uhrig, R. G., A. M. Labandera, and G. B. Moorhead. 2013. 'Arabidopsis PPP family of serine/threonine protein phosphatases: many targets but few engines', *Trends Plant Sci*, 18: 505-13.
- Ul Haq, S., A. Khan, M. Ali, A. M. Khattak, W. X. Gai, H. X. Zhang, A. M. Wei, and Z. H. Gong. 2019. 'Heat Shock Proteins: Dynamic Biomolecules to Counter Plant Biotic and Abiotic Stresses', *Int J Mol Sci*, 20.
- Urquidí Camacho, Ricardo A., Anshul Lokdarshi, and Albrecht G. von Arnim. 2020. 'Translational gene regulation in plants: A green new deal', *WIREs RNA*, 11: e1597.
- Van Aken, O., T. Pecenkova, B. van de Cotte, R. De Rycke, D. Eeckhout, H. Fromm, G. De Jaeger, E. Witters, G. T. Beemster, D. Inze, and F. Van Breusegem. 2007. 'Mitochondrial type-I prohibitins of *Arabidopsis thaliana* are required for supporting proficient meristem development', *Plant J*, 52: 850-64.
- van den Berg, Claudia, Viola Willemsen, Willem Hage, Peter Weisbeek, and Ben Scheres. 1995. 'Cell fate in the *Arabidopsis* root meristem determined by directional signalling', *Nature*, 378: 62-65.
- van Dijk, E., N. Cougot, S. Meyer, S. Babajko, E. Wahle, and B. Seraphin. 2002. 'Human Dcp2: a catalytically active mRNA decapping enzyme located in specific cytoplasmic structures', *EMBO J*, 21: 6915-24.
- Van Hoewyk, D. 2016. 'Use of the non-radioactive SUNSET method to detect decreased protein synthesis in proteasome inhibited *Arabidopsis* roots', *Plant Methods*, 12: 20.
- Van Larebeke, N., G. Engler, M. Holsters, S. Van den Elsacker, I. Zaenen, R. A. Schilperoort, and J. Schell. 1974. 'Large plasmid in *Agrobacterium tumefaciens* essential for crown gall-inducing ability', *Nature*, 252: 169-70.
- Vanderweyde, T., H. Yu, M. Varnum, L. Liu-Yesucevitz, A. Citro, T. Ikezu, K. Duff, and B. Wolozin. 2012. 'Contrasting pathology of the stress granule proteins TIA-1 and G3BP in tauopathies', *J Neurosci*, 32: 8270-83.
- Varenne, S., J. Buc, R. Lloubes, and C. Lazdunski. 1984. 'Translation is a non-uniform process. Effect of tRNA availability on the rate of elongation of nascent polypeptide chains', *J Mol Biol*, 180: 549-76.
- Vera, M., B. Pani, L. A. Griffiths, C. Muchardt, C. M. Abbott, R. H. Singer, and E. Nudler. 2014. 'The translation elongation factor eEF1A1 couples transcription to translation during heat shock response', *Elife*, 3: e03164.
- Vernoux, Teva, Robert C. Wilson, Kevin A. Seeley, Jean-Philippe Reichheld, Sandra Muroy, Spencer Brown, Spencer C. Maughan, Christopher S. Cobbett, Marc Van Montagu, Dirk Inzé, Mike J. May, and Zinmay R. Sung. 2000. 'The ROOT MERISTEMLESS1/CADMIUM SENSITIVE2 Gene Defines a Glutathione-Dependent Pathway Involved in Initiation and Maintenance of Cell Division during Postembryonic Root Development', *The Plant Cell*, 12: 97-109.
- Vickers, Tim J., and Alan H. Fairlamb. 2004. 'Trypanothione S-Transferase Activity in a Trypanosomatid Ribosomal Elongation Factor 1B\*', *Journal of Biological Chemistry*, 279: 27246-56.
- Vierling, E. 1991. 'The Roles of Heat Shock Proteins in Plants', *Annual Review of Plant Physiology and Plant Molecular Biology*, 42: 579-620.
- Voinnet, O., S. Rivas, P. Mestre, and D. Baulcombe. 2003. 'An enhanced transient expression system in plants based on suppression of gene silencing by the p19 protein of tomato bushy stunt virus', *Plant J*, 33: 949-56.
- Waese, J., J. Fan, A. Pasha, H. Yu, G. Fucile, R. Shi, M. Cumming, L. A. Kelley, M. J. Sternberg, V. Krishnakumar, E. Ferlanti, J. Miller, C. Town, W. Stuerzlinger, and N. J. Provart. 2017. 'ePlant: Visualizing and Exploring Multiple Levels of Data for Hypothesis Generation in Plant Biology', *Plant Cell*, 29: 1806-21.

- Wallace, E. W. J., J. L. Kear-Scott, E. V. Pilipenko, M. H. Schwartz, P. R. Laskowski, A. E. Rojek, C. D. Katanski, J. A. Riback, M. F. Dion, A. M. Franks, E. M. Airoidi, T. Pan, B. A. Budnik, and D. A. Drummond. 2015. 'Reversible, Specific, Active Aggregates of Endogenous Proteins Assemble upon Heat Stress', *Cell*, 162: 1286-98.
- Wang, S., J. Kurepa, and J. A. Smalle. 2009. 'The Arabidopsis 26S proteasome subunit RPN1a is required for optimal plant growth and stress responses', *Plant Cell Physiol*, 50: 1721-5.
- Wang, T. Y., J. R. Wu, N. K. T. Duong, C. A. Lu, C. H. Yeh, and S. J. Wu. 2021. 'HSP70-4 and farnesylated AtJ3 constitute a specific HSP70/HSP40-based chaperone machinery essential for prolonged heat stress tolerance in Arabidopsis', *J Plant Physiol*, 261: 153430.
- Weber, C., L. Nover, and M. Fauth. 2008. 'Plant stress granules and mRNA processing bodies are distinct from heat stress granules', *Plant J*, 56: 517-30.
- Wendrich, J. R., S. Boeren, B. K. Moller, D. Weijers, and B. De Rybel. 2017. 'In Vivo Identification of Plant Protein Complexes Using IP-MS/MS', *Methods Mol Biol*, 1497: 147-58.
- Wenig, U., S. Meyer, R. Stadler, S. Fischer, D. Werner, A. Lauter, M. Melzer, S. Hoth, M. Weingartner, and N. Sauer. 2013. 'Identification of MAIN, a factor involved in genome stability in the meristems of Arabidopsis thaliana', *Plant J*, 75: 469-83.
- Wiedner, Hannah J., and Jimena Giudice. 2021. 'It's not just a phase: function and characteristics of RNA-binding proteins in phase separation', *Nature Structural & Molecular Biology*, 28: 465-73.
- Wigge, Philip A. 2013. 'Ambient temperature signalling in plants', *Current Opinion in Plant Biology*, 16: 661-66.
- Wolozin, Benjamin, and Pavel Ivanov. 2019. 'Stress granules and neurodegeneration', *Nature Reviews Neuroscience*, 20: 649-66.
- Wroblewski, T., A. Tomczak, and R. Michelmore. 2005. 'Optimization of Agrobacterium-mediated transient assays of gene expression in lettuce, tomato and Arabidopsis', *Plant Biotechnol J*, 3: 259-73.
- Wu, Hsin-Yen Larry, Joey Jen, and Polly Yingshan Hsu. 2023. 'What, where, and how: Regulation of translation and the translational landscape in plants', *The Plant Cell*.
- Wu, J. R., T. Y. Wang, C. P. Weng, N. K. T. Duong, and S. J. Wu. 2019. 'AtJ3, a specific HSP40 protein, mediates protein farnesylation-dependent response to heat stress in Arabidopsis', *Planta*, 250: 1449-60.
- Xie, J., V. de Souza Alves, T. von der Haar, L. O'Keefe, R. V. Lenchine, K. B. Jensen, R. Liu, M. J. Coldwell, X. Wang, and C. G. Proud. 2019. 'Regulation of the Elongation Phase of Protein Synthesis Enhances Translation Accuracy and Modulates Lifespan', *Curr Biol*, 29: 737-49.e5.
- Xu, B., L. Liu, and G. Song. 2021. 'Functions and Regulation of Translation Elongation Factors', *Frontiers in Molecular Biosciences*, 8: 816398.
- Xu, D., G. Marino, A. Klingl, B. Enderle, E. Monte, J. Kurth, A. Hiltbrunner, D. Leister, and T. Kleine. 2019. 'Extrachloroplastic PP7L Functions in Chloroplast Development and Abiotic Stress Tolerance', *Plant Physiol*, 180: 323-41.
- Xu, Duorong, Dario Leister, and Tatjana Kleine. 2019. 'VENOSA4, a Human dNTPase SAMHD1 Homolog, Contributes to Chloroplast Development and Abiotic Stress Tolerance1 [OPEN]', *Plant Physiology*, 182: 721-29.
- Xu, J., Y. S. Tian, X. J. Xing, R. H. Peng, B. Zhu, J. J. Gao, and Q. H. Yao. 2016. 'Over-expression of AtGSTU19 provides tolerance to salt, drought and methyl viologen stresses in Arabidopsis', *Physiol Plant*, 156: 164-75.

- Xu, J., J. Y. Yang, Q. W. Niu, and N. H. Chua. 2006. 'Arabidopsis DCP2, DCP1, and VARICOSE form a decapping complex required for postembryonic development', *Plant Cell*, 18: 3386-98.
- Yamasaki, S., H. Matsuura, T. Demura, and K. Kato. 2015. 'Changes in Polysome Association of mRNA Throughout Growth and Development in Arabidopsis thaliana', *Plant Cell Physiol*, 56: 2169-80.
- Yan, Y., J. Gan, Y. Tao, T. W. Okita, and L. Tian. 2022. 'RNA-Binding Proteins: The Key Modulator in Stress Granule Formation and Abiotic Stress Response', *Front Plant Sci*, 13: 882596.
- Yang, P., C. Mathieu, R. M. Kolaitis, P. Zhang, J. Messing, U. Yurtsever, Z. Yang, J. Wu, Y. Li, Q. Pan, J. Yu, E. W. Martin, T. Mittag, H. J. Kim, and J. P. Taylor. 2020. 'G3BP1 Is a Tunable Switch that Triggers Phase Separation to Assemble Stress Granules', *Cell*, 181: 325-45.e28.
- Yanguez, E., A. B. Castro-Sanz, N. Fernandez-Bautista, J. C. Oliveros, and M. M. Castellano. 2013. 'Analysis of genome-wide changes in the translome of Arabidopsis seedlings subjected to heat stress', *PLoS One*, 8: e71425.
- Yeh, Ching-Hui, Nicholas J. Kaplinsky, Catherine Hu, and Yee-yung Charng. 2012. 'Some like it hot, some like it warm: Phenotyping to explore thermotolerance diversity', *Plant Science*, 195: 10-23.
- Yoo, S. D., Y. H. Cho, and J. Sheen. 2007. 'Arabidopsis mesophyll protoplasts: a versatile cell system for transient gene expression analysis', *Nat Protoc*, 2: 1565-72.
- Yoshiyama, Kaoru O., Junya Kobayashi, Nobuo Ogita, Minako Ueda, Seisuke Kimura, Hisaji Maki, and Masaaki Umeda. 2013. 'ATM-mediated phosphorylation of SOG1 is essential for the DNA damage response in Arabidopsis', *EMBO reports*, 14: 817-22.
- Zappa, F., C. Wilson, G. Di Tullio, M. Santoro, P. Pucci, M. Monti, D. D'Amico, S. Pisonero-Vaquero, R. De Cegli, A. Romano, M. A. Saleem, E. Polishchuk, M. Failli, L. Giaquinto, and M. A. De Matteis. 2019. 'The TRAPP complex mediates secretion arrest induced by stress granule assembly', *EMBO J*, 38: e101704.
- Zhang, H. Y., G. Lei, H. W. Zhou, C. He, J. L. Liao, and Y. J. Huang. 2017. 'Quantitative iTRAQ-based proteomic analysis of rice grains to assess high night temperature stress', *Proteomics*, 17.
- Zhang, H., J. Zhu, Z. Gong, and J. K. Zhu. 2022. 'Abiotic stress responses in plants', *Nat Rev Genet*, 23: 104-19.
- Zhang, Heng, Yang Zhao, and Jian-Kang Zhu. 2020. 'Thriving under Stress: How Plants Balance Growth and the Stress Response', *Developmental Cell*, 55: 529-43.
- Zhang, L., X. Liu, K. Gaikwad, X. Kou, F. Wang, X. Tian, M. Xin, Z. Ni, Q. Sun, H. Peng, and E. Vierling. 2017. 'Mutations in eIF5B Confer Thermosensitive and Pleiotropic Phenotypes via Translation Defects in Arabidopsis thaliana', *Plant Cell*, 29: 1952-69.
- Zhang, Xingqian, and Shu-Bing Qian. 2011. 'Chaperone-mediated hierarchical control in targeting misfolded proteins to aggresomes', *Molecular Biology of the Cell*, 22: 3277-88.
- Zhao, Y. 2010. 'Auxin biosynthesis and its role in plant development', *Annu Rev Plant Biol*, 61: 49-64.
- Zheng, Dinghai, Nader Ezzeddine, Chyi-Ying A. Chen, Wenmiao Zhu, Xiangwei He, and Ann-Bin Shyu. 2008. 'Deadenylation is prerequisite for P-body formation and mRNA decay in mammalian cells', *Journal of Cell Biology*, 182: 89-101.
- Zhigailov, A. V., A. M. Alexandrova, A. S. Nizkorodova, G. E. Stanbekova, R. V. Kryldakov, O. V. Karpova, N. S. Polimbetova, N. G. Halford, and B. K. Iskakov. 2020. 'Evidence That Phosphorylation of the  $\alpha$ -Subunit of eIF2 Does Not Essentially Inhibit mRNA Translation in Wheat Germ Cell-Free System', *Front Plant Sci*, 11: 936.

- Zhou, Fujun, Bijoyita Roy, John R. Dunlap, Ramya Enganti, and Albrecht G. von Arnim. 2014. 'Translational Control of Arabidopsis Meristem Stability and Organogenesis by the Eukaryotic Translation Factor eIF3h', *PLoS One*, 9: e95396.
- Zhou, Y., F. Xu, Y. Shao, and J. He. 2022. 'Regulatory Mechanisms of Heat Stress Response and Thermomorphogenesis in Plants', *Plants (Basel)*, 11.
- Zhu, Shaobo, Jinge Gu, Juanjuan Yao, Yichen Li, Zheting Zhang, Wencheng Xia, Zhen Wang, Xinrui Gui, Leiting Li, and Dan Li. 2022. 'Liquid-liquid phase separation of RBGD2/4 is required for heat stress resistance in Arabidopsis', *Developmental Cell*, 57: 583-97. e6.
- Zhu, Y., A. Dong, D. Meyer, O. Pichon, J. P. Renou, K. Cao, and W. H. Shen. 2006. 'Arabidopsis NRP1 and NRP2 encode histone chaperones and are required for maintaining postembryonic root growth', *Plant Cell*, 18: 2879-92.





## 9 List of publications

Parts of the data presented in this thesis were published in the following publications:

### Publication 1:

De Luxán-Hernández C, **Lohmann J**, Hellmeyer W, Seanpong S, Wöltje K, Magyar Z, Pettkó-Szandtner A, Péliissier T, De Jaeger G, Hoth S, Mathieu O, Weingartner M. PP7L is essential for MAIL1-mediated transposable element silencing and primary root growth. *Plant J.* 2020 May;102(4):703-717. doi: 10.1111/tpj.14655.

I have contributed to this work with:

- Analysis of embryo development by clearance of *pp7l-1* and *pp7l-3* seeds with Hoyers solution and confocal laser scanning microscopy (Fig. S1a,b)
- mPS-PI staining of mature seeds and confocal laser scanning microscopy for analysis of root meristem in mature seeds of *pp7l-1* and *pp7l-3* (Fig. S1c)
- Support of cloning of BiFC-control construct (-/PP7L) (Fig. 1c)

### Publication 2:

De Luxán-Hernández C, **Lohmann J**, Tranque E, Chumova J, Binarova P, Salinas J, Weingartner M. ‘MDF is a conserved splicing factor and modulates cell division and stress response in *Arabidopsis*’. *Life Sci Alliance.* 2022 Oct 20;6(1): e202201507. doi: 10.26508/lsa.202201507.

My contributions to this work are listed below:

- Cloning of constructs and performance of yeast-two hybrid assay for MDF and STA1 (Fig. S2B)
- Cloning and expression of nuclear speckle marker in plant cells (Fig. 2E)

### Publication 3:

**Lohmann J**, de Luxán-Hernández C, Gao Y, Zoschke R, Weingartner M. Arabidopsis translation factor eEF1B $\gamma$  impacts plant development and is associated with heat-induced cytoplasmic foci. *J Exp Bot.* 2023 Apr 18;74(8):2585-2602. doi: 10.1093/jxb/erad050.

The work for this study has mainly been performed by myself, the contributions of the co-authors are listed below:

- Cloe de Luxán Hernández: Confocal microscopy experiments with PI-stained root tips of 7-day-old WT and *eef1by1/2* double mutants (Fig. 3E); quantification of the number of cortical cells within the proximal meristem (Fig. 3F), role of the eEF1B complex  $\gamma$ -subunit in primary root growth under increased ambient temperatures conditions (Fig. S4C)
- Yang Gao and Reimo Zoschke: Performance of polysome profiling and evaluation of the obtained results (Fig. 4D, E, G)
- Magdalena Weingartner: Analysis of cytoplasmic foci formation in stably transformed lines expressing (Fig. S6)

Publication 4:

**Lohmann J**, Herzog O, Rosenzweig K, Weingartner M. Thermal Adaptation in Plants: Understanding the Dynamics of Translation Factors and Condensates. *J Exp Bot.* 2024 Apr 17: erae171. doi: 10.1093/jxb/erae171 (Review article).

## Acknowledgements

First of all, I thank Magdalena for her support, advice, patience and trust. Thank you for many hours of discussions, paper writing and correcting. Your input and ideas have had huge impact on the outcome of this work.

I thank Julia for agreeing to be the second examiner of this thesis.

I thank Stefan for the opportunity to work in his group and for discussions and input on the progress of my thesis. It has been a pleasure to work in the MPP department.

This work has profited a lot from collaborations with scientists from other institutes. I would like to thank our collaborators from Potsdam, Yang Gao and Reimo Zoschke, for conducting the polysome profiling and their help with the interpretation of the results. I thank Dominique Eeckhout and Geert Persiau from VIB-UGent Center for Plant Systems Biology for conducting the co-immunoprecipitation experiment. I thank Justin Lee and Nicole Bauer from IPB Halle for sending the plasmid pUBN-PAB8. During my research stay I had the pleasure to learn a lot from Pavla Binarova and Jana Chumova from the Institute of Microbiology of the CAS in Prague.

Many thanks goes to Steffen Ostendorp for his help with the RNA analysis using the BioAnalyser. I would like to thank Hartwig Lüthen and Kostas Lampou for their advice on confocal microscopy and automated evaluation of confocal images.

I thank Wiebke, Judith, Wenke and Teresa for their excellent technical assistance and their support with experiments. I would like to thank Christiane for her great help with all organizational matters.

I miss working together with all PhD students and PostDocs from the MPP. Special thanks goes to Lisa, Tim, Moni, Cloe and Linn. It has been the best to work together with such helpful, inspiring and funny lab companions.

I had the pleasure to work together with many great and dedicated students. I would like to thank Mahsa, Mohammed, Seinab, Felix, Jay, Florian and Christoph for their contributions to this thesis.

Big thanks to my family and Nico, who have been a big support during the last years.

At last, thanks a lot to everyone who accompanied me along the way of my “PhD journey”. It was a great experience and I am grateful for everything that I have learned.

## Affidavit

Hiermit versichere ich an Eides statt, die vorliegende Dissertationsschrift selbst verfasst und keine anderen als die angegebenen Hilfsmittel und Quellen benutzt zu haben. Sofern im Zuge der Erstellung der vorliegenden Dissertationsschrift generative Künstliche Intelligenz (gKI) basierte elektronische Hilfsmittel verwendet wurden, versichere ich, dass meine eigene Leistung im Vordergrund stand und dass eine vollständige Dokumentation aller verwendeten Hilfsmittel gemäß der Guten wissenschaftlichen Praxis vorliegt. Ich trage die Verantwortung für eventuell durch die gKI generierte fehlerhafte oder verzerrte Inhalte, fehlerhafte Referenzen, Verstöße gegen das Datenschutz- und Urheberrecht oder Plagiate.

I hereby declare and affirm that this doctoral dissertation is my own work and that I have not used any aids and sources other than those indicated. If electronic resources based on generative artificial intelligence (gAI) were used in the course of writing this dissertation, I confirm that my own work was the main and value-adding contribution and that complete documentation of all resources used is available in accordance with good scientific practice. I am responsible for any erroneous or distorted content, incorrect references, violations of data protection and copyright law or plagiarism that may have been generated by the gAI.

Hamburg, 05.11.2024

Julia Christin Lohmann

J. Lohmann